TRANSPORTATION RESEARCH RECORD 903

Bridges and Culverts

TRANSPORTATION RESEARCH BOARD

NATIONAL RESEARCH COUNCIL
NATIONAL ACADEMY OF SCIENCES
WASHINGTON, D.C. 1983

Transportation Research Record 903
Price $14.80
Edited for TRB by Mary McLaughlin

modes
1 highway transportation
3 rail transportation

subject areas
25 structures design and performance
40 maintenance
62 soil foundations

Library of Congress Cataloging in Publication Data
National Research Council. Transportation Research Board.
Bridges and culverts.

(Transportation research record; 903)
Reports for the TRB 62nd annual meeting. 1. Bridges–Testing–Addresses, essays, lectures. 2. Bridges–Design–Addresses, essays, lectures. 3. Culverts–Addresses, essays, lectures. I. National Research Council (U.S.). Transportation Research Board.
TE7.H5 no. 903 [TG305] 380.5s[624'.2] 83-17251
ISBN 0-309-03517-1 ISSN 0361-1981

Sponsorship of the Papers in This Transportation Research Record

GROUP 2–DESIGN AND CONSTRUCTION OF TRANSPORTATION FACILITIES
Robert C. Deen, University of Kentucky, chairman

Structures Section
John M. Hanson, Wiss Janney & Elstner & Associates, chairman

Committee on General Structures
Clellon Lewis Loveall, Tennessee Department of Transportation, chairman
John M. Kulicki, Modjeski & Masters, secretary
John J. Ahlskog, Dan S. Bechly, Neal H. Bettigole, Edwin G. Burdette, Martin P. Burke, Jr., Jack H. Emanuel, Dah Fwu Fine, Richard S. Fountain, J. Leroy Hulsey, Walter J. Jestings, Robert N. Kamp, Heinz P. Koretzky, Celal N. Kostem, Wendell B. Lawing, Richard M. McClure, Gordon R. Pennington, David R. Schelling, Arunprakash M. Shirole, Marcello H. Soto, Robert F. Victor, Stanley W. Woods

Committee on Steel Bridges
Frank D. Sears, Federal Highway Administration, chairman
Chris S.C. Yiu, Pavlo Engineering Company, secretary
Pedro Albrecht, Dan S. Bechly, Chester F. Comstock, J. Hartley Daniels, David A. Dock, Jackson L. Durkee, Nicholas M. Engelman, John W. Fisher, Karl H. Frank, Louis A. Garrido, Wayne Henneberger, Robert B. Jarvis, B.F. Kotalik, Richard W. Lautensleger, Albert D.M. Lewis, Abba G. Lichtenstein, Joseph M. McCabe, Jr., Roy L. Mion, W.H. Munse, Robert H. Scanlan, Frederick H. Sterbenz, Carl E. Thunman, Jr., Carl C. Ulstrup

Committee on Concrete Bridges
Robert C. Cassano, California Department of Transportation, chairman
T. Alberdi, Jr., Craig A. Ballinger, Robert C. Cassano, W. Gene Corley, C.S. Gloyd, James J. Hill, Ti Huang, Cornie L. Hulsbos, Roy A. Imbsen, Hubert Janssen, Heinz P. Koretzky, H.G. Kriegel, John M. Kulicki, R. Shankar Nair, Edward G. Nawy, Walter Podolny, Jr., Adrianus Vankampen, Julius F.J. Volgyi, Jr., Donald J. Ward, W. Jack Wilkes

Committee on Dynamics and Field Testing of Bridges
James W. Baldwin, Jr., University of Missouri-Columbia, chairman
Charles F. Galambos, Federal Highway Administration, secretary
Baidar Bakht, Furman W. Barton, David B. Beal, Harold R. Bosch, John L. Burdick, William G. Byers, G.R. Cudney, Ismail A.S. Elkholy, Hota V.S. Gangarao, David William Goodpasture, Roy A. Imbsen, F. Wayne Klaiber, Celal N. Kostem, Robert H. Lee, Robert L. McGillicuddy, Fred Moses, M. Noyszewski, Gajanan M. Sabnis, R. Varadarajan, William H. Walker, Kenneth R. White

Committee on Culverts and Hydraulic Structures
Richard A. Parmelee, Northwestern University, chairman
A.E. Bacher, Mike Bealey, Thomas K. Breitfuss, J.M. Duncan, Sam S. Gillespie, Benjamin M. Givens, Jr., Frank J. Heger, James J. Hill, Iraj I. Kaspar, Michael G. Katona, Wendell B. Lawing, L.R. Lawrence, A.P. Moser, Harold R. Sandberg, M.G. Spangler, David C. Thomas, Corwin L. Tracy, Adrianus Vankampen, Robert P. Walker, Jr., David C. Wyant

Soil Mechanics Section
Raymond A. Forsyth, California Department of Transportation, chairman

Committee on Foundations of Bridges and Other Structures
Bernard E. Butler, Reinforced Earth Company, chairman
Arnold Aronowitz, Michael Bozozuk, W. Dale Carney, Harry M. Coyle, Albert F. Dimillio, Bengt H. Fellenius, Frank M. Fuller, G.G. Goble, Richard J. Goettle III, James S. Graham, Hal W. Hunt, Gay D. Jones, Jr., Philip Keene, Hugh S. Lacy, Clyde N. Laughter, Robert M. Leary, G.A. Leonards, Richard P. Long, Lyle K. Moulton, Michael Wayne O'Neill, Arthur J. Peters, Alex Rutka, Harvey E. Wahls, John L. Walkinshaw, James Doyle Webb

GROUP 3–OPERATION AND MAINTENANCE OF TRANSPORTATION FACILITIES
Patricia F. Waller, University of North Carolina, chairman

Committee on Sealants and Fillers for Joints and Cracks
William T. Burt, III, Louisiana Department of Transportation and Development, chairman
Chris Seibel, Jr., Consulting Engineer, secretary
Craig A. Ballinger, Delmont Brown, Martin P. Burke, Jr., John P. Cook, Gary L. Fordyce, Frank D. Gaus, C.W. Heckathorn, Richard C. Ingberg, Jerome M. Klosowski, Joseph F. Lamond, Arthur Linfante, Earl W. Loucks, William G. Prince, Guy S. Puccio, Anthony L. Shloss, Charles V. Slavis, Lawrence L. Smith, J.B. Thornton, Egons Tons, Stewart C. Watson, Richard J. Worch

Lawrence F. Spaine, Neil F. Hawks and Adrian G. Clary, Transportation Research Board staff

Sponsorship is indicated by a footnote at the end of each report. The organizational units, officers, and members are as of December 31, 1982.

Contents

Authors of the Papers in This Record

Bacher, Alfred E., California Department of Transportation, 1120 N Street, Sacramento, CA 95814
Banke, Albert N., California Department of Transportation, 1120 N Street, Sacramento, CA 95814
Beal, David B., Engineering Research and Development Bureau, New York State Department of Transportation, 1220 Washington Avenue, State Campus, Albany, NY 12232
Berger, R.H., Byrd, Tallamy, MacDonald, and Lewis, 2921 Telestar Court, Falls Church, VA 22042
Browzin, Boris S., Office of Regulatory Research, U.S. Nuclear Regulatory Commission, Washington, DC 20555
Buckner, C. Dale, Department of Civil Engineering, Louisiana State University, Baton Rouge, LA 70803
Burke, Martin P., Jr., Burgess and Niple, Limited, 5085 Reed Road, Columbus, OH 43220
Callis, Eric C., Barrett, Daffin, and Carlan, Inc., 3100 Capital Circle, S.E., Tallahassee, FL 32301
Fagundo, Fernando E., Department of Civil Engineering, University of Florida, Gainesville, FL 32611
Goddard, James B., Advanced Drainage Systems, Inc., 3300 Riverside Drive, Columbus, OH 43221
Greimann, L.F., Department of Civil Engineering, Iowa State University, Ames, IA 50011
Hanson, John M., Wiss, Janney, Elstner and Associates, Inc., 330 Pfingsten Road, Northbrook, IL 60062
Hays, Clifford O., Jr., Department of Civil Engineering, University of Florida, Gainesville, FL 32611
Heins, C.P., University of Maryland (deceased)
Jorgenson, James L., Department of Civil Engineering, North Dakota State University, Fargo, ND 58105
Kirkland, Daniel E., California Department of Transportation, 1120 N Street, Sacramento, CA 95814
Koob, Michael J., Wiss, Janney, Elstner, and Associates, Inc., 330 Pfingsten Road, Northbrook, IL 60062
Kulicki, John M., Modjeski and Masters, P.O. Box 2345, Harrisburg, PA 17105
Lin, I.C., 4511 Knox Road, College Park, MD 20740
Mazroi, Ali, School of Civil Engineering and Environmental Science, University of Oklahoma, Norman, OK 73019
Moulton, Lyle K., Department of Civil Engineering, West Virginia University, Morgantown, WV 26506
Murray, Thomas M., Fears Structural Engineering Laboratory, University of Oklahoma, Norman, OK 73019
Reeve, Ronald C., Consultant, 1222 Southport Drive, Columbus, OH 43220
Rude, Lawrence C., Department of Civil Engineering, Virginia Polytechnic and State University, Blacksburg, VA 24061
Turner, H.T., Department of Civil Engineering, Louisiana State University, Baton Rouge, LA 70803
Wang, Leon Ru-Liang, Department of Civil Engineering, University of Oklahoma, Norman, OK 73019
Watkins, Reynold K., Department of Civil and Environmental Engineering, Utah State University, Logan, UT 84322
Wold-Tinsae, A.M., Department of Civil Engineering, Iowa State University, Ames, IA 50011
Yang, P.S., Department of Civil Engineering, Iowa State University, Ames, IA 50011

Field Testing of the Fremont Bridge

MICHAEL J. KOOB AND JOHN M. HANSON

In July 1979, field tests were conducted on the Fremont Bridge on the Willamette River in Oregon to obtain strain and temperature measurements that would provide information on in situ and service load stress conditions. The behavior of the bridge was more dependent on temperature than on traffic. On a hot day when the temperature reached 100° F, the temperature differential between the exposed top and shaded bottom flange plates was 50° F. The maximum daily stress range in the tie girders due to the temperature differential was about 10 ksi. Where local bending occurred in the web plates, the maximum daily stress range was about 20 ksi. Comparison of strain readings on two days of comparable temperature, with light and heavy traffic, indicated that the stress range due to traffic was about 1-2 ksi. Dynamic recordings of strain were made at 12 selected category E details during typical traffic conditions. The passage of heavy vehicles typically caused stress ranges up to 1000 psi. The largest measured stress range of about 3000 psi was associated with the passage of a heavy mobile crane. The frequency of these stress ranges was estimated to be about 50 percent of the average daily truck traffic of 5400 vehicles. The bridge was also subjected to a controlled loading of four heavy vehicles weighing a total of 177 100 lb. The maximum stress range occurring on an instrumented cross section near the junction of the arch rib and tie girder was 750 psi. The maximum stress range at any other instrumented location was 2150 psi.

A comprehensive postconstruction evaluation study of the Fremont Bridge on the Willamette River in Oregon (1) was conducted for the Oregon State Highway Division (OSHD). The purpose of this study was to assess the long-range performance of main load-carrying, nonredundant tensile members and components of the structure.

A field testing program was carried out in July 1979 as part of the study. This program was intended to provide information about the behavior of the bridge under combined traffic and environmental conditions.

During the 10-day field testing period, one day was cool and partly cloudy and several days were hot and clear. The hottest day occurred on July 16, when the ambient temperature reached 100°F. Throughout the testing period, readings were taken at intervals of one or two hours or more often if the recording station was manned and selected gages were being monitored. Dynamic recordings of strain were made during typical traffic conditions. The bridge was also subjected to a controlled loading of four heavy vehicles weighing 177 100 lb.

DESCRIPTION OF BRIDGE

The Fremont Bridge is a three-span, stiffened steel tied arch 2159 ft in length, as shown in Figure 1. In this structure, the arch is loaded in compression and the tie girder is loaded in tension to counteract the thrust of the arch as well as in flexure to resist the live-load bending moments. The main span is divided into 28 panels at 44 ft, 10 in, for a total length of 1255 ft, 4 in. Each side span is divided into 10 panels at 44 ft, 10 in, for a total length of 448 ft, 4 in. Junctions between panels are numbered from 0 through 48. A description of the bridge and its design is given by Hedefine and Silano (2).

A typical section through the bridge, in the region where the arch is above the roadway, is shown in Figure 2. The orthotropic steel upper deck, carrying four lanes of westbound traffic, acts integrally with the tie girders. The bottom deck, carrying four lanes of eastbound traffic, is a reinforced concrete slab supported on stringers and floor beams. In the middle 896 ft of the bridge, where the arch ribs are above the tie girders, the bottom deck is suspended by hangers from the tie girders. Outside of this region, the bottom deck is framed into compression struts extending between the arch ribs and the tie girders.

Representative details of the orthotropic deck and tie girders are shown in Figure 3. The top flange is A36 steel, and the bottom flange is A588. The webs are 0.5 in thick except at the junctions with the arch ribs and pier columns. Typically, the lower 6 ft is fabricated from a high-strength, low-alloy steel that meets the requirements of ASTM A441, and the upper part is fabricated from A36 steel. This hybrid design reflects the integral action of the orthotropic deck and tie girders, with the neutral axis about 6 ft below the top flange. Welded construction is used throughout the tie girders, except for high-strength bolted field splices.

The arch ribs are box shaped and have a constant width of 4 ft. The depth of the web plates is 3 ft, 10 in; hence, the overall depth of the arch ribs varies depending on the flange plates, which have a maximum thickness of 2.25 in. High-strength, quenched and tempered ASTM A514 steel is used for the arch ribs, which are welded except for bolted field splices.

At the four junctions of the girders and arch ribs located at panel points 14 and 34, the cross section of the arch rib is changed from a box shape to three A514 strap plates in a vertical plane, each 3 in thick and 3 ft, 10 in deep. These three straps are stiffened by a welded diaphragm at middepth. The straps extend through slots in the top and bottom flanges of the girder.

The center section of the bridge, between panel points 14 and 34, was fabricated off site, trans-

Figure 1. Elevation of Fremont Bridge.

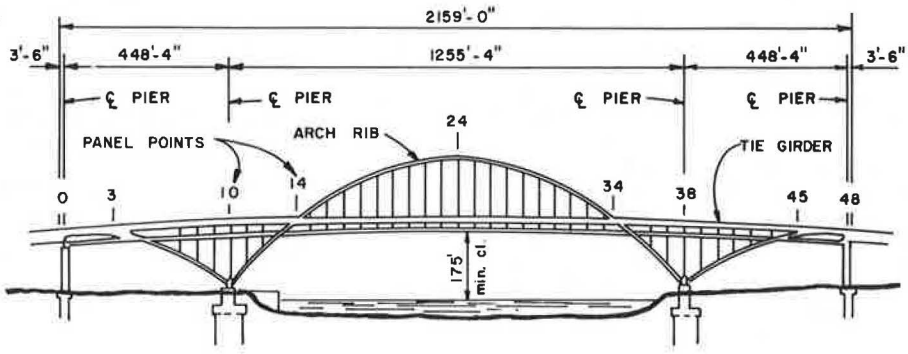

Figure 2. Typical section where arch is above roadway.

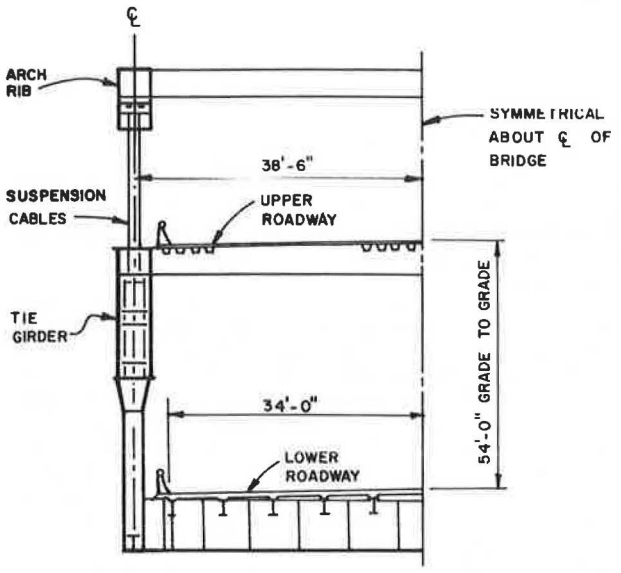

Figure 3. Representative details of deck and tie girder.

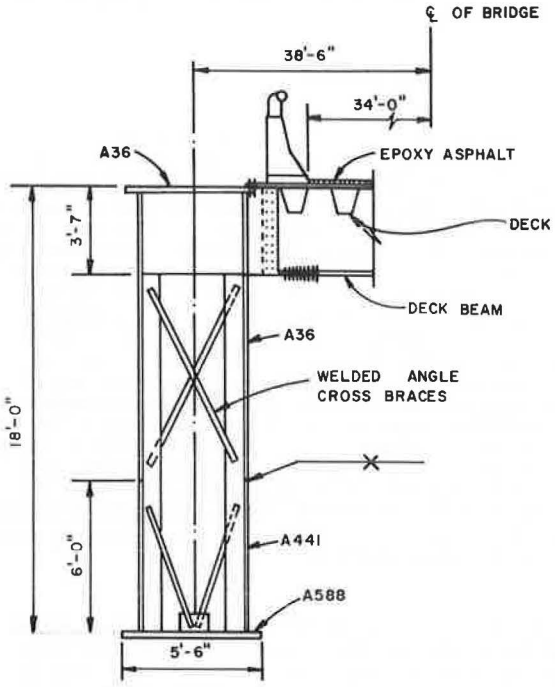

GIRDER SECTION

ported on barges, and erected by hydraulic jacking. A bolted splice connects the center and end sections, located within the junction of the tie girder arch rib. Heavy jacking stiffeners are also welded and bolted to the sides of the tie girder in this area.

The final coat of paint on the exterior of the bridge was a light shade of green.

INSTRUMENTED AREAS

It was decided that the best measure of the overall response of the bridge would be obtained by installing strain gages on four cross sections in the vicinity of panel point 14 in both the north and south tie girders. The locations of the instrumented sections, designated A, B, C, and D, are shown in Figure 4. Concern about the properties of a steel plate in the bottom flange near panel point 42 in the north tie girder led to installing instrumentation at a cross section in this region, designated section E.

Sections A, C, D, and E and section B were instrumented with six and sixteen 90° three-element strain gages, one element of which was parallel to the longitudinal axis of the member. At panel point 14 on the north tie girder, three 3-element strain gages, designated group F, were installed on the north web plate adjacent to the heavy fillet welds attaching the strap to the web.

In conjunction with the strain gage instrumentation, thermocouples were installed in both the north and south tie girders at section B.

Additional instrumentation was installed at locations of details where conditions were believed to be susceptible to fatigue crack growth or where special study of strain response was desired. These details included (a) ends of horizontal stiffeners, designated group G; (b) reinforcement around vent openings, group H; (c) openings for lower deck hangers in the bottom flange, group I; and (d) junctions of deck beams and web plates, group J, as shown in Figures 5-8. A total of 12 details were instrumented by using two-element gages. The gages were located close to the detail. Wiring diagrams for the gages are shown in Figure 9. During most of the testing period, the longitudinal and transverse elements of the three-element gages were wired together to provide a single, temperature-compensated reading. Some readings were also made with all three elements wired separately to determine principal strains. Stress was calculated from these readings by assuming a modulus of elasticity of 29 million psi and Poisson's ratio of 0.3. A correction, usually small, was made in the computed stresses to account for biaxial effects. The longitudinal and transverse elements of the two-element gages were wired together throughout the testing period.

To facilitate the strain measurements, a central recording station was established inside the north tie girder between panel points 14 and 15. Twisted, shielded, 18-gage, 3-conductor wires were used to connect the gages to the recording station.

MEASURED TEMPERATURES

Selected measurements on the tie girders are shown in Figure 10. Review of the data shows that the temperature distribution was uniform before sunrise (at 4:00 a.m.). At sunrise, or approximately 6:00 a.m., the south web and top flange of the south tie girder were exposed to the sun, if the day was clear, and would begin warming. Peak temperatures on both the south web and top flange were reached at about 1:00 p.m.

The north tie girder was shaded by the upper roadway until late afternoon. The peak temperature of the top flange was reached at about 1:00 p.m., whereas the peak temperature of the north web occurred in early evening, at about 6:00 to 8:00 p.m., after it was exposed to the sun.

The maximum temperature measured was 144°F, which occurred on the top flange of the south tie girder on July 16, 1979, when the ambient temperature was 90°F. Surfaces not exposed to the sun were always close to the ambient temperature. The maximum temperature differential between the top flange and side plates of both tie girders was about 50°F.

Figure 4. Location of instrumentation at panel point 14.

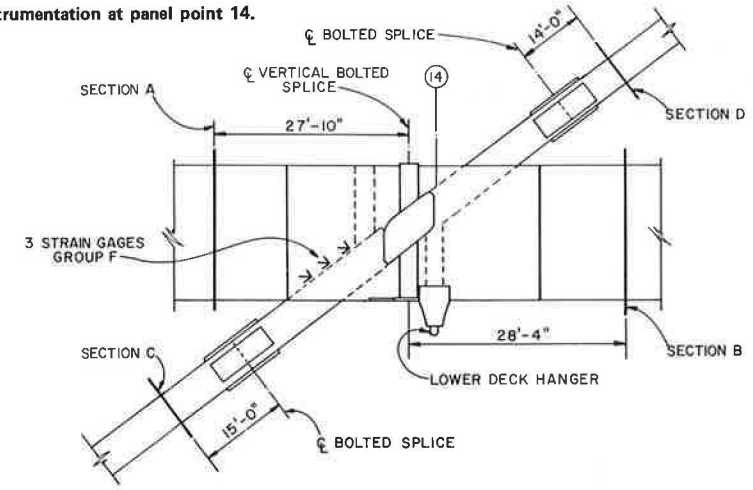

Figure 5. Group G gages at end of horizontal stiffener.

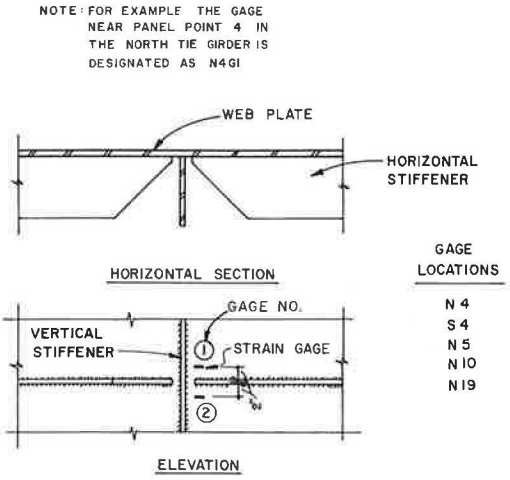

Figure 6. Group H gages at cover plates at vent opening.

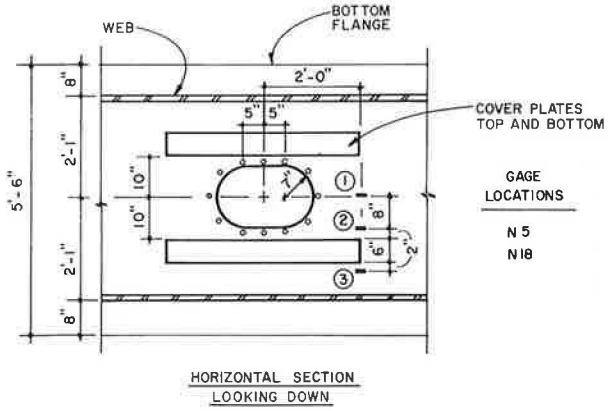

Figure 7. Group I gages at opening in bottom flange.

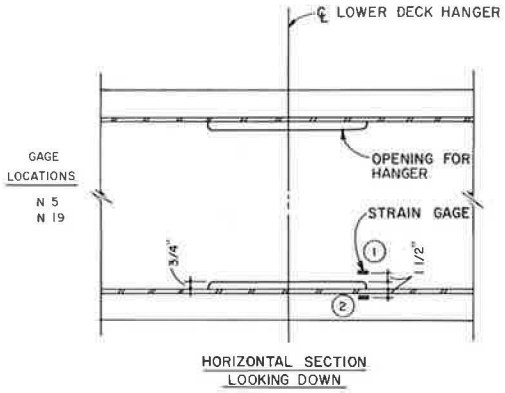

Figure 8. Group J gages at junction of deck beam and web of tie girder.

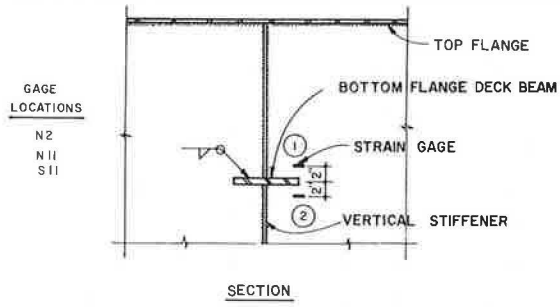

STRESSES UNDER TRAFFIC

Figures 11-15 show the change in stress at selected gage locations near panel point 14, computed from the measured strain during the period from July 12 through July 17. Data from a representative thermocouple are also presented in each figure.

Strain at gages SA1 and SA2 located on the top flange plate at section A in the south tie girder is shown in Figure 11. The temperature was obtained from thermocouple S1 located on the top flange plate at section B in the south tie girder. The abrupt change in temperature at approximately 1:00 p.m. is due to the passing of the shadow of the arch rib over section B. Maximum stress range is about 12 ksi. Note, however, that the shadow of the arch rib does not pass over the gages at section A.

Strain at gage SB2, located on the top flange plate at section B in the south tie girder, is shown in Figure 12. The temperature was obtained from thermocouple S1, which is adjacent to the strain gage. At this location, the strain responds in close relation to temperature. The maximum stress range is approximately 10 ksi.

Strain at gages NA2 and NA5, located on the top

and bottom flange plates, respectively, at section A in the north tie girder, is shown in Figure 13. Thermocouple N1 was located on the top flange plate at section B in the north tie girder. Stress ranges are about 11 and 4 ksi at these two locations.

In Figure 14, the strain at gages NB3 and NB13 is shown. These gages are located on the top and bottom flange, respectively, at section B in the north tie girder. Temperature measurements were obtained from thermocouple N1, which is located adjacent to gage NB3. Stress ranges of 8 and 5 ksi are apparent at the two locations.

Data from strain gages on the tie girder web plates indicate that out-of-plane bending occurs. Figure 15 shows this effect at section B on the

Figure 9. Strain gage wiring diagrams.

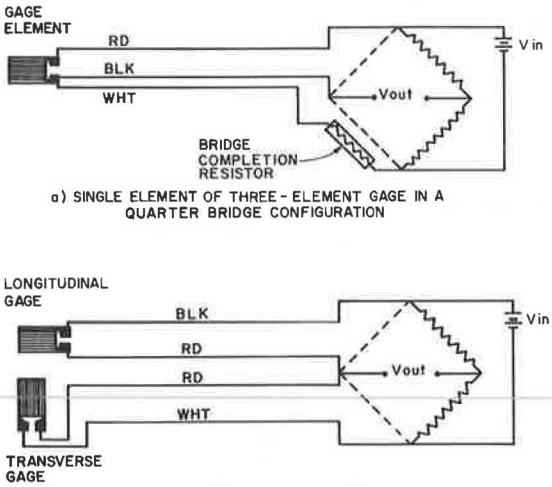

Figure 10. Measured temperatures.

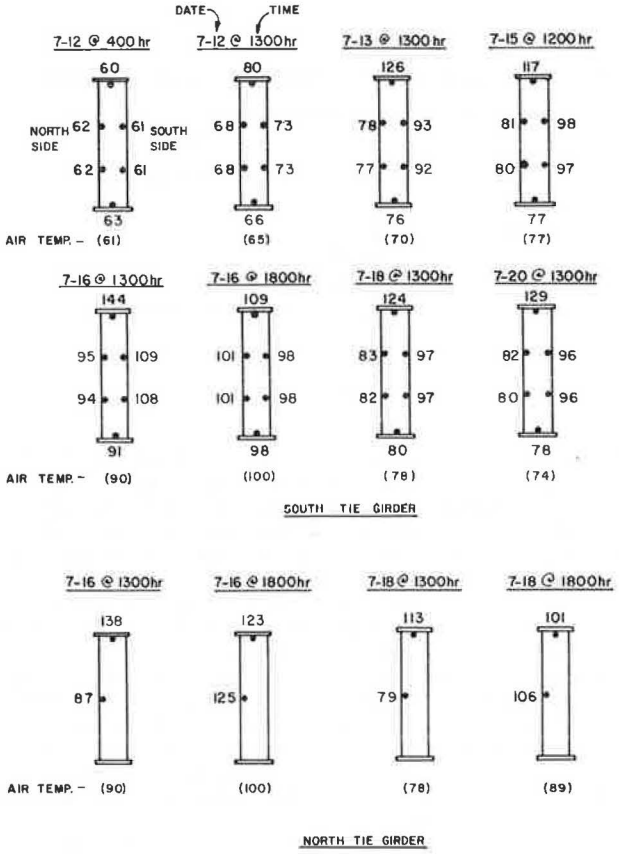

Figure 11. Strain gages SA1 and SA2 and thermocouple S1.

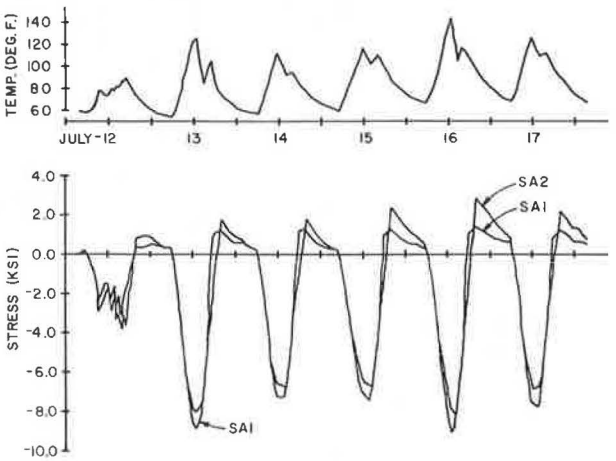

Figure 12. Strain gage SB2 and thermocouple S1.

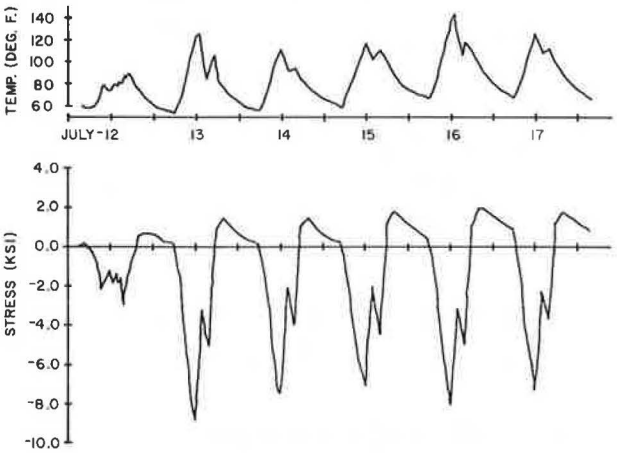

Figure 13. Strain gages NA2 and NA5 and thermocouple N1.

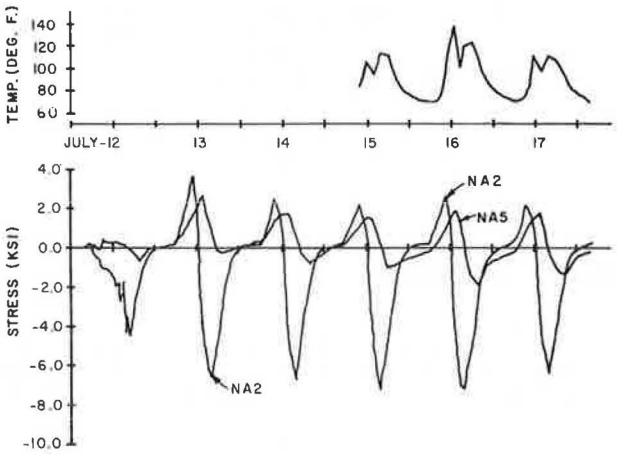

Figure 14. Strain gages NB3 and NB13 and thermocouple N1.

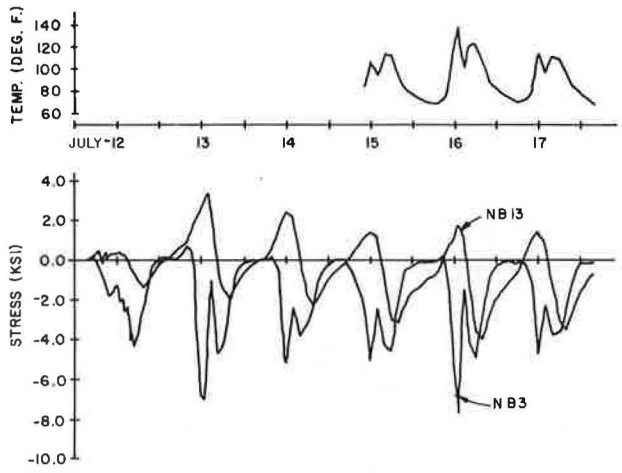

Figure 15. Strain gages NB9 and NB10 and thermocouple N2 and air.

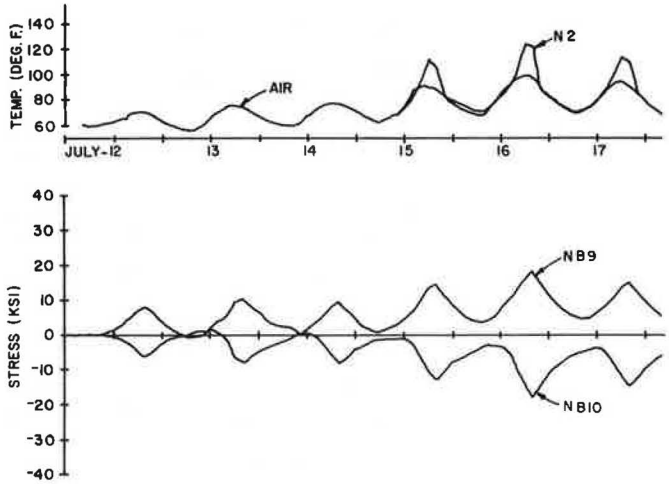

north web of the north tie girder. Longitudinal stresses computed from strains are plotted for gages NB9 and NB10, which are located on opposite sides of the web plate midway between stiffeners. Bowing of the plate apparently occurs daily. The maximum daily stress range is approximately 20 ksi, although the average stress is fairly uniform.

It is evident from these figures that the stress variations are repeatable and closely related to temperature. The heavy traffic periods in the morning and afternoon have little apparent effect.

Readings made on two days with similar temperatures but different traffic conditions were compared. These days were Sunday, July 15, when traffic was light, and Tuesday, July 17, when traffic was normal. The differences indicated that the stress range due to traffic was about 1-2 ksi.

STRESSES UNDER CONTROLLED LOADING

During the field testing, the bridge was subjected to a loading of four vehicles weighing a total of 177 100 lb. This test was conducted early in the morning on July 15 to minimize temperature effects. Both static and dynamic tests were conducted. Traffic was excluded from the bridge.

In the static loading test, the four trucks were positioned side by side in two rows on the upper deck in the two adjacent traffic lanes nearest to the north tie girder. Strain response was measured with the vehicles positioned at selected panel points along the bridge.

Figure 16. Measured strains at gages NB2 and NB4 under controlled loading.

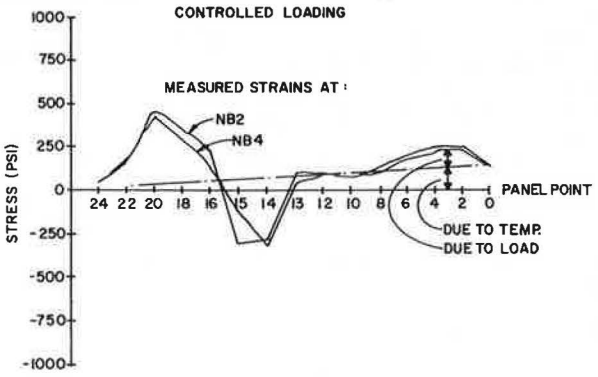

Figure 17. Strain gages NB13 and NB15.

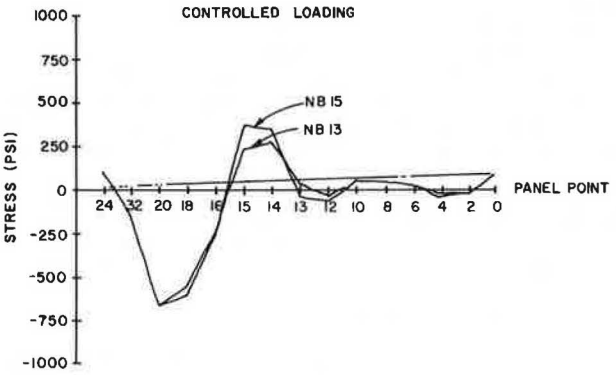

Figures 16 and 17 show computed stresses from strains measured at section B in the north tie girder. The ordinate and abscissa correspond to the longitudinal stress and the location of the vehicles, respectively. Note the departure of the ordinate from the base line at the conclusion of the test. This departure is attributed to the change in ambient temperature during the time period in which the test was conducted, between 6:00 and 7:30 a.m. The measured strains were quite small, corresponding to stresses less than 750 psi.

It may be noted that the strain response is greater when the vehicles are between panel points 14 and 24 than when they are positioned between panel points 14 and 0. This is apparently due to the varying stiffness of the structure. Between panel points 14 and 0 the tie girder is supported at each panel point by a vertical column, whereas between panel points 14 and 24 the tie girder is suspended by cables. When the vehicles were at panel point 10 (vertical column over pier), stress at all sections was essentially zero.

Data were also recorded in analog form by using a nine-channel strip chart recorder. Two groupings of gages were monitored; the first was on selected details, and the second was on gages from section B on the north tie girder.

Data were obtained during run A when the vehicles were parked at each panel point. In the dynamic test, run B, the four trucks were driven in a group across the bridge at approximately 15 mph in the same lanes used for the static tests. Data from gages recorded during the passage of vehicles in run

B are shown in Figure 18. The stress levels in both runs were quite low. The maximum static stress recorded in run A was 2150 psi at gage N19G2; the maximum dynamic stress in run B was 2100 psi at gage N19I2. The dynamic response followed the same general pattern as the static response.

To induce impact loads and provide information on impact factors, 2-in-thick boards were placed across the roadway at panel points 18.5 and 10.5. The output recorded during these runs indicated that the impact excited higher modes of vibration but there was only a slight magnifying effect on the strain readings.

STRESSES AT FATIGUE-SENSITIVE DETAILS

Dynamic recordings of strain under normal traffic were made at the fatigue-sensitive details from July 16 to July 20. The gages were divided into groups, and each was recorded for time periods of 1-4 h. Generally, significant strain response was associated with the passing of a truck. However, the representative stress "signatures" were very small. Typical data are shown in Figure 19. The maximum stress range, at gage N5I1, was 1250 psi. More typical values are 400-900 psi. As mentioned previously, the response for gages at the same detail was similar.

It is also of interest to compare these data with those obtained under the controlled loading shown in Figure 18. In all cases, the stress ranges recorded under the controlled loading were somewhat greater.

STRESS RANGES AND FREQUENCY OF OCCURRENCE

On July 17, dynamic strain recordings were made at four selected details for a period of approximately 2 h, between 10:30 a.m. and 2:30 p.m. From previous recordings, the strains at these details appeared to be larger than at other locations. Data obtained from the eight gages at these four details, during an interval of about 1 min, are shown in Figure 20.

A histogram of the stress computed from strain at one gage from each of the four details was developed from the dynamic recordings. The minimum strain that could be recognized on the recording corresponded to a stress of about 300 psi. In developing the histogram, each peak to valley or valley to peak on the recording in excess of 300 psi was therefore considered to be one-half of a stress cycle. On this basis, the number of stress cycles in 300-psi increments (ignoring cycles below 300 psi) was obtained and plotted in the histograms shown in Figure 21.

An effective Miner's stress range (S_{re}) was computed from the data in these histograms by using the following relation:

$$S_{re} = (\Sigma \gamma_i S^3_{ri})^{1/3} \quad (1)$$

Figure 19. Dynamic strain response under normal traffic.

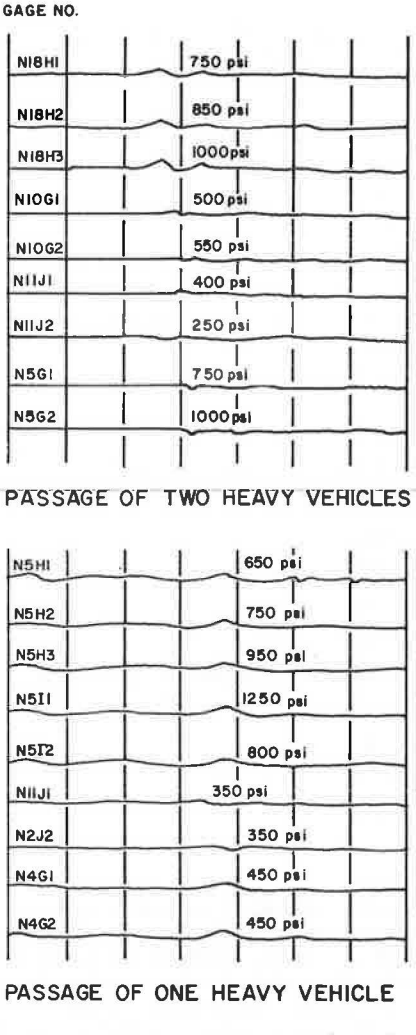

Figure 18. Data from run under moving truck loading.

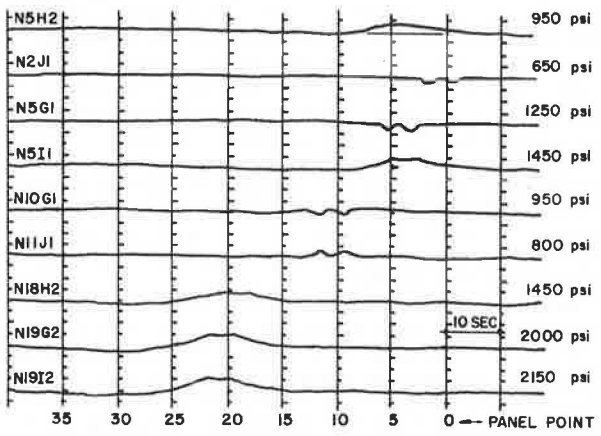

Figure 20. Dynamic strain response at four details on July 17, 1978.

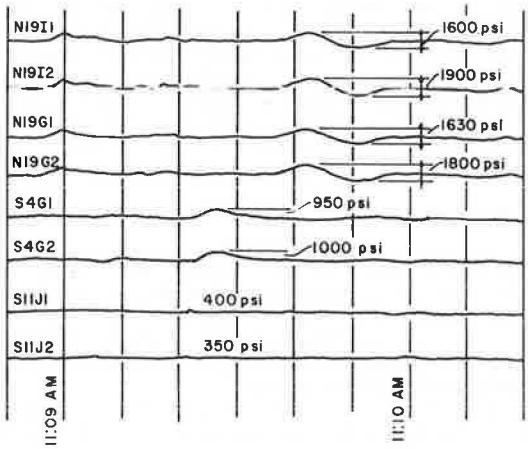

Figure 21. Histograms of stress cycles based on data obtained during 2-h period.

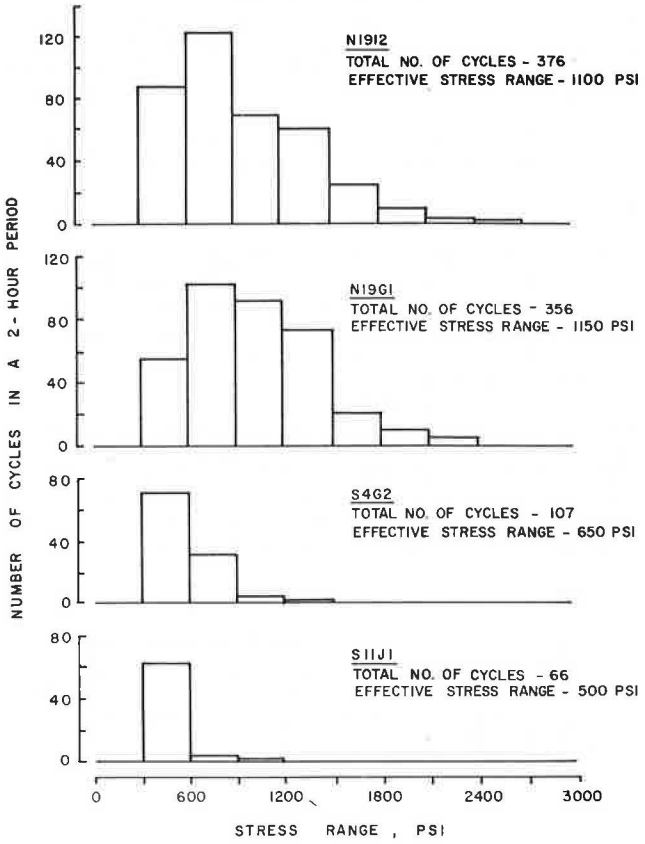

Figure 22. Dynamic strain response of gages during passing of mobile crane.

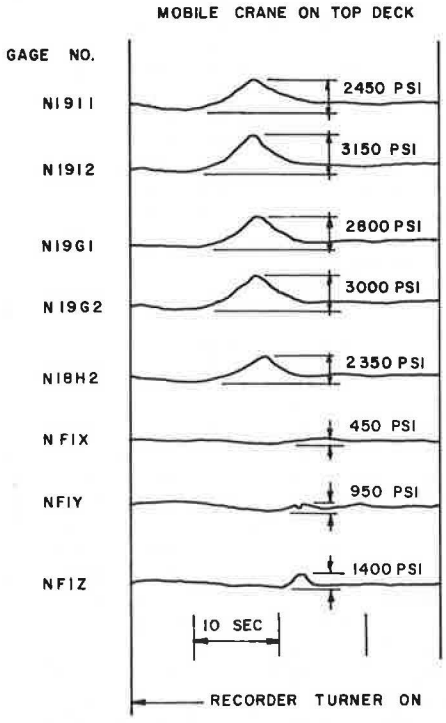

NOTE:
NFIX — ELEMENT PARALLEL TO ARCH RIB
NFIY — ELEMENT AT 45 DEGREES TO ARCH RIB
NFIZ — ELEMENT PERPENDICULAR TO ARCH RIB

where γ_i is the proportion of the total cycles falling within a particular interval i, corresponding to a stress range S_{ri}. The effective stress range for each histogram is shown in Figure 21. During this 2-h period, the maximum strain was observed at gage N19I2 and corresponded to a stress range of about 2550 psi. A total of 376 cycles were measured at this gage. The maximum effective stress range of 1150 psi was obtained at gage N19G1.

COMPARISON OF TRAFFIC WITH DYNAMIC RECORDINGS

Beginning at 2:40 p.m. on July 19, an effort was made to correlate dynamic strain recordings, or signatures, with observation of the traffic. This was found to be very difficult; only occasionally could a signature be associated with a specific vehicle such as a logging truck.

The vehicle that produced the largest recorded stress range was identified as a mobile crane on the top deck. The stress signatures from this load are shown in Figure 22. Except for the magnitude of the response, the signatures are similar to those of other heavy vehicles. It is interesting to compare the signatures for gages N19I2 and N19G2 with the signatures obtained during the controlled loading tests shown in Figure 18. The signatures are similar except that the two rows of vehicles passing in quick succession in the controlled loading test are distinguishable and the stress ranges are somewhat lower.

DISCUSSION OF RESULTS

The field testing indicated that three conditions induced stress variations in the tie girders. Most of the small-amplitude but high-cycle stress variation came from the passage of heavy vehicles. A small stress variation associated with the buildup of traffic was also observed. A large-amplitude stress variation occurred daily with temperature change.

The maximum measured stress range associated with the passage of a heavy vehicle was 3.15 ksi at a hanger slot in the bottom flange of the north tie girder near panel point 19. Most of the measured stress ranges at the instrumented details were less than 1 ksi, although stress ranges up to 2.5 ksi were measured near panel point 19. An effective Miner's stress range of 500-1150 psi was determined from data at each of four locations.

It was estimated that the number of cycles per day would be about eight times the number of cycles shown in Figure 21 for a 2-h period at midday. On this basis, the number of expected daily cycles at gages N19G and N19I is approximately 3000. The number of cycles at other locations is smaller.

Information supplied by OSHD indicated that the annual average daily traffic (ADT) on the bridge in 1978 was 58 775 vehicles. A projection to the year 2000 indicated that the ADT may be 93 400 vehicles. Approximately 9 percent of the vehicles crossing the bridge may be classified as trucks. Assuming that the ADT was 60 000 vehicles during the field testing, the average daily truck traffic (ADTT) should be about 5400 vehicles. Thus, the ADTT is about 1.8 times the rough estimate of 3000 cycles/day from the details near panel point 19. It should also be noted that the maximum stress range recorded at the details near panel point 19 under the controlled four-truck loading was 2.15 ksi, or approximately twice the maximum effective stress range under normal traffic.

The largest stress variations were related to the effects of temperature and particularly to direct exposure to the sun. As the sun passed over the bridge, the exposed surface of the south and then the north tie girder absorbed substantial heat. The maximum measured temperature was 144°F and occurred on the top flange of the south tie girder on July 16, 1979, when the ambient temperature was 90°F. Surfaces not exposed to the sun were always close to the ambient temperature. Temperature differentials of 50°F between the top and bottom flange plates and 20°F between the outside and inside web plates were measured in both tie girders.

The strain measurements indicated that the state of stress in the tie girders in the vicinity of the arch ribs is very complex. Maximum daily stress ranges in the longitudinal direction of the tie girders were about 10 ksi on the hot days. Where local bending occurred in the web plates, the maximum daily stress ranges were about 20 ksi.

Strain readings on two days of similar temperature conditions were compared in an effort to estimate the underlying stress variation due to light and heavy traffic. These days were Sunday, July 15, and Tuesday, July 17. Gages on section NB and strain gage NF1 were selected for the comparison. Readings were compared between 2:00 and 6:00 p.m. Most of the differences in stress are less than 1 ksi at section NB. Stress values obtained from gage NF1 show a change of 2 ksi in the web of the tie girder perpendicular to the arch rib. Therefore, the underlying stress variation due to traffic is believed to be about 1-2 ksi.

Because the density of the traffic may vary even during peak periods, it is thought that the underlying stress variation due to traffic should be considered to occur, at most, 50 times a day. This variation combines with the stress ranges associated with the passage of heavy vehicles.

CONCLUSIONS

Field testing indicated that stress ranges in the tie girders under traffic were generally less than 2 ksi and only infrequently 3 ksi. The number of cycles varied with the location, but it did not exceed the ADTT. However, the temperature of plates exposed to the sun may be as much as 50°F higher than the temperature of plates in the shade, which is always close to the ambient temperature. The nominal stress may change by about 10 ksi as a result of daily thermal effects. Where local bending was present, the daily stress range was about 20 ksi.

ACKNOWLEDGMENT

The field test discussed in this paper was part of a larger study conducted under the overview of a technical committee that included chairman Walter J. Hart and John C. Jenkins of OSHD and Carl Hartbower, Herbert A. Schell, and Frank Sears of the Federal Highway Administration.

Wiss, Janney, Elstner and Associates, Inc. (WJE), was assisted in the study by the following consultants and subcontractors: John W. Fisher of Lehigh University; Ammann and Whitney; Materials Research Laboratory, Inc.; and Testing Engineers, Inc. Other members of the WJE project staff included Boris Bresler, Robert Iding, and Daryl W. Boggs.

REFERENCES

1. J.M. Hanson, M.J. Koob, and B. Bresler. Post-Construction Evaluation Study, Fremont Bridge (Willamette River), I-405-Bridge 2529. Oregon State Highway Division, Salem, Dec. 30, 1981, 181 pp.
2. A. Hedefine and L.G. Silano. Design of the Fremont Bridge. ASCE National Structural Engineering Meeting, Portland, OR, Preprint 1210, April 1970.

Publication of this paper sponsored by Committee on Dynamics and Field Testing of Bridges.

Seismic Design of Curved Box Girders

C.P. HEINS AND I.C. LIN

The seismic response of single and continuous curved steel composite box girder bridges has been predicted by an equivalent structure load method. This method has been developed by computing equivalent structural stiffnesses of the entire bridge for the three displacement directions (x, y, z) and rotation. These stiffnesses are then used to evaluate corresponding natural frequencies (ω_x, ω_y, ω_z, and ω_t) by using a single degree of freedom system. The induced accelerations are then determined from the response spectrum curves. The results of these analyses are then used to develop a series of empirical equations for direct design.

As a result of the 1964 Alaskan earthquake, the 1971 San Fernando earthquake, and, more recently, the 1978 Santa Barbara earthquake (1), bridge structures in the United States have undergone considerable destructive forces. These earthquakes caused bridge professionals to reassess the design techniques that had been applied until that time for seismic design.

A prime force in such modifications has been the California Department of Transportation (Caltrans) and the California-based professional organization, Applied Technology Council (ATC). The present 1977 American Association of State Highway and Transportation Officials (AASHTO) bridge code (2), as related to seismic design, was greatly influenced by the work developed by Caltrans. This code suggests an equivalent static force method for simple structures and, when the structure is complex--as in curved bridges, for example--a computer-based response spectrum or dynamic analysis should be considered.

In the present 1977 AASHTO code, most engineers would use the seismic coefficient method (SCM) because computer-oriented dynamic programs may not be available or are not amenable for direct design. However, the SCM may give erroneous results when used for design under seismic conditions (3), as experienced by Caltrans. Caltrans in fact has used

the response spectrum technique for the design of many structures.

Because of these conditions and experience gained from recent earthquakes, the Federal Highway Administration (FHWA) decided to reassess the 1975 AASHTO code and in 1977 sponsored a research program directed by ATC (4). Part of the work of this council is to prepare a new specification (5). Although this code will be an improvement over past criteria, major areas of research still require investigation. These areas, as suggested recently by delegates attending a workshop conducted by ATC (6), include the following:

1. Conduct of parametric studies for the seismic response of common types of bridges to determine the effects of geometry and constraint on overall seismic response (parameters should include span length, curvature, column height and stiffness, material, etc.),
2. Performance of appropriate dynamic analysis on curved bridges (7,8) and development of a simple procedure for the design of curved bridges,
3. Development of a practical and accurate method to estimate the fundamental period of bridges,
4. Correlation of vibrational characteristics of existing bridges with theory, and
5. Preparation of a summary of dynamic behavior and characteristics.

These areas of research are currently being studied and will encompass curved steel and concrete box girder bridges.

Three techniques can be used in the dynamic analysis of such structures: (a) the response spectrum technique, (b) multimodal method-response spectrum, and (c) multimodal time history analysis. These methods are now being used in this research. The method that was used in the work described in this paper involves a space frame analysis of the general structure, computation of the equivalent natural frequency, and then determination of the equivalent dynamic forces for curved steel composite box girder bridges.

As this paper demonstrates, a comprehensive study of the influence of the various parameters has resulted in a proposed equivalent static load analysis technique. It should be noted that a more comprehensive study is being done that includes time history response and multimodal analysis. These results will then be compared with the results obtained by using the single degree of freedom (SDOF) system and the response spectrum data given here.

THEORY

Computer Model

The general static response of curved bridge structures requires incorporation of the interaction between the bending and torsional forces (7-12). Such interaction can be considered by solving Vlasov equations (12) or by development of the stiffness matrix (13) and appropriate restraint conditions.

The matrix-oriented technique, however, is more versatile in that a three-dimensional model (space frame) can be considered. This then permits modeling of the structure so that the support conditions can represent the physical restraints. In addition, the induced actions can be applied in three directions and thus simulate the various earthquake-induced actions.

Therefore, the study of the induced actions on a structure subjected to earthquakes was confined to the use of a space frame matrix simulation. The basic modeling consists of a series of typical elements attached rigidly together to form a continuous curved box girder bridge.

The basic properties of each beam element consist of I_z, I_y, and K_T. Although warping and distortional properties (I_w, W_n, and W_a) can be computed, they were not considered in this study because it has been shown that, with proper bracing of the box girder, warping and distortional effects are negligible (10).

Therefore, by properly evaluating the stiffness of each beam element and identifying each joint load, the static response of the continuous curved girder can be determined. The static response can then be used to determine the effective earthquake effects by using the response spectrum curves. The general procedure in which this method is used can now be described.

The support restraints to be imposed on the bridge model can be identified as releases in the computer model. Because a space frame model is being used, six releases or restraints must be identified. For the bridge under study, the following was assumed.

Equivalent Dynamic Analysis

The natural frequency response (ω) of an SDOF system can be predicted by the following (14-17):

$$\omega = \sqrt{k/m} \tag{1}$$

where k is the spring constant and m is mass [w/g (total weight of structure/gravity)] or mass moment of inertia.

If the frequency ω of the system, as computed from Equation 1 or some other technique, is reliable, then the corresponding induced vertical acceleration of the mass m created by an earthquake can be predicted by using the response spectrum curves given in Figures 1-3. The accelerations obtained are then used to determine the induced dynamic force:

$$F = m \cdot a_{RS} \tag{2a}$$

where $a_{RS} = \ddot{y}$ = linear acceleration obtained from response spectrum curves (18).

If the system is subjected to angular accelerations $\ddot{\theta}$, then the induced dynamic torque (M) is

$$M = \bar{I}\ddot{\theta}_{RS} \tag{2b}$$

where

$\bar{I}$ = mass moment of inertia = $\int pr^2 dA = \rho_{steel} \int (x^2 + y^2)dA + \rho_{concrete} \int (x^2 + y^2)dA$,
$\ddot{\theta}_{RS}$ = rotational acceleration obtained from the response curve (19), and
ρ = mass per unit area.

This type of procedure has been proposed elsewhere (3-7,18,20-25) and requires a methodology that can accurately determine the natural frequency (ω) of the structure.

Natural Frequency

As indicated by Equation 1, the natural frequency of an SDOF system is given as a function of the spring stiffnesses (k) and the spring mass (m). If the system is a bridge structure, the spring constant can be represented by

$$k = (1/\Delta) \tag{3}$$

where Δ is the induced maximum displacement caused

by a unit load. Therefore, by determining the response of a given box girder bridge when subjected to a unit load, an equivalent spring constant can be obtained. This constant (k) and the total mass of the bridge will then permit evaluation of the natural frequency as given by Equation 1.

In the instance of curved structures, the dynamic action can occur in three principal directions and one primary rotation. The resulting maximum displacement induced by these unit loads will then give the corresponding equivalent stiffnesses (k_x, k_y, k_z, and k_T) as shown in Figure 4. The corresponding natural frequencies can then be determined by applying Equation 1.

Computer Program

A general computer program has been developed (26) that will automatically determine the equivalent spring constant for the three translation directions (k_x, k_y, and k_z) and the one rotation (k_T) of a continuous, constant-radius bridge. Section properties are automatically computed and are used for determination of the stiffness matrix. Dead

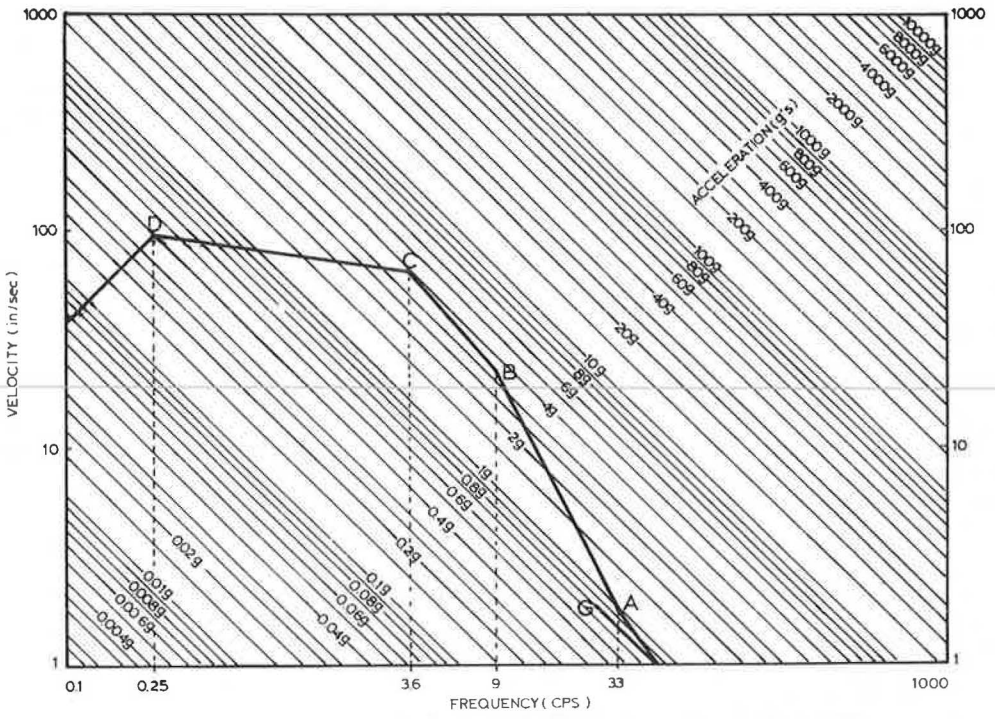

Figure 1. Vertical response spectrum for 1.0-*g* maximum ground acceleration.

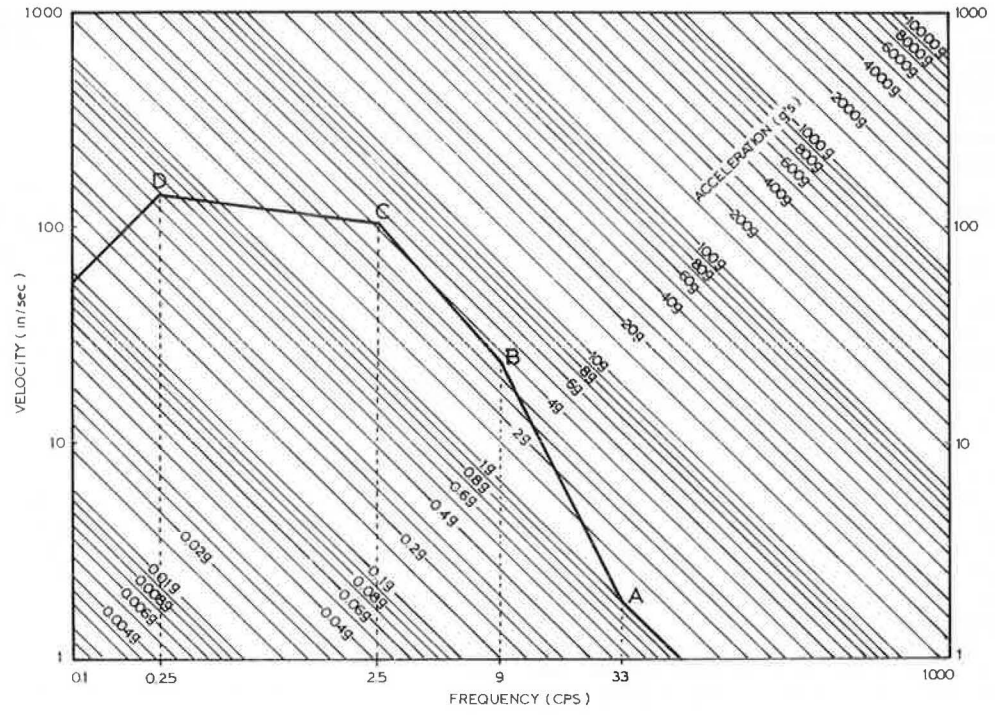

Figure 2. Horizontal response spectrum for 1.0-*g* maximum ground acceleration.

loads and masses are also computed and are used to determine the equivalent dynamic force, as given by Equation 2. This dynamic force is then applied uniformly to the structure, and the resulting deformations and actions are determined.

The response spectra (Figures 1-3) have also been incorporated into the program for direct use. Based on a constant 2 percent damping value for these types of bridges (18,22), the general curves have been written in algebraic form (26).

Figure 3. Torsional response spectrum.

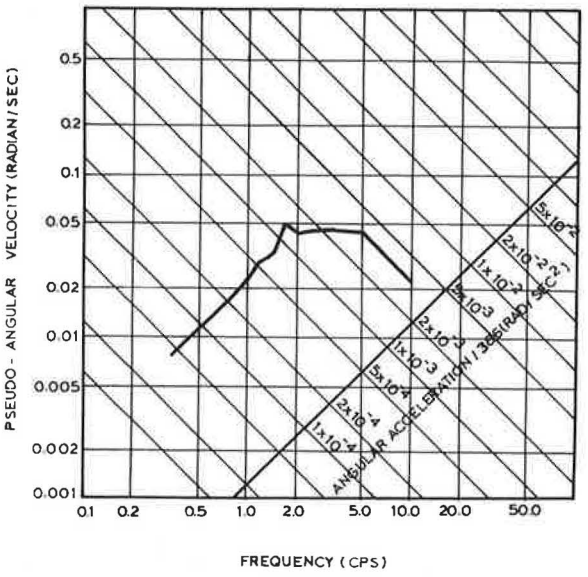

The program will automatically select 11 nodes for each span with 10 members/span between the supports. The proper member properties corresponding to the basic input section lengths are automatically determined. The interior support restraints are assumed to be flexible due to the insertion of springs in the three displacement directions.

BRIDGE STUDIES

Typical Sections

In order to develop a simplified design technique, the response of various curved box girder bridges must be examined. Such box girders, which have been used in previous studies (7), were used in this parametric study. Only the three-lane, three-girder system was considered in this study because this is most typical of curved box girder structures (10).

The basic span length configurations examined are shown in Figure 5, where length (L) = 50-150 ft and N (ratio of span length) = 1.2. The radius used for these various structures varied from 200 ft to infinity.

Column Details

In order to include the influence of the flexibility of the piers, a survey was conducted to determine typical pier configurations and sizes. Such a survey has indicated that for a roadway of 44 ft, with three boxes, a three-column bent is generally used. Such column bents generally have the following details:

Column		Steel Bars	
Type	Size (ft)	Type	No.
Round	$2.5 \leq d \leq 3.0$ (diameter)	#11	12-20
Rectangular	4x12	#8 or #9	30-40

Figure 4. Equivalent structural stiffness.

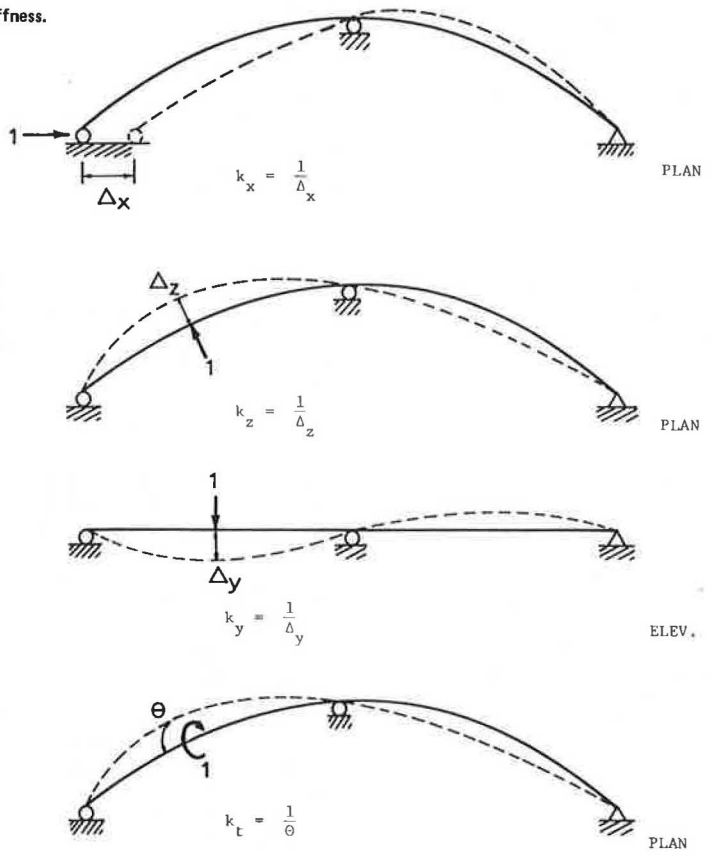

Figure 5. Modeled bridge details.

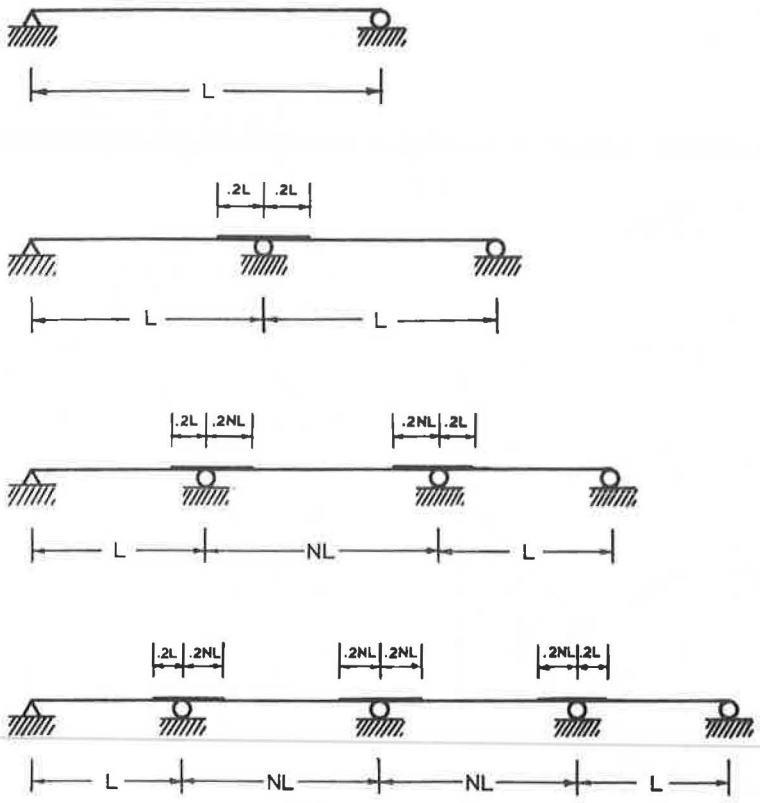

The height of the bents is 10-15 ft, and the spacing between columns is 15-18 ft.

By using this basic information, the section properties (I_x and I_z) of the round and the rectangular column have been computed (26).

These column stiffnesses were used and a three-column bent type was assumed in determining the deformation of the bent caused by a unit load in the transverse and longitudinal directions (with rigid pier caps). The equivalent spring constant was then determined from

$$k_z = (1/\Delta) = [L^3/3E(3I_x)] \quad (4)$$

$$k_x - (1/\Delta) = [L^3/3E(3I_z)] \quad (5)$$

The resulting k_z and k_x values for the column heights of 10 and 15 ft were then determined (26).

With these equivalent pier stiffnesses, the internal piers can then be modeled by using equivalent springs.

General

By using the basic box geometry and the support spring constants of $k_x = 0\text{-}2\text{x}10^3$ kip/in, $k_y = \infty$, and $k_z = 0.5\text{x}10^3$ kip/in to ∞, the equivalent seismic responses of the single-, two-, three-, and four-span structures were examined. The resulting natural frequencies (ω_x, ω_y, ω_z, and ω_t) for all bridge spans and their corresponding induced accelerations were then obtained (26). For the continuous spans, the pier flexibilities, as given by k_x and k_z, were also included as a variable. Three basic variations have been assumed:

1. $k_x = 0$, k_z = rigid;
2. $k_x = 0.66 \times 10^3$ kip/in, $k_z = 0.5 \times 10^3$ kip/in; and
3. $k_x = 2 \times 10^3$ kip/in, $k_z = 0.66 \times 10^3$ kip/in.

The analyses of the various bridges have been performed and have resulted in typical response curves for ω_x, ω_y, ω_z, and ω_t as a function of radius (R) and L. An example of such a response (ω_x) for a two-span structure is shown in Figure 6.

The induced accelerations, as determined from the response spectra, have also been plotted as a function of L/R and L for the single span (26).

However, the corresponding accelerations for the continuous spans and the single span have been plotted in Figure 7 as a function F versus the number of spans, radius, stiffnesses (k_x and k_z), and span lengths, where

$$F_x = A_x \text{ (continuous-span value)}/A_x \text{ (single-span value)} \quad (6)$$

For all span lengths of 50, 100, and 150 ft, similar relations between F_y, F_z, and F_t have been plotted (26). These data were then used to develop appropriate design criteria.

MULTIMODAL SOLUTIONS

To demonstrate the reliability of this simulated dynamic solution, the response of single-span and multispan bridges with rigid and flexible column bents has been examined by using the SAP IV computer program (13). This program idealizes the bridge as a three-dimensional unit and examines dynamic response by using dynamic mass matrix techniques.

Examination of the dynamic response of a three- and four-span continuous curved structure on flexible bents has resulted in the data (ω_x, ω_y, ω_z, and ω_t) given in Table 1. Examination of these data indicates that the comparisons between the resulting frequencies obtained from the space frame structure and SAP IV are reasonable but that only the ω_x and ω_y values are in agreement. It should be noted, however, that the SAP IV solu-

Figure 6. Natural frequency (ω_x) versus radius for two-span bridges.

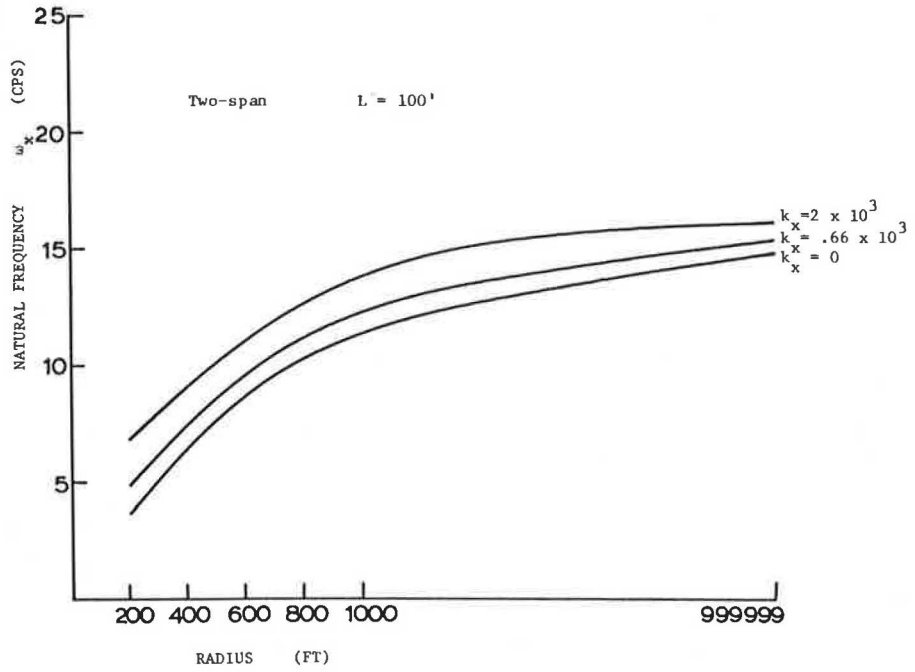

Figure 7. Continuity factor F_x versus number of spans (L = 50 ft).

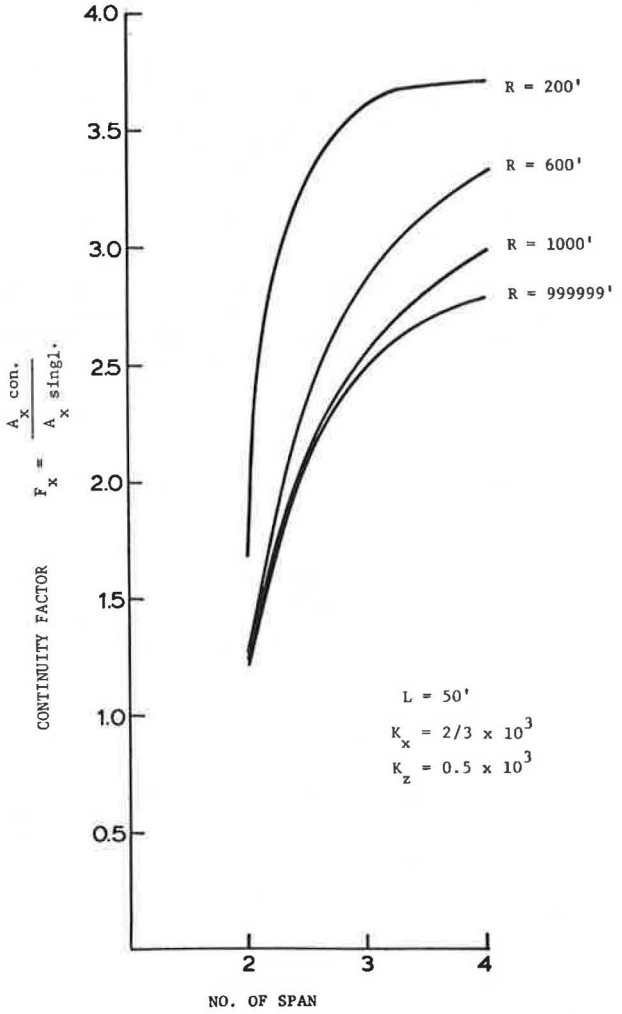

tion does not provide for the angular frequency (ω_t) and, if one compares the ω_t obtained from the space frame structure with ω_z, there is excellent agreement. Therefore, it is reasonable to assume that the space frame structure that gives ω_z and ω_t is a combination of the data given by ω_z obtained from SAP IV.

DESIGN CRITERIA

Trends

The seismic design of continuous curved box girders will be related to the response of single-span curved girders. Therefore, the single-span accelerations (A_x, A_y, A_z, and A_t) were determined with respect to the basic bridge geometry, which yielded the following:

A_x for 100 ft < L ≤ 150 ft = 2.2 $(L/R)^2$ + 0.011L + 0.45 (7)

A_y for L ≥ 100 ft = - 0.016(L) + 4.7 (8)

A_z for L ≥ 100 ft = 3.8 (9)

A_t for L ≥ 100 ft = 1.5 (10)

The continuity factors F have similarly been determined in analytic form. This results in the following four continuity factors:

F_x (longitudinal) = - 0.02(L) + 3.75 + K (11)

where K = 0.00125R for R ≤ 600 ft and K = 1.0 for R > 600 ft.

F_y (vertical) = -0.125(NS) - 0.002L + 1.35 (12)

where NS is the number of spans (2, 3, or 4).

F_z (transverse) = -0.005L + 1.5 (13)

F_t(torsion) = -0.075(NS) + 1.15 (14)

Table 1. SDOF solution (space frame) versus SAP IV.

Type of Structure	ω_x (cycles/s)		ω_y (cycles/s)		ω_z (cycles/s)		Space Frame ω_t (cycles/s)
	Space Frame	SAP IV	Space Frame	SAP IV	Space Frame	SAP IV	
Three span where L = 150, 180, and 150 ft and R = 100 ft	3.682	4.282	1.129	1.823	1.189	4.715	4.506
Four-span where L = 150, 180, 180, and 150 ft and R = 1000 ft	3.5232	3.444	0.966	1.639	1.016	3.950	3.855

Design Approach

The equivalent seismic design of curved box girder bridges will incorporate the primarily developed equations and the effective peak acceleration map (K_p) given by AASHTO (2). The general design equations for translation and rotation, respectively, are of the following form

$$EQ_n = F_n \cdot A_n \cdot m \cdot K_p \quad (15)$$

$$EQ_n = F_n \cdot A_n \cdot \bar{I} \cdot K_p \quad (16)$$

where

EQ_n = total applied seismic force in x, y, z, or t directions;
F_n = continuity factor in x, y, z, or t directions;
A_n = single-span acceleration;
K_p = effective peak acceleration modifying factor (2); and
$\bar{I}$ = rotational mass moment of section = $\rho\int(x^2 + y^2)dA$.

For the specific direction n, the continuity factor F and single-span acceleration A_n are given by Equations 7-14.

SUMMARY AND CONCLUSIONS

The seismic response of single and continuous curved steel composite box girder bridges has been predicted by an equivalent structure load method. This method has been developed by computing equivalent structural stiffnesses of the entire bridge for the three displacement directions (x, y, and z) and rotation. These stiffnesses are then used to evaluate corresponding natural frequencies (ω_x, ω_y, ω_z, and ω_t) by using an SDOF system. The induced accelerations are then determined from the response spectrum curves. The results of these analyses are then used to develop a series of empirical equations for direct design.

ACKNOWLEDGMENT

The work covered in this paper has been supported by a grant from the National Science Foundation. The support, encouragement, and guidance of the National Science Foundation are gratefully acknowledged.

REFERENCES

1. R.K. Miller and S.F. Felszeghy. Engineering Features of the Santa Barbara Earthquake of August 1978. Earthquake Engineering Research Institute, Berkeley, CA, 1978.
2. Standard Specifications for Highway Bridges, 11th ed. AASHTO, Washington, DC, 1973.
3. R.A. Imbsen, R.V. Nutt, and J. Penzien. Evaluation of Analytical Procedures Used in Bridge Seismic Design Practice. Proc., Workshop on Earthquake Resistance of Highway Bridges, Palo Alto, CA, Jan. 29-31, 1979.
4. R.L. Sharpe and R.L. Mayes. Development of the Highway Bridge Seismic Design Criteria for the United States. Proc., Workshop on Earthquake Resistance of Highway Bridges, Palo Alto, CA, Jan. 29-31, 1979.
5. Seismic Design Guidelines for Highway Bridges. Applied Technology Council, Berkeley, CA, ATC-6, Oct. 1981.
6. R.L. Sharpe and R.L. Mayes, eds. Proceedings of Workshop on Earthquake Resistance of Highway Bridges, Palo Alto, California, Jan. 29-31, 1979. Applied Technology Council, Berkeley, CA, 1981.
7. C.P. Heins and M.A. Sahin. Natural Frequency of Curved Box Girder Bridges. Journal of Structural Division, ASCE, Vol. 105, No. ST12, Dec. 1979.
8. C.P. Heins and R.S. Humphreys. Bending and Torsion Interaction of Box Girders. Journal of Structural Division, ASCE, Vol. 105, No. ST5, May 1979.
9. C.H. Yoo and C.P. Heins. Plastic Collapse of Horizontally Curved Bridge Girders. Journal of Structural Division, ASCE, Vol. 98, No. ST4, April 1972.
10. C.P. Heins. Box Girder Design: State of the Art. Engineering Journal, American Institute of Steel Construction, Vol. 15, No. 4, 1978.
11. C.P. Heins and D.A. Firmage. Design of Modern Steel Highway Bridges. Wiley-Interscience, New York, 1979.
12. C.P. Heins. Bending and Torsional Design in Structural Members. Lexington Books, Heath, Lexington, MA, 1975.
13. K. Bathe, E. Wilson, and F. Peterson. SAP IV: A Structural Analysis Program for Static and Dynamic Response of Linear Systems. Department of Civil Engineering, Univ. of California, Berkeley, June 1973.
14. N.M. Newmark and E. Rosenblueth. Fundamentals of Earthquake Engineering. Prentice-Hall, Englewood Cliffs, NJ, 1971.
15. D.J. Dowrick. Earthquake Resistant Design. Wiley, New York, 1977.
16. R.W. Clough and J. Penzien. Dynamics of Structures. McGraw-Hill, New York, 1975.
17. R.L. Wiegel. Earthquake Engineering. Prentice-Hall, Englewood Cliffs, NJ, 1970.
18. R.R. Robinson and others. Structural Analysis and Retrofitting of Existing Highway Bridges Subjected to Strong Motion Seismic Loading. FHWA, May 1975.
19. W.K. Tso and T.-I. Hsu. Torsional Spectrum for Earthquake Motions. Earthquake Engineering and Structural Dynamics, Vol. 6, Oct. 1977.
20. D. Williams and W. Godden. Effectiveness of Existing Bridge Design Methodology in Resisting Earthquakes: Phase IV. FHWA, Rept. FHWA-RD-77-91, June 1976.
21. H.E. Chapman. An Overview of the State of Practice in Earthquake Resistant Design of Bridges in New Zealand. Proc., Workshop on Earthquake Resistance of Highway Bridges, Palo Alto, CA, Jan. 29-31, 1979.
22. R.R. Robinson, A. Longinow, and K.H. Chu.

Seismic Retrofit Measures for Highway Bridges. FHWA, Rept. FHWA-TS-216, Vol. 1, April 1979.
23. T. Iwasaki. Earthquake Resistant Design of Bridges in Japan. Ministry of Construction, Tokyo, Vol. 29, May 1973.
24. M. Ohashi, E. Kuribayashi, T. Iwasaki, and K. Kawashima. An Overview of the State of Practices in Earthquake Resistant Design of Highway Bridges in Japan. Presented at Workshop on Research Needs of Seismic Problems Related to Bridges, San Diego, CA, Jan. 1979.
25. N. Yamadera and Y. Oyema. Special Considerations and Requirements for Seismic Design of Bridges in Japan. Metropolitan Expressway Public Corp., Tokyo, n.d.
26. I.C. Lin. Equivalent Seismic Design of Curved Box Girder Bridges. Department of Civil Engineering, Univ. of Maryland, College Park, M.S. thesis, April 1981.

Publication of this paper sponosred by Committee on Dynamics and Field Testing of Bridges.

Test to Failure of the Hannacroix Creek Bridge

DAVID B. BEAL

A 52-year-old reinforced concrete T-beam bridge was destructively tested to evaluate the consequences of concrete deterioration on load capacity. Instrumentation included measuring tension and compression rebar strain at midspan, end rotation, and midspan deflection. The single- and double-T test specimens were loaded symmetrically to produce a constant-moment region at midspan. The condition of the bridge was rated 2.5 on a scale from 1 (potentially hazardous) to 7 (new condition). The concrete deck was highly fractured throughout and the cement paste severely deteriorated locally. Efflorescence was common and leakage was evident. Tension rebars exposed by spalled concrete had lost 1-2 percent of their cross-sectional area. It is concluded that the deterioration noted has no significance with respect to the load-carrying capacity of the structure. Based on theoretical arguments, it is concluded that deterioration sufficient for substantial reduction in the capacity of a structure would be manifested in a local collapse and that overall failure of reinforced concrete T-beam bridges need not be a concern.

National bridge inspection standards require that highway bridges be inspected and rated for load-carrying capacity. For steel structures, the guidelines are straightforward and they can be rated without difficulty. Reinforced concrete bridges, by contrast, are not easily rated because the significance of deterioration may be unquantifiable. Because of this difficulty, in 1978 New York State initiated a research program to develop a low-cost field testing method for evaluating structural strength. This effort was abandoned when, at the load levels attainable, it was shown that bridges with sound and deteriorated concrete did not differ in behavior (1).

Because service-load tests could not show differences attributable to deterioration, a test to failure of a heavily deteriorated bridge was planned. It was believed that correlation of the results of such a test with the findings of a thorough pretest inspection and evaluation would give some insight into quantification of the effects of observable deterioration.

TEST STRUCTURE

The test structure is a reinforced concrete T-beam bridge constructed in 1930 that carries NY-32 over the Hannacroix Creek in Albany County. It consists of seven beams 39.5 in long and a 36-ft clear span between faces of the abutments. Nominal cross-section dimensions and reinforcement details for an interior beam are shown in Figure 1. In addition, a nonstructural 4-in concrete wearing surface and a 3-in asphalt wearing surface were removed before testing. The flexural reinforcement consists of eight 1.25-in-square deformed bars that provide a nominal cross-section area of 12.5 in² for a reinforcement percentage of 2.25. Compression reinforcement is negligible. In the center 21 ft, 10 in, shear reinforcement spacing exceeds the limits set by current specifications (2, p. 78).

The expansion end bearings consist of steel plates separated by a layer of graphite grease. This detail makes no provision for end rotation. At the "fixed" ends, 0.75-in-diameter rods are embedded in the abutment and end diaphragm. The beam ends and diaphragm rest directly on the abutment, a detail that restrains translation and rotation.

Bridge condition at the time of testing was poor. The most recent inspection report rates the primary members at 2-3 on a scale from 1 (potentially hazardous) to 7 (new condition). Figure 2 shows a photo montage of the underside of the structure that, except for slight transverse parallax, reliably shows its condition. Spalled concrete areas exposing the tension rebars in the beam stems are evident. The exposed rebars are rusted but do not appear to have suffered more than 1-2 percent loss of cross-sectional area. Although it is not visible in Figure 2, the vertical faces of all beams exhibited extensive cracking, generally paralleling their axes. Efflorescence (the white areas in Figure 2) is common and leakage is evident.

Cores drilled through the deck showed it to be highly fractured throughout and that the cement paste was severely deteriorated locally. The disintegration of the 4-in concrete wearing surface may be linked to its relatively high absorption (3). Failure of the structural deck concrete is judged to have resulted from the freezing of water in pores of the cement paste, aggravated by the presence of chlorides in solution. Deterioration of the T-beam stems has resulted from the same causes, plus corrosion of the steel reinforcement. These mechanisms are facilitated by increased permeability, presumed to be related to absorption. Mean absorption of seven core segments taken from the structural deck was 5.6 percent. This value is greater than about 80 percent of values measured in cores from other New York bridge decks. The upper 1 in of structural deck was disintegrated and came off with the concrete wearing surface. Thus, the structure was tested with a 6-in slab (see Figure 3).

Sonic pulse-velocity measurements through the stems of beams 3, 4, and 6 yielded values of 1700-4400 ft/s. Although precise correlation of concrete

Figure 1. Nominal dimensions.

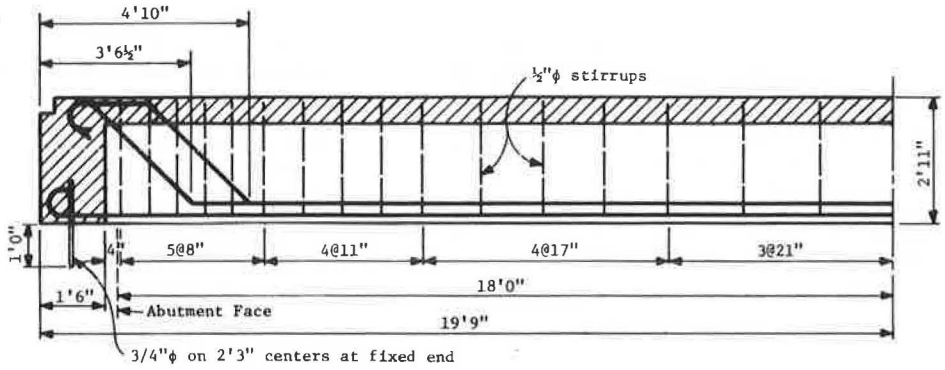

ELEVATION

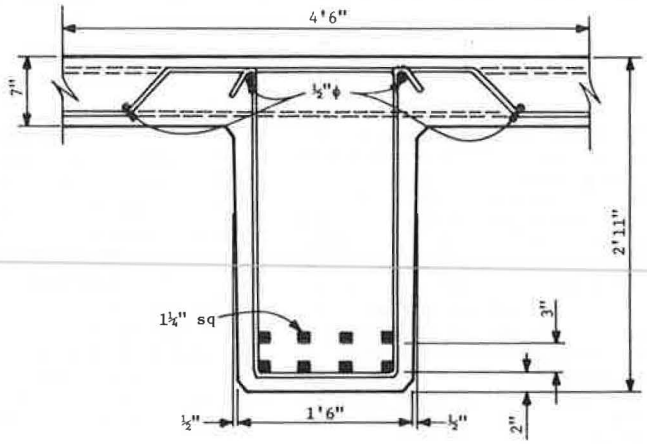

CROSS-SECTION

strength with pulse velocity has been found to be infeasible (1), such low values as these suggest concrete with low compressive strength. For comparison purposes, pulse velocities measured on 62 cylinders with compressive strengths ranging from 2000 to 5000 psi were never less than 12 500 ft/s (1).

Obtaining cores suitable for compression testing was difficult because of the extensive concrete deterioration. The mean of the two tests performed was 4200 psi and the range 1000 psi. Because of the noted disintegration of the deck and the low pulse-velocity values, this result is taken as indicating the unreliability of cylinder tests in predicting concrete strength in deteriorated structures.

Tension tests on 24 samples of the 1.25-in-square bars gave an average yield strength of 44 ksi. A single sample of the 0.5-in-diameter structural deck reinforcement had a yield strength of 46.5 ksi. Average loss of square bar cross section determined on a weight-per-unit-length basis was 2.1 percent from twenty-four 30-in samples and 2.8 percent from twenty-seven 2-in samples. Maximum loss of 6.6 percent occurred in a 2-in length; 3.2 percent loss was the maximum in a 30-in length. Loss was calculated from an assumed nominal area of 1.56 in^2. Although the structural deck steel was not randomly sampled, areas exposed during testing showed no corrosion. The chloride content of the structural deck, determined from drilled samples of concrete powder, was erratic. It averaged only 2.5 lb/yd^3, and the maximum value was 2.8 lb/yd^3. These relatively low values are probably the best explanation of the minor rebar corrosion noted. Chemical analysis of the steel showed no alloying elements expected to increase corrosion resistance.

The structure was designed to carry a live load of 20-ton trucks. With working stresses of 20 000 psi for the grade 40 steel and 1650-psi concrete (3000-psi compressive strength was assumed) (4), the maximum permissible live-load bending moment is 48 percent larger than the design moment due to HS-20 trucks (2). By using a load-factor approach (f_y = 40 000 psi, f'_c = 3000 psi), the inventory rating determined for this structure is 1.76 HS-20 design loads. The operating rating for the bridge is 2.55 or 2.93 HS-20 design loads by working stress or load factor, respectively. None of these calculations accounts for the consequences of the noted deterioration.

With respect to shear, it has been noted that spacing of stirrups in the central portion of the beam is greater than current specifications permit (2). At the supports, however, the provided reinforcement is adequate for 1.32 HS-20 trucks or 1.08 HS-20 trucks for service-load design or load-factor design, respectively.

TEST PROCEDURES

Because of site conditions that prevented detouring of traffic, the structure could not be tested as a single unit. Three separate tests were performed. Two of these were on single-stem units with the associated structural slab, and the third was on a two-stem unit with the associated slab (Figure 3).

Figure 2. Underside of Hannacroix Creek bridge (beam numbers at right).

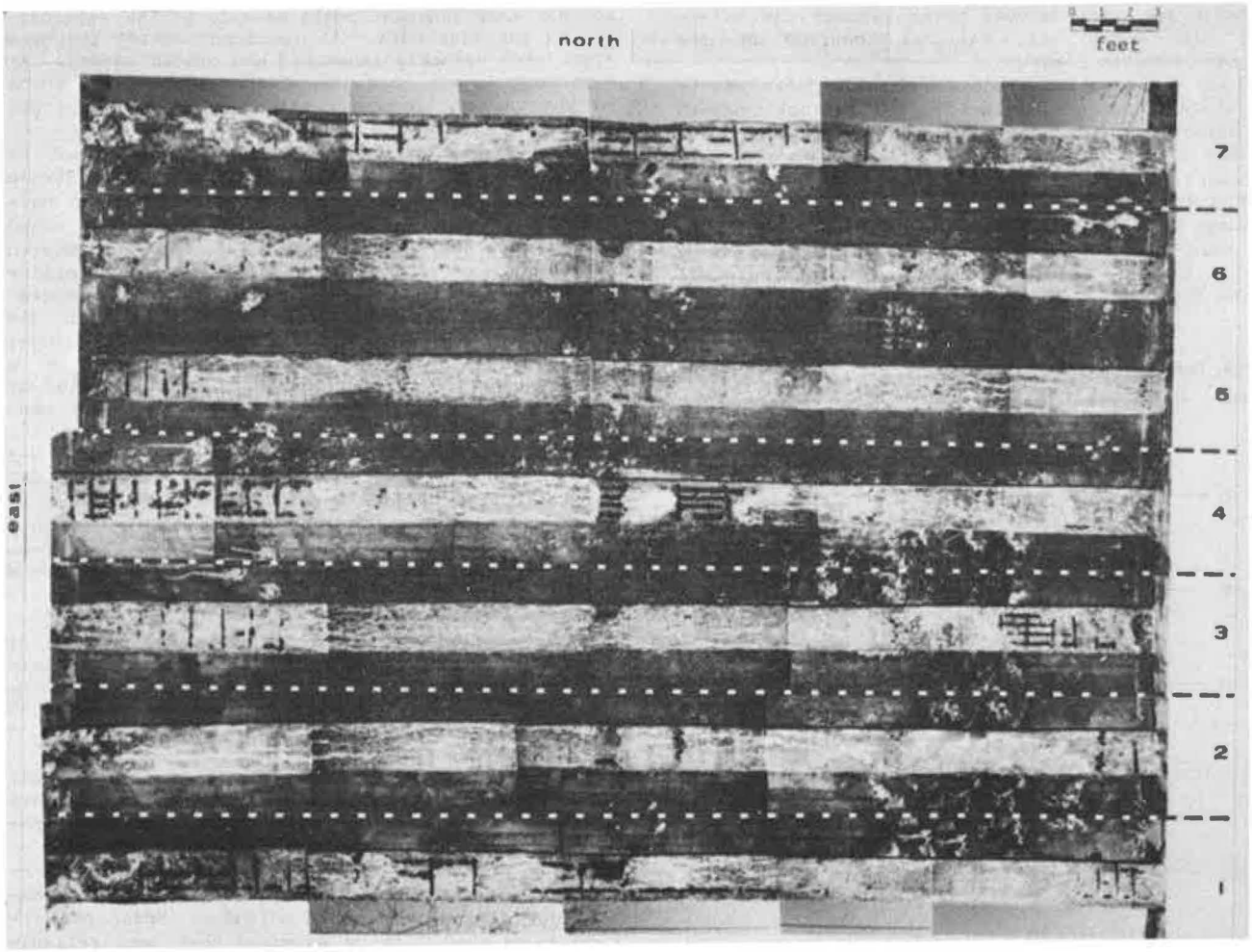

Figure 3. Test specimen details.

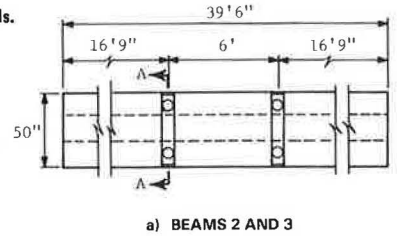

a) BEAMS 2 AND 3

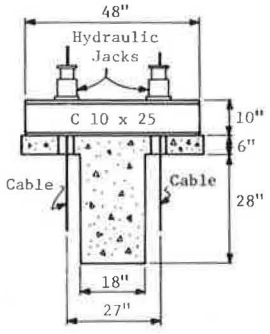

SECTION A-A

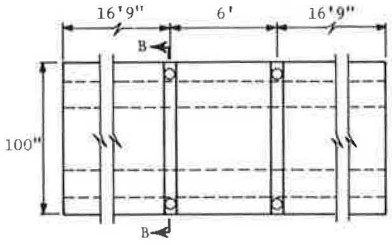

b) BEAMS 5 AND 6

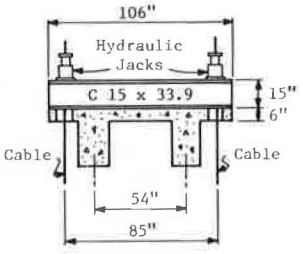

SECTION B-B

Locations of these units in the structure and their condition before testing can be seen in Figure 2. Although the cable access holes reduced the effective slab width, all failures occurred at the midpoint between loads.

Loads were applied through hydraulic jacks reacting against cables embedded in the bedrock beneath the structure. The load positions shown in Figure 3 provide a 6-ft constant-moment region. Loads were increased slowly from one load increment to the next without impact.

Loads were monitored through a pressure gage that had been calibrated with the hydraulic rams in a test machine. A manifold was used to distribute oil to the four rams. The loading scheme consisted of a series of loading-unloading cycles up to failure. This scheme provided partial replication of the test so that some judgment could be made on the reliability of the test data. At low load levels, the beam stems were visually inspected and cracks marked. At high load levels, because of the considerable force in the cables, it was considered imprudent to get close to the beams.

Instrumentation was provided for measurement of strain, displacement, and end rotation. Strain gages were bonded to each of the four tension bars in the bottom row (Figure 1) and to a 0.5-in round compression bar in the slab. Two sections located symmetrically 1 ft on either side of the centerline were instrumented. The 0.25-in-long, self-temperature-compensating gages had a resistance of 350 Ω. They provided one arm of a Wheatstone bridge, completed at the instrumentation located in a trailer near the test structure. Leads consisted of 250-ft-long, four-conductor no. 22 wire with conductors paired under separate foil shields.

Displacements were measured with a Wilde N-3 level capable of measurements to the nearest 0.001 in. Calibrated targets were placed on the bridge at the supports and at midspan. In addition, targets were placed symmetrically at points 6 and 12 ft from the supports. These latter targets were monitored at selected loads only. A fixed benchmark was positioned off the structure.

End rotation was monitored from measurement of the relative displacement of two points on a rigid bar attached to the girder ends with respect to the abutment face. The rotation measurement caused much difficulty, and the theoretical accuracy of 3×10^{-6} rad was not achieved.

The accuracy of field measurements is difficult to determine because of general inability to perform replicates. The assumed precisions of $10 \mu\varepsilon$ for strain, 0.01 in for deflection, and 0.0001 rad for rotation are based on experience with similar measurements and examination of the internal consistency of the data obtained here. Under no circumstances should it be expected that more reliable values have been obtained.

Figure 4. Tension strain versus load for all beams.

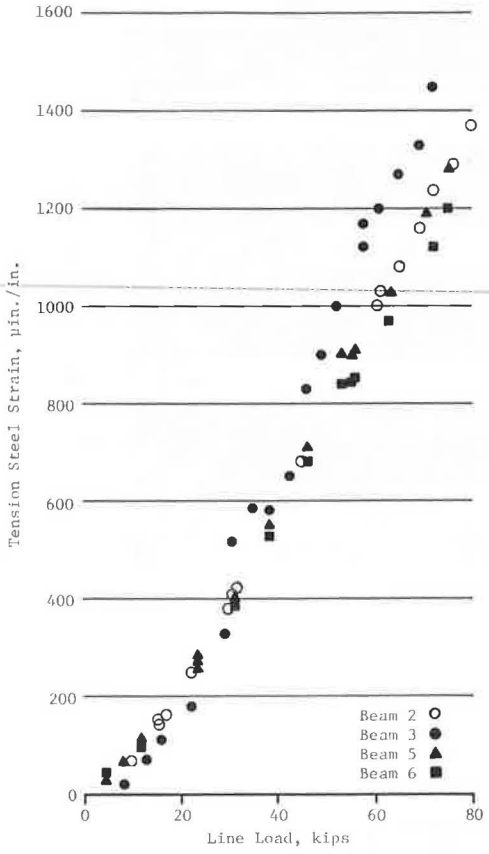

TEST RESULTS AND DISCUSSION

Analysis of the rebar strain measurements showed no trends with respect to longitudinal or transverse position of the bar in a beam cross section. Thus, despite the physical difference between rotational restraint capabilities of the fixed and expansion ends (Figure 1), the raw strain data were insufficient to demonstrate a difference. Except at high strains, the average of all eight bars was taken as

Figure 5. Load versus deflection for all beams.

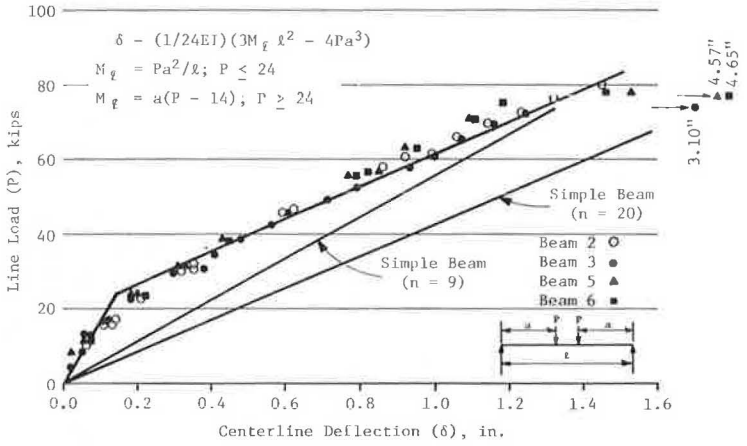

the best estimate of rebar strain. Additional details of the data analysis procedures can be found in the full report (11).

Figure 4 gives tension strain versus load for all beams. Only strains at peak loads are plotted. Data from loading-unloading cycles have been deleted for clarity. Despite variation in the magnitude of residual strains, it should be noted that the four beams behaved in a similar manner and that the relation between load and tension strain is largely linear. Extreme values are represented by beams 3 and 6, beam 3 giving the largest strain values.

Figure 5 presents a composite drawing that shows load versus centerline deflection for peak loads only. This relation is also similar to that shown for tension strains and indicates linear behavior for loads greater than 20 kips and less than 80 kips. In addition, differences between beams are less than for tension strains, an expected result since deflection represents an averaging of strain along that full length of the beam.

Load versus end rotation is shown in Figure 6. This measurement proved to be unreliable. Data were lost at the fixed end of beam 2 and the expansion end of beams 5 and 6. Some insight into the behavior of the structure can be gained, however, from the data obtained. First, it should be noted that rotations were zero in all cases for loads less than about 18 kips. For beam 3, the load needed to cause first rotation was substantially larger. Once rotation occurred, however, the relation between load and end rotation was largely linear. These data imply that both ends of the beam were supplying some moment restraint. The differing slopes of the lines for beams 3 and 2 indicate that beam 3 is slightly more flexible than beam 2 after release occurs. The flexibility for both ends of beam 3 is approximately equal, although the release load is larger at the fixed end of this beam.

Centerline bending moments for peak loads are plotted versus line load in Figure 7. The values for beams 2, 5, and 6 define a bilinear relation. Because the rotation measurements showed zero rotation or moment fixity at low loads and the strain data indicated a constant value of flexural stiffness (11), the first portion of a bilinear load versus moment relation is taken as that for a fixed-ended beam. This relation satisfactorily fits the data for moments less than 2000 kip-in. For comparison purposes, a line representing the simple-beam relation is also shown and clearly does not fit the data. The plotted relation was calculated for a span length of 37 ft.

The upper linear portion of the moment-load relation is taken with a slope equal to the shear span (a in Figure 7), the simple-beam value. Again, this

Figure 6. Load versus end rotation.

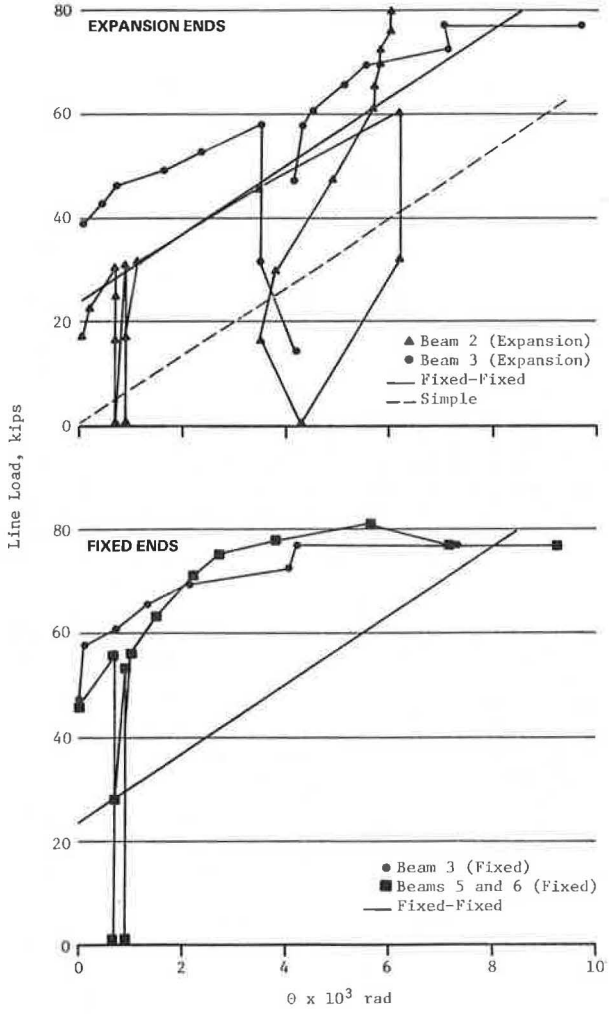

Figure 7. Load versus bending moment.

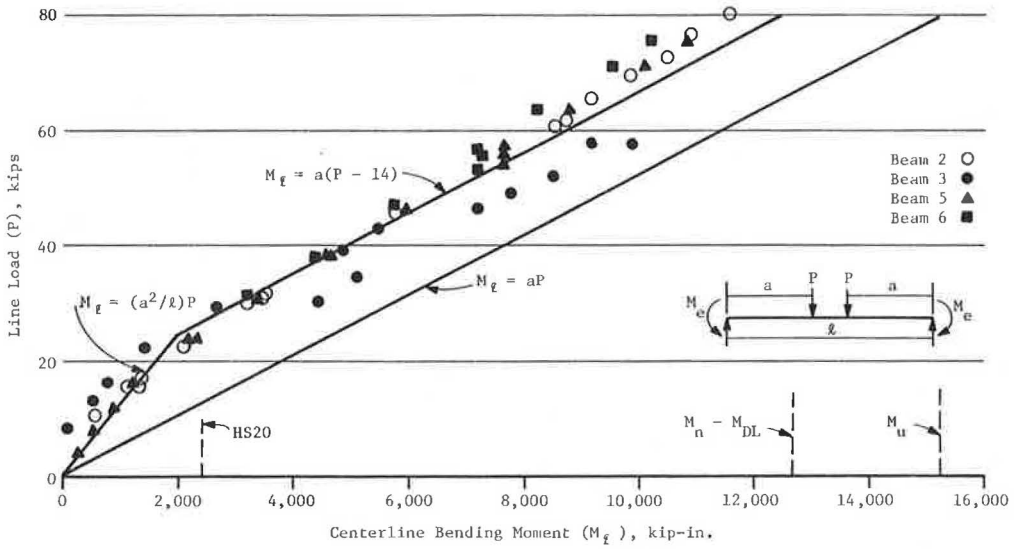

Figure 8. Influence of concrete strength on bending resistance.

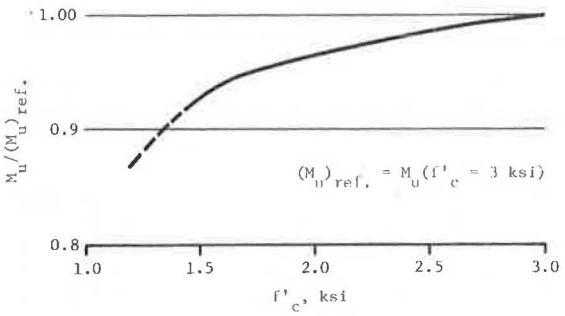

is suggested by the rotation data, which indicate a constant value of end restraint after release. The intersection point for the two linear segments was selected by fitting the "best line" with the simple-beam slope.

By using similar reasoning, a relation between bilinear load and centerline displacement was derived (Figure 5). The flexural stiffness is taken as 150×10^6 kip-in^2, as found from the strain data (11). Comparisons between calculated and measured deflections are good. Of particular note is the correspondence between the theoretical relation and beam 3 data. This result suggests that the beam 3 strain data are defective.

The slope of the relation between load and end rotation implied by the centerline moment analysis compares reasonably well with the experimental results (Figure 6). Except for the beam 2 expansion end, however, the 24-kip end-restraint release load is substantially less than the experimental value.

It is important to emphasize that no part of the preceding analysis is of particular significance with respect to the general load-rating problem. The analysis was performed to demonstrate the consistency (or lack of consistency) between the various forms of collected data and to permit estimation of the elastic modulus. From the results presented, it can be concluded that the measured values reliably represent the true behavior of the test specimens.

The only unexplained aspect of beam behavior is the end restraint indicated by all three measurements. The break point of the bilinear moment-load relation implies a maximum end moment of 2520 kip-in. It is difficult to believe that this magnitude of moment could be developed at the expansion end of the beams. Even at the fixed end with the 0.75-in-diameter dowels, the level of moment is unrealistically large. The ultimate moment of this detail (taking account of the moment enhancement due to the beam reaction) is only 660 kip-in. Nevertheless, the existence of large-magnitude end moments cannot be disputed in view of the measurements obtained.

The large difference between the modular ratio found here and the values used in design should be placed in perspective. First, the consequence of varying the modular ratio from 20 to 9 [a nominal value often assumed in design (2)] is to increase the ratio of bending moment to rebar strain by only 5 percent. Because of this small variation, it should be clear that the analysis used to obtain the experimental value is extremely sensitive to small variations in measured strain. Thus, the reported value of 20 cannot be claimed to be exact. Second, the variation in flexural stiffness over the same range is 30 percent, and this magnitude could easily be detected in the data. Comparison of measured and calculated deflections (Figure 5) demonstrates that the correct stiffness is predicted well by the modular ratio of 20 and suggests that this value is more representative of the actual stiffness of the structure than the nominal value of 9. Third, it is wrong to calculate a cylinder strength by using the modular ratio and the empirical relation devised by Pauw (7), since the inverse of this equation is not a "best fit". Thus, the only significance of the value of 20 is as a measure of stiffness and not of strength.

APPLICATION TO LOAD RATING

It is not possible or prudent to extrapolate the findings from a single test to a general set of load-rating rules. It would clearly be inappropriate, for example, to propose that a certain level of end-moment restraint be assumed for all structures because of its existence in this structure. The same is true with respect to the findings on rebar yield strength. In addition, the data obtained are for overall collapse and cannot be used to predict local failures. What, then, can be taken from the present tests and applied to the load-rating problem?

The data available can be used to estimate the reduction in load capacity, if any, from capacities predicted analytically. Unfortunately, the centerline moment at failure is unknown, but it must lie between the boundaries defined by the bilinear relation shown in Figure 7 and the relation for a simple beam. These relations establish limits for the failure moment of 1010 and 1230 kip-ft. Alternatively, the largest moment derived from the data was at the limits of elastic behavior. For this section, the theoretical ratio of maximum elastic moment to ultimate moment is 0.86. Using this value and the maximum experimental moment of 960 kip-ft gives an estimated failure moment of 1140 kip-ft (11). This value is at about the midpoint of the range defined earlier.

The theoretical failure moment determined by using actual steel yield and cross-section dimensions and accounting for the dead-load moment is 1120 kip-ft. Thus, the theoretical failure moment is at the midpoint of the possible range of actual failure moments. Because of this result, it is concluded that no evidence exists to suggest that moment resistance of the section has been decreased by either apparent concrete deterioration, loss of rebar cross section, or loss of rebar cover.

This conclusion, which is specific for the structure tested, can be generalized to apply to the complete family of concrete T-beam bridges. This is possible because the conclusion drawn from this test can be shown analytically. For example, the variation in ultimate moment resistance as a function of concrete strength is shown for the test bridge in Figure 8. Nominal section dimensions and 44-ksi yield-point reinforcement have been assumed in these calculations. From this figure, it can be seen that a 50 percent reduction in concrete strength (from 3 to 1.5 ksi) results in only a 7.5 percent reduction in ultimate bending resistance. It is assumed that local failures would occur for strengths less than 1500 psi, and thus this value is taken as a practical lower limit for rating. A similar analysis shows that a 50 percent loss of slab thickness decreases the flexural capacity of the beam by only 12 percent. It should be noted that the ability of the slab to support wheel loads would be severely reduced with a thickness loss of this magnitude and that deck failure would occur before beam failure (8).

The relation between flexural strength and tension reinforcement area is nearly linear. In practice, however, large losses in rebar area are unlikely. In this structure, the tension reinforcement is distributed in two layers and only the

exposed lower layer had any loss. Nevertheless, it may be prudent to require that inspectors record a visual estimate of cross-section loss. It is not unreasonable to assume that beams with cover intact have experienced no important loss of tension reinforcement area.

In general, it is not possible to evaluate shear capacity directly by means other than failure testing. The beams tested in this work did not fail in shear despite being subjected to loads three times larger than the maximum design value over all but the center 6 ft of the span. The shear cracks, which opened just outside the center region of zero shear (constant moment), are a consequence of the wide stirrup spacing near the centerline of this bridge. At this location the applied shear was 10 times larger than the design value, which suggests that this wide spacing is not a critical defect. In addition, the lack of bond failure is taken as evidence that loss of rebar cover is not detrimental to strength. It has been shown by others (9) that loss of cover alone has little short-term effect on the behavior and strength of reinforced concrete beams.

The test beam failed by crushing of the concrete, an apparent consequence of reduced compressive strength. This crushing failure reduced beam ductility as measured by ultimate deflection. The theoretical ultimate deflection was estimated at about 12 in (10), but the actual values ranged from 3.1 to 4.6 in. Although the actual deflections at failure are substantially less than the theoretical values, they are roughly three times larger than the elastic values predicted by the first equation in Figure 5. In addition, the lower rebars yielded before failure. Thus, the apparent loss of ductility does not compromise the load rating of the structure.

Based on the conclusion that normal forms of deterioration are not severely detrimental to the load capacity of reinforced concrete T-beam bridges, the following load-rating strategy can be used:

1. Assemble as nearly complete a set of standard sheets as possible.
2. Demonstrate that existing bridges for which no plans are available are from the standard sheets. This can be done by means of a random survey of such bridges where a set of key measurements is made. For New York State standard sheets, for example, the clear span, stem depth, and girder spacing uniquely identify the structure. Bridges with combinations of these values that are inconsistent with the standard sheets cannot be rated by this technique.
3. Analyze standard bridges for load-carrying capacity. Reduction factors can be devised for estimated losses of concrete strength, structural deck thickness, and rebar cross sections if feasible inspection procedures can be derived. Alternatively, assuming 2000-psi concrete in analysis will reduce the possible strength reduction to less than 4 percent, a tolerable value, and the minor consequences of other forms of loss can be ignored. Inspectors should be alerted to note large areas of rusted reinforcement and to estimate the area loss. In these instances, individual calculations are required. It is likely that shear capacity may control the rating in many cases, especially for short bridges such as the one tested.

CONCLUSIONS

The structure tested showed no reductions from nominal load capacity despite its apparently heavily deteriorated condition. The unexpected compression failure occurred after rebar yield and at sufficiently large displacements to give ample warning of impending collapse. It has been demonstrated that the insensitivity of the test structure to deterioration is predictable analytically. It is concluded that deterioration sufficient for substantial reduction of the capacity of the structure would be manifested in a local collapse and that overall failure need not be a concern. Finally, a strategy for load rating is outlined that is founded on the conclusions drawn in this paper and the belief that older structures were constructed with care that reliably duplicated the design.

ACKNOWLEDGMENT

Robert J. Kissane assisted in planning the testing described in this paper and was responsible for supervising the field work. Edward W. Bikowitz, Everett W. Dillon, Frank P. Pezze, and Scott P. Ross installed instrumentation and assisted in monitoring the structural response to load. This research was conducted in cooperation with the Federal Highway Administration, U.S. Department of Transportation.

REFERENCES

1. R.J. Kissane, D.B. Beal, and J.A. Sanford. Load Rating of Short-Span Highway Bridges. Engineering Research and Development Bureau, New York State Department of Transportation, Albany, Res. Rept. 79, May 1980.
2. Standard Specification for Highway Bridges: Section 1.5.10(C)--Spacing Limits for Shear Reinforcement. Structures Design and Construction Subdivision, New York State Department of Transportation, Albany, Jan. 1982.
3. D.B. Beal and W.P. Chamberlin. Effects of Concrete Deterioration on Bridge Response. TRB, Transportation Research Record 853, 1982, pp. 43-48.
4. Manual for Maintenance Inspection of Bridges. AASHTO, Washington, DC, 1974.
5. N.L. Johnson and F.C. Leone. Statistics and Experimental Design. Wiley, New York, 1964, Vol. 1, pp. 242-244.
6. E. Hognestad, N.W. Hanson, and D. McHenry. Concrete Stress Distribution in Ultimate Strength Design. Journal of the American Concrete Institute, Dec. 1955, pp. 455-480.
7. A. Pauw. Static Modulus of Elasticity of Concrete as Affected by Density. Journal of the American Concrete Institute, Dec. 1960, pp. 679-687.
8. D.B. Beal. Strength of Concrete Bridge Decks. Engineering Research and Development Bureau, New York State Department of Transportation, Albany, Res. Rept. 89, July 1981.
9. I. Minkarah and B.L. Ringo. Behavior and Repair of Deterioration Reinforced Concrete Beams. TRB, Transportation Research Record 821, 1981, pp. 73-79.
10. H.A. Sawyer. Design of Concrete Frames for Two Failure Stages. In Flexural Mechanics of Reinforced Concrete, Proc., International Symposium, Miami, FL, 1964, ASCE, New York, Publ. 1965-50, 1965, pp. 405-437.
11. D.B. Beal. Destructive Testing of a Reinforced-Concrete T-Beam Bridge. Engineering Research and Development Bureau, New York State Department of Transportation, Albany, Res. Rept. 100, Dec. 1982.

Publication of this paper sponsored by Committee on Dynamics and Field Testing of Bridges.

Load Factor Design Applied to Truss Members in Design of Greater New Orleans Bridge No. 2

JOHN M. KULICKI

The application of load factor design principles to the design of truss bridges is illustrated. The recommendations presented were developed during preliminary design of Greater New Orleans Bridge No. 2 and were applied during final design. Significant savings in construction cost resulted. A specification format version of these recommendations is currently before the American Association of State Highways and Transportation Officials Subcommittee on Bridges and Structures for possible adoption as a "guide specification".

The following general description of the load factor design (LFD) method as it applies to beam and girder bridges of moderate span is taken from the Highway Structures Design Handbook of U.S. Steel Corporation (1):

> Members designed by the Load Factor method are proportioned for multiples of the design loads. They are required to meet certain criteria for three theoretical load levels: 1) Maximum Design Load, 2) Overload, and 3) Service Load. The Maximum Design Load and Overload requirements are based on multiples of the service loads with certain other coefficients necessary to ensure the required capabilities of the structure. Service loads are defined as the same loads as used in working stress design.
>
> The Maximum Design Load criteria ensures the structure's capability of withstanding a few passages of exceptionally heavy vehicles (simultaneously in more than one lane), in times of extreme emergency, that may induce significant permanent deformations without failure.
>
> The Overload criteria ensures control of permanent deformations in a member, caused by occasional overweight vehicles equal to 5/3 the design live and impact loads (simultaneously in more than one lane), that would be objectionable to riding quality of the structure.
>
> The Service Load criteria ensures that the live load deflection and fatigue life (for assumed fatigue loading) of a member are controlled within acceptable limits.
>
> Moments, shears and other forces are determined by assuming elastic behavior of the structure, except for a continuous beam of compact section where negative moments over supports, determined by elastic analysis, may be reduced by a maximum of 10%. This reduction, however, must be accompanied by an increase in the maximum positive moment equal to the average decrease of the negative moments in the span.
>
> The moments, shears or forces to be sustained by a stress-carrying steel member are computed from the following formulas for the three loading levels. For Group I Loading:
>
> Service Load: D+(L+I)
>
> Overload: D+5/3(L+I)
>
> Maximum Design Load: 1.30 [D+5/3(L+I)]
>
> where: D = Dead Load
> L = Live Load
> I = Impact Load
>
> The factor 1.30 is included to compensate for uncertainties in strength, theory, loading, analysis, material properties and dimensions. The factor 5/3 is incorporated to allow for overloads.

The feature that most distinguishes LFD from service load design is the use of different multipliers on the dead and live loadings. Structural members designed by LFD will have a more uniform capacity for live load (in terms of multiples of live loads) than the same members designed by the service load method. The same is true of structures of various span lengths.

Section 1.2.22 of the American Association of State Highway and Transportation Officials (AASHTO) bridge specifications (2) states that "when long span structures are being designed by load factor design, the 'multipliers' should be increased if in the engineer's judgment, anticipated loads, service conditions or materials of construction are different than anticipated by the specification." In the case of long-span structures, for most elements of the structure the ratio of dead load to total load is greater than it is in moderate-length structures. Furthermore, the current AASHTO specifications do not fully treat the evaluation of truss member capacity. Therefore, design criteria that deal with proposed load factors and methods of computing member capacities are required before truss design by LFD can proceed.

SELECTION OF LOAD FACTORS

The formula for Group I "multipliers", or "load factors", given above for bending problems {maximum design load = 1.3 [D + 5/3(L + I)]} is shown as curve A in Figure 1, which relates factor of safety for bending and tension members to the percentage of total load--either dead load (upper scale) or live load plus impact (lower scale). The conventional factor of safety against first yield in the service load method is 1.82, and this is shown as curve B. It has not been uncommon in long-span bridge design to allow 10 percent overstress in members that carry mostly dead load. This corresponds to a factor of safety of 1.65. The transition to 10 percent allowable overstress often used by Modjeski and Masters occurs when the dead load is more than 75 percent of the total load. This is shown as curve C. The Group I load factors proposed here were developed by starting with a line that would intercept (a) the point corresponding to a factor of safety of 1.65 at 75 percent dead load and (b) the point at which the AASHTO service load and LFD methods have the same factor of safety--i.e., 40 percent dead load. With some rounding off, the proposed load factors result in

$$\text{Maximum design load} = 1.5\,[D + 4/3\,(L + I)] \leq \text{capacity} \quad (1)$$

The corresponding overload provision is

$$\text{Overload} = D + 4/3\,(L + I) \leq 80 \text{ percent of first yield capacity} \quad (2)$$

Comparison of the maximum design load and overload provisions shows that the overload provision does not control.

Figure 1. Load multiplier to first yield versus relative proportions of dead load and live load.

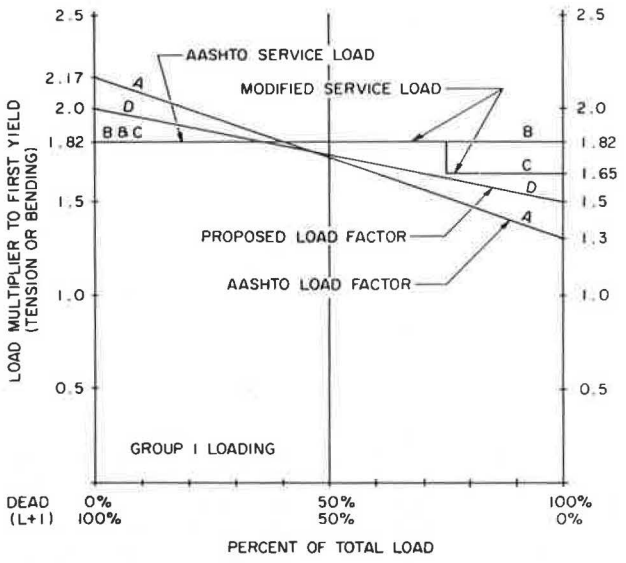

It is felt that the load factor relation proposed here is more appropriate for those truss members that carry high percentages of dead load--i.e., more than 75 percent. Similarly, the improbability of live load positioned on the structure so as to maximize member loads supports the somewhat lower total capacity required by the proposed method for members that carry high percentages of live load.

The proposed load factors for groups other than Group I have been selected to yield essentially the same results as service load design, as given below (case IIA is specifically intended for lateral truss members):

Group	Basic Factor of Safety/ Group Overstress Factor	Load Factor
II	1.82/1.25 = 1.46	1.46(D + W)
IIA	-	1.60W
III	1.82/1.25 = 1.46	1.46 [D + (L + I) + 0.3W + WL + LF]
XI	1.82/1.60 = 1.14	1.14(D + HW)

COMPUTATION OF MEMBER CAPACITY

Tension

The capacity of tension members is evaluated by using the two interaction equations shown below:

$$[P/(F_y)(A_n)] + [M/(S_n)(F_y)(f)] \leq 1.0 \quad (3)$$

$$[P/(F_u)(A_{\bar{n}})] + [M/(S_{\bar{n}})(F_u)(f)] \leq 1.0 \quad (4)$$

where

P = factored axial load;
F_y = yield point;
A_n = net area (2, Section 1.7.15);
M = factored dead load moment;
S_n = net section modulus (2, Section 1.7.15);
f = plastic shape factor computed on the basis of gross effective properties ($f = \Sigma A_y / S_g$);
A_y = statical moment of gross effective areas;
S_g = gross section modulus;
F_u = tensile strength of steel;
$A_{\bar{n}}$ = net area, all holes removed; and
$S_{\bar{n}}$ = net section modulus, all holes removed.

This interaction equation contains two simplifying assumptions. The first is that the shape of the interaction equation is a straight line joining the points ($P = P_y$, $M = 0$) and ($P = 0$, $M = M_p$). This is known to be a conservative assumption for wide-flange shapes bent about their major axis and rectangular shapes. All shapes under consideration can be considered in this range. The second assumption is that the plastic shape factor for the net section (2, Section 1.7.15), the gross effective section, and the net section with all holes removed is the same. These are reasonable assumptions, especially since the moment portion of the interaction curve is usually less than 5 percent of the total.

Compression

Two interaction equations are used, basically as discussed in Section 1.7.69(B)(1) of the AASHTO specifications (2):

$$(P/0.85\ A_{ge}\ F_{cr}) + \left(MC/M_u\left\{1 - [P/(A_{ge})(F_e)]\right\}\right) \leq 1.0 \quad (5)$$

$$(P/0.85\ A_{ge}\ F_y) + (M/M_p) \leq 1.0 \quad (6)$$

where

A_{ge} = gross effective area;
F_{cr} = critical load [2, Section 1.7.69(A)] with a suitable effective length factor (K);
C = equivalent moment factor taken as 0.85 or 1.00, as appropriate;
M_u = maximum bending strength, reduced for lateral buckling as indicated in the next section;
F_e = $(0.85)\ (\pi^2)\ (E)/(KL/r)^2$ in plane of bending;
M_p = $(F_y)(f)(S_{ge})$; and
S_{ge} = section modulus at end, reduced for access holes, if any.

Computation of Bending Strength

Box Members

Typical box-shaped truss members have such high lateral-torsional stiffness that the reduction in bending strength arising from lack of lateral support is minimal. The bending capacity can be computed as follows:

$$M_u = F_y S_{ge} \left\{1 - 0.0641\ [F_y S_{ge} L \sqrt{\Sigma(s/t)}/EA\sqrt{I_y}]\right\} \quad (7)$$

where

S_{ge} = gross effective section modulus about bending axis,
L = length of member,
s/t = length of a side divided by its thickness,
A = area enclosed within center lines of plates of box members, and
I_y = moment of inertia about the nonbending axis ("vertical axis").

H-Shaped Members Bent About Axis Parallel to Flange

H-shaped sections bent about their major axis (the axis parallel to the flanges) are very susceptible to lateral torsional buckling. The elastic critical stress at which buckling is imminent is

$$\sigma_{cr} = (1/S_{ge})\sqrt{[(\pi^2\ E\ I_y\ G\ J)/(KL)^2] + [(\pi^4\ h^2\ I_y^2\ E)/4\ (KL)^4]} \quad (8)$$

where

S_{ge} = gross effective section modulus about major axis;

I_y = minor-axis moment of inertia;
G = shear modulus;
J = St. Venant torsional constant, approximately $\Sigma bt^3/3$;
K = effective length factor for column buckling about weak axis; and
h = depth of web plate plus flange thickness.

If $\sigma_{cr} < 1/2\ F_y$, then $M_u = \sigma_{cr} S_{ge}$; if $\sigma_{cr} > 1/2\ F_y$, then $M_u = F_y S_{ge} [1 - (F_y/4\sigma_{cr})]$.

The expression for σ_{cr} above can also be used for modified H-shaped members composed of two channels (as flanges) and a web plate.

H-Shaped Members Bent About Axis Parallel to Web

H-shaped members bent about their minor axis do not exhibit lateral-torsional buckling, and their full plastic capacity may be used. Therefore, in this case,

$$M_u = 1.5\ F_y S_{ge} \tag{9}$$

Width-Thickness Ratios for Plates

Critical elastic buckling stress for plates can be written as

$$\sigma_{cr} = K\pi^2\ E/12\ (1 - \mu^2)\ (b/t)^2 \tag{10}$$

Substituting E = 29 million psi and μ = 0.3 and solving for b/t yields

$$b/t = (5120\sqrt{K})/\sqrt{\sigma_{cr}} \tag{11}$$

AASHTO shifts the curve defined by this equation to account for the observed behavior of plates, which indicates that residual stresses and out-of-flatness reduce the strength of plates of intermediate slenderness below that which would be indicated by simple elastic stability analysis. This shift is accomplished by multiplying the equation above by 0.6, which results in

$$b/t = (3072\sqrt{K})/\sqrt{\sigma_{cr}} \tag{12}$$

For the case of a simply supported plate, the minimum value of K is 4.0. This value of K and the introduction of a factor of safety that results in a working stress of $0.55\ \sigma_{cr}/1.25$ yield

$$b/t = 4073/\sqrt{\sigma_{cr}} \tag{13}$$

For main plates of truss members, the AASHTO specifications use

$$b/t = 4000/\sqrt{\sigma_{cr}} \tag{14}$$

For LFD, the maximum compressive stress is 0.85 σ_{cr}, which leads to

$$b/t = 5660/\sqrt{\sigma_{cr}} \tag{15}$$

The exact values of K, to be used for plate components of members for other conditions of support, are functions of the degree of support, which will vary from member to member. Actually, the plate strength of a fabricated member is a characteristic of the whole cross section, not of an individual plate. The existing coefficients for b/t ratios for truss members are the product of theory tempered by experience and allowances for many nonideal characteristics of plates in members. Therefore, the procedure described below has been used in developing b/t requirements.

The service load width-thickness provisions in the AASHTO specifications can be written as

$$b/t = N_{SL}/\sqrt{0.55\ \sigma_{cr}/1.25} \tag{16}$$

or

$$\sigma_{cr} = (1.25\ N_{SL}^2/0.55)(t/b)^2 \tag{17}$$

For LFD with a maximum compressive stress of 0.85 σ_{cr},

$$0.85\ \sigma_{cr} = N_{LF}^2\ (t/b)^2 = [(1.25 \times 0.85)/0.55]\ (t/b)^2\ N_{SL}^2 \tag{18}$$

Therefore,

$$N_{LF} = \sqrt{[(0.85 \times 1.25)/0.55]}\ N_{SL} \tag{19}$$

$$b/t = N_{LF}/\sqrt{\sigma_{cr}} \tag{20}$$

The resulting values are given in the second column of Table 1 along with K-values recommended by the American Institute of Steel Construction, the resulting coefficient, a recommended coefficient (N_{LF}), and a maximum b/t ratio. The recommended b/t coefficients (N_{LF}) were selected to agree, where possible, with the coefficients in the AASHTO load factor provisions for solid rib arches.

The existing AASHTO provisions for stiffened plates contained in the load factor provisions for composite box girders (adjusted for 85 percent of maximum stress) or, preferably, the load factor provisions for solid rib arches are applicable to stiffened plates in truss members.

Fatigue Design

Fatigue design proceeds exactly as in conventional service load design.

Connection Design

The load factor allowable stresses are taken from Sections 1.7.71(A) and 1.7.72(C) of the AASHTO specifications except as modified below. The overload provision, Section 1.7.72(C), will control the design of friction joints. The corresponding design capacities determined by using the proposed load factors are as follows:

Group I:	$1.5\ [D + 4/3(L + I)] = 1.5\ [1 + R/3]\ [F_v]\ [m]\ [a]$
Group II:	$1.46\ [D + W] = 1.46\ F_v\ [m]\ [a]$
Group IIA:	$1.60W = 1.60\ F_v\ [m]\ [a]$
Group III:	$1.46\ [D + L + I + 0.3W + WL + LF] = 1.46\ F_v\ [m]\ [a]$
Group XI:	$1.14\ [D + HW] = 1.14\ F_v\ [m]\ [a]$

The value of F_v is obtained from Tables 1.7.41C1 and 1.7.41C2 in the AASHTO specifications, m is the number of bolts, a is the area per bolt, and R is the ratio of live load and impact force to total force. A procedure could also be developed based on allowing friction bolts to slip into bearing at factored loads.

The design of welds is based on AASHTO Section 1.7.71(2). No modification of stated design allowables is envisioned at this time.

Eyebar Pins

The proposed allowable bearing stress on pins not subject to rotation is 1.35 F_y. This value is based on the Ontario Highway Bridge Design Code (3), which uses a value of 1.50, in which ϕ = 0.9 for steel.

Table 1. Determination of service load width-thickness ratios.

Type of Plate	Coefficient	K-Value[a]	Coefficient	N_{LF}	Max b/t Ratio
Main	5560	4	5660	5700	45
Cover	6950	5	6333	6750	50
Perforation					
Basic plate	8340	6.97	7477	8000	55
Edge of perforation	2260	0.7	2370	2200	12/16[b]

[a]Recommended by AISC. [b]Main members/secondary members.

Figure 2. Interaction curves for pins subjected to shear and moment.

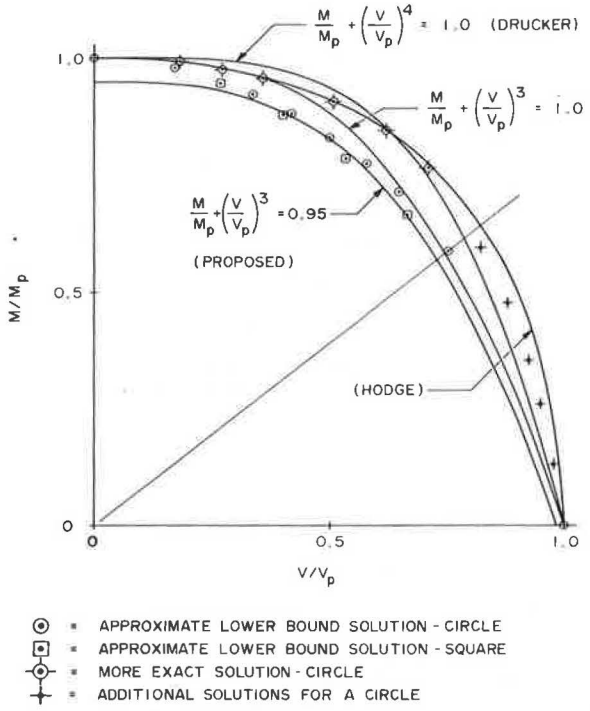

The problem of pin capacity in combined shear and bending is best approached with an interaction curve. Figure 2 shows the results of three approximations to determine a suitable interaction curve. The following considerations are noted:

1. Points marked ⊙ represent lower-bound solutions obtained for a circular shape by assuming some portion of the cross section to be yielded in bending and to carry no shear. The remainder of the cross section was assumed to be elastic in bending and shear. The maximum shear stress was equal to the shear yield stress. When plotted as a normalized interaction curve, lower-bound points computed as described above plot in the same location regardless of the choice of yield criterion. The magnitude of the shear force is, of course, a function of the yield criterion.

2. Points marked ⊡ represent lower-bound solutions, obtained as described above, for a square cross section. A square section was also analyzed because available published solutions applied to rectangular cross sections. A comparison of lower-bound results for both shapes provides a basis for evaluating previously proposed interaction curves for use in the design of eyebar pins.

3. Points marked ⊙ were obtained by a computer program that analyzed a circular cross section, broken into 20 layers, by tracing the spread of plastification through the cross section corresponding to increasing, but proportional, moment and shear. The progression of yield for each of these points was from the top and bottom toward the middle in order of layer position. The von Mises yield criterion was used in these computations because it is incorporated into the existing AASHTO load factor provisions for girder design. The calculations were repeated with the Tresca yield criterion and little difference was observed. The von Mises yield criterion is $\sigma^2 + 3\tau^2 = \sigma_y^2$; the Tresca criterion is $\sigma^2 + 4\tau^2 = \sigma_y^2$.

4. Points marked + were obtained for a circular shape by using the same computer program for ratios of shear and moment, which caused the progression of plasticity to proceed either from the middle layer out to both edges in order of layer position or to start at the middle and then proceed to total plastification in an order that did not bear any relation to the order of the layer position. This implies a discontinuous strain field, a phenomenon that can exist in plastic flow. These points are regarded as informative but less reliable than the points marked ⊙ because not all implications of the discontinuous strain field on the type of bound (i.e., upper or lower) have been evaluated.

5. The radial line in Figure 2 represents the division between ratios of shear and moment for which first yield occurs in shear or bending. Above the radial line, first yield results from bending; below it, first yield results from shear.

6. Plasticity theory indicates that the failure criterion must be convex. Therefore, the shape of the interaction curve from the lowest point marked ⊙ to the horizontal axis at $V/V_p = 1.0$ is at least a straight line; i.e., it cannot curve inward.

7. Two interaction curves for rectangular cross sections published by Drucker (4) and Hodge (5) are also shown in Figure 2. The equation by Drucker is an empirical expression developed after consideration of a number of upper and lower bounds. The curve marked "Hodge" has been scaled from the paper by Hodge (5). The analytic expression was considerably more complex than Drucker's simple expression. Both curves were developed from analyses based on the Tresca yield criterion, although Hodge noted that the von Mises criterion could also have been used. Neither paper contained experimental verification.

8. An interaction curve that is similar to Drucker's but uses an exponent of 3 instead of 4 is also shown. That curve is somewhat more conservative than either Drucker's or Hodge's curve and is suggested as the basis for eyebar pin design, modified as indicated below.

The discussion above indicates that it would be reasonable to apply Drucker's interaction curve to the design of eyebar pins. However, since neither Drucker nor Hodge published experimental verification in their respective papers, and considering the importance of eyebar pins, the more conservative interaction curve marked "proposed" in Figure 2 is suggested for use in the design of Greater New Orleans Bridge No. 2.

In summary, shear and bending in eyebar pins

Table 2. Comparative chord designs.

Chord	Member No.	Member Type[a]	Type of Steel	Dead Load Percentage of Total Service Load Design	LFD Area	Without 10 Percent Overstress: Service Load Design Area	Without 10 Percent Overstress: Service Load Area/Load Factor Area	With 10 Percent Overstress: Service Load Design Area	With 10 Percent Overstress: Service Load Area/Load Factor Area
Top	NU9-NU7	T	A572	68	287.85	326.61	1.13	NA	NA
	NU7-NU5	T	A572	76	402.60	464.19	1.15	421.99	1.05
	NU5-NU4	T	A572	81	498.60	578.35	1.16	525.78	1.05
	NU4-NU2	T	A572	81	512.10	588.81	1.15	535.28	1.05
	CU2-CU4	T	A572	86	418.35	490.45	1.17	445.87	1.07
	CU4-CU5	T	A572	86	404.85	481.65	1.19	437.86	1.08
	CU5-CU7	T	A572	86	247.98	299.81	1.21	272.55	1.10
	SU3-SU5	C	A588	85	335.06	386.95	1.15	352.36	1.05
	SU5-SU7	C	A588	85	412.06	469.88	1.14	429.41	1.04
	AU2-AU4	T	A572	82	499.35	581.19	1.16	528.36	1.06
	AU4-AU5	T	A572	82	485.85	569.35	1.17	517.60	1.07
	AU5-AU7	T	A572	79	376.23	438.39	1.17	398.53	1.06
Bottom	NL8-NL6	C	A514	72	346.59[b]	357.06[b]	1.03	NA	NA
	NL6-NL4	C	A514	78	398.22	436.94	1.10	398.69	1.00
	NL4-NL2	C	A514	84	462.75	523.69	1.13	475.66	1.03
	NL2-NL0	C	A514	84	462.75	523.69	1.13	475.66	1.03
	NL0-CL2	C	A514	86	436.94	497.81	1.14	449.84	1.03
	CL2-CL4	C	A514	86	436.94	497.81	1.14	449.84	1.03
	CL4-CL6	C	A514	86	333.69[b]	357.06[b]	1.07	354.66[b]	1.06
	SL4-SL6	T	A572	85	251.85	297.45	1.18	270.41	1.07
	SL6-SL7	T	A572	85	275.85	324.58	1.18	295.07	1.07
	AL0-AL2	C	A514	84	462.75	523.69	1.13	475.66	1.03
	AL2-AL4	C	A514	84	462.75	523.69	1.13	475.66	1.03
	AL4-AL6	C	A514	80	376.38	424.03	1.13	382.81	1.02
	AL6-AL8	C	A514	76	333.69[b]	344.19[b]	1.03	333.69[b]	1.00

Note: T = tension and C = compression.

[a] If tension member, net area is given; if compression member, gross area is given.
[b] Member design limited by b/t requirements.

should be evaluated by using the following equations:

$$M_p = (D^3/6)(F_y) \quad (21)$$

$$V_p = (\pi D^2/4)[(F_y)/\sqrt{3}] \quad (22)$$

$$(M/M_p) + (V/V_p)^3 \leq 0.95 \quad (23)$$

CONCLUSIONS

Table 2 compares designs of 25 chord members and illustrates the savings possible with strength design. The members shown were generally controlled by strength requirements rather than fatigue or minimum plate sizes; exceptions are noted. In the latter two cases, both design methods would result in the same design. Comparison of the results in which the 10 percent overstress service load criterion was not invoked shows that the ratio of service-load-design area to LFD area ranges from 1.03 to 1.21 and averages 1.14. Inclusion of the 10 percent overstress criterion results in a range from 1.00 to 1.10 and an average of 1.05.

REFERENCES

1. Highway Structures Design Handbook. U.S. Steel Corp., Pittsburgh, PA, n.d.
2. Standard Specifications for Highway Bridges, 12th ed. AASHTO, Washington, DC, 1977 (interims through 1982).
3. Ontario Highway Bridge Design Code. Ontario Ministry of Transportation and Communications, Downsview, 1979.
4. D.C. Drucker. The Effect of Shear on the Plastic Bending of Beams. Journal of Applied Mechanics, American Society of Mechanical Engineers, Dec. 1956.
5. P.G. Hodge, Jr. Interaction Curves for Shear and Bending of Plastic Beams. Journal of Applied Mechanics, American Society of Mechanical Engineers, Sept. 1957.

Publication of this paper sponsored by Committee on Steel Bridges.

Testing and Design of Longitudinal Reinforcement for Cantilevered Bridge Piers

BORIS S. BROWZIN

Deep cantilever specimens representing cantilevered bridge piers were tested for the purpose of studying their structural behavior. It has been established that the strength of the tested specimens is substantially superior to the strength predicted by conventional analysis. A new design method has been proposed for longitudinal reinforcement based on principles of static equilibrium with parameters derived from testing. The shear strength of specimens was substantially greater than was anticipated from the design. An example is provided to demonstrate the proposed design method, which provides a substantial reduction in the longitudinal reinforcement of bridge pier cantilevers.

A double cantilever system consisting of deep cantilevers at the top of bridge piers, supporting the deck, is a rational approach that leads to substantial savings in bridge construction, particularly for highly elevated intersections or deep valley crossings. The double cantilever system made it possible to build a single central pier as a replacement for the older design in which two supporting piers were used. Despite the rationality of using central piers with double cantilevers at the top, there is no research evidence on the behavior of deep double cantilevers.

Deep double cantilevers are also used to support precast beams at the top of columns or for footings.

A characteristic of deep cantilevers is a large depth-to-span ratio--say, larger than one. Other structural elements with large depth-to-span ratios are brackets (corbels) and deep beams.

The geometry of deep structural elements influences the behavior of the element. For example, brackets in most tests fail because of cracks that develop from the point of stress concentration at the intersection of the upper horizontal surface of the bracket with the vertical surface of the column face, whereas most bridge pier cantilever specimens fail because of a crack that starts at the point where the concentrated load is applied to the specimen. Therefore, design methods for deep bridge cantilevers must be different from those used in the design of brackets.

This paper is based on tests of deep double cantilever specimens. The tests are described first. Test results are used to establish a new approach for analysis and design of longitudinal reinforcement. Based on the principle of static equilibrium and test results, it has been found that the needed amount of longitudinal reinforcement is substantially smaller than that resulting from a conventional analysis. It was also observed that the shear strength of the specimens was substantially higher than is usually assumed. Consequently, the shear stresses are not governing design criteria, and shear reinforcement, depending on the slope of the bottom face, may not be required. Other design aspects of deep cantilevers, such as anchorage of longitudinal bars and temperature reinforcement, were not considered in this testing program. The conventional design practice appears adequate, particularly for anchorage. Previous work on deep structural elements has consisted of testing deep beams and brackets (corbels). Work on deep beams is not reported in this paper because the structural behavior of deep beams differs from that of deep cantilevers. The work on brackets is summarized below.

Corbels were extensively investigated in Portland Cement Association (PCA) laboratories by Kriz and Raths (1). The PCA tests resulted in empirical equations based on statistical results from tests. It is regrettable that the principles of statics were neglected in the research of Kriz and Raths. Other works on corbels are listed in a report by the American Society of Civil Engineers (ASCE) (2), among them works by Mehmel and Beckner, Mehmel and Freitag, and Commissie and others. The investigation of corbels by Niedenhoff (3) and Franz and Niedenhoff (4) resulted in new information on the mechanisms of corbel behavior. Publications oriented toward establishing a design method for corbels based on "satisfaction of the laws of statics" are reported by Mattock, Chen, and Soongswang (5) and Mattock (6). According to the best evidence available to me, cantilevers of the geometry described in this paper have never been tested.

The following sections of this paper provide the description of the experimental setup, resulting load-stress characteristics, the analysis and design of reinforcement with design examples, and a tentative analysis of the stress distribution in a cross section of a cantilever.

Because a considerable amount of effort was applied in order to achieve a careful setup of testing and measurements, it is considered appropriate to provide a detailed account of the test results in this paper. Furthermore, since these tests were used in establishing a new approach for the design and analysis of an important structural element in the development of the national transportation system--i.e., bridge piers with cantilevers--it is believed that the experimental data base presented in detail will substantiate and justify the proposed approach.

NOTATION

The following notation is used in this paper:

- A_s = cross-sectional area of reinforcement;
- a = "shear span," distance from the point of application of the load to the cross section considered;
- b = width of the cross section;
- C = resultant of normal stresses in concrete at a given cross section;
- d = depth of the cross section;
- f'_c = specified compressive strength of concrete;
- f_s = stress in reinforcement;
- f_{su} = stress in reinforcement at failure;
- f_y = yielding stress in reinforcement;
- j = parameter determining the location of the resultant of concrete compressive stresses in a cross section above the centroid of reinforcement;
- j_F = magnitude of the parameter j at failure;
- T = resultant of tensile stresses in reinforcement;
- V = reaction at tested specimens, load on cantilevers;
- $2V$ = load on tested specimens;
- V_u = V at failure;
- $2V_u$ = 2V at failure; and
- ρ = ratio of reinforcement or percentage of reinforcement.

EXPERIMENTAL SETUP AND TESTING

Experimental work was conducted at the National Bureau of Standards (specimens N1 and N2) and at Case Institute of Technology (specimens C1, C2, C3, C4, and C5). An arbitrary shape was selected for the specimens, which were tested in the upside-down position (see Figure 1). The overall dimensions of the specimens were 36x25.5x12 in (91.4x64.8x30.5 cm). The span between the supports was 27 in (68.6 cm). Axes numbered 1 through 15 were used to identify cross sections of the specimens (see Figure 2). Axes 1, 3, 5, and 7 were separated by 5 in (12.7 cm) as were axes 9, 11, 13, and 15. The specimens rested on 1x4x12-in (2.5x10.2x30.5-cm) supporting plates, which in turn rested on rollers at each side of the span. For specimens C1-C5, two rollers in contact were used at each support as a precaution against possible escape of the rollers under loading action. Specimens N1 and N2 were tested with one roller welded at support A and one free roller at support B, as shown in Figure 2.

The concrete used was Type III, which had a specified strength of 3000 psi (20.7 MPa); the strengths actually obtained ranged from 3930 to 5950 psi (27.1-41.0 MPa) and the moduli of elasticity ranged from 3.1 million to 4.8 million psi (21 400-33 100 MPa) (see Table 1).

The characteristics of the reinforcing steel in the N and C specimens were as follows:

Specimen Type	Yield Point (psi 000s)	Ultimate Strength (psi 000s)	Elastic Modulus (psi 000 000s)
N	45.3	74	26
C	45	77	29

The cross-sectional area of the reinforcement of specimens N1 and C1 was designed to provide a reinforcement ratio at the middle of the specimen, axis 8, that would approximately correspond to allowable stresses, f_s = 20 000 psi (138 MPa) and f_c = 1350 psi (9.3 MPa), at working load in steel and concrete, respectively. Normal practice was followed to obtain an approximation of 21 in (53.3 cm) for the depth of the cross-sectional area at axis 8. The distance from the bottom of the specimens to the centroid of the reinforcement was 1.5 in (3.8 cm). Specimens N1 and C1 were reinforced by two layers of bars, the others by one layer. The rein-

Figure 1. Sectional view of specimens.

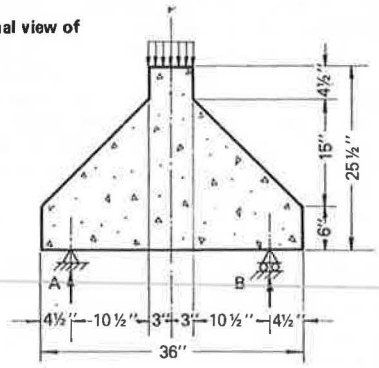

Figure 2. Structural details of specimens N1 and N2, including grid system and location of strain gages.

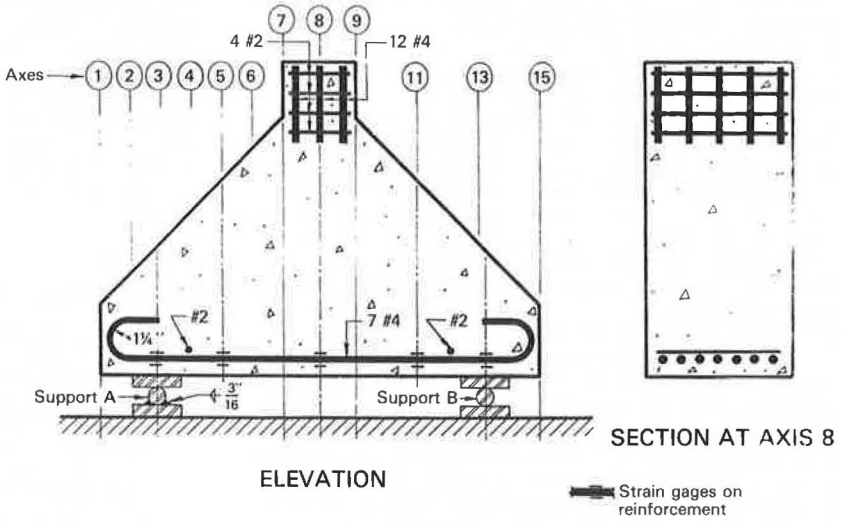

Table 1. Characteristics of specimens.

Specimen	Ultimate Strength of Concrete (psi)	Modulus of Elasticity of Concrete (psi 000 000s)	Bars		Area of Reinforcement (in^2)	Reinforcement Ratio at Cross Sections	
			Size	Number		Axes 5 and 11	Axis 8
N1	5740	4.1	#4	15	3.0	0.0172	0.0119
C1	4910	3.1	#4	15	3.0	0.0172	0.0119
N2	5950	4.1	#4	7	1.4	0.0081	0.0056
C2	5270	4.7	#4	7	1.4	0.0081	0.0056
C3	3930	4.8	#3	5	0.55	0.0032	0.0022
C4	3930	4.8	#3	3	0.33	0.0019	0.0013
C5	3930	4.8	-		0	0	0

Note: 1 psi = 0.006 895 MPa; 1 in^2 = 6.45 cm^2.

Figure 3. Location of strain gages on reinforcing bars in plan view.

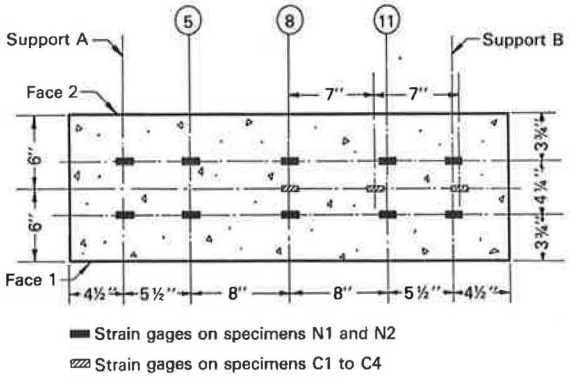

forcement of specimens consisted of 15 #4 bars for N1 and C1, 7 #4 bars for N2 and C2, 5 #5 bars for C3, and 3 #3 bars for C4 for the specimen width of 1 ft (30.5 cm). The resulting reinforcement ratio at the middle of the specimen (axis 8) varied from 0.0119 to 0.0013 and near the quarter-span (axes 5 and 11) from 0.0172 to 0.0019 (Table 1). Electrical resistance strain gages 3/8 in (0.95 cm) long were located on the reinforcing bars (see Figures 2 and 3). In specimens N1 and N2, the strain gages were located at the top and bottom of each bar, 20 gages in each specimen. In specimen N1, the gages were attached to the bars of the lower layer. In specimens C1-C4, the gages were placed at similar locations at the bottom of each bar, 3 gages in each specimen (Figure 3). The strain readings were corrected to obtain the strain and stresses at the centroid of the reinforcement in all specimens on axes 5, 8, and 11 and at the supports. Specimens N1 and N2 were equipped with strain gages placed on concrete in addition to those placed on the reinforcing. This paper includes the results of strain measurements in the steel only.

The load was applied at the top of specimens through the spherical head of 600 000-lb (2670-kN) capacity testing machines with 15 000-lb (66.7-kN) increments in the N tests and with 30 000-lb (133-kN) increments in the C tests. The test results are presented as reinforcement stress as a function of load at five locations in the N specimens, at approximately the quarter-span (axes 5 and 11), the middle span (axis 8), and the supports and at three locations in the C specimens.

EXPERIMENTAL LOAD-STRESS CHARACTERISTICS

Load-Stress Curves at Approximately Quarter-Span (Axes 5 and 11)

Specimens N1 and C1

The curves of load versus experimental stress in the reinforcement at axes 5 and 11 of specimen N1 follow the same pattern very closely from zero to failure load (see Figure 4). Both indicate elastic behavior of the concrete up to a load of about 90 kip (400 kN). Above 90 kip, the experimental stress lines begin to deviate gradually from the straight line. The first diagonal crack (shown at the left-hand side of the photograph in Figure 5) developed at a load of 135 kip (600 kN) and extended nearly half the specimen height. Further development of this crack and a new crack at the right side observed at a load of 165 kip (734 kN) are also shown in Figure 5. At 165 kip, the crack on the left side extended to about 90 percent of its final length and the crack on the right side to 60 percent of its final length. The major formation of the cracks therefore occurred between loadings of 135 and 165 kip. Correspondingly, the experimental curves exhibited a flatter pattern in this interval, indicated in Figure 4 as "major extension of diagonal cracks." This stage may be considered a transition stage, which is a stage between the elastic state of equilibrium and the cracked-elastic state of equilibrium when the steel absorbs the major portion of tensile stresses.

The new state of equilibrium of internal forces, cracked-elastic equilibrium, beginning at a load of 165 kip, is reflected by the portion of the experimental curves that follow a straight line with a slope larger than that in the transition stage but smaller than that in the elastic stage below a load of 90 kip. The left crack stopped running at 315 kip (1401 kN), as indicated in Figure 5. The experimental lines (Figure 4) indicate a flatter slope beginning with the 315-kip load. At a load of 405 kip (1801 kN), formation of a new crack starting from the existing crack at the right side was observed, beginning approximately at the 165-kip mark shown on the existing crack. The new crack extends up to the intersection of the column face (axis 7) with the sloping face of the specimen. This crack produced a sudden, explosive failure. Simultaneously, a curved crack developed at the support and there was separation of a piece behind the hooks of reinforcement. The failure occurred at stresses in the reinforcement of 38 600-39 500 psi (266-272 MPa) (see Table 2), much below the yielding stress of 45 300 psi (312 MPa). Consequently, the cause of failure was the diagonal tension (principal tensile stresses) in concrete in the direction normal to the failure crack without yielding of the steel. The experimental curve obtained from testing specimen C1 follows approximately the pattern of the experimental curves for N1 (not shown in Figure 4). Specimen C1 failed prematurely because of crushing of the specimen head at a load of 236 kip (1050 kN). Stresses for typical loads are listed in Table 2.

Specimens N2 and C2

The curves of load versus experimental stress at axes 5 and 11 of specimen N2 closely coincide (Figure 4). At the point indicating a load of 75 kip (333 kN), two curves of specimen N2 turn back, showing a drop in stress of about 1000 psi (6.90 MPa). The drop in stress in the steel at both axes 5 and 11 is local; the curve gradually returns to the normal pattern similar to that of specimen N1. The curve for specimen C2 indicates stresses consistently larger by 2000-3000 psi (13.8-20.7 MPa) than the stresses in specimen N2. The difference is probably due to the different arrangement of the supports. Similar higher stresses were observed in C1 for apparently the same cause.

Only two states of stresses can be clearly defined from the curves of specimens N2 and C2: the noncracked elastic and cracked elastic. The first crack, which was a diagonal crack at the right-hand side (see Figure 6), was observed in specimen N2 at the same load [135 kip (600 kN)] as in specimen N1; however, steel stress at 135 kip in specimen N2 (axis 11) was 18 200 psi (125 MPa) versus only 8200 psi (56.5 MPa) in specimen N1, which is almost exactly in proportion to the amount of reinforcement in N2. The second crack was observed in the middle of the specimen at a load of 150 kip (667 kN). A similar crack was not observed in the specimen with higher reinforcement, specimen N1. The third crack, a diagonal one, was observed at a load of 180 kip (801 kN) on the left side. Two minor sloping cracks developed at about half the distance between the

Figure 4. Stresses in reinforcement at axes 5 and 11 as a function of load.

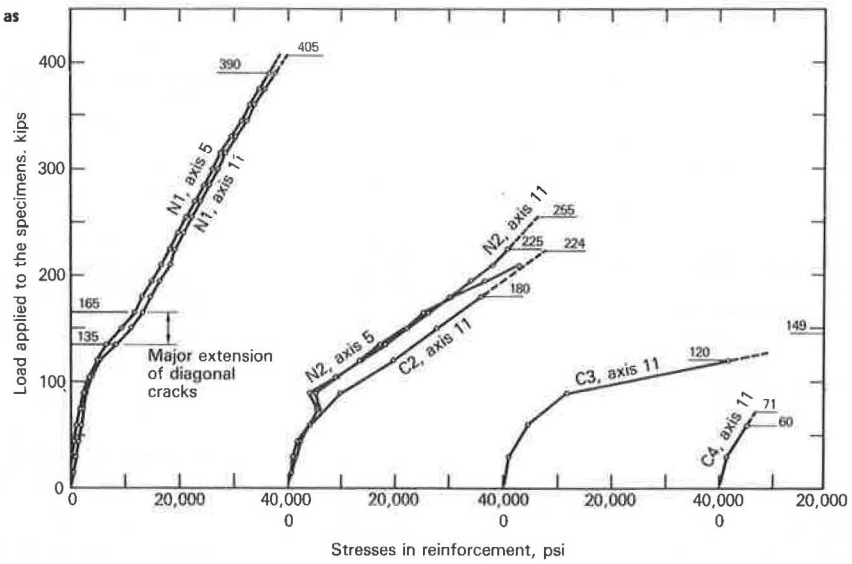

Figure 5. Specimen N1, face 2, after failure.

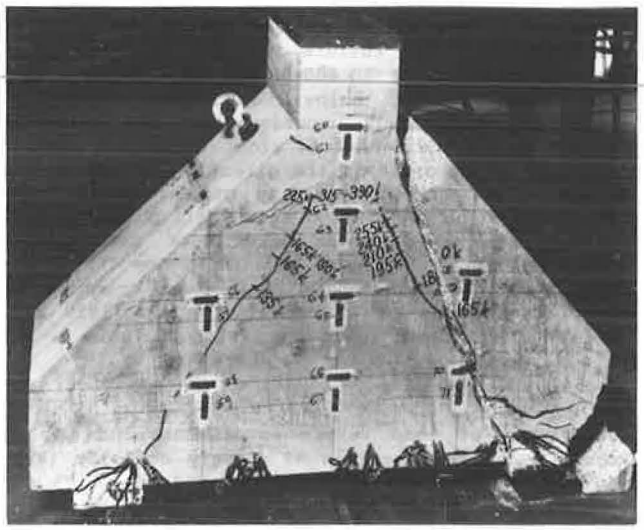

diagonal cracks, starting at the supports and the middle crack; similar cracks were also not observed in specimen N1. All five cracks were fairly symmetrically located about the center of the specimen, which may be regarded as an indication that the support conditions were symmetrical--i.e., compatible with the free support concept. A further extension of diagonal cracks was observed in both sides of the specimen at a load of 225 kip (1001 kN). The left-side crack reached the column face at axis 9, face 2, and caused the failure (Figure 6).

The appearance of the first diagonal cracks at the same 135-kip load in both specimens N1 and N2 and the extension of cracks at near the same loads in N1 and N2 (the 225-kip marks at the left side of specimens N1 and N2 are located at the same level) indicate that the amount of reinforcement does not influence the appearance and the extension of diagonal cracks. The failure of specimen N2 occurred at a load of 225 kip by a sudden, explosive failure of the concrete along the diagonal crack on the left side similar to the failure of specimen N1. A similar accompanying crack near the reinforcing bar hooks was observed as well as splitting of concrete at the hooks and at the top near the column. The failure occurred at stresses in reinforcement of 49 000 psi (338 MPa) at the middle and 46 300 psi (319 MPa) at axis 11, which were above the yield point [45 300 psi (312 MPa)]. Consequently, the cause of failure was the diagonal tension (principal tensile stresses) in concrete with simultaneous yielding of steel. The failure of specimen C2 was similar to the failure of specimen N2.

Specimen C3

The experimental curve for specimen C3 is similar to that for specimen C2 for stresses less than 10 000 psi (69 MPa). It slopes more heavily to the right at about the 10 000-psi point as a consequence of the smaller amount of reinforcement. At a load of 90 kip (400 kN), stresses were 10 000 psi in C2 and 11 700 psi (80.7 MPa) in C3. The magnitudes of these stresses are close despite a considerable difference in the amount of reinforcement. This must be explained by the assumption that concrete resists more tension in specimen C3 with less reinforcement. The cracks that developed in specimen C3 were first observed starting from the supports as in other specimens and following a diagonal direction toward the top. A vertical crack was observed near the middle of the specimen. The experimental curve indicates that, at failure, the stress in the steel reached the yield point. The type of failure is the same as that of specimens N2 and C2: by diagonal tension in concrete with simultaneous yielding of the reinforcement.

Specimens C4 and C5

The experimental curve of specimen C4 with low reinforcement is determined by only two points (Figure 4). An almost vertical crack developed in the specimen, starting near the middle. The same crack caused the failure at a load of 71 kip (316 kN), slightly above the second load, 60 kip (267 kN), which caused a stress of only 5300 psi (36.5 MPa) in the reinforcement. The widening of the crack caused a sudden increase of stress in the steel, which produced failure by yielding of the steel. A middle crack in specimen C3 did not produce failure whereas in C4, with less reinforcement, the vertical crack was fatal.

Table 2. Stresses in reinforcement calculated from measured strains and corresponding loads.

Specimen	Stage	Load (kips)	Stress (psi 000s) Support A	Support B	Axis 5	Axis 11	Axis 8
N1	At first diagonal crack	135	2.3	3.1	6.5	8.2	
	At last recorded strain	390	21.4	23.9	36.7	38.0	
	At failure load	405	23.0	26.0	38.6	39.5	
C1	At last recorded strain	180				18.7	18.8
	At failure load	236					
N2	At first diagonal crack	135	3.0	4.9	17.2	18.2	20.3
	At last recorded strain	225	23.0	28.0		40.9	41.5
	At failure load	255	28.6	32.5		46.3	49.0
C2	At last recorded strain	180		25.0		36.0	41.8
	At failure load	224		37.5		48.0	54.5
C3	At last recorded strain	120		31.2		42.0	44.7
	At failure load	149				67.0	73.0
C4	At last recorded strain	60		2.5		5.3	12.2
	At failure load	71				6.8	16.5

Note: 1 kip = 4.448 kN; 1 psi = 0.006 895 MPa.

Figure 6. Specimen N2, face 1, after failure.

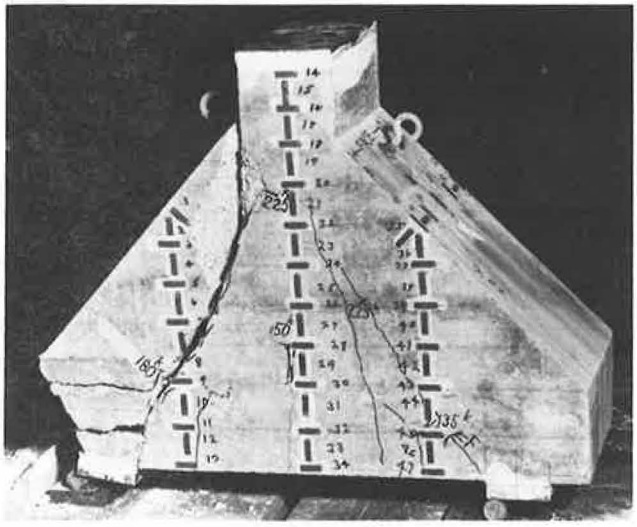

An additional specimen--C5, build with plain concrete--was tested. It failed under a load of 33 kip (147 kN), about half the load that caused the failure of specimen C4. This is an indication that even an insignificant amount of reinforcement, as in specimen C4, improves considerably the loading capacity of the specimen, a fact known by the designers of footings but not treated by the reinforced concrete design codes.

Load-Stress Curves at Middle of Span (Axis 8)

Comparison of experimental curves (see Figures 4 and 7) obtained from strain measurements at axes 5, 8, and 11 of specimen N1 shows that the curves almost coincide. The closeness of the stresses, particularly at 165 kip (734 kN) when major cracks are formed and up to failure, indicates that stresses in the reinforcement change little along the middle portion (from axes 5 to 11) of the specimen. At the last prefailure load [390 kip (1735 kN)], stresses in the steel are 36 700, 39 400, and 38 000 psi (253, 272, and 262 MPa) at axes 5, 8, and 11, respectively; i.e., there is about 6 percent difference between the average stress in 5 and 11 and the stresses at axis 8 (Table 2). This indicates that the steel absorbs almost uniformly the horizontal component of the resultant of the principal stresses directed from the applied load toward the supports. The curves and the stresses in steel at failure for specimens N2, C1, C2, and C3 confirm the same conclusion: Stresses in the steel are nearly equal from axis 5 to axis 11 (Table 2).

Load-Stress Curves at Supports

The general pattern of the experimental curves for specimen N1, representing stresses on supports versus loads (see Figure 8), is similar to that of the experimental curves plotted from observations of axes 5, 8, and 11. Stresses in the reinforcement at the supports, including stresses at failure, indicate values close to one-half those observed in bars in the space between axes 5 and 11 (Table 2). Stresses at failure in the reinforcement at the supports for specimens N2, C2, and C3 are larger than one-half the values of stresses in the space between axes 5 and 11.

NOMINAL SHEAR STRESS AT FAILURE

The nominal shear stress characteristics for loads at the first diagonal crack and at failure are given in Table 3. The nominal shear stress at failure is very large, up to 2328 psi (16.0 MPa) at axis 5. This is due to the action of the reinforcement. In such structural members as deep cantilevers, the nominal shear stress cannot be used as a design criterion because it is not a measure of the shear strength (or principal tensile strength) of concrete but rather is a measure of the strength provided by tensile reinforcement.

EQUATIONS OF EQUILIBRIUM: DESIGN OF LONGITUDINAL REINFORCEMENT

Equations of Equilibrium

The equilibrium of a free body to the left of any vertical section passing through the left portion of the cantilever specimens will result in the equation for the reaction at the support, which is the concentrated load in the prototype (V_u):

$$V_u = A_s f_{su} (jd/a) \quad (1)$$

Because the stress distribution in a vertical cross section of a short cantilever with a sloping face is unknown and differs substantially from that in a long cantilever with parallel faces or in a long (shallow) beam, the equation of equilibrium, Equation 1, cannot be used directly. The arm of the

Figure 7. Stresses in reinforcement at axis 8 as a function of load.

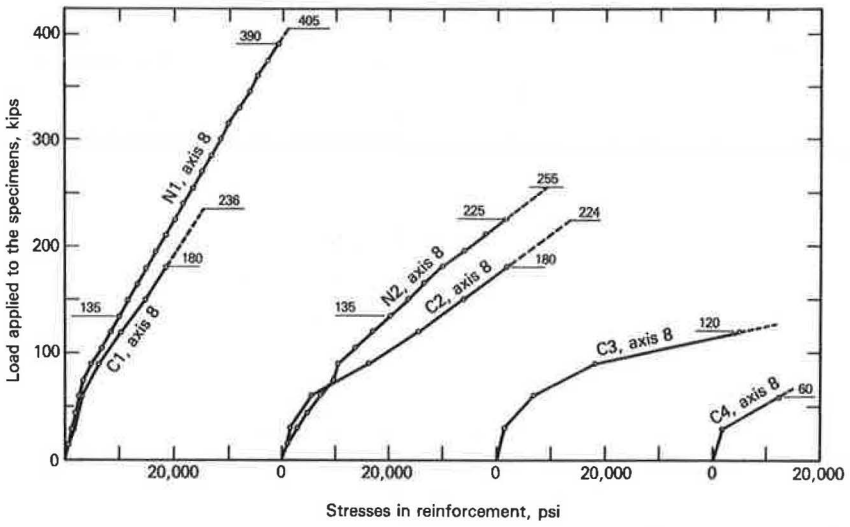

Figure 8. Stresses in reinforcement at supports as a function of load.

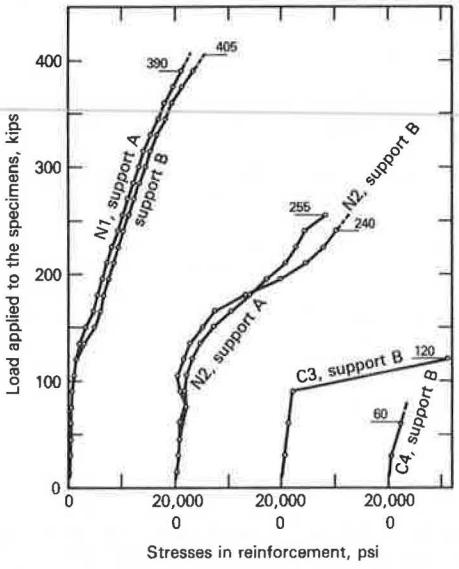

resultants of the internal normal stresses acting on a vertical section (jd) must be investigated in order to validate Equation 1 for analyzing the ultimate load (V_u). The stress of steel at failure (f_{su}) must also be assumed. Both the arm jd and the stress f_{su} may be determined from the tests reported in this paper.

By rewriting Equation 1 for j,

$$j = (V/f_s A_s)(a/d) \quad (2)$$

and using 2V for the monotonic load on the specimen (V is the reaction), f_s, the stress from the corresponding measured strain, and the known quantities a, A_s, and d, the parameter j was calculated from test data and plotted versus the quantity $V/f_s A_s$ in Figure 9 for the vertical cross sections at axes 5 and 8 of specimens N1, N2, and C3. Only a portion of the available data is shown in Figure 9. Many other points that are not shown in Figure 9 would be located, if shown, exactly on the same straight lines. It is seen that the parameter j depends linearly on the quantity $V/f_s A_s$. Moreover, for specimens N1, N2, and C3, the experimental points

Table 3. Nominal shear stress characteristics.

	Shear Stress (psi)			
	Axis 5		Axis 7	
Specimen	At First Diagonal Crack	At Failure	At First Diagonal Crack	At Failure
N1	776	2328	577	1730
N2	776	1466	577	1090
C3		856		637
C4		408		303
C5		190		141

Note: 1 psi = 0.006 895 MPa.

lie on the same straight line regardless of the amount of reinforcement. Parameter j can be regarded as an index to the stress distribution in a cross section. In the beginning of the test, $j \geq 5$ (see the upper points); i.e., the resultant of normal stresses is located outside of the section, which indicates the presence of tensile stress in the cross section that corresponds to the precracked state. With increasing load 2V (and decreasing ratio $V/f_s A_s$), the parameter j decreases and reaches the value j_F, the value at the last observed strain prior to failure. Values of j_F were calculated at sections 6 and 7 in addition to those at sections 5 and 8 (see Table 4). A graph representing the product $j_F\rho$ versus ρ, where ρ is the reinforcing ratio, was plotted (see Figure 10). Because this plot is linear with little scatter and all four lines converge to a single point (at 0-0.12), it was possible to establish a common equation for j_F as follows (for ρ in percentage):

$$j_F = (0.12/\rho) + 1.36\{[(a/d) + 0.06]\} \quad (3)$$

A verification of the accuracy of Equation 3 for ρ = 1 percent is given below:

Ratio a/d	j_F Calculated	j_F From Graph	Error (%)
0.38	0.718	0.72	-0.3
0.47	0.841	0.85	-1.2
0.54	0.936	0.87	+1.3
0.64	1.072	1.08	-0.7

The error is within 1.3 percent. This indicates

Figure 9. Internal force arm parameter (j) as a function of ratio of load to force in steel reinforcement (V/f_sA_s).

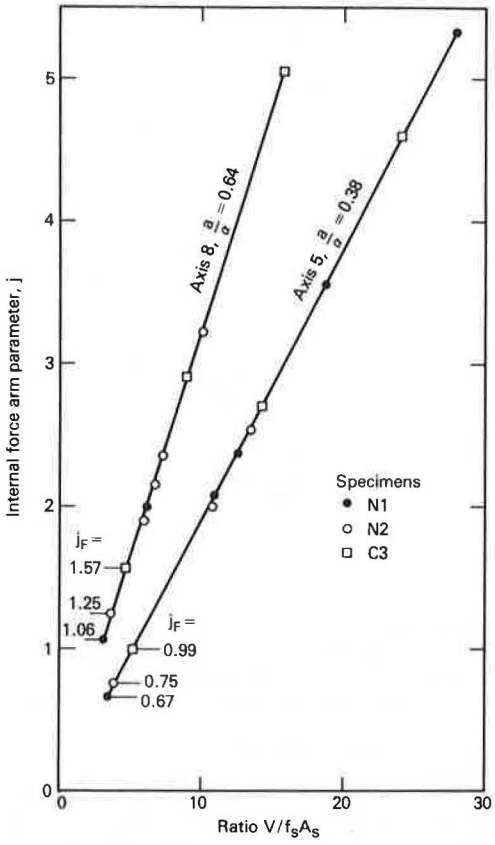

that Equation 3 provides a satisfactory method for determining the parameter j_F. Equation 3 provides the means for designing the reinforcement for a given load V_u by using Equation 1 for the stresses in steel at the failure load. Data given in Table 2 indicate that the specimens failed at stresses in steel approximately equal to yield stress. A reduction factor of approximately 0.85 can be used. The ultimate stress corresponding to the given ultimate load will consequently be $f_{su} = 0.85f_y$.

Equation 3 can be combined with the equation of equilibrium, Equation 1, and a formula for proportioning cantilevers can be obtained as follows:

$$A_s = (V_u a - 0.0012db^2 f_{su})/[1.36f_{su}(a + 0.06d)] \quad (4)$$

for consistent units.

For a given ultimate load V_u and its location determined by the shear span a, the elements of the cantilever--b, d, and A_s--must satisfy Equation 4. The width b must be selected to provide the space for placing the bars. Because Equation 3 is derived from experiments, the condition for compressive stress in concrete is satisfied if Equation 4 is satisfied. The nominal shear stress in concrete at a given cross section should not be considered as a design criterion (see above). Shear reinforcement is not required if the reinforcement is designed by using Equation 4. Because Equations 1-4 are derived based on satisfying the laws of statics, the principle of superposition can be applied when they are used; i.e., any number of concentrated loads from girders resting on a bridge pier may be included in this analysis.

Design of Reinforcement

An example of a design is provided: For an ultimate load V_u = 600 kip (2669 kN) located at a = 5.0 ft (152 cm) from the column, design the cross section at the column. Use steel f_y = 45 ksi (310 MPa), use stress at failure f_{su} = 0.85 x 45 = 38.25 ksi (264 MPa), and assume a cross section with b = 24 in (61 cm) and d = 48 in (122 cm). From Equation 4, the necessary reinforcement will be as follows:

$$A_s = [600 \times 5 \times 12 - 0.0012 \times 48 \times (24)^2 \times 38.25] \div [1.36 \times 38.25(5 \times 12 + 0.06 \times 48)] = 10.62 \text{ in}^2 (68.5 \text{ cm}^2)$$

The corresponding value for j_F for this analysis by Equation 3 is j_F = 1.92. A similar design for a shallow beam determined by using the ultimate load method results in substantially larger reinforcement. By using "Witney's block" for compressive stresses and $0.85f'_c$ stress (7, p. 50), the reinforcement is A_s = 26.8 in² (173 cm²) with j (same as j_F above) = 0.732.

Geometry

The cantilevers were tested by using specimens of particular geometry (Figures 1-3). However, the essential geometric characteristic that determines the behavior of this type of structure is the shear-span-to-depth ratio, a/d. If the slope of the lower surface of a bridge pier or the height at the end of the cantilever is different from those of the tested specimens but the essential characteristic, a/d, remains the same at a given cross section, the characteristic of the section at failure (j_F) must remain essentially the same. However, testing is desirable to confirm the applicability of the method to other cantilever shapes, particularly for bridge piers with a steeper lower surface--i.e., with larger depth-to-span ratio (d/a).

The above argument does not apply, however, to such structural elements as corbels (brackets). Because corbels (brackets) projecting from columns or walls have substantially different geometry near the column or wall face and consequently a different stress pattern near the support than deep cantilevers, Equations 3 and 4 may not provide sufficiently accurate results if applied to corbels. This conclusion follows from several trial calculations based on PCA test data (1).

INVESTIGATION OF NORMAL STRESS DISTRIBUTIONS AT A CROSS SECTION

A study of j_F values from Figure 9 and Table 4 indicates that at lower reinforcement parameter j_F is larger. When $j_F > 1$, the resultant of the normal stress in the cross section is located outside the cross section. This indicates that tension in the concrete must exist prior to failure. On the other hand, when the ratio V/f_sA_s decreases (Figure 9), the parameter j decreases. The parameter j is greater than 5 at the beginning of the test at low loads, when the precracked condition exists; it gradually drops to the value j_F indicated in Figure 9.

At the prefailure conditions concrete still resists tension, apparently at the lower portion of the cross sections, despite the fact that major cracks develop at the support. The hypothesis that concrete still resists tension at the prefailure stage (indicated by a large value of j_F) may be supported also by the fact that the concrete does not exhibit cracks at the reinforcing bars between the supports if a sufficiently large amount of reinforcement is provided (specimen N1). This also means that the bond between the bars and the concrete is not broken and therefore concrete participates in resisting tension in addition to the resis-

Table 4. Parameter j_F at last recorded strain determining location ($j_F d$) of resultant of normal stresses in concrete and corresponding ρ.

Test	Load 2V on Specimen at Last Recorded Strain (kips)	Section at Axis No. 5		6		7		8	
		j_F	ρ (%)	j_F	ρ (%)	j_F	ρ (%)	j_F	ρ (%)
N1	390	0.67	1.72	0.81	1.47	1.91	1.28	1.06	1.19
N2	225	0.75	0.81	0.92	0.69	0.97	0.60	1.25	0.55
C3	120	0.99	0.32	1.20	0.27	1.35	0.24	1.57	0.22

Note: Shear span/depth ratio (a/d) = 0.38, 0.47, 0.54, and 0.64 for sections 5, 6, 7, and 8, respectively.

Figure 10. Parameter $j_F\rho$ as a function of the reinforcement ratio, ρ, and arm-to-depth ratio a/d.

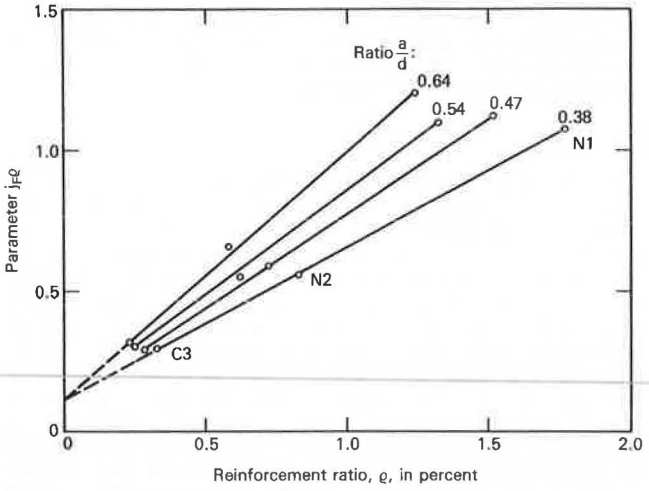

Figure 11. Normal stress distribution in concrete in specimens N1 and N2 at last observed strain at axis 7 prior to failure.

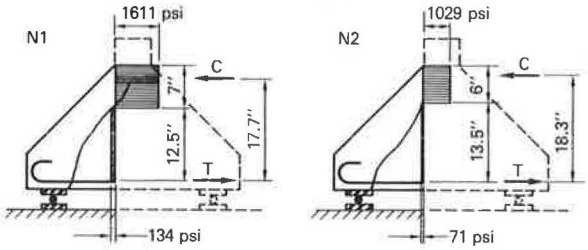

tance of the bars. In specimen N2 vertical cracks developed, so the participation of concrete in absorbing tension stress is not so obvious for this specimen.

An analysis done for specimens N1 and N2 by using the actual values of j_F results in the normal stress distribution diagrams shown in Figure 11a, b. This analysis assumes the neutral plane at the intersection of the major crack with the cross section at axis 7. Observed strain, given load, reinforcement data, and the magnitude of the parameter j_F (Equation 3) are used. The compressive stress block is assumed to be rectangular. If the rectangular compressive stress block is used, tension stress below the neutral plane must be present to satisfy the condition of equilibrium. Calculated tension stresses are shown in Figure 11. If a parabolic stress distribution or a triangular compressive stress diagram were assumed, the tension stress below the neutral plane necessary for equilibrium would still exist but would be smaller. If a similar analysis were made at axis 8 (instead of axis 7) with j_F = 1.06 (for N1) and 1.25 (for N2), the tension necessary for equilibrium would be larger than in the example analyzed for axis 7 because the resultant C of stresses in concrete is located at axis 8 outside the cross section ($j_F > 1$) (Table 4). The magnitudes of the stresses calculated for specimens N1 and N2 are shown in Figure 11.

CONCLUSION

Tested deep reinforced concrete cantilevers exhibit substantially higher resistance to applied load than that determined by conventional methods of analysis using the ultimate load or working stress method. A study based on equilibrium of tested specimens provided a method for determining the arm of the resultant of normal stresses in concrete in a vertical cross section as a function of depth-to-span ratio and reinforcement ratio. A general equation for analyzing the arm of this resultant is presented. In turn, this equation provides the means for designing the reinforcement to satisfy conditions of equilibrium prior to failure. Conditions for compression of concrete are satisfied by using this equation. It has been found that nominal shear stresses at vertical cross sections are very large, much above the shear (principal tension) strength of concrete. This is because the horizontal reinforcement provides shearing strength to the structure. For this reason, nominal shear stress should not be used as a criterion for the design. The true distribution of normal stresses prior to failure in vertical cross sections is still unknown, although the equilibrium study indicated that tension in concrete exists and contributes to the overall resistance of deep cantilevers. This in part explains their higher resistance to the applied load compared with that predicted by conventional methods of analysis.

ACKNOWLEDGMENT

The testing at Case Institute of Technology was performed under my supervision by J. Schleich, who was then a graduate student. The testing at the National Bureau of Standards was performed under my direction with the participation of R.G. Mathey and L. Catanio. I express my great appreciation to them.

REFERENCES

1. L.B. Kriz and C.M. Raths. Connections in Precast Concrete Structures: Strength of Corbels. Journal of Prestressed Concrete Institute, Vol. 10, No. 1, Feb. 1965, pp. 16-61.
2. Joint ASCE-ACI Task Committee 426 on Shear and Diagonal Tension. The Shear Strength of Reinforced Concrete Members. Journal of Structural Division, ASCE, No. ST6, Proc. Paper 9791, June 1973, pp. 1091-1187.
3. H. Niedenhoff. Untersuchungen ueber das Tragverhalten von Konsolen und kurzen Kragarmen. Karlsruhe Tech. Univ., Karlsruhe, Federal Republic of Germany, dissertation, 1961.

4. G.U. Franz and H. Niedenhoff. Die Bewehrung von Konsolen und gedrungenen Balken. Beton und Stahlbeton 5, 1963, pp. 112-120.
5. A.H. Mattock, K.C. Chen, and K. Soongswang. The Behavior of Reinforced Concrete Corbels. Journal of Prestressed Concrete Institute, Vol. 21, No. 2, March-April 1976, pp. 52-77.
6. A.H. Mattock. Design Proposals for Reinforced Concrete Corbels. Journal of Prestressed Concrete Institute, Vol. 21, No. 3, May-June 1976, pp. 18-42.
7. P.M. Fergusson. Reinforced Concrete Fundamentals, 4th ed. Wiley, New York, 1979, 724 pp.

Publication of this paper sponsored by Committee on Concrete Bridges.

Study of Cracking of Composite Deck Bridge on I-75 over Peace River

CLIFFORD O. HAYS, JR., FERNANDO E. FAGUNDO, AND ERIC C. CALLIS

Observed cracking on the Peace River Bridge on Interstate 75 near Punta Gorda, Florida, caused concern about the possibility of high maintenance cost and the structural adequacy of the bridge system. The deck system consists of precast panels resting on soft fiberboard, which serve as formwork for the road surface and later aid in carrying the traffic loads. An investigation has been completed that involved testing of the Peace River Bridge, testing of the FL-776 Bridge (a nearby structure of similar construction), analytic modeling using the finite element method, and limited laboratory testing of beam specimens. The investigation indicates that although the Peace River Bridge is adequate to carry normal traffic, the shear stresses in the bridge deck are substantially higher than those of deck systems that have positive bearing at the ends of the panels. Further experimental studies are under way to determine the shear fatigue life of the bridge. The causes of cracking and separation at the ends of the panels are identified as differential shrinkage and creep due to prestress forces. Recommendations for future construction projects are made.

Rising costs of formwork, materials, and labor have greatly increased the cost of reinforced concrete bridges constructed with conventional field forming techniques. Construction techniques that reduce the amount of forming done under field conditions increase the economy of the bridge. Prefabricated prestressed girders have been in common use in bridges for approximately 30 years. Precast stay-in-place forms of concrete and steel replaced wooden forms in recent years and eventually led to the development of precast composite deck panels. Composite deck panel bridges contain precast prestressed panels that span between bridge girders and support the cast-in-place topping, eliminating most of the field formwork. Research in Florida, Pennsylvania, and Texas led to their widespread acceptance and incorporation into the American Association of State Highway and Transportation Officials (AASHTO) specifications (1). Figure 1 shows typical composite bridge panel construction, as built in Florida, prior to this research.

Recent research in Florida (2) and Louisiana (3) dealt with full-span form panels that span directly between piers without using prestressed girders. Additional research on deck panels was recently completed in Texas (4). Although there are significant differences in these two types of construction, they both exhibit more regular cracking patterns than bridges with reinforced concrete decks constructed by using conventional forms. The combination of (a) shrinkage due to placing a thin layer of fresh concrete on top of a deck panel that has already undergone a major portion of its shrinkage and (b) vertical joints between panels and cast-in-place concrete in regions of high stress (due to traffic) will cause cracking and the cracking will follow a regular pattern. However, extensive research and experience have shown that these systems can be safely used in bridge construction.

The Peace River Bridge on I-75 near Punta Gorda, Florida, was constructed with prestressed girders and composite deck panels. During the construction of the bridge, an unusually large number of cracks were observed in the deck. As pointed out earlier, some cracking is inherent in this type of construction, but the extensive early cracking that was observed caused concern about the possibility of excessively high maintenance costs due to deterioration of the deck with time.

Preliminary studies of the plans for the Peace River Bridge indicated one major difference from details used in other states. On the Peace River Bridge, and other bridge work in Florida, the precast panels are supported, as shown in Figure 1, by fiberboard so that the panels do not have positive bearing on the girders. One series of the Florida panel tests (5) was made without positive bearing for the panels, and satisfactory performance of the panels was observed. However, these test panels had prestressed strands that extended a short distance into the cast-in-place concrete. In addition, these laboratory test specimens were not exposed to temperature, creep, and shrinkage stresses, which aggravate the cracking near the end of the panels under field conditions.

The panels are designed to act compositely with the cast-in-place concrete in resisting live loads and are assumed to act as a continuous slab with negative moment developed in the slab over the girders. The ability of the panels to transfer shear across their ends and provide continuity was questioned due to the observed cracking. Prior research concentrated heavily on demonstrating that adequate bond could be developed between the top of the panels and the cast-in-place topping. Only minimal attention was given to the bond between the end of the panels and the cast-in-place concrete over the girders. The exact mechanism of the shear transfer and the degree of continuity in this region of interfaces between various concretes with creep, shrinkage, and temperature cracks is difficult to predict with any degree of certainty. Thus, a thorough investigation of the Peace River Bridge was warranted.

Figure 1. Typical composite bridge panel construction.

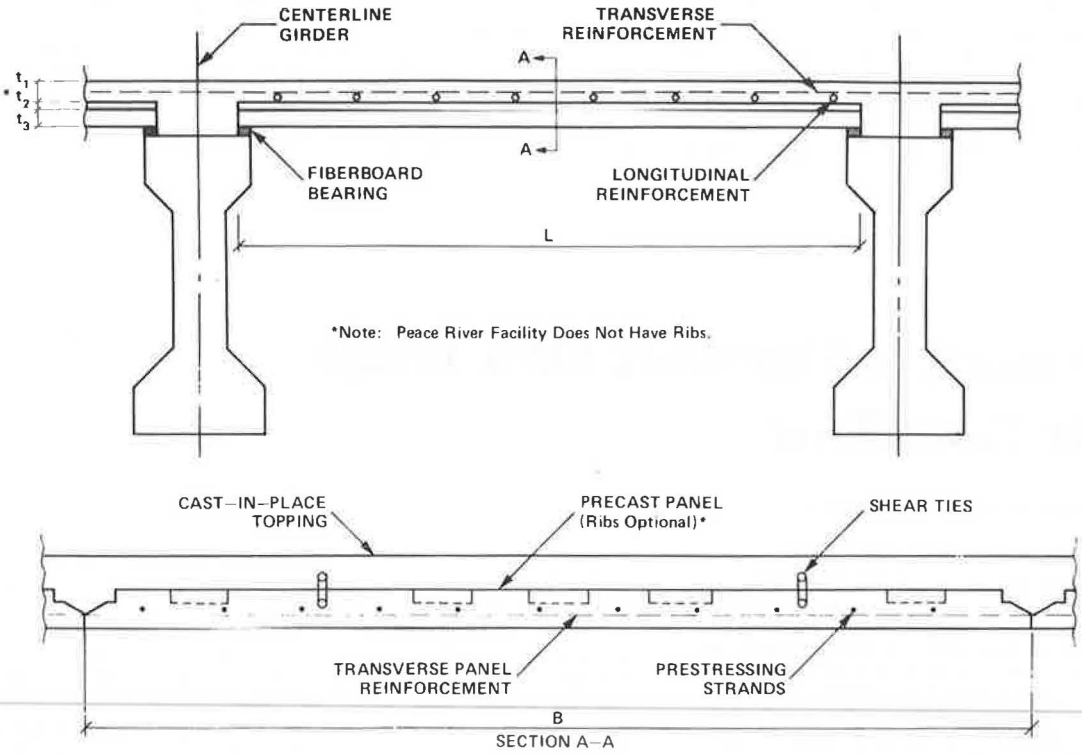

FIELD TESTS

Static and dynamic tests of the Peace River Bridge were made to determine the degree of composite action and structural adequacy of the decks. Tests were performed under three conditions:

1. Present condition--Testing was performed on (a) sections with typical reinforcement used in most areas of the bridge and (b) sections with increased reinforcement.
2. Remedial improvements--The fiberboard under several panels was removed and the void so created was grouted. These panels were later retested.
3. Comparison tests--For comparative purposes, a nearby bridge on I-75 crossing FL-776 was tested. The FL-776 bridge had similar details but shorter panel spans and less extensive cracking.

LABORATORY TESTS

After a preliminary study of the field data, the major area of concern became the shear behavior of the joints at the ends of the precast panels. Thus, a series of laboratory tests was made on slab specimens constructed by using strips sawn out of panels left over from the construction of the Peace River facility. These strips or "beam" specimens were loaded cyclically to study their shear fatigue strength. The results of these beam tests (6), although only applicable in a qualitative way to actual bridge decks, indicated that testing of wider specimens was necessary to determine the shear fatigue life of the Peace River Bridge. Tests are already in progress at the University of Florida to evaluate the shear strength and behavior of wide-slab specimens with joint details similar to those on deck systems of the Peace River type.

FIELD TESTING PROCEDURES

Peace River Bridge

The Peace River Bridge consists of two parallel structures that have a number of simple girder spans between 65 and 105 ft. A Florida Department of Transportation (DOT) water tanker was used for loading the bridges, either hydraulically or as a vehicle load. A data acquisition system was stored in an instrument trailer and used to record deflection and strain measurements. Figure 2 shows the configuration used for most of the tests in which deflection measurements were made by using two wooden gage support beams attached to the center three girders. Two other displacement gages were supported on top of the deck to measure the relative slip across longitudinal cracks.

FL-776 Bridge

The FL-776 Bridge also had two parallel structures. Each FL-776 structure consisted of two simple skewed spans with seven Type IV girders. Girder spans were 108.5 ft, and slabs spanned transversely approximately 4.5 ft between girders. The test layout for the FL-776 Bridge was similar to that described above for the Peace River Bridge.

Test Loadings

Figure 2 shows the truck in position for one of the hydraulic tests with the load in the center of a panel. All figures that show transverse sections of the bridge were drawn facing north. Figure 3 shows the detailed plan location of the loadings. Figure 3a shows the positions of the hydraulic loadings. Loads A, B, C, and D refer to different positions of

the wheel plate (2), whose dimensions are shown in Figure 3b. Two positions are shown for the gage line. The primary gage line was in the longitudinal center of the panel. In most cases the testing pattern was load positions A, C, B, and D with the gages located on the primary gage line. However, for a few of the tests, the test gages were moved to a secondary position 6 in north of the end of the panel and tests C and D were performed for the gages on the adjacent panel.

The hydraulic loads were applied in 8-kip increments up to a maximum load of 32 kips, which is approximately 1.5 times the AASHTO HS-20 design wheel load of 16 kips with an impact factor of 0.3. The hydraulic load was applied by jacking against the water tanker. The jack was centered over the wheel plate and located with respect to the truck axles as shown in Figure 3d.

Figure 3c shows the location of the axle loads for the static and dynamic truck tests. For each static truck test, the three axles were each separately placed over the gage lines. The symbols TA,

Figure 2. Schematic of field test arrangement for Peace River Bridge.

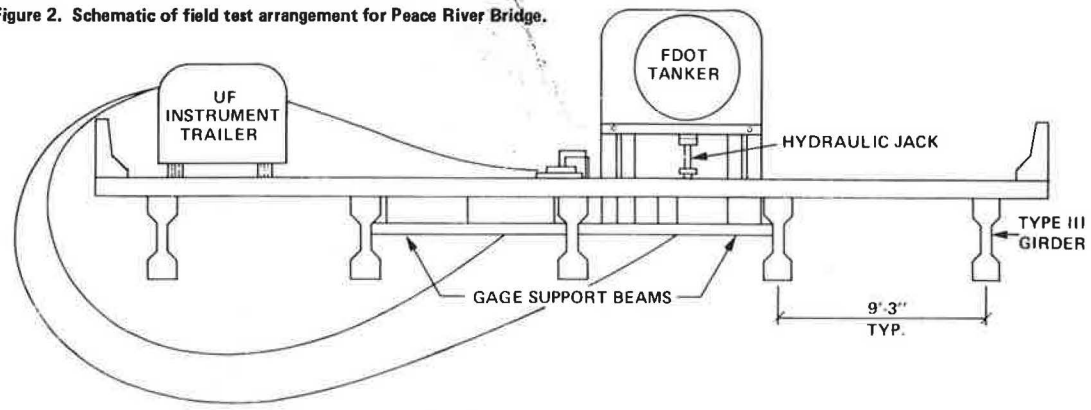

Figure 3. Plan location of loads.

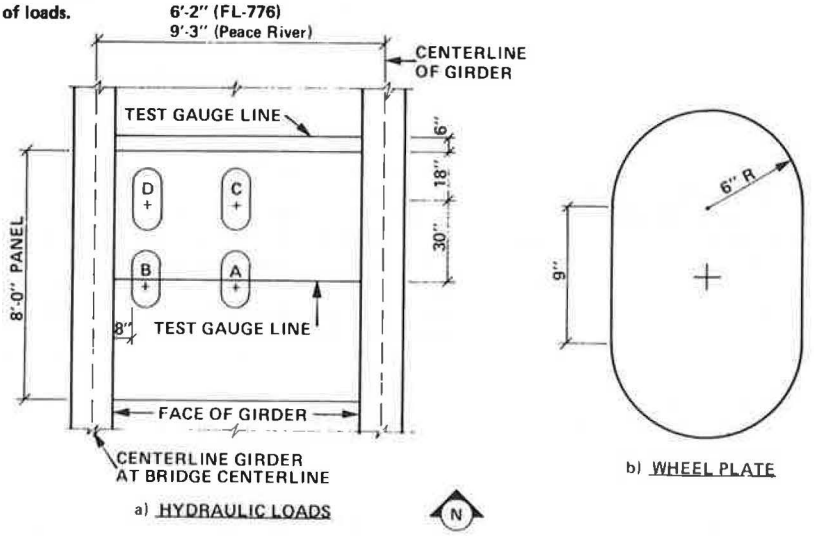

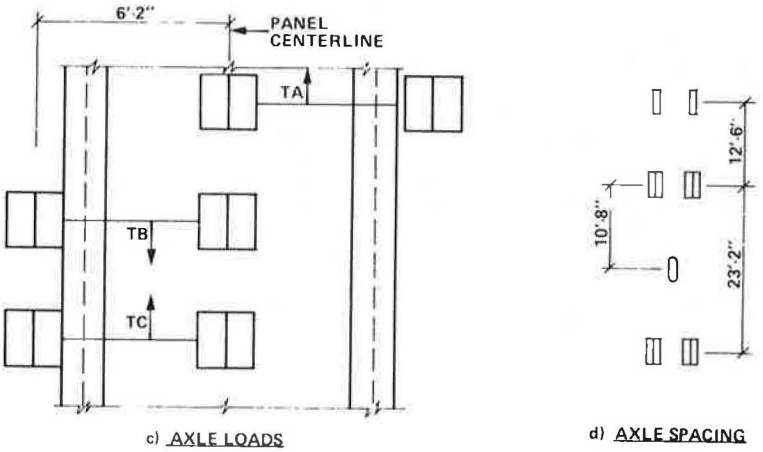

Figure 4. Location plan of gages for span 11R of Peace River Bridge.

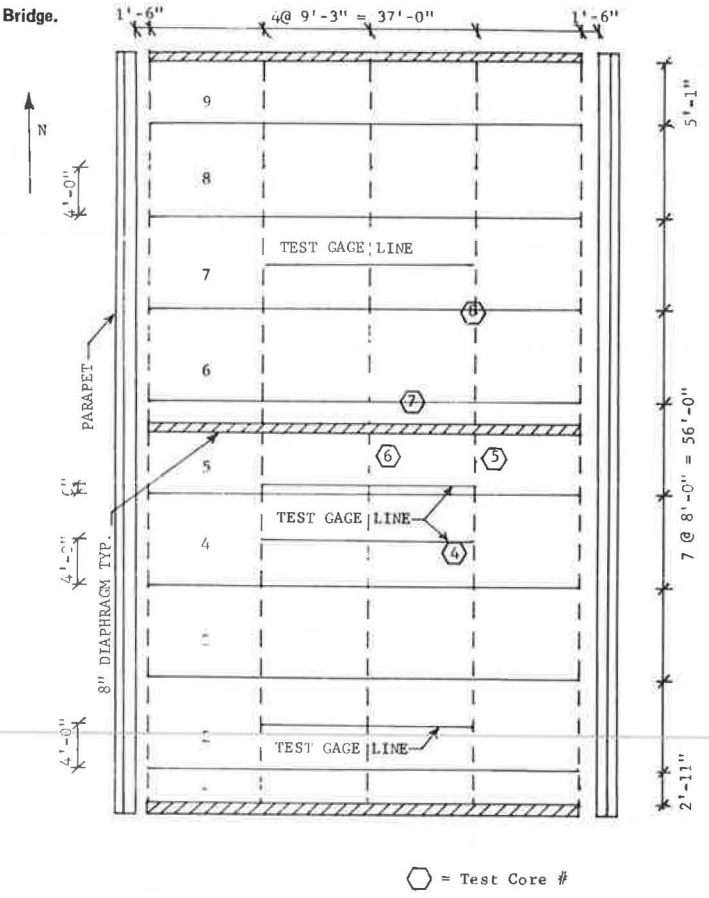

TB, and TC refer to three different orientations of the truck wheels. The arrow shows the direction in which the truck was facing. In the dynamic tests, the transverse position of the wheels was the same as in the corresponding static tests (as closely as could be maintained) and the truck was driven over the bridge at speeds ranging from 5 to 40 mph.

Deflection Gage Locations

Figure 4 shows the plan location of the gage lines for one span of the Peace River Bridge. Deflections were measured by a series of linear variable differential transformers (LVDTs) located on the gage lines previously discussed. An LVDT is an electrical-mechanical transducer that produces an electrical output proportional to the displacement of a separate inner core. One end of a threaded rod attached to the core was connected to a threaded tube that was epoxied to a magnetic block. This block was then attached magnetically to a steel plate that had been epoxied to the bottom of the bridge slab. The plastic LVDT holder was attached to an aluminum bar that was held onto the gage support beam by a C-clamp. Figure 5 shows a section of the gages for the FL-776 Bridge as well as the Peace River Bridge. Wooden end blocks were epoxied to the sides of the prestressed girders. The wooden gage support beams were then connected to the end blocks by dowels. One end of each gage support beam had a circular hole and the other end was slotted. With this configuration, the gage support beams would not restrain the movement of the girders and should have moved as a rigid body during the testing. The gage support beams were made out of plywood and could be adjusted in length to accommodate minor variations in girder spacing.

Gages 1-10 were supported on the gage support beams under the bridge deck. Gages 11 and 12 were supported by a wooden fixture over the girder on top of the deck. The two top gages were located approximately 2 in on either side of the longitudinal crack that ran close to the edge of the girder. The difference in deflection between gages 11 and 12 was therefore a measure of the deformation at the end of the panel.

Strain Gage Locations

Strain gages were also used in some tests and were located along the same gage line as the LVDTs. Figure 6 shows the locations of the strain gages in relation to the girders and the LVDT gages. No strain readings were made on the FL-776 Bridge.

Ground Reference Tests

Due to the large number of spans tested and their precarious locations (generally over water or high above the ground), it was felt that the deflections of the slab relative to the girder would be easier to obtain than absolute deflections measured from the ground. However, some measurements were obtained with LVDT gages attached to scaffolding supported on the ground as means of referring relative measurements to absolute deformations.

Data Acquisition System

The 3052A data acquisition system manufactured by Hewlett Packard consists of a 9825A system controller, a 3495A multiplexer, a 3497A system volt-

Figure 5. Location of LVDT gages.

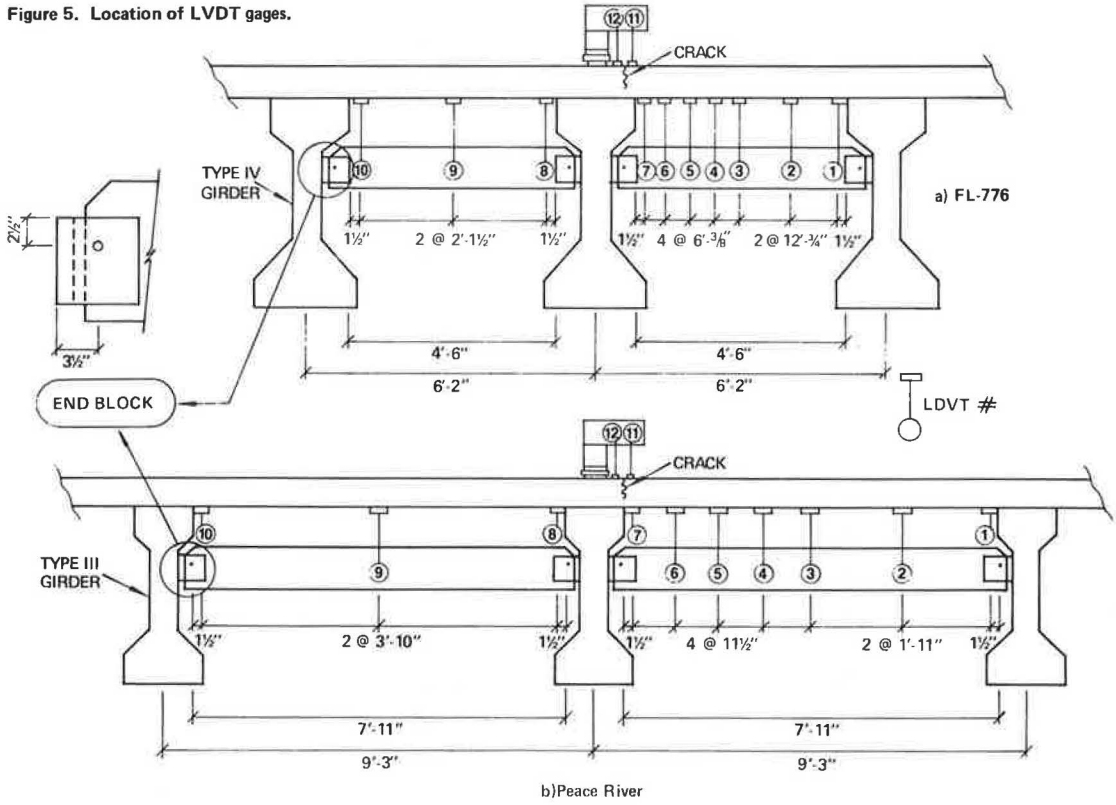

Figure 6. Location of strain gages for Peace River Bridge.

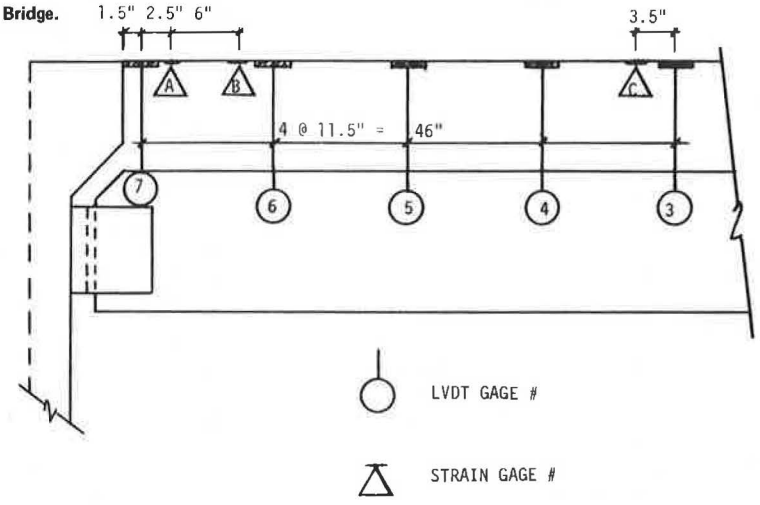

meter, and a 9871A printer-plotter. The 9825A system controller is a 23K desk-top computer that controls and services all peripherals through the HP-IB interface bus. A cassette tape unit and a small thermal printer are built into the 9825A. The 3495A multiplexer is a high-speed scanning device capable of a switching rate of 1000 channels/s. All transducer output signals are received by the 3495A, which relays them to the 3497A voltmeter. The 3497A is a 3.5-digit voltmeter that converts analog signals to digital signals. These signals are then transmitted through the HP-IB to the 9825A for storage and/or reduction. With the 9871A printer-plotter, hard copies of raw or reduced data are obtainable.

Displacements were measured by using Schaevitz LVDTs. Input to the LVDTs consisted of an excitation of ±15 V direct current and a common tied to the ground of the LVDT output signal. The output signals were passed through lowpass filters to reduce noise and alternating current spikes. Each filter consisted of a parallel circuit of two 100-MF capacitors and one 5000-ohm resistor. Each LVDT core was attached to one end of an 8-in-long stainless steel rod. Both input and output cables were approximately 50 ft in length. The input (excitation) cables were three-conductor, 22-gage telephone cables. Output cables were two-conductor, 24-gage microphone cables.

Strains were monitored with either a two-channel Hewlett-Packard 7404A strip chart oscillographic recorder or a BLH 1200B portable strain indicator

Figure 7. Finite element model.

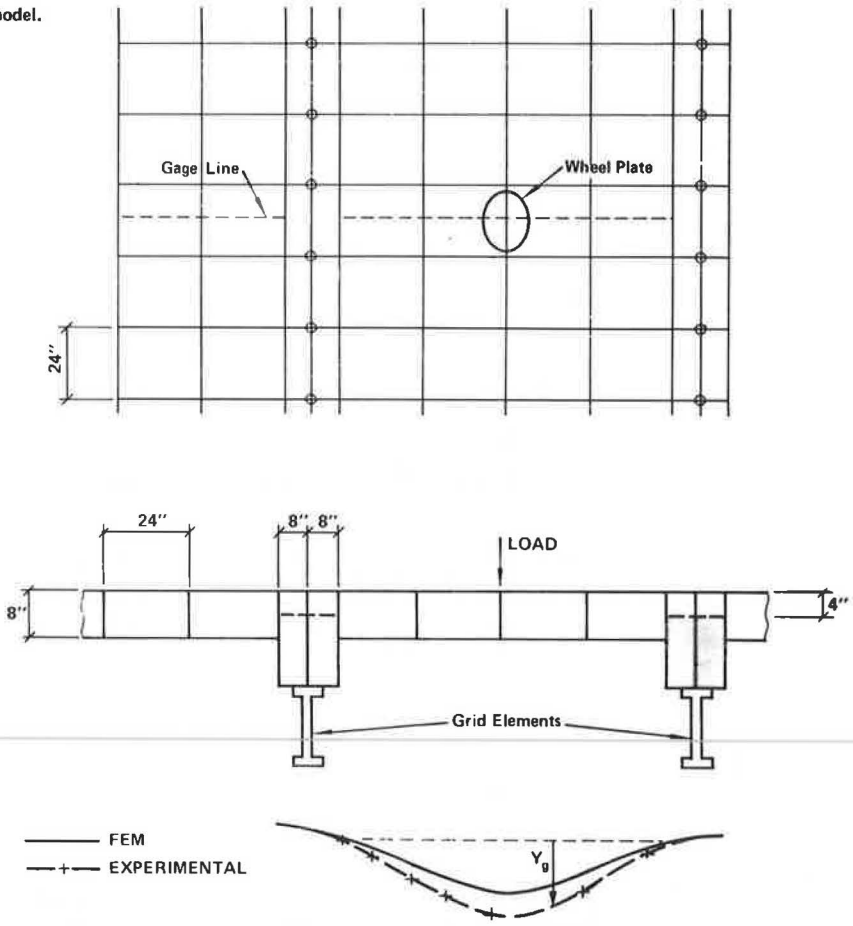

and its accompanying switching and balancing unit (model 1225). A Wheatstone Bridge configuration was used for every active gage with temperature-compensating gages attached to a concrete cylinder maintained under similar environmental conditions as the active gages.

EVALUATION OF FIELD TESTS

Load-Deflection Plots of Hydraulic Tests

Automatic load-deflection plots of all gages for the hydraulic loading tests were made at a small scale to see whether the response to the hydraulic loads was generally linear and to spot any obvious malfunctioning gages. The majority of the load-deflection plots indicated quite linear response.

Transverse Deflection and Moment Profiles

Finite Element Model

In order to have a reference against which to compare the observed data, finite element models were made of the bridges. A given span was modeled as a collection of plate bending and grid (beamlike) elements.

Figure 7 shows a portion of the model for the Peace River Bridge. The pairs of 8-in-wide elements are used over the width of the top flange of the girders. The full model (not shown) has all five girders and a total of 832 plate bending elements. The wider elements were used to represent the slab (precast panel and cast-in-place topping) between girders. An average value of the modulus of elasticity was used for all elements (6).

When the hydraulic load was applied down onto the deck, the reaction to that load was developed by a decrease in the loads on the wheels of the water tanker. These decreases in the wheel loads represent upward loads on the finite element models and were computed by assuming that the trailer acted like a simple beam with supports at the drive wheels and the rear wheels of the trailer unit. This procedure was used because the gages were "zeroed" with the truck in position prior to the application of the hydraulic loads. Because the nearest wheel was approximately 11 ft from the hydraulic load, the upward wheel loads would have almost no effect on the deflections measured relative to the girders but would appreciably affect the absolute deflections of the finite element models.

The thickness of the elements in the vicinity of the girder was increased to account for the torsional stiffness of the girder. This also gives extremely stiff elements (little bending deformation) across the width of the girder. The sum of the moments of inertia of these thickened elements was still below that of the composite girder and slab. Therefore, grid elements were added along the centerline of the girder with moment of inertia such that the combined moment of inertia of the thickened plate and grid elements was equal to that of the composite girder and slab. Grid elements were also used for the diaphragms. If the precast panels and cast-in-place topping were acting as one integral unit, it was felt that the observed results would be in close agreement with those predicted by this finite element model.

When it became apparent that the observed deflections were larger than those from the finite element model and that the field results were indicating

much smaller negative moment than that predicted by the model, a new reduced-thickness model was developed to include the effect of a discontinuity at the ends of the panels. The thickness of the plate elements in the girder region was reduced to 4 in, the thickness of the cast-in-place topping. Both the torsional stiffness and the moment of inertia of the grid elements were increased to the values for the composite girder.

This reduced-thickness (thin element) model clearly does not represent the exact conditions in the deck if bond is lost at the end of the panel. It should not be expected that this thin element model could be used to study the detailed behavior of the joint. It does, however, give deflections and moments that are very close to those observed in the field. This close correspondence is used as substantial evidence that the moments are quite small at the edges of the girder.

Reduction of Field Deflections

Most of the field deflection measurements were made from gages supported on the girders. Thus, these deflections are the deflections of the slab relative to the girder. To make the visual comparison of the theoretical and experimental deflections easier, the theoretical girder deflections were added to the field deflections. Figure 7 shows how this was done. The gage support beam is shown as a dashed line. The deflections from the gage support beam (Y_g) are added to the deflections of the gage support beam at the proper point along the axis. The solid line represents the deflected shape of the slab as predicted by the finite element solution, and the + signs and the dashed line represent the deflected shape observed in the field.

Computation of Experimental Moments

The bending moments in the slab were computed by two procedures outlined by Callis, Fagundo, and Hays (6). First, the deflections along transverse gage lines were numerically differentiated by using the finite difference technique. Second, the measured strains were used to compute the bending moments by assuming linearly elastic response and the flexural stress formula to be valid.

Comparisons of Finite Element Model and Experimental Data

Figure 8 shows the type of behavior exhibited by most of the hydraulic tests of the Peace River Bridge. The analysis made by using the full-continuity model indicates both smaller deflections and positive moments than that based on the field data. Figure 9 shows the same field data as Figure 8 but in comparison with the thin element model. Clearly, the correlation between the model and the experimental data is quite good. This type of behavior indicates that the panels are approaching a simply supported condition.

Figure 10 shows results for a test that had strain gage data as well as deflection data. The correlation between the computed moments based on displacement data and those based on strain gage data is quite good.

Tests for the FL-776 Bridge (6) showed larger negative moments near the face of the girder, which indicated that this bridge was behaving more like a continuous deck.

Comparison of static truck tests generally showed better agreement between the continuous solution and the experimental than did the hydraulic tests. This was probably due to the fact that in the truck test the double wheels spread out the load more than did the single-wheel plate used for the hydraulic tests.

Joint Deformations

Gages 11 and 12 (Figure 5) were mounted on top of the deck directly above the girder and approximately 2 in on either side of the longitudinal crack near the end of a panel. The difference in deflection (Δ) between gages 11 and 12 is a good measure of the deformation at the ends of the panel. Because A and B tests generally gave about equal magnitudes of Δ ($\approx$0.0012-in slip for a 32-kip load), the deformation must be a combination of shearing and flexural deformations. The flexural deformations in this short 4-in length are probably due to the hinging action at the ends of the panels.

The panels on the Peace River Bridge that were retested after being grouted showed smaller joint deformations than in the original tests. The A tests that were repeated showed a 28 percent reduction, and the B tests that were repeated showed a 42 percent reduction. A reasonable conclusion would be that the grouting eliminated essentially all of the joint shearing deformation and had little effect on the flexural deformation. The joint deformations were smaller for spans 31 and 32, which had the extra reinforcement in the cast-in-place topping. Span 31, which had the extra transverse reinforcement, exhibited less joint deformation for the B load, whereas span 32 with the extra longitudinal steel showed a decrease for the A and A + 30 loads. Both of these reductions in joint deformations are encouraging.

CREEP AND SHRINKAGE STUDIES

PCA Method

Precast, prestressed girders are sometimes used to make continuous bridges. The continuity is achieved by supporting simple-span girders on piers, adding continuity steel at the piers, and pouring the deck concrete compositely with the girders. The system then acts continuously to support live load. The major portion of the continuity steel is for negative moment at the piers. However, some positive moment steel is added for live load on adjacent spans and the effects of creep and shrinkage. A Portland Cement Association (PCA) publication (7) has been used to design this positive moment reinforcement.

Calculations based on the PCA method (6) indicated that initially high tension stresses would develop on top of the deck due to shrinkage and would be sufficient to cause cracking either by themselves or in conjunction with load stresses; then, with time, creep in the panels due to prestress would cause a separation of the end of the panel from the cast-in-place concrete.

Core Specimens

Several cores were taken from the Peace River Bridge for the purpose of examining the interface between the ends of the prestressed panels and the cast-in-place topping. Prior to these coring operations, epoxy grout was pumped into the cracks around the coring locations by a contractor selected by the Florida DOT. This was done in an attempt to prevent the coring operation from possibly increasing the panel-topping interface separation. After the cores had been examined and photographed, two cores were sawn apart along the transverse panel-topping interface so that the effectiveness of the grouting operation could be examined. Neither of these two

cores showed much grout penetration into the interface region. However, several of the other cores showed that the grout reached the interface and in a few instances completely filled up the crack. The separation at the ends of the panel was approximately the same for the cores with epoxy penetration as for those without penetration. In addition, cores taken at the ends of the panels from a laboratory

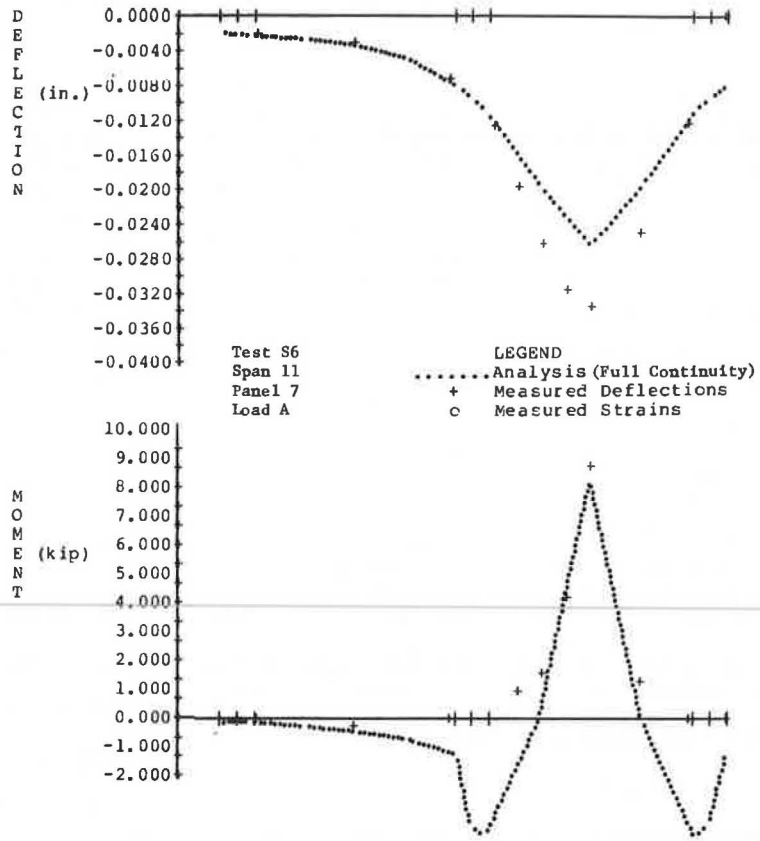

Figure 8. Deflection and moment profiles from test S6.

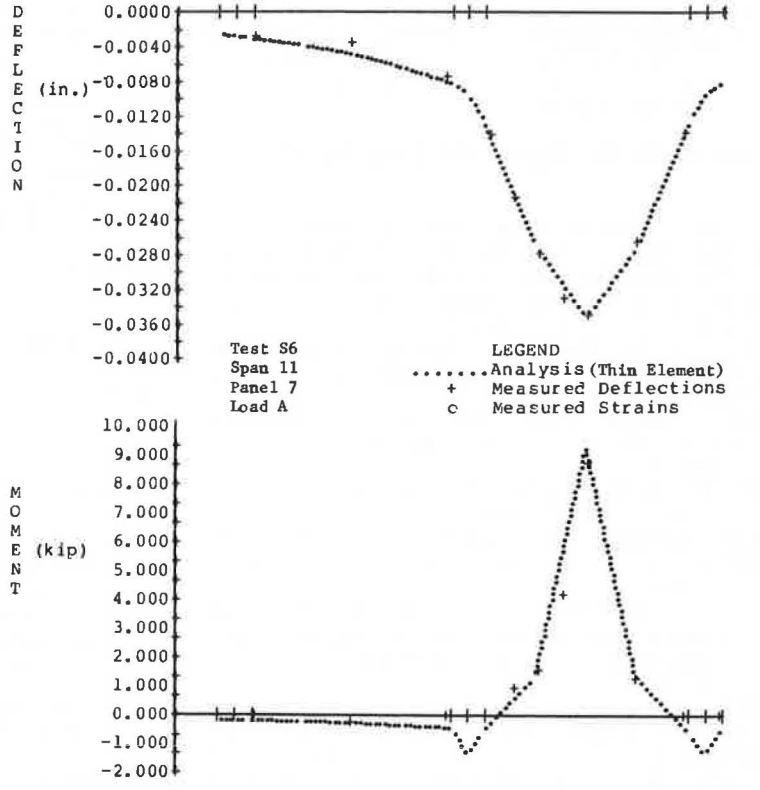

Figure 9. Deflection and moment profiles from test S6 (thin element).

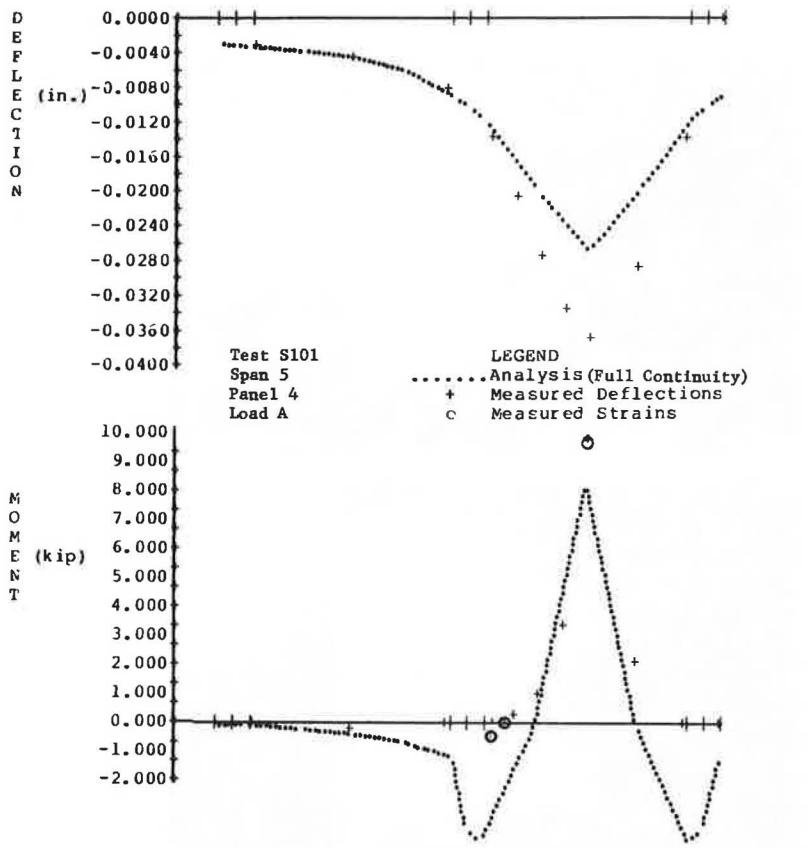

Figure 10. Deflection and moment profiles from test S101.

specimen (6) did not exhibit any separation in spite of the coring operation, which was similar to the field coring procedure except that no epoxy grouting was done. Thus, it is felt that the coring operation does not significantly affect the separation of the panel-topping interface. It should also be noted that the bottom portions of the cores completely separated once the topping was sawed off, which indicated very little bond on the end of the panels.

The photograph at the top of Figure 11 shows core 1. The separation at the end of the panel is about 0.01 in. The lower photograph shows core 3, which had essentially full penetration by the epoxy grout. The thickness of the epoxy appears to be about 0.01 in. The thicknesses of the topping of cores 1 and 3 are only 3.5 and 3.25 in, respectively. However, all of the other cores taken from the Peace River Bridge had at least a 4-in topping. It should also be noted that both cores 1 and 3 had hairline cracks extending about 1 in up the panel-topping interface. The fact that these cracks passed through both paste and aggregate indicated that the crack occurred after the topping had cured.

SUMMARY

An investigation of the Peace River Bridge was conducted in response to reports of extensive cracking in the deck of the facility. This investigation involved testing of the Peace River Bridge and a nearby structure, analytic modeling using the finite element method, and limited laboratory testing of "beam" specimens constructed with panels similar to those used in the Peace River Bridge. Close cooperation between the University of Florida and Florida DOT personnel was maintained throughout the investigation.

The investigation clearly indicates that the behavior of the Peace River Bridge deck is more like that of simple spans than that of continuous ones. This behavior is indicated by comparisons of the field tests and predictions made by using finite element models.

The lack of continuity causes positive flexural stresses near midpanel that are higher than for conventional decks. Analyses indicate, however, that these stresses are within allowable limits. Consequently, this effect of the loss of continuity is not serious. Unfortunately, the loss of bond at the ends of the panels and the corresponding separation of the ends of the panels from the cast-in-place concrete over the girders mean that the shear (in the deck at the face of the girder) must be carried essentially by the cast-in-place topping. This separation has been confirmed by cores taken from the Peace River Bridge and a comparison of the joint deformations measured in the field with the joint deformations of a laboratory specimen (6) that had an artificial bond breaker inserted at the end of the panel.

Creep and shrinkage studies indicate that the most probable cause of the separation of the ends of the panels and the cast-in-place concrete is creep of the panels under the action of the prestress.

The decks that had more transverse and longitudinal steel in the topping concrete than the normal decks exhibited both smaller overall deflections and smaller joint deformations than the decks that had regular reinforcement. This reduction could indicate that the separation of the ends of the panels from the cast-in-place concrete has been diminished and consequently the shear fatigue life would be improved. It is not felt, however, that extra reinforcement is a satisfactory substitute for positive bearing at the ends of the panels.

It appears, based on the relatively few tests of the FL-776 bridge, that this bridge deck slab was

Figure 11. Peace River cores: (top) core 1 and (bottom) core 3.

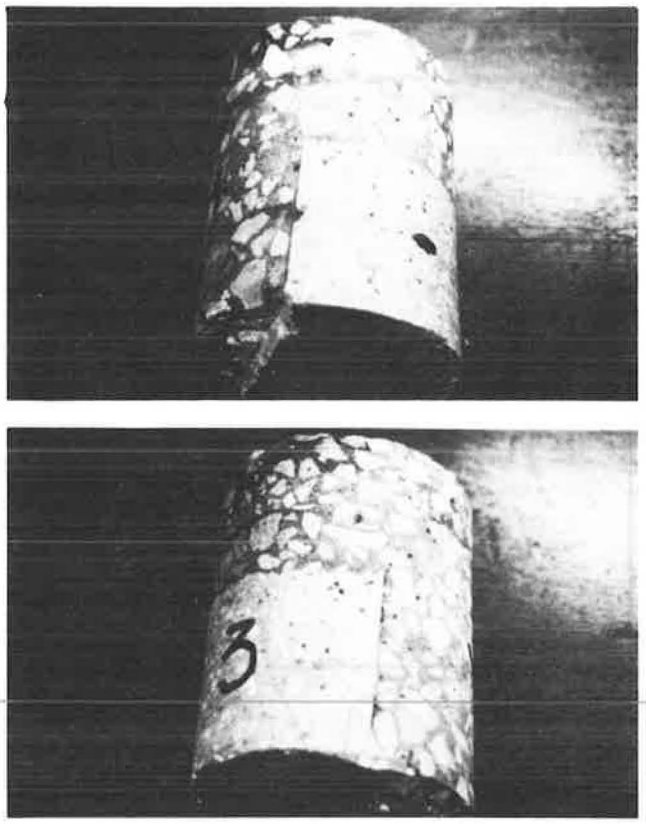

acting more like a continuous system than the Peace River Bridge deck slab. Because the amount of separation at the ends of the panels is a function of the panel length, the more continuous behavior of the FL-776 bridge is at least partly due to its shorter panel length. Shorter panels are likely to have less prestressing and thus less creep than longer ones. It is very difficult to predict whether this higher degree of continuity will be maintained for the FL-776 facility, particularly since under some load conditions positive moments will be developed at the ends of the panels. However, it appears that panel bridges with deck spans shorter than that of the Peace River Bridge will probably have longer fatigue lives.

CONCLUSIONS

The following conclusions have been made based on the research presented in this paper:

1. The two decks in their present cracked condition are structurally adequate to carry normal traffic. In spite of the simple action of the decks, flexural stresses are not excessive.
2. The shear stresses in the Peace River Bridge are substantially higher than those of conventional bridge decks or panel bridges with positive bearing at the ends of the panels. Because of this, the fatigue life of the Peace River Bridge deck is substantially less than that of conventional bridge decks or panel bridges with positive bearing at the ends of the panels. However, studies are under way that involve extensive field coring of bridges built with details similar to the Peace River facility and laboratory testing to destruction of wide deck specimens. Preliminary studies of this work indicate that, although panel bridges built without positive bearing may exhibit increased cracking and some spalling with time, the punching shear strength is sufficient to prevent structural shear fatigue failures under normal traffic loads.
3. The observed cracking on the top of the deck is probably primarily due to volume changes brought about by differential shrinkage between the panels and the cast-in-place topping. However, temperature changes and live load stresses certainly increase the tensile stresses and the degree of cracking.
4. Adding extra transverse or longitudinal steel is not felt to be sufficient to ensure adequate fatigue life of panel bridges.
5. Removing the fiberboard and replacing it with mortar would greatly increase the fatigue life expectancy of the Peace River Bridge. Whether this action is economically justifiable depends on further studies of the shear fatigue behavior of the bridge under way at the University of Florida.
6. Future panel construction projects should include a detail that provides positive bearing for the panels. Strand extensions may also be useful.

ACKNOWLEDGMENT

We would like to acknowledge the Florida DOT and the Federal Highway Administration for their financial support of the research on which this paper is based.

The opinions, findings, and conclusions presented are ours and not necessarily those of the Florida DOT or the Federal Highway Administration.

REFERENCES

1. Standard Specifications for Highway Bridges, 12th ed. AASHTO, Washington, DC, 1977.
2. C.O. Hays, Jr., R.L. Cox, and G.O. Obranic, Jr. Full Span Form Panels for Short Highway Bridges. Department of Civil Engineering, Engineering and Industrial Experiment Station, Univ. of Florida, Gainesville, Final Rept. U17F, Sept. 1980.
3. C.D. Buckner and H.T. Turner. Performance Tests of Full Span Panel Form Bridges. Division of Engineering Research, Louisiana State Univ., Baton Rouge, Aug. 1981.
4. L.A. Bieschke and R.E. Klingner. The Effect of Transverse Strand Extensions on the Behavior of Precast Prestressed Panel Bridges. Center for Transportation Research, Univ. of Texas at Austin, Res. Rept. 303-1F, Dec. 1981.
5. R.W. Kluge and H.A. Sawyer. Interacting Pretensioned Concrete Form Panels for Bridge Decks. Department of Civil Engineering, Engineering and Industrial Experiment Station, Univ. of Florida, Gainesville, Final Rept. D610-635F, Dec. 1974.
6. E.G. Callis, F.E. Fagundo, and C.O. Hays, Jr. Study of Cracking of I-75 Composite Deck Bridge over Peace River. Department of Civil Engineering, Univ. of Florida, Gainesville, Final Rept. U49F, July 1982.
7. Design of Continuous Highway Bridges with Precast, Prestressed Concrete Girders. Portland Cement Assn., Skokie, IL, Engineering Bull. 014.01E, Aug. 1969.

Publication of this paper sponsored by Committee on Concrete Bridges.

Performance of Full-Span Panel-Form Bridges Under Repetitive Loading

C. DALE BUCKNER AND H.T. TURNER

An experimental program to determine the effects of repetitive loading on the serviceability and strength of composite panel form bridges is described. Six simply supported bridge decks were tested. The specimens consisted of three precast, pretensioned panels spanning in the direction of traffic and composite with a cast-in-place topping slab. Bond between the topping slab and the roughened interface surfaces of the panels provided the only means of shear connection. Items considered in the study include the topping slab thickness, panel joint type (flat or beveled-edge), and the effect of longitudinal cracks in the topping slab. The specimens were loaded repetitively with 2 million cycles of design load (HS20-44 axle load with allowance for impact). The loading arrangement was such that maximum transverse shear and longitudinal bending stresses were produced during each cycle. Performance was evaluated primarily on the basis of flexural rigidity, differential deflection between panels, and the strength and ductility of the composite system. Several states have constructed bridges by using precast panels as full-span stay-in-place forms. Many of these bridges have developed longitudinal cracks in the topping slab over the panel joints. The study indicates that cracks of this type do not have a detrimental effect on the strength and serviceability of the bridge deck for the expected repetitive loading.

The number of highway bridges in the United States currently in need of replacement has been estimated to be in the tens of thousands. This need, coupled with increasing construction costs, has intensified the search for more economical bridge systems.

One recent development in bridge construction is the use of precast panels as stay-in-place forms for the bridge deck. Most of the applications of these panels have been for short spans in which the panels span transverse to the roadway and are supported by the girders. The panels serve initially to support the weight of a cast-in-place topping slab. After the slab hardens, the panels act compositely with it to resist traffic loads. Adequate performance of this system has been demonstrated in several research programs and by approximately 20 years of use in actual bridges (1).

Tests of short-span precast-form panels for use in highway bridge decks have been conducted in Florida (2), Pennsylvania (3), and Texas (4). The results of these tests have been summarized in a state-of-the-art report by Barker (5). Based on these tests and the performance of panels in actual bridges, design criteria were developed for stay-in-place precast panels (5). These have been incorporated in the latest American Association of State Highway and Transportation Officials (AASHTO) specifications (6).

Based on the satisfactory performance of the short-span stay-in-place panels, at least two states, Florida and Louisiana, have constructed bridges by using precast panels as full-span stay-in-place forms. These bridges are constructed with the panels spanning parallel to traffic and supported either by abutments or pile bents.

Many of the bridges built in this way have developed cracks in the topping slab approximately over the longitudinal joint between panels. These cracks are believed to be initiated by stresses induced by the drying shrinkage of the topping slab. Cracks of this type were detected in bridges built in Louisiana shortly after they were opened to traffic, and similar cracks have been documented for several recently constructed bridges in Florida (7).

Hays, Cox, and Obranic (7) have performed extensive numerical and experimental studies of the static behavior of full-span panel-form bridges. These studies involved both prototype bridges, which had been in service for periods of up to three years, and half-scale laboratory specimens. Both flat and ribbed form panels were considered in the studies.

It was concluded from these studies that the AASHTO effective width criterion for a one-way slab provides a reasonable and conservative estimate of the effective width of the composite panel-form deck. Finite element studies were performed that indicated that transverse bending moments caused tension in the bottom of the cast-in-place topping and predicted better performance from the ribbed than from flat panel decks. The authors recommended a panel that would result in a thickened topping slab with supplementary U-bar reinforcement over the joints between panels.

The formation of cracks in the topping slab so soon after the bridges were built has caused concern among some bridge designers. They perceive a need to verify and refine the design criteria for the full-span panel-form bridges under controlled laboratory conditions. The experimental program described in this paper was performed to fulfill these objectives.

The program involved testing six simply supported composite decks for 2 million cycles of service load and following this with a test to failure. Loads were applied so as to produce maximum transverse shear stresses in the topping slab under an HS20-44 design load.

The items considered in the study included the topping slab thickness, panel joint type (flat or beveled), and the effect of longitudinal cracks in the topping slab. Performance was evaluated primarily on the basis of the flexural rigidity of the deck, the differential deflection between adjacent panels, and the strength and ductility of the composite deck. Visible cracks in the concrete, slip of prestressing strands, and strains in transverse steel were also considered in evaluating the specimens.

DESCRIPTION OF SPECIMENS

Six simply supported composite specimens were constructed. Each specimen had an overall thickness of 13 in, an overall width of 125 in, and a span length of 20 ft.

The thicknesses of the precast panels and the cast-in-place topping slab were varied, while a constant overall thickness of 13 in was maintained. One set of two specimens was constructed of panels 5.5 in thick with a complementary topping slab thickness of 7.5 in. The 5.5-in thickness was established as a lower bound for an unshored panel on a 20-ft simple span. Two specimens were constructed of 10-in-thick panels with 3-in topping slabs. The 3-in thickness was selected as a lower bound for the topping slab to allow for a minimum cover of 2 in. A slab of this thickness would probably not be considered a practical minimum when tolerances in precast dimensions and differential cambers are considered. It is believed that the satisfactory behavior of the upper- and lower-bound thicknesses will indicate satisfactory behavior for similarly

Figure 1. Details of test specimens.

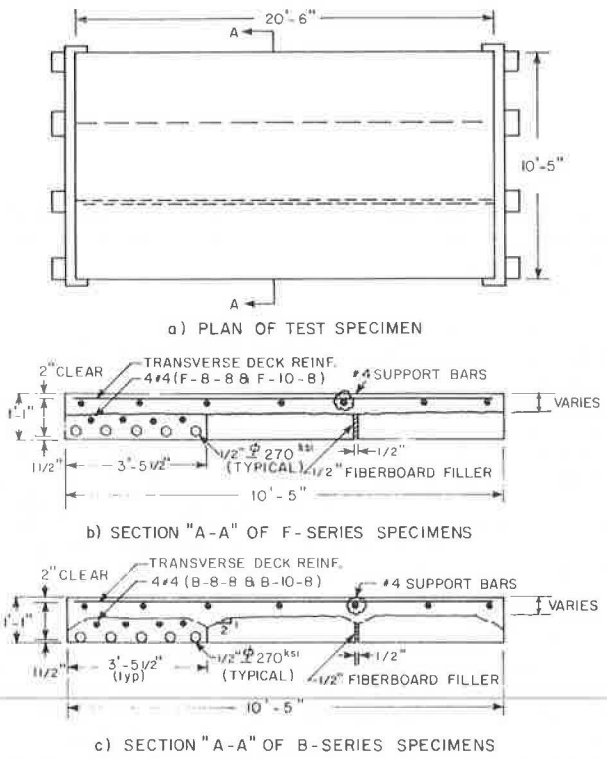

designed specimens of intermediate thickness.

Two specimens with 8-in panel thickness and 5-in topping were also tested. These specimens were used to study the effect of longitudinal cracks in the topping slab on the behavior of the composite decks.

For each set of specimens of a particular panel thickness, one was constructed by using flat precast panels and one had beveled edges, as shown in Figure 1. It was thought that the composite decks constructed with beveled panels might perform better than those with flat panels due to improved shear transfer between panels.

Each specimen was constructed of three panels 3 ft, 5.5 in wide. One of the longitudinal joints between panels had a 0.5-in gap filled with fiberboard to minimize shear transfer by friction and to allow more freedom for transverse shrinkage. The other joint was a tight butt joint, which is the usual construction procedure.

Details of the test specimens are shown in Figure 1. Test specimens are identified by a symbol of the form F-n_1-n_2 or B-n_1-n_2. The letters F and B refer to flat and beveled panels, respectively; n_1 is the overall panel thickness and n_2 is the number of 0.5-in-diameter, 270-ksi strands per panel.

Design of Specimens

The test specimens were designed as a one-way slab with an effective width for distribution of wheel loads computed in accordance with the 1977 AASHTO specifications (6). The design live load was the HS20-44 highway loading. The effects of this loading were increased by 30 percent to allow for impact, in accordance with AASHTO.

Complete composite action was assumed between the panels and the cast-in-place slab. Design was based on normal-weight concrete with specified compressive strengths of 5000 psi in the precast and 4200 psi in the cast-in-place topping.

The computed stresses in the specimen at various loading stages are summarized in Table 1. These stresses were computed based on the transformed concrete section but neglecting the transformed steel areas. Sample calculations for these stresses are included in the final report of the study (8).

Manufacture of Precast Panels

The precast concrete panels were manufactured by Biloxi Prestress Concrete Company of Biloxi, Mississippi. The long-line production system was used with all 8-strand panels cast on one line and all 10-strand panels cast on another.

The beveled edges of the B-series panels were rough-shaped by using an appropriate screed and then hand-floated to yield an acceptable shape. At the approximate time of initial set, the top and beveled surfaces of each panel were raked transversely to depths of approximately 0.125 in.

The panels were steam-cured for 12 h, at which time control cylinders indicated a compressive strength in excess of 4000 psi. The panels were stored at the prestress plant until the control cylinders had reached a compressive strength in excess of 5000 psi. The panels were then shipped to Louisiana State University, unloaded, and stored outside until they were moved inside the laboratory for construction of the test specimens.

Construction of Specimens

The precast panels were moved into the laboratory and set over concrete support beams as indicated in Figure 1. After the panels had been placed and aligned, the support beams were shimmed so that the soffits of the panels were bearing accurately at 25 in above datum. The panels were cambered due to the prestress force and therefore were 0.25-0.5 in higher near midspan. Differential camber between adjacent panels was less than 0.125 in in all specimens.

Formwork for the cast-in-place topping slab was then erected. The elevation of the formwork was adjusted by shimming the base so that the top edge was 38 in above datum. The top edge of the formwork supported a steel angle that was used to screed the concrete after it was placed.

Steel reinforcement for the topping slab was placed and supported so that there was 2-in cover from the top of the transverse steel to the top surface. Lifting loops, which were embedded in the top of the precast panels, were burned off to eliminate mechanical shear connection between the precast and cast-in-place concrete. Formwork and reinforcement for a typical specimen are shown in Figure 2.

Approximately 15 min before concrete was to be placed, the top of the panels was saturated with water (water puddled in low spots and in scratch marks on the panel). The panels were then air-blasted until all free water was removed. The surface was still wet when concrete placement began.

Concrete was discharged directly from the truck onto the panels and consolidated by vibration. The top was screeded and finished with a float. The specimen was then covered with polyethylene sheet for curing.

Four of the specimens (B-5.5-10, B-10-8, F-5.5-10, and F-10-8) were cured under plastic for seven days and then exposed to air. None of these specimens developed visible shrinkage cracks on the top surface. The temperature and relative humidity of the air in the vicinity of the specimen were recorded during the curing period by using a hygrothermograph. The mean and range of these values are documented (8).

Table 1. Summary of computed design stresses.

Specimen	At Transfer of Prestress[a]						Service Load (Dead + Live + Impact) at Midspan[b]				Stress Range (Live + Impact) at Midspan (psi)	
	2 ft from Ends			At Midspan				Stress (psi)				
	Prestress Force (kips)	Stress (psi)		Prestress Force (kips)	Stress (psi)		Prestress Force (kips)	Bottom	Top Panel	Top Slab	Horizontal Shear at Interface	Prestress Strands
		Bottom	Top		Bottom	Top						
F-5.5-10	260	2132	142	261	1712	578	220	-319	1426	695	19	3700
B-5.5-10	259	2121	223	261	1701	701	220	-433	1676	695	19	3700
F-8-8	212	1541	-268	213	1256	28	176	-61	583	695	18	3700
B-8-8	212	1576	-297	213	1291	43	176	-116	750	695	18	3700
F-10-8	213	1377	-351	214	1147	-115	176	40	492	686	13	3700
B-10-8	212	1420	-437	213	1187	-141	176	13	584	686	13	3700

[a] Assuming strands initially stressed to 189 ksi and 24 h of relaxation prior to release.
[b] Assuming total prestress loss of 45 ksi prior to placing topping slab; based on gross transformed area of concrete.

Figure 2. Formwork and reinforcement for topping slab.

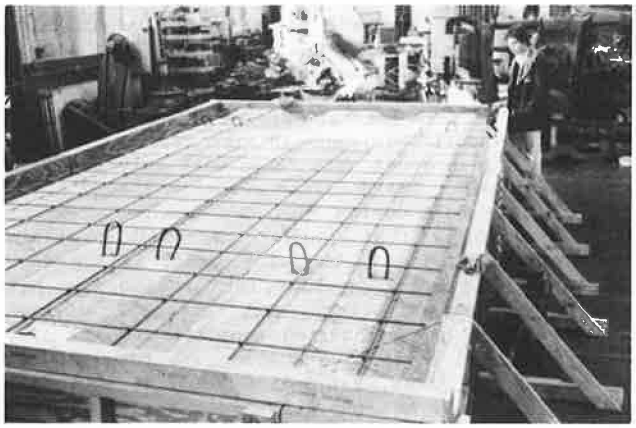

It was not practical to cure the specimens until all potential drying shrinkage had occurred. Thus, although there were no visible longitudinal cracks of the type that have been primarily attributed to shrinkage in prototype bridges, there is no assurance that such cracks would not have occurred in the specimens eventually.

As a measure of potential shrinkage, three volume-change prisms, conforming to ASTM C341, were cast for each specimen. These prisms were cured with the specimen and used to measure the unrestrained drying shrinkage that occurred during the curing period. The measurements indicated shrinkage at time of test of about one-half the ultimate value expected for the class of concrete.

Two of the specimens (B-8-8 and F-8-8) were cured under plastic for only 48 h and then exposed to air. The shorter curing time was intended to simulate the relatively poor curing conditions that are likely to occur in real bridges. In each of these specimens a longitudinal crack was induced in the topping slab approximately over the joint that contained the 0.5-in-wide fiberboard-filled gap. This crack was induced by holding down the outside edge of the deck and jacking up on the panel soffit along the joint. This produced a fine flexural crack that was visible in the top surface along the entire length of the deck. A chalk line was snapped on the top surface above the longitudinal joint. The crack meandered across this line several times and deviated from the line by less than 2 in at all points.

Six locations, at approximately 3-ft intervals along the crack, were monitored for crack width growth. Locations were selected where the crack approximately paralleled the chalk line. The width was measured by using a direct reading microscope graduated to 0.01 mm.

Material Properties

The materials used in the test decks were specified to conform to the standard specifications of the Louisiana Department of Transportation and Development (9).

The concrete in the precast panels was specified as air-entrained, normal weight, with minimum cement content of 6.5 sacks/yd^3, compressive strength of 5000 psi, and air content in the range of 3-7 percent by volume. The concrete was placed with a slump of approximately 3 in. Twenty-one 6-in-diameter by 12-in cylinders were cast with the panels. Three of these were cured under standard conditions and tested at age 28 days. The remaining cylinders were cured with the panels and tested on the day that the topping slab was cast.

The concrete for the cast-in-place topping slab was air-entrained, of normal weight, with specified cement content of 6.5 sacks/yd^3, compressive strength of 4200 psi, and air content 3-7 percent by volume. The concrete was placed with a slump of 3-5 in. Nine 6-in-diameter by 12-in cylinders and three 3x3x11-in volume-change prisms were cast with each pour. Three of the cylinders were cured under standard conditions and tested at age 28 days. Six of the cylinders were cured with the deck. Three of these were tested on the day that repetitive loading began, and three were tested on the day that ultimate loading was performed. The results of the tests for both the panels and the topping slab are summarized in the study final report (8).

The prestressing strand was specified to be 0.5-in-diameter, uncoated, seven-wire strand conforming to ASTM A416 Grade 270K. Mild steel reinforcement was specified as ASTM A615 Grade 60K.

EXPERIMENTAL PROGRAM

The test specimens were loaded 2 million times with a cyclic load to simulate the stresses expected during the life of an actual bridge. The performance criteria used to evaluate the deck were the flexural rigidity of the composite unit, the differential deflection between adjacent precast panels, strains in transverse reinforcing bars, slip of the prestressing strands, visible cracks in the concrete, and the strength and ductility of the composite deck.

Loading Arrangement

In most previous studies that have involved repetitive loads on simple-span bridges, the loads have

Figure 3. Test equipment.

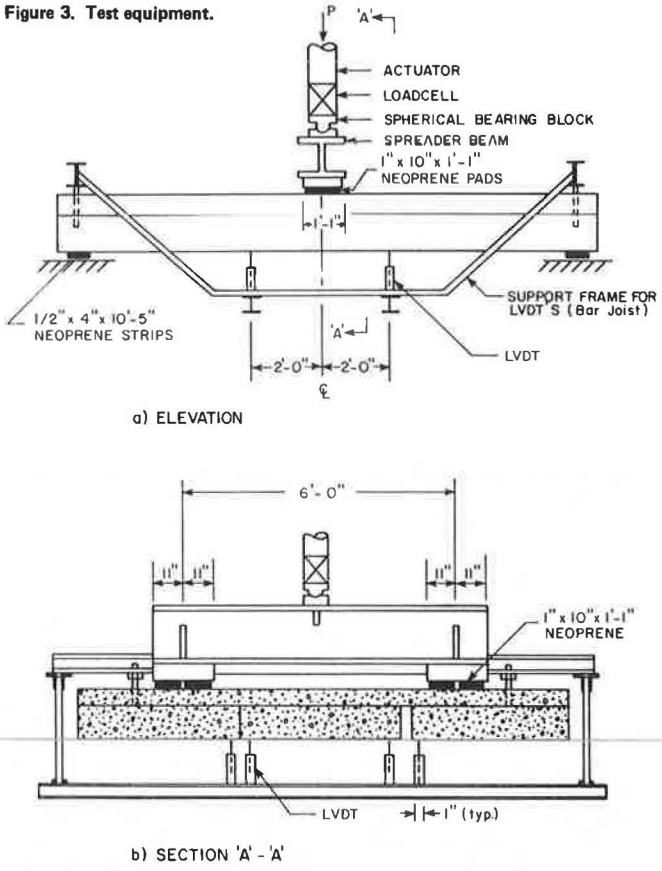

been applied as a series of concentrated loads positioned to approximate the moment envelope. Because a primary consideration in this study is the shear transfer across the joint between panels, it was decided that a better loading arrangement would be a single concentrated load applied at midspan. This arrangement creates maximum shear stress at the longitudinal joint and maximum bending stress at the critical (midspan) section during each cycle.

The load was applied by an actuator controlled by an Instron Series 2150 servohydraulic system. The concentrated load was spread into two "wheel" loads and applied to the slab through 1-in-thick neoprene bearing pads that were sized and positioned to simulate tire prints. The arrangement for the loading is shown in Figure 3.

With the load applied through the spreader beam, approximately one-third of a wheel load is transferred across each longitudinal joint into the middle panel. This yields a reasonable approximation to the maximum shear transfer that would occur in an actual bridge.

Instrumentation

Vertical deflections were measured at transverse sections located 2 ft on each side of the span centerline, as indicated in Figure 3. Four Schaevitz linear variable differential transformers (LVDTs) with a range of ±1 in were positioned at each transverse section. Data from the LVDT units were recorded with the aid of a multichannel data logger.

Strain gages were mounted in a half-bridge on two transverse bars in each cast-in-place topping slab. The active bridge arms were approximately over the longitudinal joints between the precast sections. The bars were approximately above the location where the LVDTs were mounted. Strain readings were obtained with the aid of a Vishay-Ellis switch and balance unit with a digital indicator.

Strand slip was measured by using a caliper with dial gage graduated to 0.001 in. Metal tabs were epoxied to the strands and to the end of the panel approximately 0.5 in above the strand to serve as reference points for these measurements. Two strands on each end of every panel were monitored in this fashion.

Test Procedure

Application of repetitive loads began when the concrete in the topping slab had reached an age of 32 days. The design load, including the allowance for impact, is 41.6 kips. The spreader beam and bearing blocks produced a tare of approximately 1.5 kips. To prevent separation between the actuator and the bearing block, an additional 1.5-kip load was maintained; thus, the repetitive load was varied between 3 and 41.6 kips. The repetitive load was applied at a rate of 500 000 cycles per 48 h (2.89 Hz). This rate was such that dynamic stresses were negligible, and it yielded a convenient stopping time for intermediate static tests that were performed after each 500 000 cycles.

Initial measurement of strand slip and crack width (when applicable) and initial readings of the LVDTs and strain gages were taken with only the tare on the specimen. The specimen was then loaded statically to the full design load, and the measurements were repeated at that load. Intermediate static tests were performed in the same manner as the initial static test except that strand slip was not measured until the final test after 2 million cycles. These tests required approximately 10 min, after which the repetitive loading was resumed. In two of the specimens, F-5.5-10 and B-8-8, equipment breakdowns caused an interruption in the repetitive loading. For specimen F-5.5-10, this interruption occurred after approximately 1.3 million cycles were applied and lasted for two days; for specimen B-8-8, it occurred after approximately 1.8 million cycles and lasted for three days. Otherwise, the repetitive loading was applied continuously except for the brief interruptions for the static tests.

The specimen was then loaded to failure. This loading was applied in increments of 10 kips but was reduced to 5-kip increments near ultimate. The LVDT readings were recorded after each load increment.

TEST RESULTS

The measured structural performance of the composite decks was satisfactory in all six specimens tested. There was no evidence of fatigue in either concrete or reinforcement or of deterioration of composite action, shear transfer strength, or bond during the cyclic loading. Generally, the LVDT readings indicated a slight increase in panel stiffness during the test period. This increase can be attributed to the small increase in modulus of elasticity of the concrete due to cement hydration during this period.

The specimens were loaded to failure after 2 million cycles of design load. Primary failure in every specimen was in flexure by yielding of the reinforcement. Secondary failures were either by crushing of concrete or in a shear mode. The measured loads at secondary failure were in all cases above the computed ultimate load and occurred after the specimen had demonstrated adequate ductility.

The behavior of the test specimens and the analysis of the test data are described below.

Primary Performance Criteria

The performance of the test specimens was evaluated

Table 2. Deflection readings at LVDT locations.

Specimen	Avg Initial Deflection (in)	Avg Deflection/Avg Initial Deflection by No. of Cycles				Maximum Ratio Differential Deflections by No. of Cycles				
		0.5×10^6	1×10^6	1.5×10^6	2×10^6	0	0.5×10^6	1×10^6	1.5×10^6	2×10^6
B-5.5-10	0.0739	0.995	0.980	0.946	0.946	1.08	1.08	1.08	1.08	1.07
F-5.5-10	0.0682	0.970	0.994	N.A.	0.990	1.04	1.03	1.04	N.A.	1.06
B-8-8	0.0926	0.975	0.966	0.966	0.950	1.02	1.02	1.03	1.03	1.03
F-8-8	0.0842	1.000	1.002	1.003	1.017	1.02	1.02	1.02	1.02	1.02
B-10-8	0.0780	0.949	0.933	0.932	0.946	1.02	1.03	1.02	1.03	1.04
F-10-8	0.0746	1.005	0.996	1.006	0.998	1.04	1.08	1.02	1.03	1.04

Table 3. Moment strength and cracking load of composite deck.

Specimen	Age of Precast at Time of Test (days)	Computed Loss of Prestress (ksi)	Moment Strength (kip-ft)			Cracking Load (kips)	
			Computed (M_n)	Experimental (M_u)	M_u/M_n	Computed	Experimental
B-10-8	99	33.3	856	957	1.12	79.2	125.5
B-5.5-10	127	42.1	1012	1213	1.20	54.8	87.5
F-5.5-10	160	43.1	1010	1130	1.12	61.4	118.2
F-10-8	194	35.7	860	886	1.03	81.7	113.5
B-8-8	243	38.2	884	992	1.12	72.7	103.5
F-8-8	242	38.4	886	942	1.06	76.6	110.8

primarily on the basis of flexural rigidity, differential deflection between panels, and moment strength and ductility of the composite deck. The computed flexural rigidities of the composite specimens, based on linear elastic theory for an uncracked section, are 2.06-3.80 times larger than for their cast-in-place topping and precast panels acting noncompositely. Because the deflection of the deck is inversely proportional to its flexural rigidity, the measured deflection is a sensitive indication of deterioration of composite action. The deflections of the deck at locations 2 ft to either side of midspan are tabulated in Table 2. These deflections are essentially the same at the end of 2 million load applications as at the beginning, which indicates that there was no significant loss of composite action.

The differential deflection between adjacent panels is a measure of shear transfer across the longitudinal joint. If there were a differential deflection between panels, then one panel would have to resist a larger proportion of load and hence be subjected to larger bending stress than was assumed in the design.

The differential deflection readings after each stage of cyclic loading are summarized in Table 2, where comparison is made on the basis of the ratio of larger to smaller adjacent deflections. These data indicate a maximum value of this ratio of 1.08. By a simple elastic analysis, if the panels resist an equal share of load when their deflections are equal, when the deflection ratio is 1.08 the share of load resisted by the more severely stressed panel would be increased about 4 percent. This computed increase is not considered significant. Thus, the measured differential deflections indicate satisfactory shear transfer behavior for all specimens under the cyclic loading.

The moment strength and ductility of the deck provide vital measures of endurance under the cyclic loads. To alleviate stress concentrations at the supports, the precast panels were supported at both ends by neoprene bearing pads measuring 0.5 in by 4 in by 10 ft, 5 in. The pads restrain horizontal movement and create a horizontal thrust that was believed to be negligible under service loads but significant at loads near ultimate. To account for this thrust, the shear stiffness of the support pads was determined and the soffit chord extension was measured as the specimen was loaded to failure. These values, together with the measured applied load and deflections, were used to determine the bending moment at the critical midspan section and are given in Table 3.

The moment strength of the deck was computed based on generally accepted assumptions of the strength design method (10). The stress-strain relation for the prestressing steel was furnished by the manufacturer. The compressive strength of the concrete was taken as the average cylinder strength of concrete in the cast-in-place deck at the time of test. The effective stress in the prestressing steel was estimated by the general method recommended by the Prestressed Concrete Institute (PCI) Committee on Prestress Loss (11). The stress in the prestress strands at ultimate was computed by a trial-and-error procedure by using the appropriate strain-compatibility and equilibrium equations.

The computed and experimental moment strengths of all specimens are given in Table 3. In every case, the experimentally determined moment is larger than the computed moment strength.

A typical load-deflection curve for one of the specimens is plotted in Figure 4. For comparison all of the curves are shown superimposed in Figure 5. These curves indicate that primary failure occurred in each specimen in flexure and that the specimens exhibited adequate ductility prior to secondary failure.

Secondary failure of specimens B-10-8, B-5.5-10, F-5.5-10, and B-8-8 occurred by crushing of the concrete at midspan. Secondary failure in specimen F-10-8 was by shear transfer in the 3-in-thick topping slab. Inspection of the topping slab after secondary failure indicated that a vertical crack had formed over the longitudinal joint and a U-shaped diagonal crack around the load point. The cracks in this region indicated both direct shear and diagonal tension failure.

The failure load for F-10-8 was 168 kips, which corresponds to a wheel load of 84 kips--5.25 times the design load of 16 kips. This indicates that an uncracked topping slab of the thinnest feasible size has adequate shear transfer strength for an HS20-44

Figure 4. Typical load-deflection curve for specimen B-8-8.

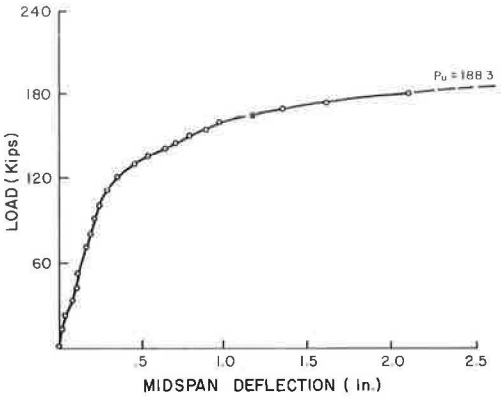

Figure 5. Load-deflection curves for all specimens.

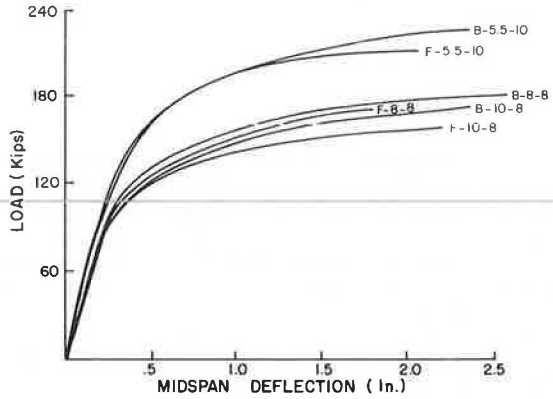

Figure 6. Visible top surface cracks after repetitive loading.

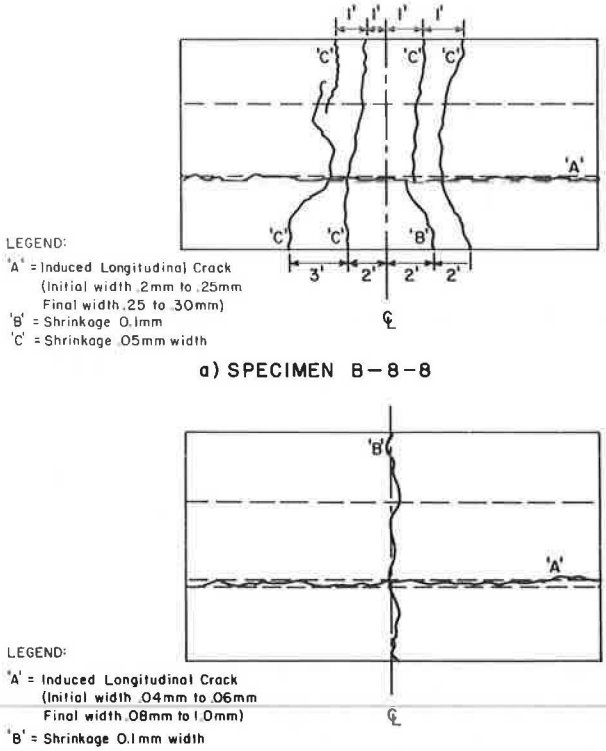

loading. However, it should be noted that a preexisting crack across a shear transfer plane, such as can be caused by shrinkage in an actual deck, has been shown to significantly reduce the shear transfer strength (12).

Specimen F-8-8, which had a 5-in topping slab and an induced longitudinal crack over a panel joint, failed at a measured load of 179.6 kips. This indicates that a 5-in topping slab, when transversely reinforced with pf_y = 200 psi, has adequate shear transfer strength even across a preexisting crack. Secondary failure of this specimen occurred in horizontal shear on the exterior panel of one quadrant.

In a sense, the behavior of specimens B-10-8 and B-8-8 was better than that of the companion specimens F-10-8 and F-8-8 because secondary failures occurred at larger loads and deflections in these specimens. However, since all specimens developed resisting moments in excess of their computed capacities and demonstrated adequate ductility prior to secondary failure, the behavior of all specimens is considered adequate.

Additional Performance Criteria

The flexural cracking load, visible cracks in the specimen, slip of the prestressing strands, and strains in several transverse rebars were recorded for each specimen.

The cracking load is defined as the load at which the first flexural crack was observed in the exterior side of the specimen. This load was in every case more than 40 percent greater than the computed cracking load when based on a modulus of rupture of $7.5\sqrt{f'_c}$ and on the effective prestress and concrete strength at time of test. The discrepancy between computed and observed values can be partly attributed to the simplifications made in computing the cracking moment. Another likely factor is that visual observation was limited to the exterior edges of panels. The first cracks very likely occurred in the interior. The cracking load was not considered an important indication of performance in this test.

Visible cracks provided information that was useful in explaining failure modes and certain aberrations in the load-deflection curves for the specimens. The only visible cracks in the top surface of the topping slabs after 2 million cycles of design load were in specimens B-8-8 and F-8-8. One of the cracks was the induced longitudinal crack that was discussed earlier in this paper. The other cracks are believed to have been caused by shrinkage. The approximate locations of visible cracks are shown in Figure 6.

The longitudinal cracks were measured shortly after they were induced and periodically during the curing and loading periods. In both specimens they were found to widen about 0.05 mm during the curing period, but there was no measurable increase in width during the cyclic load period.

The transverse cracks had a significant effect on the stiffness of the decks in the service load range, as can be seen from the data given in Table 2. The service load deflections in specimens B-8-8 and F-8-8 are approximately one-quarter greater than in the specimens that did not contain transverse cracks. These cracks are believed to be a consequence of the relatively poor curing condition for these specimens.

The transverse crack in specimen F-8-8 is believed to have caused the reduction in rigidity that

was measured between the initial and subsequent static tests. All other specimens showed a small increase in rigidity during the cyclic loading, but the rigidity of specimen F-8-8 was found to diminish about 2 percent. The transverse crack in this specimen was approximately across the midspan, and it is believed that the expansion of the neoprene pads under the load points caused this crack to enlarge during the first series of cyclic loads.

Bond and development of the prestressing strands were not thought to be likely problems with the specimens. However, the slip on two strands per panel was measured to verify this performance. There was no indication of strand slip in any of the specimens tested at any stage of loading. The strain gages that were mounted on the transverse rebars did not provide a reliable basis for evaluating the performance of the transverse reinforcement. Several of the gages were apparently damaged during placement or curing of the topping slab and could not be initially balanced. The readings that were obtained varied erratically from one quadrant to another.

The strain measurements did provide some qualitative information on the performance of the decks. The measured strains in the transverse rebars were relatively small for application of the live loads. The strains were in every case less than 75×10^{-6} in/in, which corresponds to a stress of about 2 ksi. This indicates that, regardless of the actual stress level caused by shrinkage plus live load effects in the rebars, the stress range due to live load is likely to be so small that fatigue of these bars should not be a problem.

CONCLUSIONS

All of the specimens tested in this program performed satisfactorily for the 2 million cycles of repetitive load. Visible cracks did not develop in any concrete surface, and there was no measurable increase in the width of any preexisting crack during the cyclic loading period. Primary failure was in a ductile flexural mode, and there was no indication of fatigue in the reinforcement.

The only factor that caused a significant variation in behavior among the specimens was the transverse cracking of the topping slab that occurred in two of the specimens. These cracks developed approximately one week after the topping was cast and are attributed to the relatively poor curing conditions for the two. The cracks caused an increase in measured service load deflection of approximately 25 percent compared with the uncracked (better-cured) specimens. These transverse cracks closed as the specimen was loaded, and they did not appear to affect the behavior near ultimate. Whereas cracks in the cast-in-place topping slab did not significantly affect the structural performance of the test decks, such cracks could possibly have an important influence on the long-term durability and serviceability of actual bridges.

The conclusions drawn from this experimental program apply to full-span panel-form composite decks designed by the AASHTO specifications by using the effective width criteria for a one-way slab. Concrete in both the precast panels and the cast-in-place topping slab is of the type commonly classified as normal weight.

Based on the limited number of specimens tested, the following conclusions can be drawn:

1. The composite deck can withstand 2 million cycles of design load without significant loss of serviceability or strength. Adequate composite action is obtained by roughening the interface surfaces of the precast panel and by waterblasting this surface immediately prior to placing the topping slab.
2. Adequate serviceability and strength can be obtained by using flat, precast panels rather than more expensive, beveled-edge panels.
3. There is no indication that the thickness of the topping slab relative to the total thickness affects the fatigue strength of the composite deck up to 2 million cycles.
4. For HS20-44 live loads, adequate shear transfer strength is provided by a 5-in topping slab reinforced transversely with no. 4 grade 60 rebars spaced 12 in on centers. This shear transfer strength is available even when a longitudinal crack exists in the topping slab over the panel.

Specific design recommendations based on this study and on other related studies are given in the study final report (8).

ACKNOWLEDGMENT

The investigation described in this paper was sponsored by the Louisiana Department of Transportation and Development (LaDOTD) in cooperation with the Federal Highway Administration, U.S. Department of Transportation. Technical liaison with LaDOTD was provided by Sheldon Law and J.W. Porter and by Mitchell Smith, who represented the Federal Highway Administration.

The experimental work was carried out in the Structural Research Laboratories of Louisiana State University. We are indebted to Robert Taylor of the University and to student workers John Brogue, William King, and Ray Battalora for their assistance with the construction and testing of the specimens. Contributions to the typing and drafting of figures for the final report were made by Ellen Donner, Susan Sartwell, Meredith Whaley, and Carolyn Sharp.

REFERENCES

1. J.M. Barker. Research, Application and Experience with Prestressed Concrete Bridge Deck Panels. PCI Journal, Vol. 20, No. 6, Nov.-Dec. 1975, pp. 66-85.
2. R.W. Kluge and H.A. Sawyer. Interacting Pretensioned Concrete Form Panels for Bridge Decks. PCI Journal, Vol. 20, No. 3, May-June 1975, pp. 34-61.
3. R.M. Barnoff, J.A. Orndorft, R.B. Harbaugh, and D.E. Rainey. Full Scale Test of a Prestressed Bridge with Precast Deck Panels. PCI Journal, Vol. 22, No. 5, Sept.-Oct. 1977, pp. 66-86.
4. A.L. Furr and L.L. Ingram. Cyclic Load Tests of Composite Prestressed-Reinforced Concrete Panels. Texas Transportation Institute, Texas A&M Univ., College Station, Res. Rept. 145-4F, 1972.
5. PCI Bridge Committee. Tentative Design and Construction Specifications for Bridge Deck Panels. PCI Journal, Vol. 23, No. 1, Jan-Feb. 1978, pp. 32-39.
6. Standard Specifications for Highway Bridges, 12th ed. AASHTO, Washington, DC, 1977.
7. C.O. Hays, Jr., R.L. Cox, Jr., and G.O. Obranic, Jr. Full Span Form Panels for Short Span Highway Bridges. Department of Civil Engineering, Univ. of Florida, Gainesville, Final Rept. U17F, 1980.
8. C.D. Buckner and H.T. Turner. Performance Tests of Full Span Panel Form Bridges. Research and Development Section, Louisiana Department of Transportation and Development, Baton Rouge, Final Rept. 80-1C, 1981.

9. Louisiana Standard Specifications for Roads and Bridges. Office of Highways, Louisiana Department of Transportation and Development, Baton Rouge, 1977.
10. A.H. Nilson. Design of Prestressed Concrete. Wiley, New York, 1978.
11. PCI Committee on Prestress Losses. Recommendations for Estimating Prestress Losses. PCI Journal, Vol. 20, No. 4, July-Aug. 1975, pp. 43-75.
12. A.H. Mattock and N.M. Hawkins. Shear Transfer in Reinforced Concrete: Recent Research. PCI Journal, Vol. 17, No. 2, March-April 1972, pp. 55-75.

Publication of this paper sponsored by Committee on Concrete Bridges.

Full-Depth Modular Precast, Prestressed Bridge Decks

R. H. BERGER

Precast modular deck construction has been used successfully since 1967. It is still used in a modest but effective fashion, as exemplified by several installations. The details used to connect the panels to the supporting structures, provide composite action, permit vertical adjustment, and develop shear resistance between adjacent panels are critical. A deck protection system to prevent chemical penetration should be incorporated in the design. Construction costs were estimated for four design examples and compared with costs of conventional cast-in-place construction. In each case, the modular system proved to be more economical. Benefits of precast, prestressed decks include greater structural efficiency, reduction in the number of support elements required, less construction time, reduction in interruption to traffic for replacement decks, potential for increasing capacity of existing structures through reduction in dead load, and better quality control.

Current practice in the construction of concrete bridge decks supported by a structural framing system uses cast-in-place reinforced concrete. This is predominantly used for bridge deck replacement and for new bridge construction.

Some of the problems generated by this construction technique have been overcome through the development of new materials and improved procedures, such as concrete overlays, epoxy-coated rebars, and stay-in-place forms. However, others have not. These include the very time-consuming and labor-intensive procedures inherent in the use of cast-in-place concrete and the inefficient use of the materials that occurs when the full advantage of the compressive strength of concrete is not exploited.

One alternative to conventional cast-in-place bridge deck construction that could be more cost efficient is full-depth, precast, prestresssed bridge deck panels. This system is equally adaptable to new construction and to deck replacement projects.

STATE OF THE ART

In 1967, Purdue University, in cooperation with the Indiana State Highway Commission, initiated research to establish design criteria for a full-depth, precast, prestressed deck system (1). This study was followed by an implementation phase consisting of the replacement of decks on two structures: IN-37 over Bean Blossom Creek and IN-140 over Big Blue River. This work was completed in 1970 (2). Subsequently, the deck on a third structure in Indiana (Tonkel Road over Cedar Creek) was replaced with precast elements.

Deck panels for these bridges were cast full width in sections approximately 1.2 m (4 ft) wide. The panels were prestressed in the transverse direction of the bridge and were posttensioned in the longitudinal direction after erection. Composite action between the deck and the supporting members was not developed.

Slabs for the IN-37 bridge were match-cast with a tongue-and-groove joint assembly. Spring clips bolted to concrete inserts were used to anchor the panels to the top flange of the system. Vertical adjustments at the stringer bearing areas were achieved by welding shim plates of variable thickness to the top flange of the structure.

The replacement deck for the IN-140 bridge was constructed in a similar fashion except that the slab had a variable thickness to obtain the desired roadway crown. This was necessary since the steel framing was constructed in a level plane.

The Tonkel Road replacement deck was attached to the beams by using a "Z-clip" in lieu of the spring clip. A fiberglass expansion joint material was placed between the slab and the stringer flange. The adjacent panels were connected to each other on the top surface by a plate welded to inserts cast in the panels. An asphalt wearing surface was placed with variable thickness to provide the required roadway crown.

These structures are performing reasonably well after 12 years of service. Minor problems have developed with concrete spalling at the joints between panels and in connections used to attach the panels to the supporting members.

Since this pioneering effort, a number of agencies have designed replacement decks with precast panels. The New York Thruway has probably constructed more square footage of precast deck than any other agency. These designs did not call for prestressing but rather used mild reinforcing. This was a policy decision based primarily on concern about corrosion of the steel due to the heavy application of salts for snow and ice control.

Precast slabs used by the Thruway Authority were cast with block-outs over the supporting stringers. The slabs were placed on a thick epoxy bed applied to the stringer flange to provide uniform bearing. Studs were welded to the stringer flange through the block-outs, and the void was filled with additional epoxy mortar. This provided a positive connection between the slab and the stringer and also developed some horizontal shear capacity, although the Thruway does not rely on composite action. Keyed transverse joints between adjacent slabs were filled with epoxy. Longitudinal posttensioning was not used. A waterproof membrane and asphalt wearing surface were placed over the completed deck.

In 1979, the Pennsylvania Turnpike Authority replaced the deck on the Clark Summit Bridge near Scranton, Pennsylvania, using precast mild rein-

forced deck panels. Panels were cast with haunches over the girders to allow for variable thickness of cover plates. Neoprene strips were glued to the supporting members as a side form for the placement of epoxy grout between the slabs and the flange. Posttensioning ducts were provided in the longitudinal direction. Threaded rods with sleeve nuts were inserted and used to pull adjacent slabs together snugly. A keyed joint was then filled with a nonshrink grout.

The deck on the High Street Overhead Bridge near Oakland, California, was also replaced by using precast panels. A unique feature of this project was the use of two-headed bolts placed through threaded inserts in the slab and located over the supporting stringers. These bolts were used to adjust the panels to the desired elevation. Wooden side forms were attached to the stringer flange, and a fast-setting concrete mortar was placed between the slab and the stringer.

Railroads have also used precast elements in deck replacement programs. The Atchison, Topeka and Santa Fe Railway Company has developed precast, prestressed deck slab construction standards for use in replacement of timber decks (3). The concept differs from those already discussed in that there are no mechanical attachments between the slabs and the supporting structure. Bolts with spring clips are used at two points on each slab in place while curing of the mortar is completed.

After removal of the timber deck, the girder flanges are sandblasted. Plywood forms are attached to the edges of the flange, and a pourable epoxy bedding material is placed. Slabs are then erected while the mortar is still plastic. The spring clips are used to hold the slab in place while curing of the mortar is completed.

The railroad reports that the epoxy mortar between the slab and the beam develops sufficient shear capacity to ensure composite action between girder and slab (3). This provided sufficient increase in the live-load capacity of the structure to overcome the additional dead load resulting from the concrete deck. In most instances, it also eliminated the need to make structural repairs to the supporting girders to increase capacity.

The primary concern in constructing the replacement deck for each of the examples cited was to minimize the interruption of traffic on the facility. Spin-off benefits included increased capacity, improved quality control in the concrete deck, and economy. Minor problems that developed included details to compensate for the irregular surface of the top girder flange connection of the slab to the girder and joints. Overall, each of these projects was judged to be highly successful by the responsible agency.

DESIGN CONSIDERATIONS

The American Association of State Highway and Transportation Officials (AASHTO) Standard Specifications for Highway Bridges (4) provide load distribution formulas, procedures for developing maximum design moments, and the magnitude of wheel loads to consider in the design of concrete bridge decks. These are applicable to either cast-in-place concrete decks or precast decks. These specifications permit the use of more sophisticated procedures for the analysis of forces. This should be considered in those instances where very wide spacing of beams is used or where savings could be realized by a more precise analysis.

The current AASHTO specifications permit tension in the concrete under service loads of $6\sqrt{f'_c}$. This is reduced by 50 percent in corrosive environments. For bridge decks, tension should be allowed only where significant economy can be achieved and with due consideration for the possibility of harmful chemicals penetrating the slab through resulting tension cracks. Whenever tension is permitted, mild reinforcement should be provided.

Composite action between the framing system and the precast deck can be used to provide an efficient design. Careful attention to details is required to provide for the horizontal shear at the interface.

The design of the slab cantilever must include provision for proper development length for moment resistance from the prestress force. Mild reinforcement should be included when the length available for the stress transfer from the prestressing strand is insufficient.

CONSTRUCTION DETAILS

To obtain the maximum utility from the precast concept, it is important to develop details that will provide an efficient procedure for construction, provide the flexibility necessary to accommodate variable geometrics, and permit the structure to operate in accordance with the design assumptions. Critical details include joints, slab-support interface, geometrics, strand and duct placement, and protection for the deck surface.

Joints

Several types of joints have been used between adjacent precast slab elements. These include keyed or tongue-and-groove joints, butt joints, and grouted keyway joints.

The butt joint is simple to cast and erect but has the disadvantage of providing no inherent shear transfer capacity. This can be developed through frictional resistance from longitudinal posttensioning.

The keyed joint required careful fabrication and minimum fabrication tolerance. When match-casting techniques are used, this can provide a superior end product as well as develop adequate shear transfer. Several configurations of this joint are shown in Figure 1.

The grouted joint, shown in Figure 2, has been effectively used by the New York Thruway Authority and the Pennsylvania Turnpike Authority. It permits greater construction tolerance than the other joints and, when properly grouted, provides the desired shear transfer.

Bridge decks for structures that carry more than two traffic lanes will usually require multiple-width slabs. The longitudinal joint between these sections can be placed over a supporting stringer or somewhere between supporting stringers. In the former case, a lapped joint such as that shown in Figure 3 can be provided. This should not be considered to develop continuity over the support. When continuity is required, a cast-in-place concrete section should be used, properly reinforced with mild reinforcing steel. Sufficient reinforcing should extend from the precast units to provide the required development length.

Where the joint falls between supports, an open joint can be provided. If drainage runoff is a potential problem, the joint should be sealed. Details should include edge-reinforcing protection to minimize maintenance.

Framing Connections

Details must be developed to provide a positive attachment between the precast slab elements and the support frame. Where composite action is required,

Figure 1. Keyed joints.

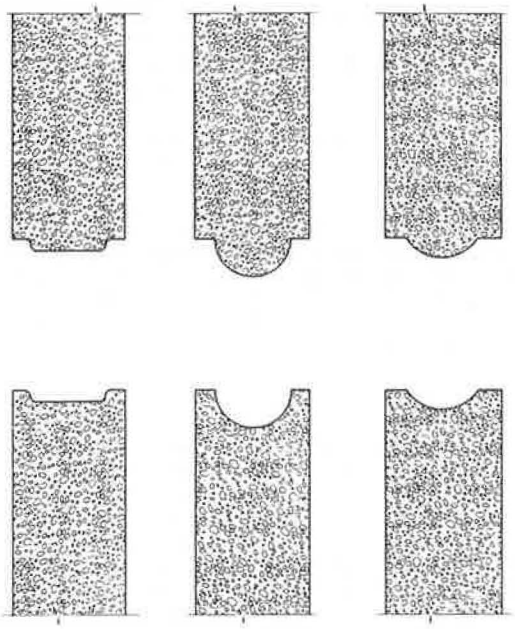

Figure 2. Grouted joint.

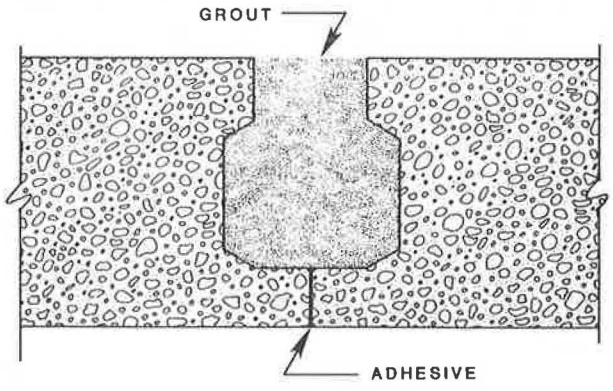

the construction must be adequate to transfer horizontal shear and provide lateral stability to the girder flange. Several systems have been developed, including shear studs, bolt clips, and bolts, adaptable to either steel framing or precast concrete framing.

Bolt clips, shown in Figure 4, were used on some of the earlier installations for connecting the slab to steel stringers but have not proved to be satisfactory except for providing a temporary connection during construction. This detail was used on the Tonkel Road Bridge in Indiana.

A more durable detail incorporates high-strength bolts placed in recessed holes in the slab and connected to the top flange of the steel stringer. The bolt head is on the underside of the flange, and the nuts and washer are placed in the recessed hole in the concrete deck. A similar system used by the New York Thruway, which included a cast steel bushing, is shown in Figure 5.

The connection can also be made with shear studs attached to the supporting steel girder through preformed openings in the deck slab. The void is then filled with a nonshrink or epoxy mortar. This detail provides a very simplistic construction procedure and does not call for extremely tight con-

Figure 3. Lap joint over stringer.

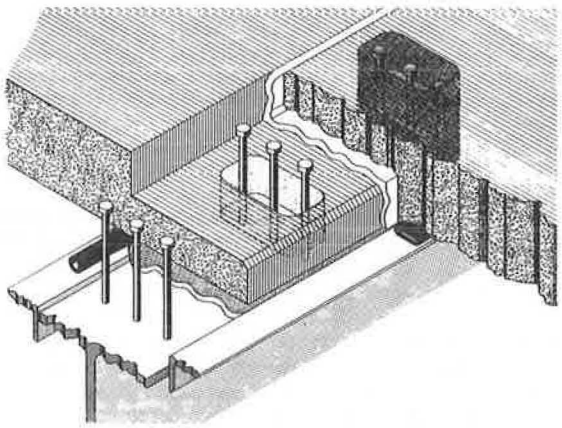

Figure 4. Typical bolt clip.

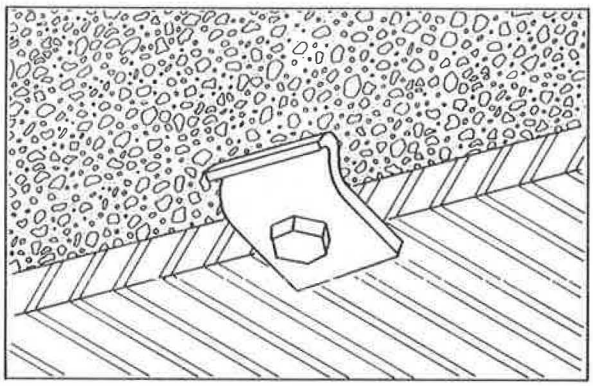

struction tolerances. This procedure, like the others discussed, is adaptable to either new construction or replacement decks on steel framing.

For precast concrete support framing, different details are required. Figure 6 shows an example of a detail for precast girders. A plate is anchored to the girder during prefabrication and later used to attach shear studs. Slotted holes in the plate provide additional horizontal shear capacity. Studs are attached to the girder through preformed openings in the deck unit. These cavities are later filled with nonshrink grout or a suitable epoxy mortar.

A similar detail can be developed for replacement decks. After removal of the existing slab, stirrup shear connector bars are cut off several inches above the concrete. A slotted plate is placed over these bars. The bars are then bent over and welded to the plate as shown in Figure 7. After placement of the precast unit, shear studs are welded to the plate through preformed holes. Again, cavities are filled with grout.

A high-strength bolt connection similar to that already described for steel beam supports can be used for new construction. The bolts are placed in inserts cast in the concrete beam.

An alternative to this is grouting bolts in preformed holes cast in the concrete beam. The precast deck units are then placed, and the tie downs are completed as shown in Figure 8.

Geometrics

Superelevation, transitions, and vertical and hori-

Figure 5. High-strength bolt connection.

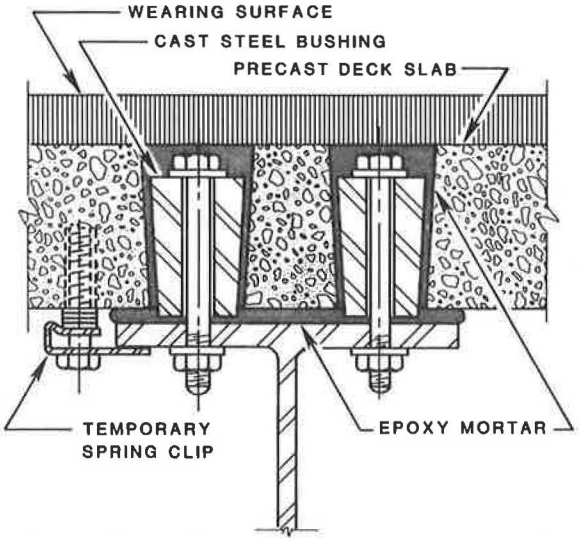

Figure 6. Precast slab connection to precast girder.

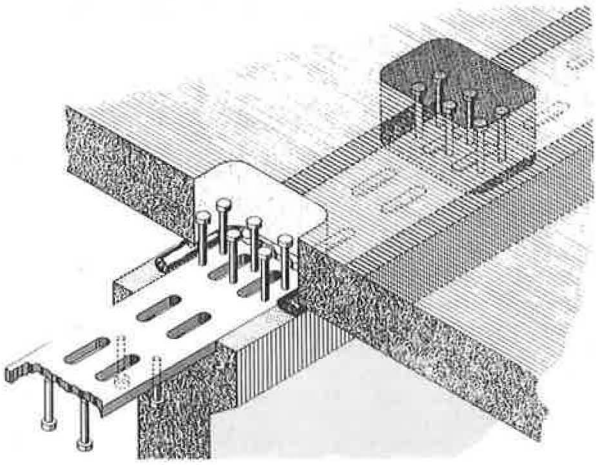

Figure 7. Precast slab connection to precast girder for replacement decks.

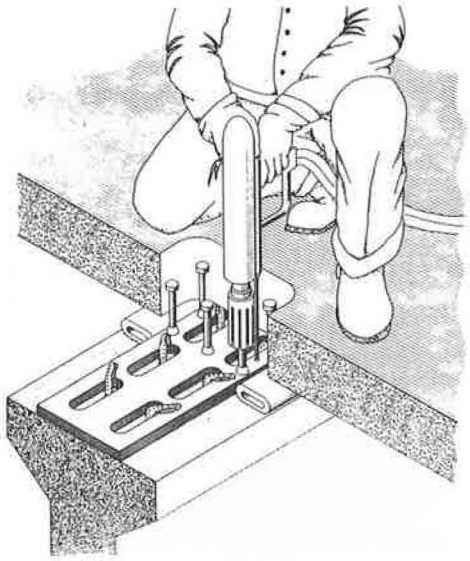

zontal curvature can be handled satisfactorily during the deck unit precasting operation. However, significant field problems are created as a result of irregularities in the supporting elements. Details must be developed that permit vertical adjustment of the individual slab units in the field. These details must also ensure proper temporary support as well as final bearing on the supporting beams.

Several systems have been developed to accomplish these objectives. One system requires the "buttering" of the top flange of the support elements with grout. The slab is placed while the grout remains plastic, and the excess material is squeezed out as the slab reaches the desired position. Hardening of the grout provides the final bearing.

A second method uses shim pads, which are placed under the slab in sufficient thickness to satisfy the required vertical alignment. Epoxy mortar is placed between the deck slab and the beam flange to provide final bearing.

Figure 3 shows a detail that incorporates side angles welded to the top flange of a steel support member. These angles are placed to compensate for variable flange plate thickness. Grout is placed by using the angles and a neoprene sealing tube as a side dam. This detail is equally adaptable to new construction and to replacement decks. Careful attention must be given to welding details to ensure that undesirable fatigue characteristics do not result.

A detail that provides excellent versatility for vertical adjustment and adequate temporary support during construction and meets all requirements for final bearing is shown in Figure 9. It consists of a bolt extending through a threaded insert cast with the deck slab. The slab can be adjusted to the proper elevation by increasing or decreasing the extension of the bolt below the bolt head. The number of bolts provided is dictated by design requirements for dead load and the requirements for adjustment. After the slab has been adjusted to the proper elevation, the void below the slab and beam flange is filled with grout. Collapsible neoprene tubes are used for side dams to contain the grout. After the grout has cured, the leveling bolts are removed and the remaining void is filled with grout.

Deck Protection

Because the same factors that have caused the rapid deterioration of cast-in-place bridge decks are present with precast decks, a protection system should be provided where deicing chemicals are used. In most instances, it is also desirable to place a wearing surface of either concrete or bituminous material over the precast deck. A bituminous overlay provides a mechanism for eliminating irregularities in the roadway surface and, when constructed with a waterproof membrane, provides protection from the intrusion of chloride ions. In lieu of a membrane, the concrete surface could be treated with a penetrating sealer. Dense concrete or latex-modified concrete overlays will also provide an effective protection system. It is highly desirable to specify epoxy coating for all mild reinforcing in close proximity to the deck surface.

COST ANALYSIS

Design Examples

To assess the potential cost benefits of using precast deck panels, four hypothetical examples were developed. Two of the examples involve an existing

Figure 8. Precast slab connection to concrete beam.

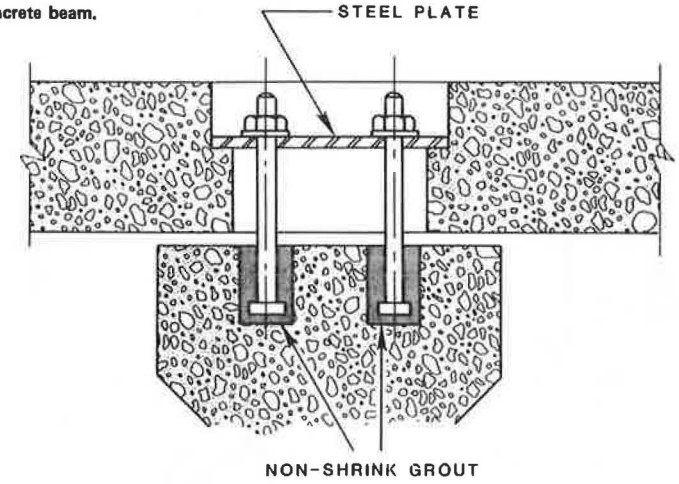

Figure 9. Adjustable support.

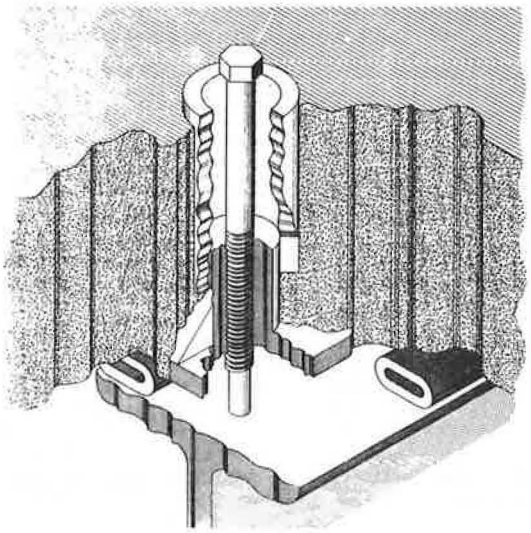

deck that requires replacement, and the other two are related to new construction. Each example involves a different support framing system.

The examples and the estimated construction cost include only the deck itself and not other parts of the structure. Changes in dead load and in the cost of the framing system have not been included in the economic analysis.

Each example is developed by using current AASHTO specifications and an HS20 live load.

Example 1

Example 1 involves the replacement of an existing deck on a 24-m (78-ft) simple-span, multiple steel girder bridge. The shoulder width on the deck is increased to provide additional safety, and a minimum of one lane of traffic in each direction is maintained at all times. A typical section of the existing and proposed bridge superstructure, which uses precast slab construction, is shown in Figure 10.

The precast deck is composed of 2.4-m (8-ft) wide modules. Units are cast for each half of the deck with a lap joint over the center stringer. Attachment to the steel stringers is made by welding studs through preformed openings in the precast deck unit, which are then filled with grout. Bedding and vertical adjustment is obtained as described earlier with the screw-type inset (Figure 9). The bridge is longitudinally posttensioned. The precast deck is 178 mm (7 in) deep and the cast-in-place concrete is 203 mm (8 in) deep to comply with current specifications.

Example 2

In example 2, the deck on an existing 29-m (95.5-ft) span through truss bridge is replaced with a modular deck slab system that spans between existing floor beams (existing stringers are removed). Figure 11 shows a typical cross section for the existing bridge and for the proposed precast deck replacement.

The precast deck units are 2.1 m (6.9 ft) wide and cover one-half of the bridge length. The slabs are continuous over intermediate floor beams. A lap joint is used between the ends of adjacent panels at the center floor beams, and a grouted keyway is used in the longitudinal direction between adjacent units. Attachment to the floor beams is by shear studs, as in example 1. Vertical adjustment is obtained with screw-type inserts.

The precast slab is 241 mm (9.5 in) deep, and the cast-in-place alternative requires a 330-mm (13-in) deep slab to carry the same live load.

Example 3

Example 3 is a new bridge design. A single-span, 19.8-m (65-ft), prestressed concrete, multiple-I-beam bridge was selected. The bridge was designed for composite action between the deck slab and the I-beam. Roadway width accommodates two lanes of traffic with 1.5-m (5-ft) shoulders. A typical section of the structure is shown in Figure 12.

The precast modular deck units are 1.4 m (8 ft) wide and cover the full cross section of the bridge. Curbs are cast monolithically with the slab. Stringers have been spaced to optimize the efficiency of the precast slab. The required slab thickness is 190 mm (7.5 in) for the prestressed alternative and 241 mm (9.5 in) for the conventional cast-in-place concrete design (with the same stringer spacing).

Joints between adjacent slabs are tongue and groove. The slabs are connected to the support stringers by welding studs to a steel plate embedded in the top flange of the I-beam through preformed holes. These connectors also develop sufficient horizontal shear capacity for composite action.

Figure 10. Typical section: example 1.

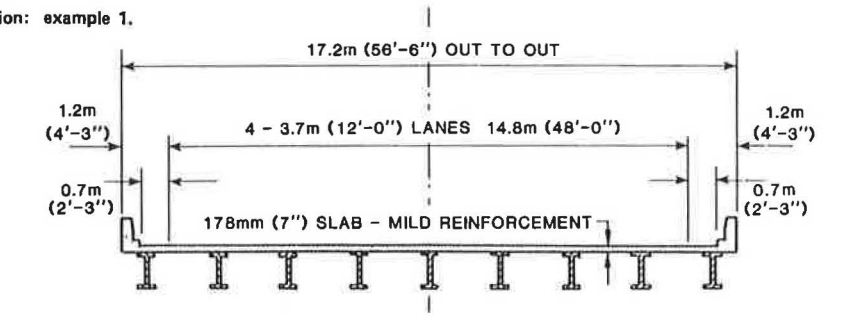

TYPICAL CROSS-SECTION OF EXISTING BRIDGE

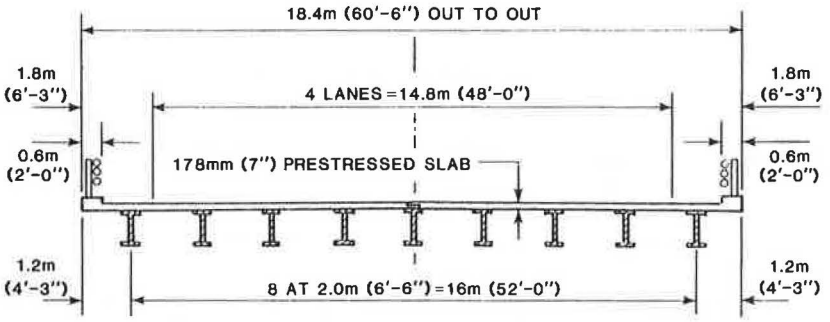

PRESTRESSED PRECAST SLAB REPLACEMENT

Figure 11. Typical section: example 2.

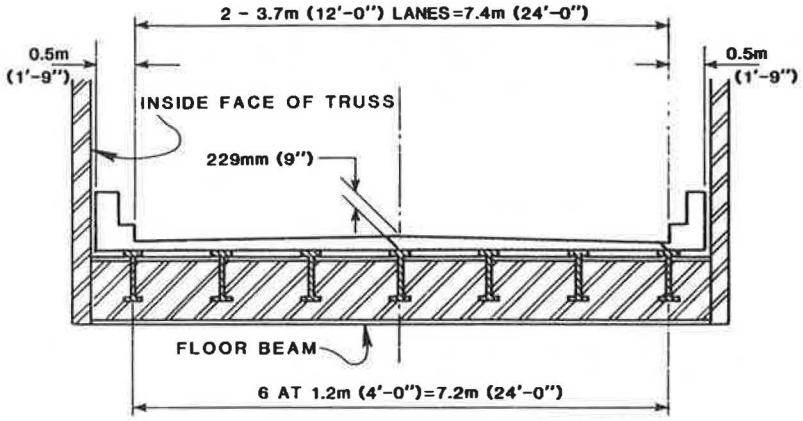

TYPICAL CROSS-SECTION OF EXISTING BRIDGE

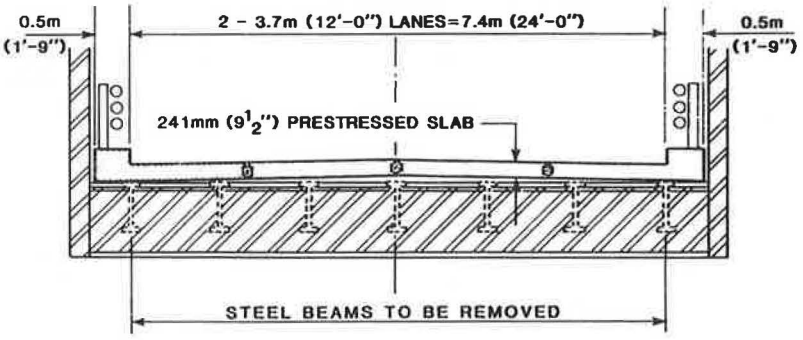

PRESTRESSED PRECAST SLAB REPLACEMENT

Figure 12. Typical section: example 3.

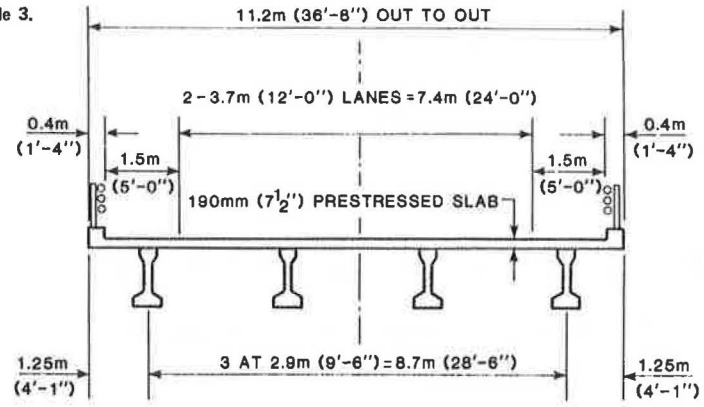

Figure 13. Typical section: example 4.

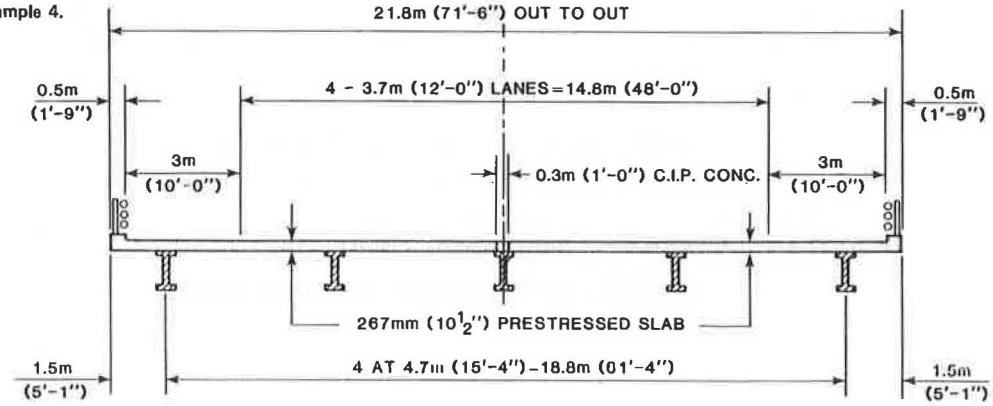

Leveling bolts, as in the previous examples, are used for vertical adjustment. The void between the top flange and the underside of the deck panel is filled with grout by using O-ring sealers.

Example 4

Example 4 demonstrates the applicability of using a prestressed, precast deck to minimize the number of required stringers and thereby improve overall economy. A multiple-steel-beam, 34.2-m (112-ft), single-span structure was selected. The roadway accommodates four lanes of traffic with full-width shoulders. Composite action is developed between the beams and the deck slab. Continuity of the deck over the center support is achieved by casting in place the section directly over the center stringer. This section is reinforced and made continuous with the adjacent deck panels. A typical section of the structure is shown in Figure 13.

The precast modules are 2.4 m (8 ft) wide and cover one-half of the deck. Longitudinal posttensioning is specified. Joints, leveling procedures, and grouting requirements are similar to those for the other design examples. The precast, prestressed deck requires a thickness of 267 mm (10.5 in) and the cast-in-place, conventionally reinforced deck requires a thickness of 318 mm (12.5 in).

Results

A construction cost estimate has been developed for each of the examples described above for the precast alternative and for the cast-in-place alternative. Estimates are based on complete installation of the deck, including curbs and appurtenances. Costs associated with the supporting framework have not been included. Costs have been included for traffic control for the two examples that involve deck replacements. No consideration has been given to those costs associated with user delays and the like. Estimates are based on 1980 dollars.

A summary of the results of the analyses is given in Table 1. In each case, the modular system is less costly, although marginally so for example 1. However, the significant saving in field construction time, which translates into additional savings in user cost, has not been considered.

CONCLUSIONS

The concept of transverse prestressed, precast modular bridge deck construction has definite advantages when compared with conventional cast-in-place deck construction using mild reinforcement. A review of bridges with precast decks that have been in service for a number of years indicates that they have performed favorably compared with cast-in-place construction.

The concept is applicable to both new bridge construction and replacement deck construction. In each of the design examples investigated, a cost estimate was made, and in each instance the precast alternative proved to be more economical. In addition, the time for field construction was significantly reduced.

Improved economy is primarily the result of a decrease in the amount of materials required due to the increased structural efficiency of the prestressed deck. Where time is a factor that has quantifiable costs, this further enhances the economic viability of the concept of precast, prestressed construction.

Other benefits of modular construction for new bridge construction and for deck replacement have been identified:

Table 1. Cost analysis.

Construction Type	Example	Span (m)	Curb-to-Curb Width (m)	Framing System	Cast-in-Place			Precast				Potential Savings over Conventional Construction
					Thickness (mm)	Field Erection Time (days)	Deck Construction Cost ($)	Thickness (mm)	Field Erection Time (days)	Deck Construction Cost ($)	Cost Savings (%)	
Deck replacement	1	23.8	16.0	Multiple steel I-beams	203	41	64 900	178	7	63,700	7	-
	2	29.1	7.3	Steel-thru truss with floor beams	330	25	37,200	241	5	33,200	5	Member strengthening not required
New bridge	3	19.8	10.4	Multiple prestressed concrete I-beam	241	20	35,200	190	4	27,400	4	Fewer supporting members required
	4	34.2	20.7	Multiple steel I-beams	317	26	119,000	267	13	102,600	13	Fewer supporting members required

1. New bridge construction--(a) Improved structural efficiency, (b) fewer support elements, (c) decreased manpower requirements, and (d) less construction time;
2. Replacement deck construction--(a) Decreased on-site construction time and manpower requirements, (b) less time required for traffic control, (c) less inconvenience to the traveling public, and (d) decreased dead-load weight and potential for increase in live-load capacity.

In addition, precast concrete elements fabricated in a controlled environment under "factory" conditions provide for improved quality control, which can ultimately result in improved durability of the completed deck.

REFERENCES

1. M.J. Gutswiller, R.H. Lee, and C.F. Scholer. Feasibility Report: The Use of Precast, Prestressed Concrete for Bridge Decks. Joint Highway Research Project, Purdue Univ., West Lafayette, IN, and Indiana State Highway Commission, Indianapolis, Project C-36-56N, File 7-4-14, July 1968.
2. P.K. Kropp. The Use of Precast, Prestressed Concrete for Bridge Decks. Joint Highway Research Project, Purdue Univ., West Lafayette, IN, and Indiana State Highway Commission, Indianapolis, Project C-36-56N, File 7-4-14, March 1973.
3. W.F. Hyma. Replacing Timber Decks on Railroad Bridges with Prestressed Concrete Slabs. Concrete International, Vol. 1, No. 5, May 1979, pp. 18-21.
4. Standard Specifications for Highway Bridges, 12th ed. AASHTO, Washington, DC, 1977.

Publication of this paper sponsored by Committee on Concrete Bridges.

Abnormal Rotations of Skewed and Curved Bridges

MARTIN P. BURKE, JR.

The abnormal rotation of skewed and curved bridge superstructures is described and illustrated. Various types of compound bearings that accommodate this type of rotation are described. Specific examples of structure distress due to abnormal rotation and inappropriate bearing selection are given. Although present design specifications are mute concerning this phenomenon and research that is specifically focused on it is scarce, it is suggested that the designers of severely skewed or curved bridges should consider the consequences of abnormal rotation and furnish an appropriate bearing design for such structures.

The present American Association of State Highway and Transportation Officials (AASHTO) Standard Specifications for Highway Bridges (1) recognize the need for other than flat bearing surfaces for bearings of bridge spans of 50 ft or more. Section 1.7.32 of the specifications states that "spans of 50 feet or greater shall be provided with a type of bearing employing a hinge, curved bearing parts, elastomeric pads, or pin arrangement for deflection purposes." However, nothing is stated about the need to make similar provisions for bridges with severe skews or curves, yet the need of accommodating the actual rotations of skewed or curved bridge superstructures, laterally as well as longitudinally, is in some cases equally important (2).

This paper attempts to highlight this subject of combined lateral and longitudinal superstructure rotations (abnormal rotations). Some of the major bearing types that have been developed during the past two decades to accommodate these rotations are described as well as the bearings that some Ohio bridge engineers have chosen for their bridges.

For example, consider bridge CUY-480-1572 de-

Figure 1. Framing plan of Ohio bridge CUY-480-1572.

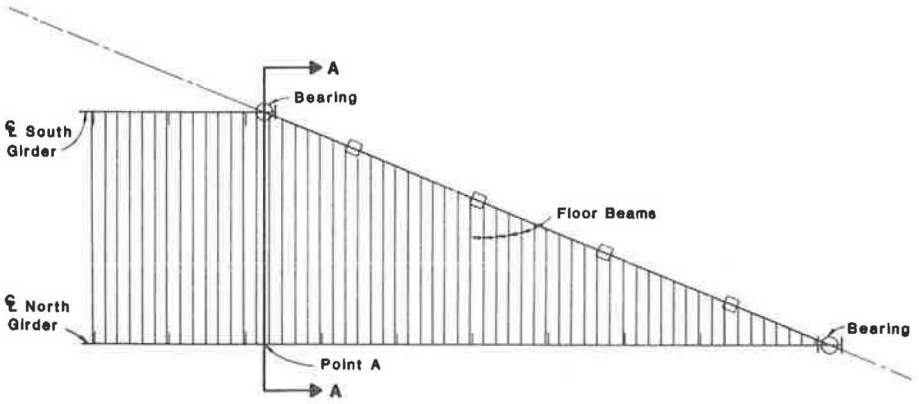

Figure 2. Cross section of bridge CUY-480-1572 at point A: vertical deflection without rotation.

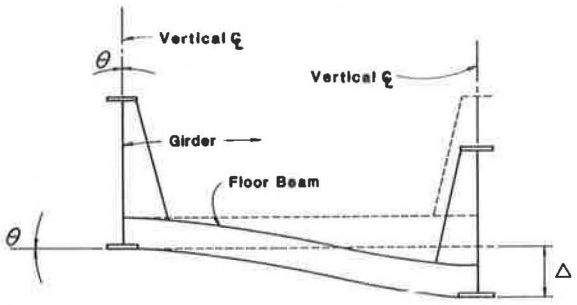

Figure 3. Cross section of bridge CUY-480-1572 at point A: vertical deflection with rotation.

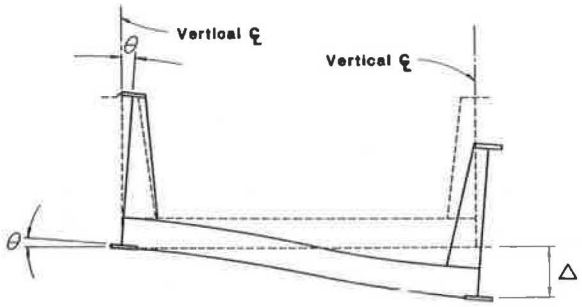

signed by Murray of Alden E. Stilson and Associates. It is a bridge with a two-span, continuous through-girder superstructure designed to carry the two tracks of the Penn Central Railroad over I-480 in Cleveland, Ohio. It has spans of 159 and 190 ft and a skew of about 67°. Part of the framing plan of this structure is shown in Figure 1. In this framing plan, notice that point A of the north girder is located more than 90 ft from its girder bearing but only 37 ft from the bearing of the adjacent south girder. A schematic cross section of the superstructure at point A is shown in Figure 2. The dashed lines represent the girders and transverse floor beams in an unloaded position and the solid lines the members deflected due to live load. In this exaggerated sketch showing girder deflection in a vertical plane, the type of deflection usually assumed in bridge design, it should be obvious that the reverse bending of the floor beams should be accompanied by lateral bending and/or rotation of the girders.

A more realistic assumption of structure deformation is shown in Figure 3, where the deflection of the girder at point A is associated with bending of the floor beams and rotation of the girders. Because the rotation of the left girder is occurring at a bearing, the type of bearing used at this location must be able to accommodate not only longitudinal rotation but lateral rotation as well; otherwise, bearing edge loading will occur and be followed by girder, bearing, and bridge seat distress.

During the past two decades, several types of bridge bearings have been developed for applications in which abnormal rotations must be accommodated. These various bearing types have come to be known as pot, spherical, elastomeric, and disk (3).

For his Penn Central Railroad structure, Murray selected and designed pot bearings to accommodate the skew-related abnormal rotation of the structure. The bearings he designed will accommodate all abnormal rotations and longitudinal translation and will support reactions of up to 4000 kips. They will be the largest bearings of their kind in Ohio.

Typical pot bearing details are shown in Figure 4. These bearings are circular in plan and rather flat in outline. The bottom cylindrical section, or pot, which contains an elastomer of either natural rubber or neoprene, is covered by an upper cylindrical section, or piston. The elastomer confined within the pot is subjected to a vertical pressure of about 3500 psi, which causes the elastomer to behave much like an incompressible fluid. Rotation of a bridge superstructure causes a redistribution of the elastomer within the pot, thereby minimizing the eccentricity of the vertical reaction. To aid in the redistribution of the elastomer within the pot, some manufacturers use a lubricant on the elastomer; others sandwich the elastomer between two thin disks of Teflon. To prevent the elastomer from being extruded from the pot by the pressure of the loosely fitted piston, manufacturers have developed a number of different types of sealing rings.

Because of the fit of the piston within the pot, differential horizontal translation between the superstructure and the bridge seat is prevented by the pot design shown in Figure 4. To provide for horizontal translation, this basic design is modified by the addition of an abutting pair of sliding surfaces, one faced with stainless steel and the other with Teflon. This type of pot bearing design is shown in Figure 5. The pair of guide bars shown in this figure is intended to restrict the lateral translation of the superstructure. Without guide bars, the bearing would be capable of accommodating both lateral and longitudinal translation.

Figure 6 shows a pot bearing that was designed by Kopetz of Howard Needles Tammen and Bergendoff for

bridge STA-30-1507. This is one of the first pot bearings fabricated for an Ohio structure. The two pot bearings of this structure were used to support a transverse box girder pier cap, where the deflection and lateral rotation of the transverse supporting girder and the longitudinal rotation of the integrally constructed and supported deck girders were clearly evident. These bearings were designed for an axial load of 3000 kips. Note that in this design the pot and the piston are reversed so that the pot is positioned on top of the piston. This placement of pot and piston, along with the closed-cell foam seal, will aid considerably in keeping the interior of the pot from becoming contaminated by water and debris. In this design, it should also be noted that the top sole plate and bottom masonry plate were designed to facilitate the removal of the bearing without extensive structure modification. A relatively thick masonry plate is required to distribute the 3500-psi pot pressure to the 1000-psi concrete bridge seat pressure.

To allow for the abnormal rotations of the curved superstructure of bridge COL-30-3661, Hendricks of Glaus, Pyle and Dehaven chose a spherical bearing design that has details similar to those illustrated in Figure 7. Note that this type of bearing has two sliding surfaces: a curved or spherical lower surface to provide for the abnormal rotations of the superstructure and an upper flat surface to provide for horizontal translation. In this particular design, lateral translation of the superstructure is prevented by the use of twin guide bars.

With respect to the sliding surfaces, these bearings were designed with two different types of sliding surfaces. The spherical surfaces were lubricated bronze, and the upper flat surfaces were faced with stainless steel and Teflon. A lubricated bronze surface is a bronze surface that has trepanned concentric recesses that are filled with a compressed lubricant. The recommended design coefficient of friction for such a surface is 10 percent. The upper sliding surfaces were faced with stainless steel and Teflon fabric, the first time that Teflon fabric was used in a compound bearing for an Ohio structure. This is one of the more efficient and durable forms of Teflon available to the bearing designer. The coefficient of friction for such a surface is well below 5 percent.

Recent improvements have been made in the spherical bearing designs by the Merriman Company. Instead of using lubricated bronze for the spherical sliding surface, manufacturers are now able to furnish a spherical convex surface faced with stainless steel (by welding with stainless electrodes) and a spherical concave surface faced with Teflon fabric.

Based on recent conversations with an official of a metallizing company, it now appears practicable to apply a stainless surface on regular structural steel--A588, for example--by the metallizing process. In metallizing, a spray of heated particles of the desired facing metal is applied to a structural substrate. After the particles have fused with the substrate to an appropriate thickness, the metallized surface is then machined and polished to the desired finish.

A third type of bearing is the elastomeric. Elastomeric bearings are unique in that, for short structures, they provide for both abnormal rotation and horizontal translation without any moving parts. All anticipated movements are accommodated by deformation of the elastomer within the bearings. For long structures, the basic elastomeric bearing is also supplemented with sliding surfaces similar to those that are incorporated in the other types of compound bearings.

In Ohio, the first use of large-diameter elastomeric bearings began two decades ago when Dorian of the Ohio Department of Transportation Bureau of Bridges chose them as replacements for the severely corroded and inoperative rocker bearings of bridge ROS-50-0667, a bridge with a through-truss superstructure. The bearings were installed in 1964. Periodic inspections of these now 18-year-old bearings indicate that they are in very good condition and it appears that they will survive the structure.

Shortly after this first installation, Ericksson of Ericksson Engineering provided elastomeric bearings for bridge BEL-7-2789 (see Figure 8). This structure consists of continuous steel beams supported on integrally framed transverse girders, which in turn are supported on widely spaced pier columns. Because of the deflection and rotation of the transverse girders and the simultaneous deflection and rotation of the longitudinal beams, it was obviously necessary to provide for the combined rotational effects (abnormal rotation) with compound column-top bearings. All of the intermediate pier bearings of this structure are elastomeric. The largest of those bearings are 3 ft in diameter and 7.5 in thick. They were installed in 1966.

Designs for elastomeric bearings have become quite large. Some bearings with 3-ft, 10-in diameter were manufactured by the General Tire and Rubber Company for a New York State structure. The bearings were tested at Lehigh University with one of the largest machines of its type in the country. Axial loads of up to 3 million lbf (about 3000 psi bearing pressure or about four times the maximum allowable design pressure) were applied to the bearings without apparent adverse effect.

The roof of the Dallas Sports Arena is supported on eight column-top structural bolsters. To provide for rotation and some translation, these structural bolsters are set on top of elastomeric bearings that are 4 ft square and 10 in thick. Harris of Oil States Industries, the fabricator of these bearings, said that his firm has just completed the fabrication of even wider bearings, probably the largest bridge bearings fabricated in the United States to date. These new bearings are 5 ft, 4 in long, 2 ft, 6 in wide, and 9.625 in thick. They are destined for a segmental concrete structure now being constructed for I-75 in Dade County, Florida.

Currently, elastomeric bearing manufacturers do not appear to be aggressively promoting the design and manufacture of compound elastomeric bearings for abnormal rotation and translation applications. However, we feel that this type of bearing, properly designed and manufactured, would be functionally efficient and an economical alternative for the more expensive pot, spherical, and disk bearings. Part of the reason for the lack of interest may be the present restrictive AASHTO design code. However, present elastomeric bearing research being conducted at the University of Washington under the direction of the National Cooperative Highway Research Program (4) should result in a new AASHTO elastomeric bearing specification that will furnish design guidance for this important application.

Until just recently, bridge engineers could only select from among these three types of compound bearings (pot, spherical, and elastomeric) for abnormal rotation applications. A fourth type of compound bearing, shown in Figure 9, has been introduced into the United States by Watson-Bowman Associates, Inc. It has come to be known as the disk bearing since its primary element, which is designed to facilitate abnormal rotations, is a disk composed of Adiprene, a hard plastic form of polyurethane developed by the DuPont Company. Unlike the pot bearing, which uses a confined elastomer under high pressure, or the

Figure 4. Pot bearing: rotation.

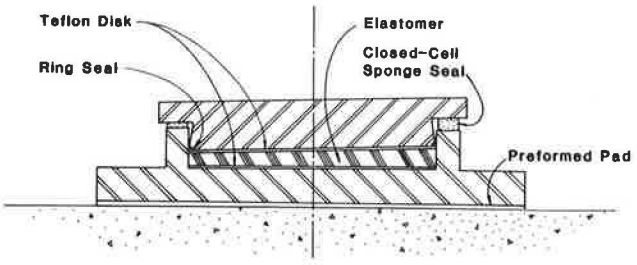

Figure 5. Pot bearing: rotation and translation.

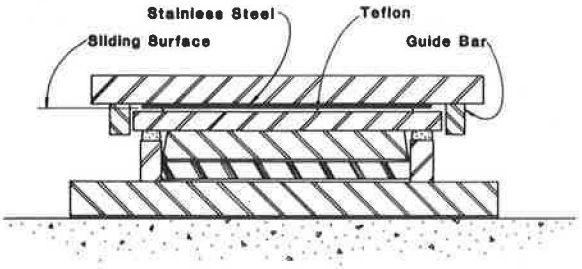

Figure 6. Pot bearing designed for Ohio bridge STA-30-1595.

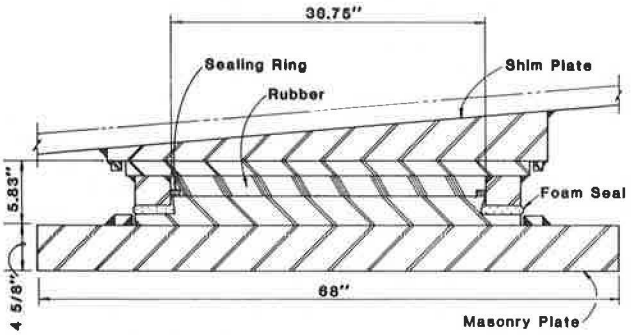

Figure 7. Spherical bearing.

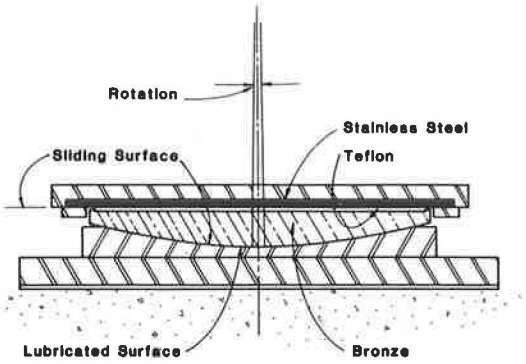

Figure 8. Elastomeric bearing designed for Ohio bridge BEL-7-2289.

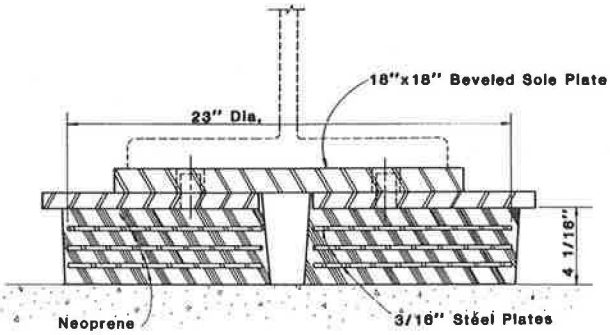

Figure 9. Disk bearing.

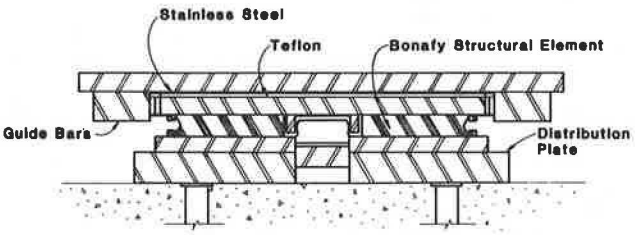

elastomeric bearing, which uses an unconfined but restrained elastomer under moderate pressure, the disk bearing is based on the use of a specially compounded unconfined elastomer under high pressure (up to 3800 psi). Apparently, the characteristics of the Adiprene disk, identified in Figure 9 as the Bonafy Structural Element, are such that it can withstand these high pressures and imposed rotations of more than 2° without apparent distress. We are familiar with Adiprene and its impressive properties, but we have no experience with this material in such a demanding application. However, Grant of Arvid Grant and Associates chose these bearings for his Pasko-Kennewick cable-stayed structure that was recently completed in Washington State. They have also been chosen for many other major structures throughout the world.

As Figure 9 shows, lateral and longitudinal translation is provided for by sliding surfaces similar to those of the other three types of compound bearings.

In view of the availability of these four basic types of compound bearings, we have wondered why so many bridge engineers fail to consider their use when they are choosing bearings for skewed or curved bridges. Probably the traditional use of rockers, rollers, pinned bolsters, and other similar structural bearings has conditioned many engineers to their use. The existence of Federal Highway Administration (FHWA) and state standard bearing design drawings that are designed for normal rotations but contain no limitations in this respect has probably supported such conditioning. The simplified design procedure that must be used in the design of multibeam or girder-deck-type structures has probably also contributed to such conditioning. We conceptually isolate a primary member and consider it acting alone, supporting a specific portion of the dead load and the superimposed live load. We size the member, calculate its required camber, verify the live load deflection, calculate the bearing reaction, and, in some instances, compute the amount of member rotation at the bearings. And in all of those calculations, we visualize the behavior of a single member deforming in a vertical plane, not a portion of a well-integrated structural system responding to randomly located vehicular live loads. Finally, the conditioning process appears to be supported by the actual performance of standard single-axis structural bearings. Bearing performance is

Figure 10. Bell River bridge pier 1 expansion bearing.

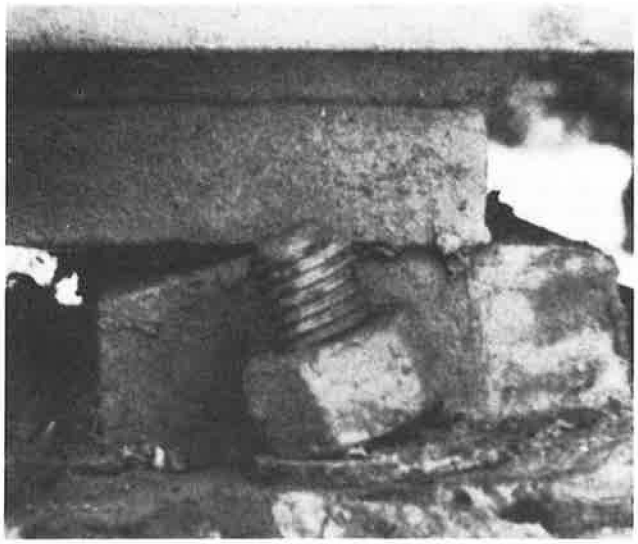

generally considered very good. If a structure is experiencing some distress, seldom is it recognized that the distress may be associated with, or indeed may even be caused by, a type of bearing that is not accommodating the actual superstructure rotations.

The standard specifications contain no clue to this potential problem. Article 1.7.32 of the AASHTO specifications (1) requires rotational provisions in bearings of spans "50 feet or greater... for deflection purposes." Since deflections are generally visualized as occurring in a vertical plane, this terminology tends to guide the design engineer to the choice of a bearing with a rotational axis that can be placed normal to the vertical plane.

Article 15.6.1.1 of the Ontario Highway Bridge Design Code (5) is somewhat better. It states, "bearings...shall accommodate the required translation and/or rotation of the structure." At least in this code, the engineer is directed to consider the rotation of other than a "member" when choosing a bearing type and bearing components.

Finally, Article 1.7 of the AASHTO Guide Specifications for Horizontally Curved Highway Bridges (6) is more specific. However, its very specificity only compounds the problem of bearing selection and bearing orientation. Consider a portion of the second paragraph of this article: "Thus, regardless of the direction of displacement allowed at a support, if rotation is permitted about only one axis, that axis should be perpendicular to the centerline of the web at the bearing." This text is probably appropriate for a slightly curved structure with radially placed substructures. It obviously is not intended for sharply curved structures on parallel substructures or for superstructures with severely skewed substructures. The text of this article is unfortunately worded in several respects. First, the choice of bearing or its orientation will not enable the engineer to "permit" the rotation of a bridge about only one axis; second, the use of a bearing with only one axis of rotation will generally be inappropriate; and, finally, if the one axis is placed normal to the web of the member, it will probably not coincide with the axis of rotation of the structure.

As pointed out in the introductory section of this paper, the AASHTO design specification requires special bearing designs to facilitate the deflection of bridge spans of 50 ft or more. But, since the average bridge engineer appears to have been conditioned to contemplate vertical deflections and normal rotations with respect to span length, the effects of skew and curvature on the deflection and rotation of the structures under consideration are generally ignored. This oversight has little consequence for shallow skews and moderate curves, for superstructures with unstiffened rolled beam flanges, or for superstructures that have been provided with compound bearings. However, for large skews and sharp curvatures, especially for longer spans, this omission of specification recognition is in large measure responsible for the fact that many bridge design engineers fail to consider the effects of these geometrics on the function, integrity, and durability of their bearing and bridge designs.

Consider the bearings that were used on the curved approaches to the Poplar Street bridge in St. Louis, Illinois. They were standard cast steel pinned rockers and bolsters. They failed to function appropriately and had to be replaced with elastomeric bearings after substantial girder distress was discovered (7).

In Ohio, the pinned rocker bearings of the 154-ft single-span deck girder bridge carrying I-76S over East Market Street in Akron, Ohio, have failed to function as designed (2). The bridge is skewed 67°, and the abnormal rotation of the superstructure at the bearings has caused the extrusion of the lead bearing pads from beneath the bearings. The pinned portions of the bearings are inoperative since the rotation of the superstructure at the bearings is about an axis that parallels the abutment rather than the rotational axis of the individual bearings.

One of the few reported examples of structure distress related to abnormal rotations is contained in a paper by Karol (8), who writes, "The performance of roller, rocker, or cylinder bearings can only be satisfactory if the 'door hinge' analogy is followed, that is, if all the hinges are in line." With respect to the condition of the bearings shown in Figure 10, he writes, "Although several causes of the described failure were considered (too low strength of mortar pads, incorrect setting of bearings, blocked expansion joints) the type of failure points to the main cause being associated with the geometry of the bridge and bearings and their inability to rotate laterally."

To help focus attention on this subject, Bishara of Ohio State University is currently engaged in a research project funded by the State of Ohio and FHWA to study the abnormal rotations of skewed superstructures. It is hoped that the results of this research will result in an AASHTO specification that requires the recognition of actual superstructure rotations in the choice and design of superstructure bearings. In the interim, the bridge engineer given the responsibility of designing heavily skewed and/or sharply curved structures, especially long-span structures, should choose a bearing design that will facilitate the abnormal rotations of the actual bridge superstructure and function well within reasonable stress limits.

REFERENCES

1. Standard Specifications for Highway Bridges, 12th ed. AASHTO, Washington, DC, 1977.
2. M.P. Burke, Jr. Orientation of Rocker Bearings on Curved Structures. Ohio Department of Transportation, Columbus, 1969.
3. Bridge Bearings. NCHRP, Synthesis of Highway Practice 41, 1977.

4. J.F. Stanton and C.W. Roeder. Elastomeric Bearings: Design, Construction, and Materials. NCHRP, Rept. 248, 1982.
5. Ontario Highway Bridge Design Code. Ontario Ministry of Transportation and Communications, Downsview, 1977.
6. Guide Specifications for Horizontally Curved Highway Bridges. AASHTO, Washington, DC, 1980.
7. F.K. Jacobson. Investigation of Bridge Approach Spans to Popular Street Bridge. Bureau of Materials and Physical Research, Division of Highways, Illinois Department of Transportation, Springfield, 1975.
8. E. Karol. Bearings: Part B--Design Factors. NAASRA Bridge Maintenance Seminar, Department of Main Roads, Sydney, New South Wales, Australia, 1979.

Publication of this paper sponsored by Committee on General Structures.

Notice: The Transportation Research Board does not endorse products or manufacturers. Trade and manufacturers' names appear in this paper because they are considered essential to its object.

Skewed Bridges with Integral Abutments

L.F. GREIMANN, A.M. WOLDE-TINSAE, AND P.S. YANG

As background to a theoretical investigation to establish tentative recomendations on maximum safe lengths and skew angles for concrete and steel skewed bridges with integral abutments, a survey of the highway departments of all 50 states was made to obtain information on the design and performance of skewed bridges with integral abutments. The findings of the survey are summarized, including various design criteria and limitations being used; typical pile orientations being used in bridge design by the different states and types of analysis used for thermal expansion and contraction; assumptions being made regarding selected design parameters; specific construction details being used, such as approach slab, backfill, and pile cap; long-term performance of skewed bridges with integral abutments; and previous research on skewed bridges with integral abutments. The variation in design assumptions and length limitations among the various states in their approaches to the use of integral abutments is discussed. The problems associated with thermal-induced abutment movement and the solutions developed by the different states for most of the ill effects of abutment movement are summarized. In view of the lack of theoretical and experimental research in this area, it is hoped that the survey will provide some useful empirical experience and information on the design of skewed bridges with integral abutments.

The routine use of integral abutments to tie bridge superstructures to foundation piling began in the United States about 30 years ago (1-4). Kansas, Missouri, Ohio, and Tennessee were some of the early users. This method of construction has steadily grown more popular. Today, more than half of the state highway agencies have developed design criteria for bridges without expansion joint devices.

Most of the states that use integral abutments began by building them on bridges less than 100 ft long. Allowable lengths have been increased based on good performance of successful connection details. Full-scale field testing and sophisticated rational design methods were not commonly used as a basis for increasing allowable lengths. This led to wide variations in criteria for the use of integral abutments from state to state. In 1974, the variation in the criteria between Kansas and Missouri was 200 ft (1). A survey conducted by the University of Missouri in 1972 (5) indicated that allowable lengths for concrete bridges with integral abutments were 500 ft in some states and only 100 ft in others.

Continuous steel bridges with integral abutments in the 300-ft range have performed successfully for years in such states as North Dakota, South Dakota, and Tennessee. Continuous concrete structures 500-600 ft long with integral abutments have been constructed in Kansas, California, Colorado, and Tennessee (6). In Iowa, the maximum bridge length for which integral-abutment construction is allowed has been limited to 265 ft (1). The Federal Highway Administration (FHWA) recommends integral abutments for steel bridges less then 600 ft long and for unrestrained bridges, those in which the abutment is free to rotate as with a stub abutment on one row of piles or an abutment hinged at the footing (6).

The primary purpose for building integral abutments is to eliminate bridge deck expansion joints and thus reduce construction and maintenance costs. A sketch of a bridge with integral abutments is shown in Figure 1. Conventional bridge bearing devices often become ineffective and are susceptible to deterioration from roadway runoff through open or leaking deck joints. A cross section of a bridge with stub abutments and deck joints is shown in Figure 2.

In an integral-abutment bridge with flexible piling, the thermal stresses are transferred to the substructure by way of a rigid connection. Various construction details have been developed to accomplish the transfer; one such detail from the state of Iowa is shown in Figure 3. The abutments contain sufficient bulk to be considered a rigid mass. A positive connection to the girder ends is generally provided by vertical and transverse reinforcing steel. This provides for full transfer of temperature variation and live load rotational displacements to the abutment piling.

PREVIOUS RESEARCH

Several of the states that use integral abutments have performed research to develop guidelines for the use of integral abutments. A summary of these research efforts follows.

California

California (7) began informal studies of some of its long structures without expansion joints about 15 years ago. Efforts consisted of identifying appropriate structures and conducting periodic inspections to monitor performance. A total of 27 bridges, varying in length from 269 to 566 ft, were studied; 18 of the bridges had integral abutments, and the others had semi-integral abutments.

Although a final report on this study is not yet available, the Office of Structures Design, California Department of Transportation (Caltrans), in

Figure 1. Cross section of a bridge with integral abutments.

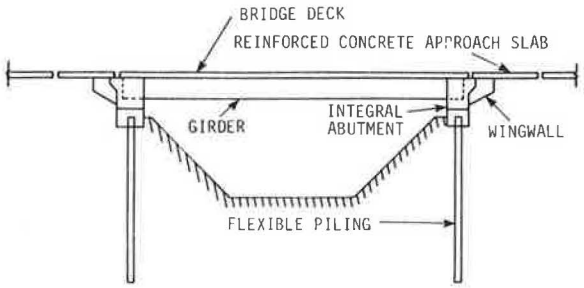

Figure 2. Cross section of a bridge with expansion joints.

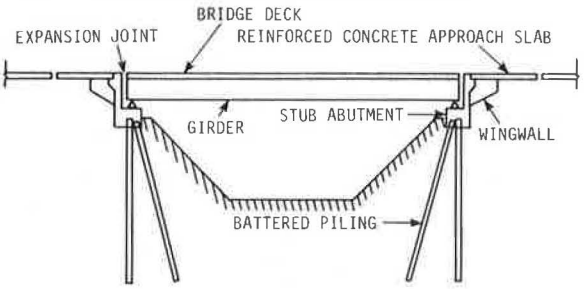

Figure 3. Integral abutment details (Iowa).

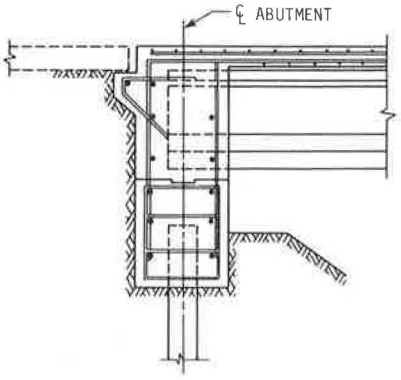

informal communications has reported the following interim findings:

1. There is no apparent distress at end bent columns.
2. There is no cracking on girder soffits related to the lack of deck joints.
3. No structural distress is apparent at the abutments.
4. There have been some problems with erosion and piping of abutment support soils due to small amounts of water flowing down behind the abutments.
5. There are no apparent deck cracking problems associated with expansion stresses.

The interim report recommends that a reinforced concrete approach slab be used with all jointless structures.

In 1971 and 1972, Caltrans and FHWA sponsored a research project to correlate theoretical solutions for laterally loaded piles with full-scale field tests in bridge embankments. Most of the work was done by Yee of the University of California at Sacramento. Yee reached the following conclusions (8):

1. The use of a linear variation in soil modulus with depth is a good approximation.
2. The influence of the soil below about 12-20 ft on pile stresses was practically negligible.
3. The effective length of the pile was about 15 ft for a free-head condition and about 21 ft for a fixed-head condition.

The results of this research were used to develop guidelines for the use of integral abutments in California. They are used when up to 1.5 in of total movement due to thermal forces is expected in a reinforced concrete bridge. In addition, to avoid rotation problems at the abutment, the end span is limited to 160 ft. The use of integral abutments is limited on prestressed bridges to those where the elastic shortening due to posttensioning is less than 0.375 in and the end span is less than 115 ft long.

Iowa

A final report on nonlinear pile behavior in bridges with integral abutments was published by Iowa State University in February 1982 (2). The research was sponsored by the Iowa Department of Transportation (DOT). The report included a survey of the highway departments of all 50 states to find the extent of use of integral abutments and the different guidelines used for analysis and design of nonskewed bridges with integral abutments. The variation in design assumptions and length limitations among the various states in their approaches to the use of integral abutments is discussed. The problems associated with lateral displacements at the abutment and the solutions developed by the different states for most of the ill effects of abutment movements are summarized in the report.

An algorithm based on a state-of-the-art nonlinear finite element procedure was developed and used to study piling stresses and pile-soil interaction in bridges with integral abutments. The finite element idealization consists of beam-column elements with geometric and material nonlinearities for the pile and nonlinear springs for the soil. An idealized soil model (modified Ramberg-Osgood model) was introduced in this investigation to obtain the tangent stiffness of the nonlinear spring elements.

Several numerical examples are presented in order to establish the reliability of the finite element model and the computer software developed. Three problems with analytic solutions were first solved and compared with theoretical solutions. A 40-ft H-pile (HP 10 x 42) in six typical Iowa soils was then analyzed by first applying a horizontal displacement (Δ_H) to simulate bridge motion and no rotation at the top and then incrementally applying a vertical load (V) until failure occurred. Based on the numerical results, the failure mechanisms were generalized to be of two types: lateral and vertical. It appears that most piles in Iowa soils (sand, soft clay, and stiff clay) failed when the applied vertical load reached the ultimate soil frictional resistance (vertical type of failure). In very stiff clays, however, lateral failure occurs before vertical failure because the soil is sufficiently stiff to force a plastic hinge to form in the pile as the specified lateral displacement is applied.

Preliminary results from this investigation showed that the vertical load-carrying capacity of H-piles is not significantly affected by lateral displacements of 2 in in soft clay, stiff clay, loose sand, medium sand, and dense sand. However, in very stiff clay (average blow count of 50 from standard penetration tests), it was found that the

Figure 4. Integral abutment system with pressure relief strips.

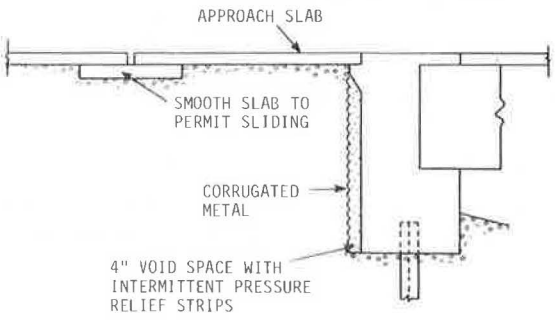

vertical load-carrying capacity of the H-pile is reduced by about 50 percent for 2 in of lateral displacement and by about 20 percent for lateral displacement of 1 in.

On the basis of the preliminary results included in the report, the 265-ft length limitation in Iowa for concrete bridges with integral abutments was termed to be very conservative. A summary of state length limitations for bridges with integral abutments is given below (9):

Maximum Length (ft)	No. of States by Bridge Type		
	Steel	Concrete	Prestressed
800	-	1	1
500	-	1	2
450	-	1	3
400	2	3	4
350	1	3	1
300	8	8	8
250	2	1	-
200	5	1	2
150	1	-	-
100	-	1	-

Missouri

In 1972, the University of Missouri conducted a survey and feasibility study of integral and semi-integral abutments (5). The following conclusions were drawn from the survey:

1. The use of superstructures connected to flexible substructures was becoming generally acceptable.
2. Design limitations were more restrictive for steel than for concrete bridges.
3. There was no simple design criterion that accounted for shrinkage, creep, temperature, or substructure flexibility.
4. Induced stresses resulting from thermal effects, creep, shrinkage, backfill movement, and the like are recognized by bridge engineers as potentially significant, but there is wide variance in methods of considering them.
5. Bridge design engineers are interested in induced stresses and associated problems, are generally uncertain as to the significance of and suitable methods for consideration of these stresses, and would welcome a simple, rational design criterion and specific recommendations as to design details.

North Dakota

In August 1979, the State of North Dakota built a 450-ft prestressed concrete box beam bridge on a 0° skew near Fargo. The piles in the integral abutments were instrumented with strain gauges and had inclinometer tubes attached. Jorgenson of the Civil Engineering Department, North Dakota State University, was commissioned to monitor the movements and strains in the bridge for one year. He had a preliminary report prepared in late summer 1981 (10). It appears that the maximum total movement at each end of the bridge is about 2 in. This is equivalent to a temperature variation of about 117°F.

The installation contains a unique feature designed by Moore Engineering of West Fargo, North Dakota. A special expansion joint material several inches thick is placed behind the abutment backwall. Behind it is a sheet of corrugated metal. The mechanism is designed to reduce passive earth pressures on the abutment and to help reduce the formation of a void space on contraction of the superstructure. The system is shown in Figure 4 (10).

South Dakota

In 1973, South Dakota State University conducted full-scale model tests on integral abutments to determine induced stresses in the superstructure and the upper portion on the piling (1). The model consisted of two HP 10 x 42 steel piles on 8.5-ft centers cast into a rigid concrete abutment with two plate girders about 26 ft long. The 32-ft piles were driven into silty clay over glacial till to a bearing capacity of 23 tons. The pile tops were welded to the bottom flanges of the girders.

Various lateral displacements within ±1 in were induced at the abutment by jacking at the free end during four construction stages. The results of interest are with the slab and backfill in place. Strains in the piling corresponding to stresses of up to 42 ksi were measured. This occurred just below the bottom of the concrete abutment. Several conclusions were drawn by the investigators (they were referred to as qualitative results that would require further verification):

1. Stresses were induced in the girders that in some cases were additive to dead and live load stresses. The induced stresses were generally within the 40 percent overstress allowed by the American Association of State Highway and Transportation Officials (AASHTO).
2. Horizontal movements greater than about 0.5 in will cause yielding in the piles.
3. Free-draining backfill is recommended since frozen soil against the abutment can greatly increase induced girder stresses by limiting free movement.
4. The use of approach slabs that allow rotation and translation of the abutment and, if possible, avoid continuing compaction of the backfill by traffic is recommended.

As part of this study, a questionnaire was sent to 10 north-central states. Two trends can be identified when this survey is compared with the responses of the same states to the survey recently conducted by Iowa State University (2). Idaho, Missouri, North Dakota, and South Dakota have substantially increased their bridge-length limitations for use with integral abutments. Iowa, Kansas, Nebraska, and Wisconsin have retained the same limits. Two states still do not routinely use integral abutments. Also of interest is the fact that since 1973 three of the states have begun to routinely use integral abutments with steel bridges; four of them already had and one still has not.

SURVEY OF CURRENT PRACTICE ON SKEWED BRIDGES WITH INTEGRAL ABUTMENTS

As background to a theoretical investigation to establish tentative recommendations on maximum safe

Figure 5. Questionnaire for skewed bridge with integral abutments.

Part One. Questionnaire for Skewed Bridges with Integral Abutments.

1. If you design skewed bridges with integral abutments, which of the kinds of pile orientations shown below do you use in the integral abutments? If neither, please sketch the type of pile orientation you use.

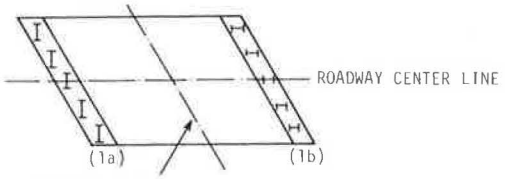

CENTER LINE PARALLEL TO ABUTMENT

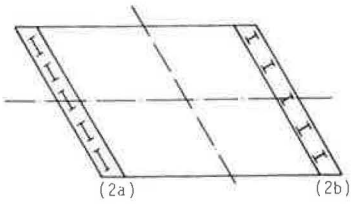

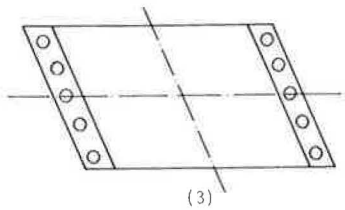

2. If you use either orientation, what structural assumptions are made for (1) the top of the pile, (2) thermal expansion or contraction (one direction or both directions) and (3) diagonal thermal expansion or contraction?

3. When you design skewed bridges with integral abutments, how do you treat the approach slab, backfill, and pile cap?

4. Any additional comments on skewed bridges with integral abutments?

lengths and skew angles for concrete and steel skewed bridges with integral abutments, a survey of the different states was made to obtain information on the design and performance of such bridges. This paper summarizes the findings of the survey, including

1. Various design criteria and limitations being used;
2. Typical pile orientations being used in bridge design by the different states and types of analysis used for thermal expansion and contraction;
3. Assumptions being made regarding selected design parameters;
4. Specific construction details being used, such as approach slab, backfill, and pile cap; and
5. Long-term performance of skewed bridges with integral abutments.

Method of Investigation

Responses to previous surveys concerning the use of integral abutments (2,4) have indicated that most state highway departments have their own limitations and criteria in designing integral abutments. The bases of these limitations and criteria are shown to be primarily empirical.

Today, the use of integral abutments in design has been accepted by 28 state highway departments and the District Construction Office of FHWA Region 15 (2). A survey questionnaire was prepared in cooperation with the Office of Bridge Design, Highway Division, Iowa DOT, to obtain information on the use and design of skewed bridges with integral abutments. A copy of the questionnaire is shown in Figure 5.

The survey questions concerned pile orientations in the integral abutments. The states were asked what structural assumptions were being made in determining fixity conditions on pile head and directions of thermal expansion and contraction of the integral abutments of skewed bridges. In addition, questions included the treatments of approach slab, backfill, and pile cap. Sketches of different types of pile orientations in integral abutments were also included in the questionnaire.

Trends of Responses

Of the 28 responses received, 26 states indicated that they use an integral type of abutment on skewed bridges. Among these states, Virginia has designed its first integral-abutment skewed bridge with a small skew (10°) and a relatively small anticipated movement at each abutment (±3/8 in). The states of Connecticut and Oklahoma indicated that they do not use integral abutments on skewed bridges. Although Connecticut has not constructed any integral abutments on a skew, they have constructed one nonskewed bridge with integral abutment. The other

state, Oklahoma, indicated that it felt integral abutments on skews are inappropriate because of the integral displacement.

One of the purposes of this study is to present methods of analysis and design details of integral abutments on skewed bridges. Many of the states that use integral abutments on skewed bridges provided useful empirical experience that sheds some light on this problem.

Summary of Responses

The following discussion of questionnaire responses received from states that use integral abutments on skewed bridges is keyed to the survey question numbers shown in Figure 5. A comprehensive summary of the survey responses is given in Table 1.

Question 1

The pile orientations in the integral abutments on skewed bridges shown in the first survey question in Figure 5 can be classified into two parts: (a) the web of the pile perpendicular or parallel to the roadway centerline--e.g., types 1a and 1b, respectively; and (b) the web of the pile parallel and perpendicular to the centerline of the abutment--e.g., types 2a and 2b, respectively. The responses indicated that 6 states use type 1a orientation, 1 state uses type 1b, 10 states use type 2a, and 16 states use type 2b. In addition, 3 states use circular piles (type 3) in integral abutment on skewed bridges.

One major difference between skewed and nonskewed bridges with integral abutments is that when both are subjected to thermal expansion and contraction the skewed will have thermal-induced biaxial bending stresses on piles if pile orientation 2a or 2b is specified. This becomes a three-dimensional analysis problem. For types 1a, 1b, and 3, pile orientations will have the same thermal effects as with nonskewed integral-abutment bridges (2). The responses showed that 15 of 26 states have adopted the pile orientations so that bending will be primarily about the strong axis.

A second questionnaire was sent out to investigate whether there are any theoretical, experimental, or empirical bases for the orientation of the piles and to find out whether any distresses or problems associated with orientation of the piles have occurred. The responses received from the second questionnaire indicated that most states do not have any clear theoretical, experimental, or empirical bases.

Idaho officials assumed some creep in the soils surrounding the piles and that a redistribution of stresses will occur since thermal forces are generally applied gradually. In addition, the restraint provided by the integral abutment was assumed to reduce the magnitude of the thermal movement; orienting the piles with the strong axis parallel to the centerline of the bearings was assumed to give more rigidity for earthquake loads when liquification of embankment is assumed. Vermont oriented the piles to resist the force of earth pressure from the abutment backfill rather than the force of thermal expansion.

California explained its policy of orienting the web of piles perpendicular to the centerline of the abutment (Figure 5) as follows: For a square bridge, such orientation of piles results in bending about the strong axis of the piles due to both thermal forces and active soil pressure. When the bridge is skewed, however, temperature forces would act along the centerline of the roadway, not parallel to the pile web, and active soil pressure would act against the strong axis of the pile. A particular concern is rotational action caused by the active soil pressure on skewed bridges. Temperature effects are somewhat compensated for by predrilling for driven piles and filling the voids with pea gravel or sand.

Colorado respondents replied that they were unaware of any distress in the piling. In a few cases, with cast-in-place, posttensioned bridges with integral abutments, cracks have been detected in the abutment wall at the intersection of the superstructure with the abutment. The state suspected that the cracks are due primarily to the movements of the superstructure caused by elastic shortening and creep from the posttensioning forces.

North Dakota has been using this method of building bridges for about 18 years and so far was unaware of any problems.

According to Iowa bridge engineer Gee (3), pile orientation 1a is not considered in design because of construction work difficulty in arranging the reinforcement in the integral abutments. Thermal-induced biaxial bending stresses on piles can be avoided by using type 3 circular pipe piles. The major disadvantages are that their vertical bearing capacities are usually less than those of the steel H-piles and they are stiffer than H-piles about the weak axis.

Question 2

The second survey question, regarding structural assumptions (Figure 5), revealed the following. Two states indicated that at the pile top a roller assumption was made, eight reported a pinned assumption, one assumed partial fixity, and eight states assumed the pile top to be totally fixed. These assumptions were actually based on the restraint conditions on the pile top. In Iowa, the pile top is completely restrained by spiral reinforcement in the pile cap and total fixity is assumed. For a pinned assumption, the top portion of piling is enclosed with a flexible material before casting in the concrete abutment (3).

Only a few states consider thermal, shrinking, and soil pressure forces when calculating pile loads. For a long skewed bridge with integral abutment, temperature-induced stresses become very critical to the piling load capacities. If pile orientations 2a and 2b are adopted, the thermal expansion or contraction along the roadway center can be divided into two components, one parallel to the pile web (transverse) and the other perpendicular to it (longitudinal). Thus, the piles in integral-abutment skewed bridges will be subjected to biaxial bending due to thermal movement. It is also possible that in long skewed bridges diagonal thermal expansion and contraction will cause a serious problem. However, none of the states indicated concern about it. The following are some of the remarks made regarding thermal effects on integral abutments on skewed bridges:

1. Assume that the pile is fixed a certain depth below the bottom of the pile cap and any thermal movement is accomplished by bending in the pile.
2. Thermal expansion parallel to the pile cap can be resisted by the friction force between the backfill and the end wall.
3. For large skews, one state batters selected piles (say, every other pile) 3 in/ft to resist rotation caused by road fill against the abutment backwall.
4. Use shear keys on the bottom of the pile cap to prevent lateral movement of the pile cap on extreme skews (±40°).

Table 1. Summary of responses by the different states.

State	Pile Orientation					Structural Assumption				Design Consideration			Comment
							Thermal Expansion and Contraction						
	1a	1b	2a	2b	3	Pile Head	Longitudinal	Transverse	Diagonal	Approach Slab	Backfill	Pile Cap	
Arkansas	-	-	-	-	-	-	-	-	-	-	-	-	-
Arizona	No	No	No	Yes	No	Roller	Yes (due to roller)	Restrained by abutment cap	No	Tied to abutment with dowels and moves back and forth with superstructure	No	No	-
California	No	No	No	Yes	No	Hinge	No	No	No	-	-	-	Battered piles used to resist active earth pressure
Colorado	Yes	Yes	Yes	Yes	No	-	-	-	-	Bridge length >200 ft, use approach slab	No	No	Steel bridge ⩽250 ft; concrete bridge ⩽350 ft; no problem in skew; use predrilled oversized hole
Connecticut	No	No	No	No	No	No	No	No	No	No	No	No	-
Georgia	Yes	No	No	No	No	Free translation; free rotation; roller	Yes	Yes	No	Expansion joint between approach slab and bridge slab	-	-	-
Iowa	No	No	Yes	No	No	Fixed	Yes	No	No	Neglect	Neglect	Neglect	Conservative design
Idaho	No	No	Yes	Yes	No	Fixed	Yes	Yes	-	Expansion joint specified between rigid pavement and approach slab; no special treatment specified for flexible pavement	Use free-draining granular material as backfill	Rigid pile cap	Skewed three-span steel girder bridge with integral abutment was built; rotational forces from lateral earth pressure on end wall caused failure in pier anchor bolts on exterior girder
Indiana	No	No	No	Yes	No	Hinge	No	No	No	20-ft approach slab integrally attached to bridges	Use select granular fill	Pile cast in pile cap 1 ft	150 ft maximum
Kansas	No	No	Yes	Yes	No	Hinge	Yes	Yes	No	Uses slab support at backwall and pavement rests on slab with about 30 ft from end of wearing surface	Backfill compaction has settlement just off end of bridge	Pile caps not used	Cast-in-plate bridges with end of steel beams into abutment concrete, reinforcing to make them essentially integral
Kentucky	Yes	No	No	No	No	Partially restrained	Yes	No	-	No special treatment with flexible pavement	Special granular backfill specified	-	Bridge length 300 ft, max skews ⩽30°, pile prebored for distance of 8 ft before bottom of pile cap
Missouri	No	No	No	Yes	No	Fixed	No	No	No	-	-	Use shear key on bottom of pile cap to prevent lateral movement of pile cap on extreme skews (±40°)	Piles designed for direct load only: <500 ft for prestressed bridges, <400 ft for steel bridges
Montana	No	No	No	Yes	No	No	No	No	No	Not fixed to abutment	Granular material as backfill	No	⩽30° skews
North Dakota	No	No	No	Yes	No	Fixed	Yes	Yes	No	Assume approach slab has no effect	Select granular material	Abutment wall is pile cap and is re-	Hold skew to max of −30°

Table 1. Continued.

State	Pile Orientation					Structural Assumption				Design Consideration			Comment
							Thermal Expansion and Contraction						
	1a	1b	2a	2b	3	Pile Head	Longitudinal	Transverse	Diagonal	Approach Slab	Backfill	Pile Cap	
North Dakota continued												inforced to resist bending below superstructure	
Nebraska	Yes	No	No	No	No	-	Yes	No	No	Same as square bridges with integral abutments	Select granular material	Abutment wall is pile cap and is reinforced to resist bending below superstructure	15° skew for integral abutment
New Mexico	No	No	Yes	No	No	Fixed	Yes	No	No	Used on some bridges and not on others	Do not use specified backfill anymore	-	Have built bridges with 15° skew; skew angle neglected
New York	No	No	Yes	No	No	-	No	No	No	Construction joint provided between approach slab and bridge slab	Granular fill behind backwall and wing walls	No	Neglect stress caused by rotation, designed to take vertical load only; in skewed bridges, neglect some twisting induced in piles when structure deflects, use predrilled oversized hole
Ohio	No	No	Yes	No	No	-	No	No	No	Tie approach slab to abutment	Same as nonintegral abutments for usual short bridge	Pile cast in pile cap 2 ft	Oil country pipelines not used in integral abutments because they are stiffer than H-piles about weak axis
Oklahoma	No	No	No	No	No	-	-	-	-	-	-	-	Integral abutments only with zero skews
Oregon	No	No	No	Yes	No	Hinge	-	-	-	Approach slab was tied to pile cap	-	Pile cast in pile cap 1 ft	-
South Dakota	Yes	No	Yes	No	No	Fixed	Yes	No	No	Tied with bridge to prevent erosion of shoulder	-	No	-
Tennessee	No	No	No	Yes	No	-	Yes	No	No	Construction joint between abutment backwall and approach slab	No	No	-
Utah	No	No	No	No	Yes	Hinge	-	-	-	Expansion joint between approach slab and bridge slab	96 percent of optimum	No	Steel piles used primarily through granular material over bed rock; no problem in thermal movements
Virginia	No	No	Yes	No	No	Fixed	No	No	No	No approach slab	Used 1.5 ft of porous backfill with 0.5-in diameter pipe underdrain	Uniform width and parallel to bridge skew	Max skew 10°; relatively small movement at each abutment (±3/8 in)
Vermont	No	No	No	Yes	No	Fixed	Yes	No	No	Approach slab anchored to abutment	No special treatment	Rigid pile cap	≤30° skew
Washington	Yes	No	No	Yes	Yes	Hinge	Yes	No	No	Approach slab at-	Backfill	Designed	Calculate mo-

Table 1. Continued.

State	Pile Orientation					Structural Assumption				Design Consideration			Comment
	1a	1b	2a	2b	3	Pile Head	Thermal Expansion and Contraction: Longitudinal	Transverse	Diagonal	Approach Slab	Backfill	Pile Cap	
Washington continued										tached to abutment with allowance for expansion	earth pressure applied normal to abutment	as cross beam on simple supports	ments of inertia along roadway center
Wisconsin	No	No	No	Yes	Yes	-	No	No	No	Designed for vertical load only	-	Designed as reinforced continuous beam over piling	Piles designed for vertical loads ≤30° for slabs; ≤15° for prestressed or steel girders
Wyoming	No	No	No	Yes	No	Plastic hinge	Yes	Yes	No	Neglect	Neglect	Assumed to be a mass attached to end of girder	Max length ≤300 ft
FHWA Region 15	No	No	Yes	No	No	Hinge	No	No	No	-	-	Pile cast in pile cap 1 ft	-

5. If the bridge design has a small skew (≤10°) and a relatively small anticipated move- ment at each abutment (±0.375 in), no special consideration need be given beyond that of a 0° skew condition.

Question 3

Most states indicated that a free-draining granular material is used as backfill behind the abutment. One state uses 1.5 ft of porous backfill from subgrade to bottom of integral abutment along with 6-in-diameter pipe underdrain. Beyond that, normal material available at the job site is used. Some respondents, however, indicated that backfill compaction has always been somewhat of a problem with settlement just off the end of the bridge. Otherwise, no special treatment has been used. Several states indicated that rigid pile cap has been used, and pile was cast into pile cap 1-2 ft long. Two states indicated that pile cap is designed as reinforced continuous beam over the piling.

The survey responses show, in general, that the approach slab can be tied to the abutment with dowels and can move back and forth with the superstructure if a construction joint is provided between the approach slab and the bridge slab. The reply from South Dakota stated that at least one approach slab panel with curb-and-gutter section attached to the bridge end is necessary to prevent erosion of the shoulder behind the abutment wing. One state indicated that, whereas its criteria specify an expansion joint between rigid pavement and the approach slab, no special treatment is specified for flexible pavement. In Colorado, the approach slab was used if the bridge length was greater than 200 ft.

Question 4

The following are some additional comments on skewed bridges with integral abutments:

1. Some of the piles in the abutment have to be battered to resist the active earth pressure acting behind the abutment.
2. Rotational forces from the lateral earth pressure on the end walls cause a failure of the pier anchor bolts on the exterior girders.
3. For a cast-in-place bridge, the end of steel beams may be cast into the abutment concrete, reinforcing to the extent that they are considered essentially integral.
4. Piles may be prebored for a distance of 5-20 ft below the bottom of the pile cap.
5. Because the piles are oriented to allow bending about the weak axis, any stresses caused by rotation will only occur in the outermost flange fibers and not the web and center portions of the flanges. When the abutment is skewed, some twisting may be induced in the piles when the structure deflects, but this can be assumed to be of a minor nature and may be neglected.

SUMMARY AND CONCLUSIONS

Previous research work in the area of integral abutments includes surveys of detailing and design criteria used by the state highway agencies, full-scale model tests, and monitoring of the performance of actual bridge installations. The present survey responses indicated that 26 states use integral-type abutments on skewed bridges. Most states design integral abutments on skewed bridges based on empirical experience and no theoretical analysis is introduced in design.

For integral abutments on skewed bridges, 15 states orient their piles with the web of the piles perpendicular to the centerline of the abutment (type 2b) so that bending will be primarily about the strong axis. Thus, thermally induced biaxial bending stresses will be introduced into the piles. But the survey responses show that most states ignore the thermally induced bending stress due to transverse thermal movement. Kansas indicated that transverse thermal movement can be eliminated by using shear keys on the bottom of the pile cap. The major reasons given for using pile orientation 2b are as follows:

1. The restraint provided by the integral abutment will reduce the magnitude of the thermal movement. Orienting the pile with the strong axis parallel to the centerline of the bearings gives more

rigidity for earthquake loads when liquification of embankment is assumed.

2. Thermal expansion is actually very small, and the backfill material around the abutment and the piling seems to yield sufficiently so that no distress is apparent. The piling was oriented to resist the force of earth pressure from the abutment backfill rather than the force of thermal expansion.

3. Temperature forces would act along the centerline of the roadway, not parallel to the pile web, and active soil pressure would act against the strong axis of the pile. Temperature effects are somewhat compensated for by predrilling for driven piles and filling the voids with pea gravel or sand.

No special treatments are usually given to backfill and pile cap on skewed bridges, and they might be constructed in the same way as on nonskewed bridges. As for the approach slab, it can be tied to the abutment with dowels or an expansion joint may be provided between the approach slab and the bridge slab. Some states put an expansion joint a certain distance behind the approach slab. In this case, the approach slab will act integrally with the abutment.

It has been more than 15 years since the first integral abutments on skewed bridges were constructed. No serious problems or distresses have yet been discovered. In view of the lack of theoretical and experimental research in this area, it is hoped that this survey will provide some useful empirical experience and information on the design of skewed bridges with integral abutments.

ACKNOWLEDGMENT

The study discussed in this paper was conducted by the Engineering Research Institute of Iowa State University and was sponsored by the Highway Division of the Iowa DOT through the Iowa Highway Research Board. We wish to express our gratitude to the bridge engineers in all 50 states for the 100 percent return rate on the survey questionnaire. In particular, special thanks go to those who provided additional information concerning their design and detailing procedures. We also wish to extend sincere appreciation to the engineers of the Iowa DOT for their support, cooperation, and counseling. Special thanks are extended to Bruce Johnson, Charles A. Pestotnik, Henry Gee, Vernon Marks, Kermit L. Dirks, and Wallace W. Sanders, Jr.

REFERENCES

1. H.W. Lee and M.B. Sarsam. Analysis of Integral Abutment Bridges. South Dakota Department of Highways, Pierre, March 1973.
2. A.M. Wolde-Tinsae, L.F. Greimann, and P.S. Yang. Nonlinear Pile Behavior in Integral Abutment Bridges. Iowa State Univ., Ames, ERI Project 1501, ISU-ERI-Ames-82123, Feb. 1982.
3. P.S. Yang, A.M. Wolde-Tinsae, and L.F. Greimann. Nonlinear Finite Element Study of Piles in Integral Abutment Bridges. Iowa State Univ., Ames, ERI Project 1501, ISU-ERI-Ames-83068, Sept. 1982.
4. A.M. Wolde-Tinsae, L.F. Greimann, and B. Johnson. Performance of Integral Bridge Abutments. Journal of International Assn. for Bridge and Structural Engineering, IABSE Periodica 1/1983, Feb. 1983.
5. J.H. Emanuel and others. An Investigation of Design Criteria for Stresses Induced by Semi-Integral End Bents. Univ. of Missouri, Rolla, 1972.
6. Integral, No-Joint Structures and Required Provisions for Movement. FHWA, T5140.13, Jan. 28, 1980.
7. Memo to Designers. Office of Structures Design, California Department of Transportation, Sacramento, Nov. 15, 1973.
8. W.S. Yee. Lateral Resistance and Deflection of Vertical Piles: Final Report--Phase I. Bridge Department, Division of Highways, California Department of Transportation, Sacramento, 1973.
9. State Highway No. 44 Over Pine Creek, Mellette County, South Dakota. U.S. Steel Corp., Pittsburgh, Bridge Rept., ADUSS 887126-01, March 1977.
10. J.L. Jorgenson. Behavior of Abutment Piles in an Integral Abutment Bridge. Engineering Research Station, North Dakota State Univ., Fargo, ND(1)-75(B), Nov. 1981.

Publication of this paper sponsored by Committee on General Structures.

Behavior of Abutment Piles in an Integral Abutment in Response to Bridge Movements

JAMES L. JORGENSON

A field study of the behavior of abutment piles for a bridge that has integral abutments, piers, concrete box girders, concrete deck, and six 75-ft spans is discussed. To compensate for anticipated thermal movements, two unique features were built into the bridge. Expansion joint material was placed between the back side of the abutment and the soil backfill, and compressible material was placed on the webs of the abutment piles to create low soil resistance to pile movement. Over a one-year period, monthly readings were taken of bridge length (by using steel tape), gap between soil backfill and back side of abutment, openings in the expansion joints on the concrete approach slabs, vertical elevation of abutments and piers, slope indicator readings on the four corner abutment piles, and temperatures of concrete deck and air. A formula involving air temperatures was developed to estimate the maximum change in bridge length due to thermal changes. The changes in bridge length agree with changes measured from steel tape and expansion joint openings. The study concluded that these changes did not result in equal abutment movements at each end of the bridge, and the maximum abutment movement resulted in stresses at the top of the piles sufficient to initiate a yield stress in the steel but not sufficient to form a plastic hinge. An analytic model was used to predict stresses in the abutment piles due to movements of the abutments.

Bridge engineers recognize that changes in air temperature result in changes in the temperature of bridge materials, which in turn result in movements of the bridge. So long as the bridge components

(girders, piers, and abutments) are not restrained from movement, the movements do not create stresses in the bridge. However, if the girders, piers, and abutments are integral, thermal movements result in stresses in those bridge components. The bridge designer must then elect to use expansion joints, an integral structure, or some combination of the two.

My own observations and those of others (1) indicate that in many cases the expansion devices do not function as assumed by designers. This behavior has interested designers in eliminating the expansion devices and considering the use of integral structures.

A survey of bridge designers on the use of integral-abutment bridges (2) indicates that the maximum bridge length without an expansion joint is 400-450 ft for concrete structures. In addition, the induced stresses from thermal effects are recognized as being potentially significant.

The North Dakota State Highway Department has been using integral abutments on structures up to 350 ft in length. However, the Department is concerned about the magnitude of thermal movements and resulting stresses in long bridges. To respond to this need, the Department contracted with the Engineering Experiment Station of North Dakota State University to study the behavior of a 450-ft integral-abutment bridge in Cass County (see Figure 1).

The bridge studied is on Cass County Road 31, about 2 miles north of Fargo, and provides a crossing of the Cheyenne River. Construction took place between July 1978 and August 1979. In 1978 the old bridge was removed, rough grading was completed, all piles were driven, abutment and pier caps were poured, and the prestressed concrete girders were placed. In addition, at least one pier diaphragm and one intermediate diaphragm were poured. Work on placement of the concrete deck began in the spring of 1979, and the deck was poured in July. The remaining items were completed in time for the August 1979 opening to traffic.

The Cass County Bridge is a 450-ft-long concrete bridge with integral abutments and piers. There are no expansion joints on the bridge, but expansion joints are located in the approach slab about 30 ft from each end of the bridge.

A transverse section through the bridge deck is shown in Figure 2. Prestressed concrete box girders were used to support a poured-in-place concrete deck. The girders and deck were designed to act as a monolithic unit even over the piers (see Figure 3). The concrete curb is tied into the concrete deck; however, the curb does have expansion joints at 15-ft intervals.

Continuity at the piers is also shown in Figure 3. The steel pile, pier cap, diaphragm, concrete girder, and concrete deck were all reinforced to behave as a single unit. For the center three piers, the piles are oriented with their strong direction of bending in the longitudinal direction of the bridge. A concrete wall was placed between the pile in each pier. The piles in the piers adjacent to the abutments have their weak direction of bending in the longitudinal direction of the bridge.

A section through the abutment is shown in Figure 4. As with the piers, the pile cap, diaphragm, concrete girder, and concrete deck are reinforced to act as a single monolithic unit. The pile is oriented with its weak direction of bending in the longitudinal direction of the bridge and is reinforced within the abutment cap and diaphragm to transmit the full plastic movement of the pile. In anticipation of thermal changes in the length of the bridge, a pressure relief system was set up between the back side of the abutment and the backfill soil. The system consists of 3-1/3-in-wide by 4-in-thick pressure relief strips placed vertically at about a 4-ft spacing on the back side of the abutment. Corrugated metal was used to retain the granular backfill behind the pressure relief strips. The material used for pressure relief strips was "Pressure Relief Joint", manufactured by W.R. Meadows. According to data sheet 324 on this product, the material will recover 96 percent of its thickness after being compressed to 50 percent of its thickness.

To permit longitudinal movement of the abutment piles without generating significant resistance to movement, a 2-in layer of compressible material was placed on each side of the web of the pile. The soil was predrilled to a 16-in diameter and a 20-ft depth. Compressible material was glued to the pile; after pile driving, the void space was filled with sand (see Figure 5). The compressible material was Ray-Lite with a density of 1.25 pcf and a compressive strength of 8-16 psi.

There is an expansion joint in the approach slab at 20 ft from each end of the bridge. One end of the approach is tied into the bridge abutment, and the other rests on the smooth surface of a supporting slab. As the bridge changes in length, the expansion joint will open and close.

The soil profile consisted of a glacial-lake-deposited clay to a 100-ft depth underlaid by glacial till. The soil profile under the north abutment was as follows: 15 ft of fat clay of medium stiffness, 6 ft of soft silty clay, 4 ft of stiff fat clay, 70 ft of fat clay of medium stiffness, and 17 ft of very stiff sandy clay, followed by silty sand that was very dense. The piles were about 110 ft long and extended into the silty sand.

MEASUREMENTS OF BRIDGE MOVEMENTS

Measurements of bridge movements were taken during the period from August 8, 1979, through September 7, 1980. Some measurements were taken prior to August 8, but they were not complete sets of data. The readings were taken at about one-month intervals except during September 6 and 7, when they were taken at 6-h intervals. (Because early morning temperatures will not contain the highest daily temperature, it was decided to take additional readings at about 6-h intervals over a 24-h period.)

Readings were taken early in the morning just after daylight. When the sun is shining on the bridge, the exposed concrete surface increases in temperature at a higher rate than the remaining concrete. Hence, the sun causes unequal temperatures within the concrete. After sundown, the concrete temperature is influenced by the current temperature of the concrete and the air temperature. By daybreak, the air will have had the best possible chance to equalize the temperature throughout the concrete. Other researchers have found the temperature of the concrete to be fairly uniform at daybreak (3).

Change in Bridge Length

The length of the bridge was measured by placing a 500-ft-long steel tape on top of the concrete curb and measuring the distance between markers, which were cast into the concrete near the ends of the curb. The tape length was corrected for temperature change with the air temperatures taken as the tape temperature.

One way to determine the change in length of the bridge would be to sum the movements of the abutments. This is shown in Figure 6 along with the change in bridge length determined by tape measure-

Figure 1. Plan and elevation of integral-abutment bridge.

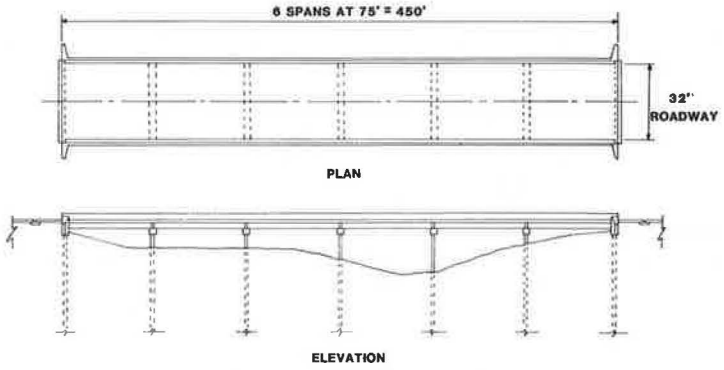

Figure 2. Transverse section through deck.

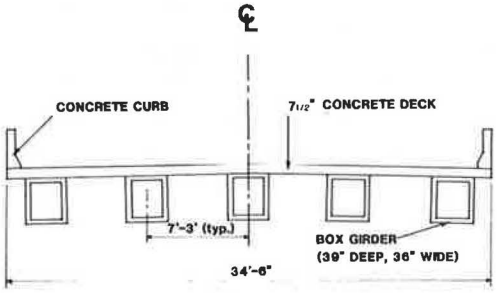

Figure 3. Longitudinal section through pier.

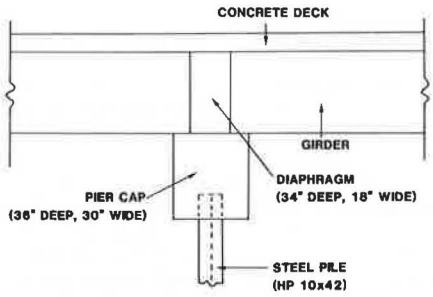

Figure 4. Section through abutment.

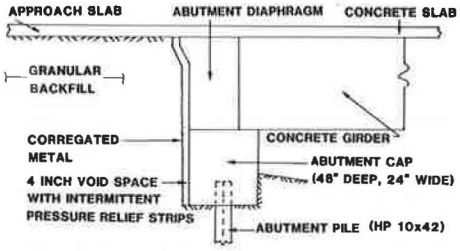

Figure 5. Compressible material on abutment piles.

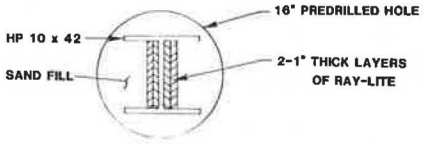

ment. One line shows the sum of movements in the expansion joints on the approach slabs. Another line shows the sum of the changes in gap openings between the abutment and the backfill. Note that the readings are about equal except for the tape readings at 12:00 p.m. Because the expansion joints are located 20 ft from the end of the bridge, changes in the temperature of the approach slab will cause expansion joint readings to be slightly different.

Bridge Temperature

Air temperature versus average concrete deck temperature for the 24-h period is shown in Figure 7. Air temperature (67°) and deck temperature (65°) were about equal at 7:00 a.m. During the morning there was a 17° rise in air temperature but only a 5° rise in deck temperature. The following 6 h brought the opposite effect--a 10° rise in air temperature and a 23° rise in deck temperature. The same pattern occurs for a drop in temperature--i.e., the change in deck temperature lagging the change in air temperature. The 7:00 a.m. readings indicated the deck and air temperature to be within 2° of each other.

An interesting question is whether the change in deck temperature can explain the change in length of the bridge. Information on this question is presented in Figure 8. One line represents the change in bridge length determined by tape measurement. The other line shows a calculated change in length based on change in deck temperature. A thermal coefficient of 6×10^{-6}/°F was used in the calculations. Nearly equal changes in length occur at 12:00 midnight and 7:00 a.m. the next morning. The largest difference occurs at 6:00 p.m. The results suggest that the deck temperature is not the temperature of the entire bridge at least during portions of the day. The slab is open to the direct sun while the box girders are shielded from the direct sun. The lower temperature of the box girders accounts for the reduced change in length of the bridge.

Over a one-year period, tape measurements taken indicate that, for the nine readings shown in Figure 9, the average error in readings was 0.40 in and the range was 0.0-1.1 in. There is a correlation between these measurements and the data obtained from slope indicators fixed to each of the corner piles in each abutment, although individual slope indicator readings may contain errors.

What are the maximum measured movements of each abutment during the one-year period? By using the measured value of the expansion joint opening as the best indicator for the north abutment movement, a value of 0.73 in was obtained on February 26, 1980. With 2.34 in as the change in bridge length for that date, the south abutment moved 1.60 in. On January

Figure 6. Change in length of bridge: abutment movements.

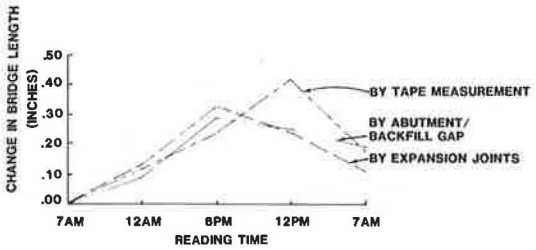

Figure 7. Air temperature versus concrete deck temperature over one day.

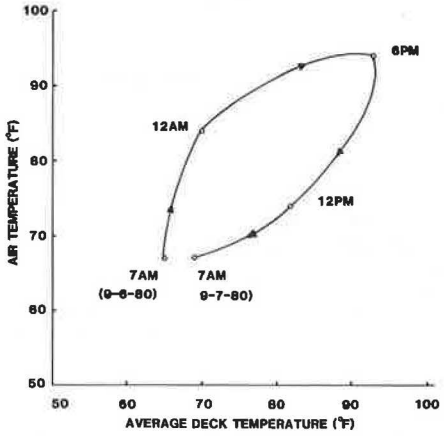

Figure 8. Change in length of bridge: deck temperature.

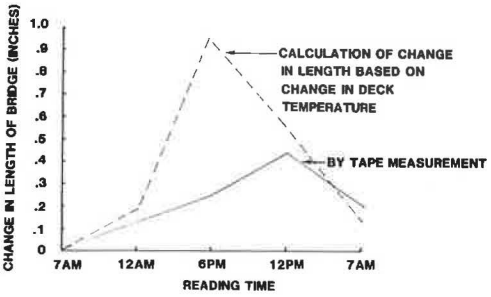

30, 1980, the change in bridge length was measured by tape to be 0.37 in greater than on February 26, 1980. Hence, the south abutment could have moved 1.96 in depending on the expansion joint opening, which was not measured that day due to ice in the joint.

Two sources of temperature measurements were used: the air temperature and the temperature of the concrete deck. A plot of these two temperatures is shown in Figure 10. If the air and deck temperatures were equal, all points would be on the diagonal line. The temperatures would not necessarily be equal since fluctuations in air temperature take place much quicker than fluctuations in deck temperature. However, the fact that air temperatures decreased to less than 17°F while the deck temperature remained at 17°F is questionable. Did the deck temperature stay at 17°F or did the temperature reading equipment malfunction in that temperature range? That question can best be answered by determining which temperature (air or deck) relates to change in bridge length.

This information was calculated and is shown in Figure 11. Two lines represent the calculated change in bridge length based on changes in air temperature and deck temperature. The third line is the change in length of the bridge based on tape measurement. For the two temperatures in question in January and February, the changes in deck temperature do not account for the changes in bridge length. Hence, the equipment used to measure deck temperature malfunctioned at temperatures below 17°F. Figure 11 shows the closeness of change in length based on air temperature at sunrise.

Temperature Influence on Length

The maximum change in bridge length due to temperature change can be estimated by first calculating the change in length from dawn on the coldest day of the year to dawn on the hottest day of the year and then adding an estimate of the change in length during the hottest day of the year. For the one 24-h period studied, the dawn air temperature was 67°F and the maximum air temperature was 94°F. However, the measured change in length during that air temperature change was about 0.27 in (Figure 6), which is equivalent to an average temperature change in the bridge of about 8.3°F. That is, for a 27° change in air temperature, about one-third of that change (8.3°) resulted in change in bridge length.

MEASUREMENT OF ABUTMENT MOVEMENTS

Three independent measurements were taken on the longitudinal movements of the abutments. They were (a) the gap between the backfill and the abutment, (b) the opening of the expansion joint on the approach slabs, and (c) slope indicator measurements on the piles in the abutments. Do the three methods provide consistent readings on abutment movements? That question is answered by the data shown in Figure 12. Abutment movements from 7:00 a.m. on September 6, 1980, are plotted for each approximate 6-h interval during a 24-h period. Note that the average backfill to abutment gap and average expansion joint openings provide nearly equal displacements whereas the displacements from the average of the slope indicator readings are much larger. Two reasons are suggested as to why the slope indicator readings do not agree with the other readings. The first is that the slope indicator displacements are calculated on the assumption that the deflection of the pile at the 35-ft depth does not change. A second reason is that each displacement at the top of the pile (actually 3 ft below the deck surface) results from the difference among 18 sets of readings. If any one of those readings were in error, the displacement would be in error.

Movements Between Abutments and Soil Backfill

As Figure 4 shows, there is a partial void space between the solid side of the abutment and the backfill. This void space is held open by using pressure relief strips between the abutment and the backfill. When the abutment was poured, four steel pipes were cast in the form to provide openings through the abutment into the void space. The width of the opening of the void space is measured by placing a rod through the opening in the abutment and measuring the extension of the rod from the abutment to the corrugated steel. Four readings were taken on each abutment.

As stated earlier, there is an expansion joint in the approach slab at each end of the bridge. Measurements were made on the size of openings in the joint at the north end of the bridge. Three readings were taken, one on each side and one in the middle of the slab.

Figure 9. Change in length of bridge over one year.

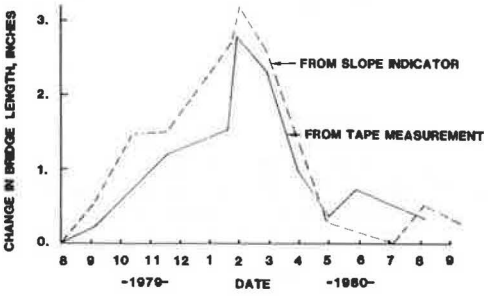

Figure 10. Air and concrete deck temperatures over one year.

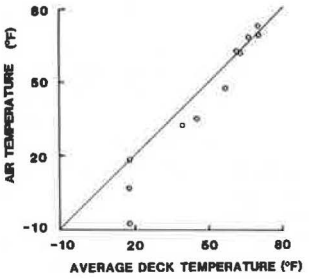

Figure 11. Change in length of bridge: temperature readings.

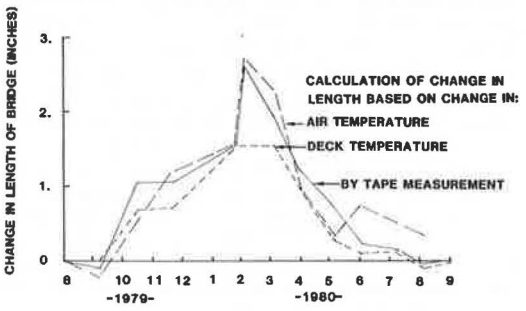

Vertical Movement and Displacement of Abutments, Piers, and Piles

To determine any changes in the elevation of the piers and abutments, two permanent benchmarks were constructed and a level circuit was run each time bridge data were collected. Elevation changes over the year were less than 0.03 ft.

A slope indicator casing was attached to each edge pile of each abutment. Readings were taken periodically to measure the slope of the pile. These slopes were used as a measure of pile movement as well as of bending stresses in the pile.

The casing extended from the top of the concrete deck to depths of 31-35 ft and had pairs of grooves in perpendicular planes. One pair of grooves was oriented to the weak plane of the pile. The casing was placed on the piling by holding angles welded in place before pile driving. When the driving was completed, a section was added to the casing that permitted it to extend to the top surface of the concrete deck. The slope indicator casing was encased in concrete throughout the height of the abutment.

The series 200-B slope indicator instrument from the Slope Indicator Company was used to measure the slope or the casing. All readings were taken at

Figure 12. Abutment movements over one day.

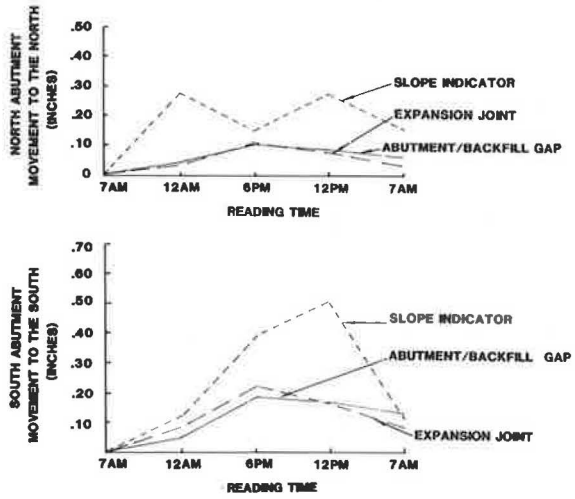

2-ft intervals with the instrument in the plane of weak direction of the pile, which is also the longitudinal plane of the bridge. If, at a particular point on the casing, the slope changes with time, that is an indication of pile movement. The magnitude of pile movement between any two slope readings is determined by multiplying the length of the pile between readings by the change in slope of the lower reading. If it is assumed that there is no movement at the bottom end of the pile, then the displacements at each reading point along the casing can be assumed to determine the displaced position for the casing.

MEASUREMENT OF STRESSES IN PILES AND CONCRETE TEMPERATURE

To determine the bending stresses in the piles, electrical resistance strain gages were attached to the two edge piles on the north abutment, wired, and moisture-protected in the laboratory. After the piles were driven, the wires were placed in plastic pipe inside the concrete and brought to a junction box encased in the abutment wing wall. Stable readings were observed in the laboratory check of the gages and again in the fall of 1978 after the abutment was poured. The next spring the area was flooded to a level above all the strain gages. Following the flood, the readings for most gages would not stabilize. Due to the erratic readings, the electrical resistance strain gage data were not used.

Four thermocouples were installed in the concrete deck. They were of copper constantan material manufactured by Honeywell. A Model 199-1F digital thermometer manufactured by Omega Engineering was used to read the temperature. The thermocouples were checked for accuracy at 40°F and 70°F. The thermocouples were located midway between the edge and adjacent girders at about 25 ft from each end of the bridge.

The thermocouples were installed by first forming a void space in the slab. When the slab forms were removed, the thermocouples were inserted and the remaining space was filled with concrete.

ANALYTIC MODEL DEVELOPED TO MEASURE STRESSES IN PILES

A secondary objective of this bridge study was to develop a model to measure the stresses in the abutment piles. Pile stresses depend on the relative

Figure 13. Model for calculating pile stresses.

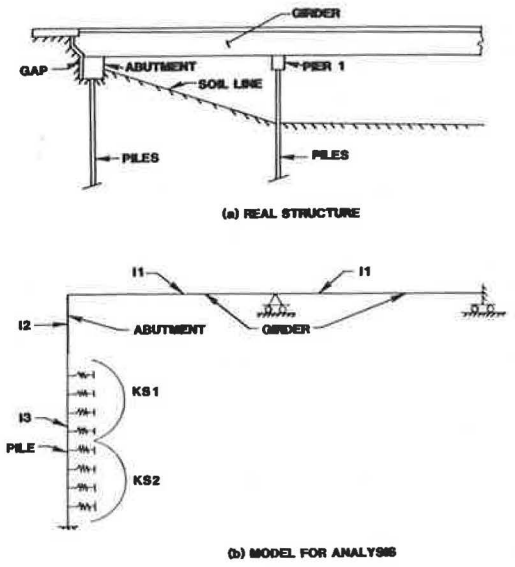

Figure 14. Measured and calculated pile movements.

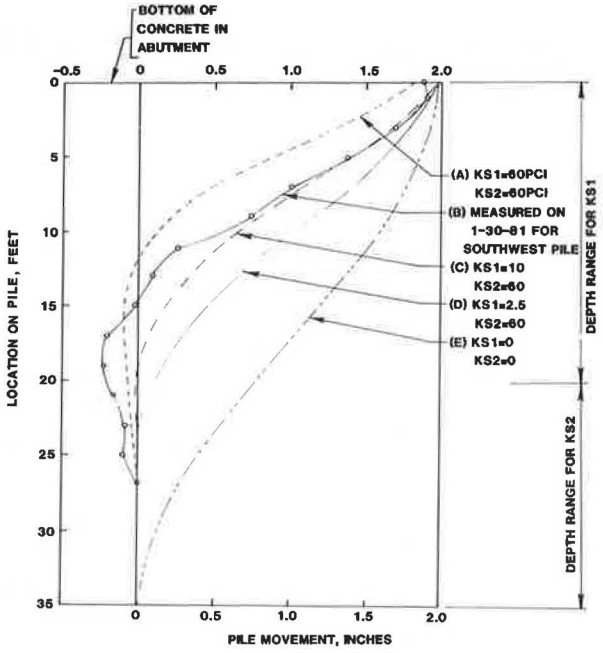

stiffness of bridge, abutment, pile, and soil as well as the abutment and pile movement and method of pile installation. To analyze this situation, it is necessary to devise mathematical models that describe the behavior of each element in the problem.

The model used is shown in Figure 13. Figure 13a is a sketch of the real structure that shows the bridge girder, abutment, piles, soil line, and first pier. The gap between the abutment and the backfill soil is also shown. Figure 13b illustrates the mathematical model. The beams are on rollers in order to place a specified displacement in the abutment. I1 represents the moment of inertia of that portion of the bridge deck that reacts with a single pile, and I2 is the moment of inertia of an equivalent portion of the abutment. The moment of inertia of a single pile is represented by I3. The model is considered to follow elastic behavior.

The remaining parameter in the model is the modulus of subgrade reaction, which is represented by the symbol KS. The modulus of subgrade reaction is a measure of the load-deformation relation for soil. It is the ratio of the stress on a loaded plate divided by the magnitude of the displacement of the plate into the soil. Bowles (4) indicates that the best method of obtaining the KS for the soil is to conduct a lateral load test on the pile. In this case a load test was not conducted. Other estimates are that, for clays, KS is primarily dependent on the unconfined compressive strength of the clay. Soil tests in the region of the pile under study give an average unconfined compressive strength of 1.50 kips/ft^2. This was multiplied by 72 (from Bowles) to obtain a modulus of subgrade reaction in kips per cubic foot. After changing to pounds per cubic inch (pci) units, 60 pci was used where the pile was in contact with clay.

The KS for that portion of the pile with compressible material attached to the web depends on the load-displacement relations for the compressible material, the sand around the pile, and the clay around the sand. Load-displacement tests were run on the two 1-in-thick layers of Ray-Lite. For a displacement up to 0.17 in, the KS was 42 pci; for displacements from 0.17 in, the KS was 13 pci. Load-displacement tests were not run on the sand or clay. The KS for the combined materials will be less than what it is for any one of the materials. With that as background, two values of KS--2.5 and 10.0 pci--were used as estimates where compressible material was attached to the pile.

Pile Displacement

Earlier it was pointed out that the maximum recorded movement for the south abutment occurred on January 30, 1980. The movement of the west pile on the south abutment for that date is plotted in Figure 14 along with calculated pile movements by using the model shown in Figure 13 and different values of modulus of subgrade reaction.

The left side of Figure 14 indicates the location on the pile measured from the bottom of the concrete in the abutment. That point is about 8 ft below the roadway. Measurements of pile displacements were taken with the slope indicators to a depth of 24 ft below the bottom of the concrete. The calculation mode was extended to 35 ft below the bottom of the abutment concrete. Modulus-of-subgrade-reaction springs were placed at a 2-ft spacing along the pile. The left side of the figure indicates the range in depth over which the two modulus-of-subgrade reactions apply.

The solid line indicates the measured location of the pile on January 30, 1980. The remaining four lines are calculated pile movements based on different values of KS. All calculated movements are based on a 1.96-in movement of the top of the abutment. Movement will extend over the entire length of the pile if the soil provides very little resistance to the movement--i.e., a low modulus of subgrade reaction, as shown by curve E. In contrast, for high values of KS (60 pci in both regions), the pile movements are very small, as shown by curve A. Curves C and D are for what was considered to be reasonable values for the subgrade modulus--i.e., from 2.5 to 10 pci for the top 20 ft of pile and 60 pci for the remaining depth. Note that curve C closely matches the measured pile movement down to the 9-ft depth. Models could be developed to obtain closer agreement at lower pile depths, but this was not pursued since the pile stresses at those depths are likely to be less than those near the top of the pile.

Figure 15. Bending moment in pile.

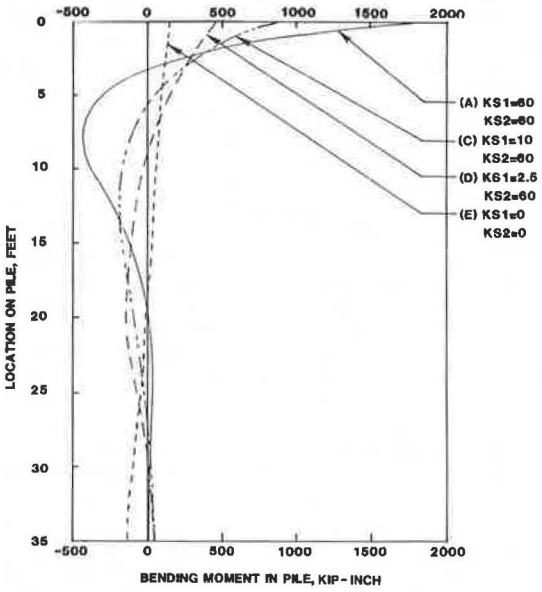

Figure 16. Comparison of calculated, yield, and plastic moments.

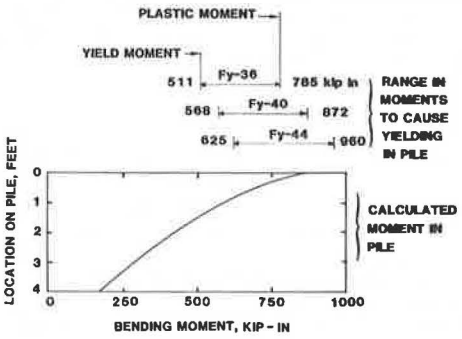

Pile Stresses

Pile bending moments for four sets of soil constants are shown in Figure 15. For the more firm soil (KS = 60 pci), the maximum moment is 1842 kip·in. The maximum moment at the top of the pile is controlled primarily by the modulus of subgrade reaction KS1. Holding KS1 constant and doubling KS2 will have less than a 5 percent influence on the maximum moment. At the top of the pile, the maximum moment causes tension on the inside edge of the flange. Going down the pile, the moment goes to zero and increases to cause tension on the outside edge of the flange. These maximum moments are about 23 percent of the top maximum moments and occur at 7-10 ft below the top of the pile.

Bending moments are related to bending stress by F = M/S, where F is the bending stress, M is the bending moment, and S is the elastic section modulus for the pile. HP10x42 piles were used in the abutment with the minor axis of the pile in line with the longitudinal axis of the bridge. The elastic section modulus for the pile is 14.2 pci. Based on the maximum bending moments from Figure 15, the maximum bending stresses are 9.6, 33.4, 59.3, and 129.7 ksi. Since some of these moments are beyond the yield strength for the steel, the assumed elastic behavior for the analysis model was not correct.

Bending moments for that case that most closely fits the actual pile deflections are shown in Figure 16. The lower portion of Figure 16 shows a plot of the calculated moment in the pile, and the upper portion shows a plot of the range in moments to cause yielding in the pile for different yield strengths of steel. The yield moment occurs when the outer fiber of the flange reaches the yield stress. The plastic moment occurs when the strain has been sufficient to cause yielding at middepth of the member. The guaranteed minimum yield strength (F_y) for the pile steel was 36 ksi. Very little steel would be produced at that level, and the average value would be closer to 40 or 44 ksi. If 44 ksi is used as the yield strength of the steel, then yielding took place in less than the top 1 ft of the pile, and at the top of the pile the yielding was only on each outer one-fourth depth of the flange.

Are the calculated stresses in Figure 16 correct, since the model was based on an elastic analysis and the stress near the top of the pile was beyond the elastic limit? The error is believed to be minor because the yielding was not sufficient to form a plastic hinge.

CONCLUSIONS

Based on the one year of measurements at the bridge and study of the data, the following conclusions were made:

1. The maximum change in length of the bridge due to thermal change can be estimated by using a temperature change equal to

$$DT = T1 - 72 + (T3 - T1)/3 \quad (1)$$

where

T1 = air temperature at dawn on the hottest day,
T2 = air temperature at dawn on the coldest day, and
T3 = maximum air temperature on the hottest day.

2. The above change in bridge length agrees well with changes in length determined from tape measurement and measurements of openings in expansion joints.
3. The change in bridge length did not result in equal movement at the two ends of the bridge. At the point of maximum bridge shortening, the south abutment moved in 1.96 in and the north abutment moved in 0.74 in from their initial August positions.
4. In one year, the gap between the abutment and the backfill closed about 0.5 in on the north abutment and 0.75 in on the south abutment.
5. The vertical movements of the abutments and piers were nearly zero.
6. The method of measuring pile stresses failed. However, pile stresses were calculated and resulted in pile displacements that matched those from the slope indicator measurements. For the maximum measured abutment movement of 1.96 in, the stress at the top of the pile was sufficient to initiate a yield stress in the steel but not sufficient to cause the formation of a plastic hinge.
7. An analytic model was used to predict stresses in the piles due to movements of the abutments. The two parameters that have the most influence on pile stresses are the amount of abutment movement and the modulus of subgrade reaction near the upper portion of the pile.

REFERENCES

1. C.E. Ekberg, Jr., and J.H. Emanuel. Current Design Practice for Bridge Bearing and Expansion

Devices. Engineering Research Institute, Iowa State Univ., Ames, Project 547-S, Final Rept., Aug. 1967.
2. J.H. Emanuel and others. An Investigation of Design Criteria for Stresses Induced by Semi-Integral End Bents: Phase I--Feasibility Study. Civil Engineering Department, Univ. of Missouri, Rolla, 1974.
3. C. Berwanger. Thermal Stresses in Composite Bridges. Proc., ASCE Specialty Conference on Steel Structures, Engineering Extension Series, No. 15, Univ. of Missouri, Columbia, June 1980, pp. 27-36.
4. J.E. Bowles. Foundation Analysis and Design, 3rd ed. McGraw-Hill, New York, 1982.

Publication of this paper sponsored by Committee on Foundations of Bridges and Other Structures.

Effective Coefficient of Friction of Steel Bridge Bearings

ALI MAZROI, LEON RU-LIANG WANG, AND THOMAS M. MURRAY

A study to determine experimentally the effective coefficient of friction of four classes of steel bridge bearings used by the Oklahoma Department of Transportation is reported. As-built, rusted, and in situ (debris at the moving surfaces) conditions were tested by using full-scale bearings under normal loads to 250 000 lb. In addition, the effects of manufacturing tolerances on bearing performance were analyzed. From the tests it was found that unturned pipe rollers exhibit the lowest effective coefficient of friction of the four rolling devices tested. For turned pipe rollers it was found that the equivalent coefficient of friction is a function of the amount of horizontal movement from the centerline. A geometric explanation was devised, and excellent agreement between predicted and measured results was achieved. Tests with a pintle rocker showed that fabrication inaccuracies, especially in the sole plate socket radius, can significantly affect the performance and effective coefficient of friction of the bearing. In all cases, tests with rusted bearing plates or with sand spread over the lower bearing plate showed significant increases in the effective coefficient of friction.

Expansion and contraction caused by temperature changes, deflection, relative support settlement, creep, and other factors will produce motion in a bridge. The movement is very slow, but the forces involved can be tremendous and usually are accommodated by bearings at piers or abutments. If the bridge does not have the ability to move, because either it does not have a bearing or the bearing is not working, it pushes and tears at its supports until it achieves the ability to move.

Even if the bearing is working properly, horizontal force is transmitted to the pier or abutment through friction caused by relative motion of the bearing parts or by eccentric loading of the bearing as found in certain "pipe" bearings. This force must be accommodated in the design of the supporting structure; if not, structural damage can occur.

The purpose of this study was to determine experimentally the effective coefficient of friction of several classes of bridge bearings used by the Oklahoma Department of Transportation (ODOT). Both as-built conditions and simulated conditions, as found after several years of use, were used in the testing program. A thorough literature search revealed that very few studies of the behavior of complete bearing assemblies have been conducted and that specification provisions have been based on classic values of coefficients of friction between sliding parts without regard to effects of manufacturing tolerances or environmental effects. This study is an attempt to assess these effects and to provide guidelines to establish accurate estimates of horizontal force requirements for the class of bearings tested.

For the purpose of this study, the effective coefficient of friction (μ_{eff}) is defined as

$$\mu_{eff} = F/N \quad (1)$$

where F is the horizontal force to overcome the resistance to allow motion and N is the normal force applied to the bearing. The value of F was determined experimentally for the entire assembly for an applied normal force N, from which μ_{eff} is calculated.

BACKGROUND

Many types of bearing devices are used to accommodate bridge movement: single rollers, groups of rollers, rockers, elastomeric pads, sliding plates, sliding tetrafluorethylene (TFE), etc. In general, bridge bearings can be classed in two categories: elastomeric and mechanical (1). According to a recent National Cooperative Highway Research Program synthesis on the design, fabrication, construction, and maintenance of bridge bearings (2), the elastomeric bearing pad is perhaps the best expansion bearing because it is unaffected by weather (e.g., it has no moving parts to freeze), has nothing to corrode, is low in cost, and requires almost no maintenance. However, elastomeric bearing pads are limited to 700 psi for vertical load capacity and 3 in for horizontal movement and their success depends on the quality of the material. On the other hand, for mechanical bearings the movements and rotations are accommodated by rolling, rocking, or sliding actions, usually on metal parts that can accommodate much larger bearing pressures. Furthermore, mechanical bearing devices can be designed for virtually unlimited horizontal motion (2).

One of the simplest types of mechanical bearing is the roller or "pipe roller", simply a piece of steel pipe with a stiffener as shown in Figure 1a. The load-carrying capacity of the roller is a function of its radius and can be found from the following formula (3): For diameters up to 25 in,

$$P = [(F_y - 13\,000)/20\,000]\ 600\ d \quad (2)$$

and for diameters from 25 to 125 in,

$$P = [(F_y - 13\,000)/20\,000]\ 3000\ \sqrt{d} \quad (3)$$

where

P = allowable bearing (lb/linear in),
d = outside diameter of the roller (in), and
F_y = minimum yield point in tension of the steel in the roller or bearing plate, whichever is the smaller (psi).

Figure 1. Roller expansion bearing.

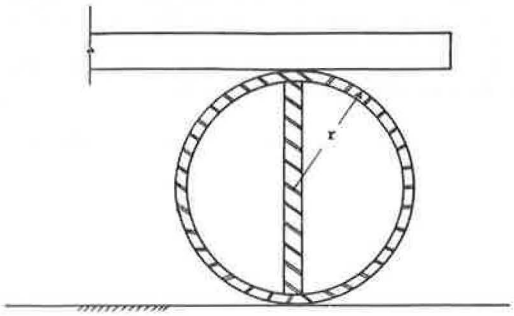

(a) Pipe Roller (Single Roller)

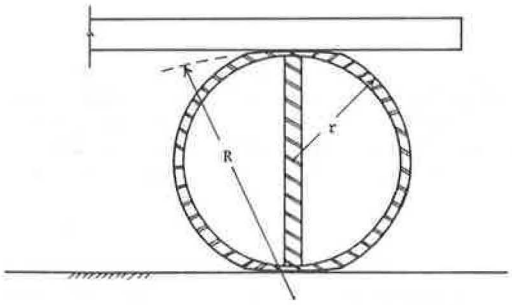

(b) Turned Pipe Roller

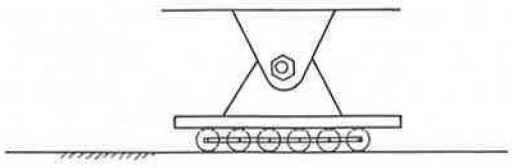

(c) Roller-nests

For a roller diameter of 12 in and a length of 12 in, the capacity of a single roller is slightly less than 100 000 lb. The principal advantage of this type of roller is the low effective coefficient of friction--generally less than 0.01 (4).

To increase load-carrying capacity without increasing the diameter, a single roller can be machined (turned) to increase the radius at the contact surface as shown in Figure 1b. This type of roller, which in this paper is called a "turned roller", has geometric properties that cause a high horizontal resistance. The equivalent effective coefficient of friction of a turned roller is a function of the amount of movement.

Rollers can be used in combination to increase load-carrying capacity, as shown in Figure 1c. Because roller nests only work well when they are clean, maintenance is required. Furthermore, this type of bearing is relatively expensive.

Several different types of rockers are used as expansion bearings: for instance, the segmental rocker, pinned rocker, and pintle rocker shown in Figures 2a, 2b, and 2c, respectively. The double-segmented rocker shown in Figure 3 has been described as a "modern rocker bearing for long steel girders" (2). Because the radius of this rocker is greater than half the depth, the resisting force (equivalent friction force) would be tremendous for large movements.

Very few experimental studies of full-scale bridge bearings were found in the literature. Specification requirements seem to have been developed from classic values of friction coefficients and from experience. Jacobson (5) has concluded that certain pin-connection details can accumulate rust between the contact surfaces of the pin and the housing. Resulting increased horizontal forces can cause major structural damage to the main supporting members of a bridge. Laboratory tests of models similar to these bearings showed that the life of the bearing can be improved by using a case-hardened pin and by lubricating the bearing with a heavy-duty grease. Jacobson concluded that the use of pin-connected details subjected to large rotations and the use of untreated, corrosive mild steels should be avoided.

Chang and Cohen (6) have suggested coefficients of friction of 0.2 for steel bearing on steel, 0.1 for steel bearing on self-lubricating bronze plate, and 0.06 for polytetrafluorethylene (PTFE) on PTFE or stainless steel. For rocker-type bearings, they suggest that the force be calculated based on a 20 percent friction coefficient but reduced in proportion to the radii of the pin and rocker as shown in Figure 4.

British Standard 153, Specification for Steel Girder Bridges, specifies the coefficients of friction for sliding bearing as 0.25 for steel on steel or cast iron and 0.15 for steel on copper alloy. The coefficient of friction with one or two rollers is taken as 0.01.

Jacobson (7) has conducted experimental work to investigate the potential use of TFE as a sliding surface. He concluded that the TFE bearings are suitable for use as highway bridge bearings. A substantial increase in the coefficient of friction for filled TFE was found after 7000 cycles of testing.

Taylor (8) has found that the coefficient of friction of PTFE is influenced by a number of parameters, including pressure across sliding surfaces, rate of movement, presence or absence of lubrication, previous loading-movement history, and temperature. The coefficient of friction decreased with higher compressive stress across the bearing but increased slightly at lower temperatures.

SCOPE OF RESEARCH

Because few published data are available on the effective coefficient of friction of standard bridge bearings, a testing program was undertaken to investigate the performance of several types of standard ODOT bearings under several conditions. Mechanical bearing types were as follows:

1. Typical single roller bearing (Figure 1a),
2. Typical single turned roller bearing (Figure 1b),
3. Typical pinned rocker shoe (Figure 2b), and
4. Typical pintle rocker bearing (Figure 2c).

To determine the effect of environmental changes on the frictional coefficients, the following conditions were studied: (a) unlubricated (as-built condition), (b) rusted, and (c) with debris on the lower bearing plates. The unturned pipe roller, turned pipe roller, and pinned rocker shoe bearings used in the study were new bearings. The pintle rocker bearings were removed from a bridge prior to testing.

To increase the reliability of the experimental results, several increments of loading were used and

Figure 2. Rocker expansion shoes.

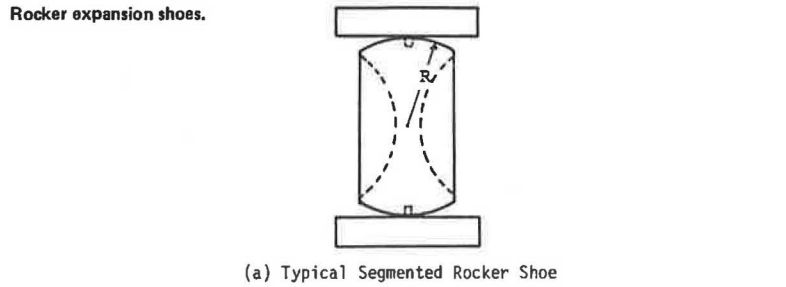

(a) Typical Segmented Rocker Shoe

(b) Typical Pinned Rocker Shoe

(c) Typical Pintle Rocker Shoe

Figure 3. Double-segmental rocker.

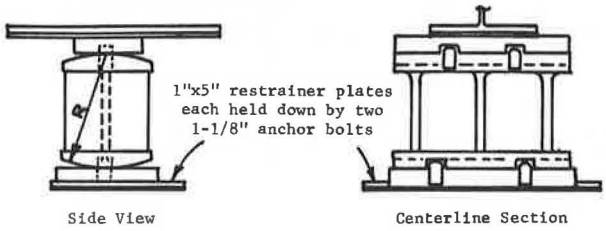

Figure 4. Forces on rocker bearings.

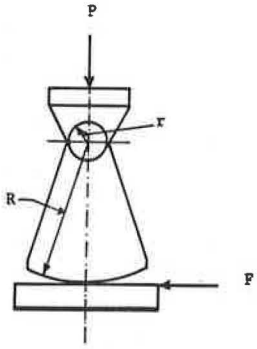

P = Superstructure D.L.
$F = (P \times 0.20)\frac{r}{R}$
r = radius of pin
R = radius of rocker

at least three tests were done at each loading for each combination.

TEST SETUP

To determine the experimental coefficient of friction of bridge bearings, a test setup that simulated the actual bridge was built as shown in Figure 5. The normal force was applied with a 750 000-lb-capacity hydraulic ram and the horizontal force with a 55 000-lb-capacity closed-loop hydraulic testing system. The data were recorded by using a microcomputer system.

The test setup was erected on the reaction floor inside the Fears Structural Engineering Laboratory at the University of Oklahoma. The setup was erected directly over two W36 beams spaced 8 ft apart and consisted of three parts: (a) an H-frame that was designed for a 250 000-lb maximum vertical reaction and that supported the hydraulic ram, (b) a triangle frame that was designed for a 55 000-lb maximum horizontal reaction and that supported the closed-loop hydraulic testing system, and (c) a W33x130x15-ft girder that simulated the actual bridge girder.

The vertical load chain consisted of the H-frame, hydraulic ram, load cell, swivel head, roller nest with a known effective coefficient of friction, a steel plate with a highly polished surface, the simulated bridge girder, the test bearing, a steel reaction plate, and the reaction floor. The horizontal load chain consisted of the triangle frame, the actuator of the closed-loop hydraulic testing system, the load cell, a loading linkage to prevent out-of-plane forces, and the simulated girder (Fig-

Figure 5. Side view of test setup.

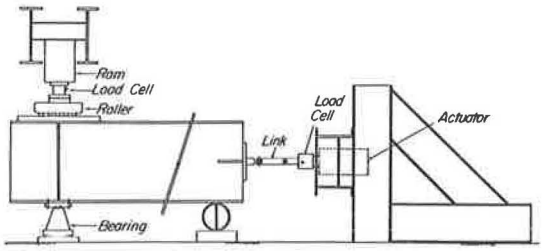

ure 5). Lateral brace mechanisms were used to stabilize the girder against out-of-plane rotations, and a pipe roller was used to support the unloaded end of the bridge girder.

INSTRUMENTATION

Instrumentation consisted of the two calibrated load cells, a horizontal displacement transducer, an analog-to-digital signal converter, and a microprocessor. The applied normal force was measured by using a calibrated 300 000-lb-capacity load cell; the horizontal force was measured by using a calibrated 100 000-lb-capacity load cell; and the horizontal movement (girder movement) was measured by using a calibrated transducer that is part of the closed-loop hydraulic testing system.

The analog signals from the three instruments were digitized by using a 16-channel differential input A/D converter with direct interface to the microprocessor. The microprocessor was used to reduce and plot the data in real time. In this manner, changes in normal force due to uncontrollable vertical movement in the vertical force chain were accounted for and the instantaneous relation of the two force variables and one displacement variable was known.

TEST PROCEDURES

For each test, the centerline of the bearing was first positioned relative to a fixed vertical plane. A nominal normal force was then applied, usually in multiples of 25 kips but not exceeding the rated capacity of the bearing. The simulated girder was then pulled at a slow rate (approximately 1 in/min) by using the closed-loop hydraulic testing system. As previously mentioned, all data were recorded in real time with the microprocessor.

Approximately 100 data sets (each consisting of one displacement and two force readings) were recorded for each test. The effective coefficient of friction was automatically calculated by the microprocessor by taking into account the initial force on the bearing due to the weight of the system and the effective coefficient of friction of the roller nest. The graphics capabilities of the microprocessor system were used to display and plot the relation between the horizontal force and horizontal movement.

To simulate in situ conditions, the steel bearings were subjected to rusting and debris environments. To achieve the rusting condition, the bearings were placed inside a closed bucket in an acidic environment for about two months. Muriatic acid (HCl) was used to accelerate the rusting. The bearings were supported approximately 10 in above the acid surface, and the bucket was kept outside where temperatures varied from 25° to 80°F.

To achieve the debris environment, an approximately 0.125-in-thick layer of graded sand was spread on the lower bearing plate. The sand, supplied by ODOT, was obtained by vacuuming areas near in-place bridge bearings.

TEST RESULTS

The details of the test data for this project have been given elsewhere (9) and will not be repeated here. The essential results and conclusions are summarized below.

Unturned Pipe Roller (Single Roller)

A 10-in-diameter, unturned, stiffened, painted pipe roller (Figure 1a) was used for this phase of the study. The specimen was tested under three conditions:

1. Clean roller and bearing plates,
2. Clean roller with rusted lower bearing plate, and
3. Roller with sand spread over the lower bearing plate.

The roller was tested at four increments of vertical loading--25, 50, 75, and 100 kips--for each condition based on a load-carrying capacity of 103.5 kips, as determined from Equation 2. Typical horizontal force versus horizontal deflection plots for conditions 1-3 are shown in Figure 6. For a perfectly rigid system, horizontal displacement would not take place until the rolling frictional resistance was overcome. The initial horizontal motion shown in Figure 6 (and all subsequent similar plots) is from the elastic deformation of the test fixtures.

The results for all tests are shown in Figure 7 as effective coefficient of friction versus normal force. The straight lines shown are the result of regression analyses conducted for each condition.

The average effective coefficient of friction for condition 1 (clean roller and bearing plate) was found to be 0.33 percent with a standard deviation of 0.14 percent over 12 tests and with a range of 0.12-0.58 percent. For condition 2 (rusted lower bearing plate), the average effective coefficient of friction increased to 0.69 percent with a standard deviation of 0.10 percent over 12 tests and with a range of 0.47-0.85 percent. Approximately 0.125-in-thick graded sand was placed on the lower bearing plate in front of the roller for condition 3. In this condition, the average coefficient of friction was found to be 3.38 percent with a standard deviation of 1.2 percent for 14 tests and with a range of 2.1-5.8 percent.

From the results of the 38 tests conducted, the following results were noted:

1. The effective coefficient of friction seems to increase with increasing normal force (Figure 7). It is more pronounced for the condition with sand.
2. The effective coefficient of friction increases 400-1000 percent if sand is placed on the lower bearing plate.
3. The effective coefficient of kinetic friction is essentially equal to the effective coefficient of static friction.
4. The results for condition 2 were obtained for a rusted lower bearing plate and a clean upper plate. If the upper plate were also rusted, the increase of the effective coefficient of friction could conceivably double.

Turned Pipe Roller

A 10-in-diameter, turned, stiffened, painted pipe roller (Figure 1b) was used in this phase of the

Figure 6. Typical displacement versus friction force plots for pipe-roller bearing.

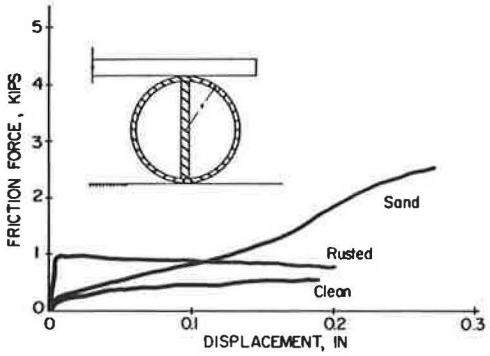

Figure 7. Normal force versus effective coefficient of friction of pipe-roller bearing.

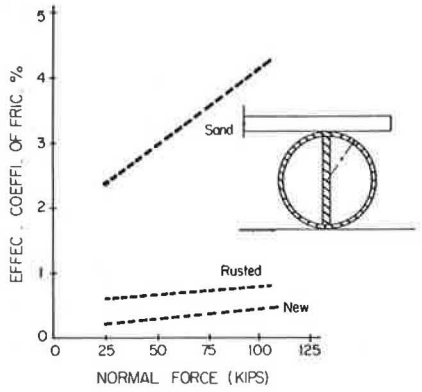

study. The roller was identical to the unturned roller except a 12-in radius was turned on opposite sides to increase the contact surface at the upper and lower bearing plates and thus increase the load-carrying capacity. Based on Equation 2, the allowable load is 248.4 kips.

Because the radii at the two contact surfaces are greater than half the roller depth, the supported bridge girder rises slightly with horizontal movement. In addition, an eccentricity between the lines of action of the resultant vertical contact forces is created. A set of horizontal resisting forces is therefore needed to maintain equilibrium if the roller is moved on either side of its centerline. The magnitude of this resisting force increases with movement from the centerline as long as the turned portions of the roller are in contact with the plates. Movement beyond the turned area (usually 1-2 in on each side of the centerline) results in a rapid decrease in horizontal force requirements, since the roller is essentially an unturned roller under this condition. For the purposes of this study, the resisting force is related to an equivalent effective coefficient of friction defined as follows:

$$\mu_{equiv} = F/N = (R \cdot d)/(R - d/2)h \quad (4)$$

where

R = turned radius at the contact surfaces,
d = total depth of the roller, and
h = total horizontal movement from either side of the centerline.

The roller was tested under the following two conditions:

Figure 8. Friction versus displacement for turned pipe roller.

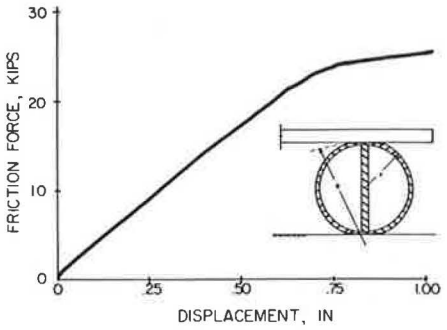

Figure 9. Resisting force versus movement for turned pipe roller.

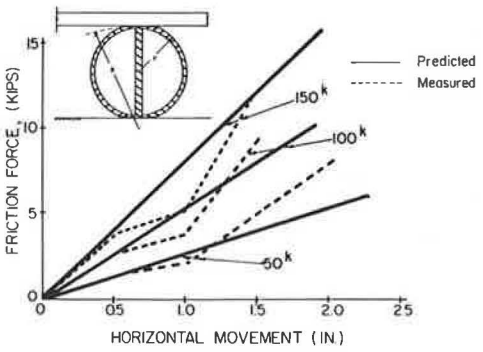

1. Clean roller and bearing plates and
2. Roller with sand spread over the lower bearing plate.

Three increments of vertical load were used: 50, 100, and 150 kips.

Typical coefficient of friction and horizontal force versus horizontal deflection plots are shown in Figure 8. Figure 9 compares measured and theoretical results. Correlation is good except at a horizontal movement of approximately 1 in. Close inspection of the bearing showed an imperfection in the turned surface, which is believed to account for the discrepancy.

From the results of the 21 tests and the theoretical analyses, the following observations are noted:

1. The equivalent coefficient of friction is a function of horizontal displacement and increases rapidly with displacement.
2. Small imperfections in the turned surfaces can cause significant changes in the equivalent coefficient of friction.
3. The presence of sand on the lower bearing plate can increase the equivalent coefficient of friction 250-400 percent.

Pinned Rocker Shoe

A pinned rocker shoe, similar to that shown in Figure 2b, was tested for the following three conditions:

1. Clean and unlubricated,
2. Rusted, and
3. With sand spread over the lower bearing plate.

The load-carrying capacity was calculated as 232 kips by using Equation 2, and the shoe was tested in approximately 25-kip increments from 50 to 225 kips.

Figure 10. Friction force versus normal force for pinned rocker shoe.

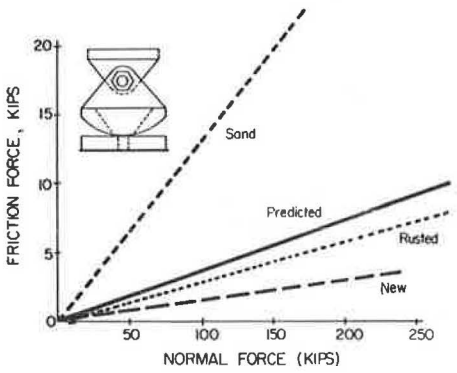

Figure 11. Friction force versus normal force for pintle bearing 1, condition 1.

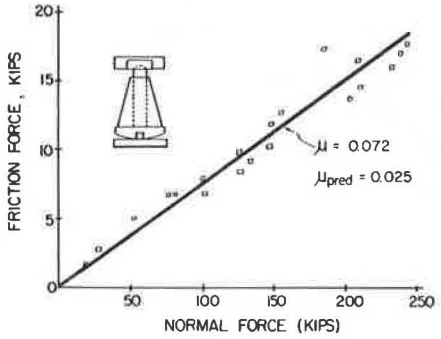

The average effective coefficient of friction for condition 1 (clean and unlubricated) was found to be 0.99 percent with a standard deviation of 0.001 37 over 16 tests and with a range of 0.71-1.18 percent. For condition 2 (rusted), the average effective coefficient of friction increased to 1.85 percent with a standard deviation of 0.31 percent over 23 tests and with a range of 1.38-3.23 percent. Approximately 0.125-in-thick graded sand was placed on the lower bearing plate for condition 3. The average effective coefficient of friction was found to be 8.95 percent with a standard deviation of 0.071 percent over 12 tests and with a range of 4.42-10.40 percent.

The results of all tests are plotted in Figure 10 as friction force (horizontal force) versus normal force. The straight lines shown are the result of regression analyses conducted for each condition.

The following observations are noted from the 51 tests:

1. The effective coefficient of friction for a rusted rocker can be as high as 185 percent of the value for a clean, unlubricated rocker.
2. The presence of sand significantly alters the effective coefficient of pinned rocker bearings.

Pintle Rocker Shoe

Two pintle rocker bearings similar to that shown in Figure 2c were tested under three conditions:

1. As removed from a bridge site,
2. Partly rusted, and
3. With sand spread over the lower bearing plate.

By using Equation 2, the load-carrying capacity of the bearing was calculated to be 260 kips. Tests were conducted from 25 to 225 kips in increments of approximately 25 kips.

Figure 12. Measured and specified dimensions of pintle rocker bearings.

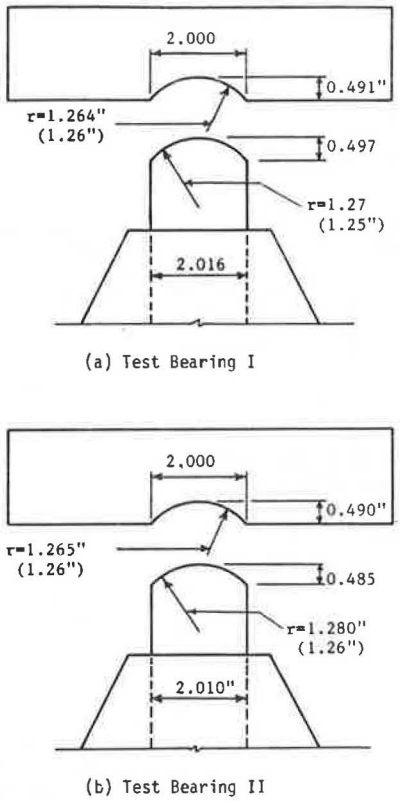

Results for test bearing 1 in condition 1 (as received) are shown in Figure 11. The average coefficient of friction was 7.6 percent with a standard deviation of 0.111 percent over 24 tests and a range of 6.15-9.88 percent.

In conducting these tests, it was noticed that the bearing exhibited significantly different effective coefficients of friction depending on the initial position of the centerline of the rocker relative to the direction of movement. A series of tests for each bearing was then conducted in which the starting position was varied from before dead center to after dead center. In the 55 tests conducted, the effective coefficient of friction varied from 3.13 to 7.94 percent, a variation not found in tests of ther bearings. In addition, the effective coefficient of friction predicted by the equation shown in Figure 4 was 2.4 percent.

In an attempt to determine the cause of the discrepancy, the outside radius of the top portion of the rocker and the inside radius of the sole plate were carefully measured. Actual and specified dimensions are shown in Figure 12. In both cases, the outside radius of the rocker was found to be larger than specified and larger than the inside radius of the sole plate. Because of this geometry, the top part of the rocker tends to wedge inside the socket of the sole plate, which causes a high effective coefficient of friction.

To verify this contention, sole plates with inside radii of 1.27 and 1.35 in were used for additional testing. For the series with the 1.27-in radius, the average effective coefficient of friction was 4.31 percent with a standard deviation of 0.49 percent and a range of 2.22-5.45 percent. The average coefficient of friction decreased from 7.60 to 4.31 percent with an increase in inside radius of only 0.01 in. Typical results are shown in Figure 13.

Figure 13. Friction force versus displacement for pintle rocker bearing.

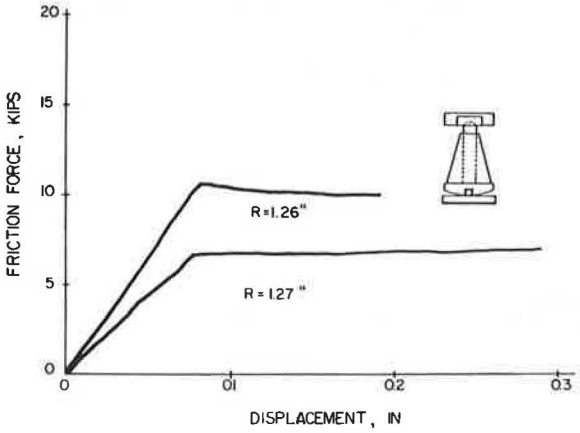

Table 1. Summary of results.

Bearing Type	Condition	Effective Coefficient of Friction: Predicted (%)	Effective Coefficient of Friction: Measured (%)	Radius of Sole Plate/Radius of Rocker (in)
Single roller	Clean		0.5	
	Rusted		1.0	
	With sand		5.0	
Pinned rocker shoe	Clean	2.5	1.0	
	Rusted		2.0	
	With sand		9.0	
Pintle rocker	Clean	2.5	6.2-9.9	1.26/1.27
	Clean	2.5	2.2-5.5	1.27/1.27
	Rusted	2.5	3.6-5.5	1.27/1.27
	With sand	2.5	12.1-14.1	1.27/1.27

Note: For the turned roller, a geometric relation was found and sand increased the coefficient of friction 250-400 percent.

A series of tests was also attempted with a large-radius (1.35-in) sole plate. Since the radius in the sole plate was significantly larger than the outside radius of the rocker (by 0.07 in), the rocker was rolling inside the sole plate rather than sliding. The rocker was observed to roll in the sole plate socket until the required coefficient of friction was greater than that possible between the steel surfaces, and then the parts suddenly "jumped" to an initial position and the process was repeated. Results achieved by using the large-radius sole plate were too scattered to be of use.

The tests were repeated with the 1.27-in-radius sole plate for condition 2 and with the original sole plate for condition 3 (with sand). The average effective coefficient of friction for the rusted condition increased to 4.8 percent with a standard deviation of 0.18 percent over 15 tests and a range of 3.64-5.48 percent and for the sand condition to 13.13 percent with a standard deviation of 0.14 percent and a range of 12.08-14.11 percent for 12 tests.

From the numerous tests, conditions, and configurations of this phase of the study, the following observations are noted:

1. Fabrication accuracy is necessary if the predicted effective coefficient of friction (Figure 4) is used to estimate the horizontal friction force of pintle bearings.
2. Slight inaccuracies in the radii of mating parts can result in a substantial increase in the effective coefficient of friction.
3. Rust and particularly sand can substantially increase the effective coefficient of friction of pintle bearings.

SUMMARY

The results of this study, summarized in Table 1, show that an unturned pipe roller exhibits the lowest effective coefficient of friction of the four rolling devices tested. The effective coefficient of friction was found to be less than 0.5 percent for a clean 10-in-diameter pipe roller. The value increased to about 1 percent when the roller was tested in a rusted condition and to 5 percent when sand was spread over the lower bearing plate.

Tests with a turned roller showed the equivalent coefficient of friction to be a function of the amount of horizontal movement from the centerline (median line). A geometric explanation was found, and excellent agreement between predicted and measured results was achieved.

An effective coefficient of friction of 1 percent was found from tests with a clean pinned rocker. The value increased to 2 percent for a rusted condition. Both values are lower than a predicted value of 2.5 percent determined by using a published criterion. The effective coefficient of friction for this rocker increased to 9 percent when sand was placed on the lower bearing plate.

Tests with a pintle rocker showed that fabrication inaccuracies, especially in the radius of the sole plate socket, can significantly affect the performance and effective coefficient of friction of the bearing. Tests with a sole plate socket radius slightly smaller than the rocker radius resulted in effective coefficient of friction values from 6.15 to 9.88 percent compared with 2.4 percent from published criteria. Tests with rusted bearing plates or with sand spread over the lower bearing plate showed significant increases in the effective coefficient of friction.

ACKNOWLEDGMENT

This paper is derived from a research project sponsored by ODOT. The financial support of ODOT is appreciated. We wish to thank Tim Borg, Jim Schmidt, and Dwight Hixon of the ODOT Research and Development Division and Veldo Goins of the ODOT Bridge Division for their helpful suggestions and assistance during the course of the investigation.

REFERENCES

1. J.E. Long. Bridge Bearings and Joints. Highways and Public Works, Vol. 46, No. 1825, Dec. 1978, pp. 9-20.
2. Bridge Bearings. NCHRP, Synthesis of Highway Practice 41, 1977.
3. Standard Specifications for Highway Bridges, 12th ed. AASHTO, Washington, DC, 1977.
4. J.E. Long. Bearings in Structural Engineering. Newnes-Butterworths, London, 1974.
5. F.K. Jacobson. Investigation of Bridge Approach Spans to Poplar Street Bridge: A Preliminary Study. Bureau of Materials and Physical Research, Illinois Department of Transportation, Springfield, Oct. 1975.
6. F.-K. Chang and E.C. Cohen. Long-Span Bridges: State-of-the-Art. Journal of the Structural Division, ASCE, Vol. 107, No. ST7, July 1981, pp. 1145-1213.
7. F.K. Jacobson. TFE Expansion Bearings for Highway Bridges. Bureau of Materials and Physical Research, Illinois Department of Transportation, Springfield, Physical Research Rept. 71, April 1977.

8. M.E. Taylor. PTFE in Highway Bridge Bearings. Transport and Road Research Laboratory, Crowthorne, Berkshire, England, Rept. LR491, 1975.
9. A. Mazroi, L.R.-L. Wang, and T.M. Murray. Effective Coefficient of Friction of Bridge Bearings. School of Civil Engineering and Environmental Science, Univ. of Oklahoma, Norman, Final Rept., Feb. 1982.

Publication of this paper sponsored by Committee on General Structures.

Observations of Highway Bridge Movements and Their Effects on Joints and Bearings

LYLE K. MOULTON

Data on bridge movements and their effects were collected from 314 highway bridges in 39 states, the District of Columbia, and 4 Canadian provinces. These data have been analyzed to compare the movements that occurred with evidence of structural damage and to gain some insight into the basic causes of the movements and the resulting damages. The tolerance of the bridges to the various types and magnitudes of movements was also evaluated. It was found that, in general, bridge structures have much greater tolerance to differential vertical movements than is generally thought. However, in many instances, it was found that the design and/or construction practices used led to bridges in which structural damage, particularly to joints and bearings, was produced by relatively small horizontal movements of abutments and piers and the level of these damages was more severe when the horizontal movement was accompanied by vertical movement. In many instances, it was possible to identify the cause or causes of the bridge movements and the resulting structural damage. These causes suggested possible changes in design and construction practice that could help to reduce the probability of damaging movements. It is concluded that, although many highway bridge structures can tolerate significant vertical and horizontal movements, depending on span length and stiffness, there are relatively simple design and construction techniques available that can greatly reduce the possibility of movements and thus reduce the potential for structural damage and the resulting maintenance.

Throughout the years, a great deal of data has been collected that relates observed deformations of buildings and industrial structures to structural damage. These data have then been used to establish criteria for tolerable movements that can be used jointly by geotechnical and structural engineers to decide how a structure should be founded in order to minimize costs while maintaining an appropriate level of safety against structural damage. Among the most significant published accounts of this work are papers by Skempton and MacDonald (1); Polshin and Tokar (2); Feld (3); Grant, Christian, and Vanmarcke (4); and Burland and Wroth (5). Unfortunately, however, no such criteria have been available for highway bridges. Although there is a significant body of literature dealing with the investigation of bridge approach embankments and bridge foundation movements, until recently there was virtually nothing of a specific nature in the literature that related bridge foundation movements to structural damage or dealt with the tolerance of bridges to these movements. The 1978 papers by Grover (6), Keene (7), Walkinshaw (8), and Bozozuk (9,10) and more recent papers and reports by Moulton (11), Moulton and Kula (12), GangaRao and Moulton (13), and Moulton, GangaRao, and Halvorsen (14) constitute notable attempts to remedy this situation.

As part of an extensive investigation designed to develop rational criteria for the tolerable movements of bridges, data on bridge movements, their effects, and the tolerance of bridges to these movements were collected for a total of 314 bridges distributed across 39 states, the District of Columbia, and 4 Canadian provinces. The starting point for this data collection process was the acquisition of data, contained in the files of Transportation Research Board Committee A2K03, that were the result of surveys conducted in 1967 and 1975. Supplementary data on 115 of these bridges, including as-built plans, were obtained by direct contact with the state bridge and/or geotechnical engineers who had been involved in the original surveys. In addition, data were also obtained for a substantial number of bridges that were not included in the original surveys, including 28 bridges in the State of Washington that were contained in a Federal Highway Administration staff study (15), 89 bridges from Ohio, 9 from Maine, 5 from South Carolina, and 3 from Utah.

The collected field data were analyzed to compare the movements that had occurred with evidence of structural damage and to gain some insight into the basic causes of the movements and the resulting damages. It was also possible to obtain a very important insight into the magnitude of movements that had proved to be tolerable and intolerable in actual practice.

It is the purpose of this paper to summarize the results of these analyses, to identify the most common causes of these movements and their effects on bridge structures, particularly joints and bearings, and to suggest possible changes in design and construction practice that could help to reduce the possibility of damaging movements and minimize future bridge maintenance.

INFLUENCE OF SUBSTRUCTURE VARIABLES ON BRIDGE MOVEMENTS

A general summary of the substructure data incorporated into the investigation of the influence of substructure variables on bridge abutment and pier movements is presented in Table 1. For the abutments, the variables considered were (a) general soil conditions, (b) type of abutment (full height, perched, or spill-through), (c) type of foundation (spread footing or piles), and (d) height of approach embankment. Additional variables considered for the piers were (a) span type (simply supported or continuous) and (b) abutment-embankment-pier geometry. In addition to considering the effect of each of these variables on abutment and pier movements, various combinations of variables were considered in an effort to determine combinations that may or may not result in foundation movement. A general summary of the superstructure data that have

Table 1. General summary of substructure data.

Substructure Variables	No. of Bridges	Substructure Variables	No. of Bridges
General soil conditions		Abutment type	
Fine-grained soil	104	Full height	35
Granular soils	78	Perched	235
Fine-grained soils over granular soils	15	Spill-through	15
Granular soils over fine-grained soils	30	Full height and perched	2
Interlayered or intermixed soils	50	Perched and spill-through	3
Bedrock	14	Not given or unknown	24
Permafrost soils	3	Height of approach embankment	
Not given	20	Cut	4
Foundation type		0-9 ft	13
Spread footings	125	10-19 ft	56
Piles	95	20-29 ft	114
Abutments on spread footings or piers on piles	21	30-39 ft	77
Abutments on piles or piers on spread footings	39	40-49 ft	16
Abutments and piers on both spread footings and piles	20	50 to >100 ft	19
Miscellaneous combinations of spread footings, caissons, etc.	3	Not given	15
Not given	11		

Note: 1 ft = 0.3048 m.

Table 2. General summary of abutment movements.

Movement Type	Frequency		Range (in)	Avg (in)
	No. of Abutments	Percentage Moved		
All	439	100.0		
Vertical	379[a]	86.3	0.03-50.4	3.7
Horizontal	138	31.4	0.1-14.4	2.6
Vertical and horizontal	77	17.5	0.1-50.4	6.9
			0.1-14.4	2.2

Note: 1 in = 25.4 mm.

[a]Two abutments that raised vertically are not included in total, range, or average.

been incorporated into these analyses, including type of span, is presented below:

Superstructure Variable	No. of Bridges
Type of span	
Simple	97
Continuous	158
Simple and continuous	14
Rigid frame	7
Cantilever	10
Miscellaneous or not given	28
Type of structural material	
Steel	197
Concrete	78
Steel and concrete	4
Not given	35
Number of spans	
1	25
2	24
3	120
4	67
5	25
>5	50
Not given	3

These analyses resulted in the generation of a large amount of data on the influence of substructure variables on bridge movements. Because of space limitations, only a limited portion of the data can be presented here. The rest of the results are presented in the report by Moulton, GangaRao, and Halvorsen (14).

Abutment Movements

A total of 580 abutments had sufficient data to be included in the analysis. A general summary of the movement data for the 439 abutments that experienced some type of movement is presented in Table 2. These data show that the great majority of the abutments moved vertically, a little less than a third of them moved horizontally, and a significant number experienced simultaneous vertical and horizontal movement. The vertical movements tended to be greater than the horizontal movements. This can be explained in part by the fact that in many instances the abutments moved inward until their back walls became jammed against the beams or girders, which acted as struts preventing further horizontal movement. For those "sill"-type abutments that had no back walls, the horizontal movements were often substantially larger, the abutments moving inward until the beams or girders were, in effect, extruded out behind the abutments. However, a significant number of abutments (39) did move outward away from the bridge superstructure and toward their approach embankments. These were almost invariably perched abutments founded on piles driven through approach fills placed over deep compressible foundation soils. This type of movement has been described by Stermac, Devata, and Selby (16). The data given in Table 2 also show that abutment movements tended to be larger for those abutments that experienced both vertical and horizontal movements.

Of those abutments with sufficient data to be included in the analysis, substantially more perched abutments were reported than either full-height or spill-through abutments. Both the full-height and perched abutments tended to move more frequently than the spill-through abutments. However, the summary of abutment movements in terms of abutment type, given in Table 3, shows that perched and spill-through abutments tended to undergo a wider range of movements than did the full-height abutments. This was true with respect to both the vertical and horizontal movements. These movements are a manifestation of a variety of problems experienced by those abutments that were founded in approach embankments, regardless of foundation treatment (i.e., spread footings or piles). The two most common and most significant of these problems were (a) settlement of the embankment and/or foundation soil and (b) instability of the embankment slope, caused by excessively steep slopes, excessively high fills, low shear strength in the embankment or foundation soil, or streambed scour at the toe of the slope. It is significant that, whenever the preloading technique was applied (17-19) or whenever there was a waiting period between completion of embankment and abutment construction, the foundation movements were generally substantially lower than when abutment construction was initiated immediately after

Table 3. Summary of movements by abutment type.

Abutment Type	Movement Type	Frequency: No. of Abutments	Frequency: Percentage Moved	Range (in)	Avg (in)
Full height	All	64	100.0		
	Vertical[a]	56	87.5	0.3-17.0	3.8
	Horizontal	32	50.0	0.1-8.0	2.1
	Vertical and horizontal	24	37.5	0.3-17.0	4.8
				0.1-8.0	2.1
Perched	All	357	100.0		
	Vertical	307	86.0	0.03-50.4	3.5
	Horizontal	93	26.0	0.3-14.4	2.9
	Vertical and horizontal	43	12.0	0.1-50.4	7.9
				0.3-14.4	2.5
Spill-through	All	21	100.0		
	Vertical	16	76.2	1.2-24.0	8.2
	Horizontal	13	61.9	0.5-8.8	2.4
	Vertical and horizontal	8	38.1	1.2-24.0	7.8
				0.5-3.0	1.4

Note: 1 in = 25.4 mm.

[a]Two full-height abutments that raised 3 in are not included.

Table 4. Summary of movements of perched abutments on spread footings on fill by construction sequence.

Construction Sequence	Movement Type	Frequency: No. of Abutments	Frequency: Percentage Moved	Range (in)	Avg (in)
Preload and/or waiting period	All	81	100.0		
	Vertical	81	100.0	0.2-5.2	1.8
	Horizontal	2	2.5	0.3-0.3	0.3
	Vertical and horizontal	2	2.5	4.0-5.0	4.5
				0.3-0.3	0.3
No preload or waiting period	All	63	100.0		
	Vertical	60	95.2	0.1-35.0	7.3
	Horizontal	13	20.6	0.3-5.0	3.5
	Vertical and horizontal	10	15.0	0.1-35.0	18.2
				0.3-5.0	3.7

Note: 1 in = 25.4 mm.

completion of the embankment. This is illustrated rather clearly in Table 4.

In terms of foundation type, abutments founded on spread footings had a higher incidence of movement than abutments founded on piles. However, the summary of abutment movements in terms of foundation types, presented in Table 5, shows that abutments founded on piles actually experienced a larger range and slightly larger average vertical movement than did those founded on spread footings. This situation also existed with respect to horizontal movements. These same general trends were observed when the data were further broken down in terms of abutment type. This finding, coupled with the relatively large number of pile foundations that did move, would tend to suggest that the mere use of pile foundations does not necessarily guarantee that abutment movements will be within acceptable limits, particularly for the case of perched and spill-through abutments in fills. In fact, there is an existing body of evidence that, under some circumstances, bridges founded on piles or other deep foundations can move, sometimes substantially (16, 20-25).

Although some of the pile foundations of abutments were designed to provide some resistance to horizontal loading (i.e., batter piles were provided), in a substantial number of cases, where horizontal movement was experienced, no provisions were included to resist horizontal loading. In fact, it

Table 5. Summary of abutment movements by foundation type.

Foundation Type	Movement Type	Frequency: No. of Abutments	Frequency: Percentage Moved	Range (in)	Avg (in)
Spread footings	All	266	100.0		
	Vertical	254	95.5	0.1-35.0	3.7
	Horizontal	40	15.0	0.1-8.8	2.4
	Vertical and horizontal	28	10.5	0.1-35.0	6.1
				0.1-8.0	2.2
Piles	All	173	100.0		
	Vertical	122	70.5	0.03-50.4	3.9
	Horizontal	99	57.2	0.3-14.4	2.7
	Vertical and horizontal	48	27.7	0.3-50.4	5.6
				0.3-14.4	2.3

Note: 1 in = 25.4 mm.

was found that a significant number of perched abutments were founded on a single row of vertical piles driven through the approach embankment, often with only one pile under each beam or girder seat.

Although some general trends were evident, approach embankment heights did not correlate particularly well with the frequency and magnitude of abutment movements. In fact, the available data seem to suggest that the compressibility and shear strength of the embankment and foundation soils are as important as or more important than the height of the embankment in controlling embankment settlement and stability. This tends to agree with the findings reported by Grover (6) for Ohio bridges.

Pier Movements

The results of the analysis of pier movements showed that piers generally moved less often than abutments. In addition, the general summary of pier movements given in Table 6 shows that vertical movements tended to be considerably less than for abutments. Unlike the abutment movements, average horizontal pier movements tended to be larger than the vertical movements.

Table 7, which summarizes the pier movements in terms of foundation type, shows that the average magnitude of vertical movement was greater for pile foundations than for spread footings. However, the vertical movements for the piers on spread footings had a wider range than those for piers founded on piles, although there was a much larger number of piers founded on piles than on spread footings. This would suggest that the rate of success in founding piers on piles is substantially greater than that of founding abutments on piles, particularly for perched and spill-through abutments. The data show that, for the majority of piers founded on piles, the piles were driven in natural ground. This is in contrast to the situation for perched and spill-through abutments on piles, where in most instances the piles were driven through fill materials. In my judgment, this is the key to the indicated difference in performance between piers founded on piles and perched and spill-through abutments founded on piles. Piles simply cannot be expected to limit significantly the movements of a compressible or unstable embankment unless they are specifically designed to do so.

Piers located in or near the toe of approach embankments experienced movement almost twice as frequently as piers that were located away from the embankment. The data showed that, contrary to what might be expected, the magnitudes of vertical movements tended to be slightly larger for piers located away from the embankments: The average movement was 4.0 in (101.6 mm) compared with 2.2 in (55.9 mm) for

Table 6. General summary of pier movements.

Movement Type	Frequency: No. of Piers	Frequency: Percentage Moved	Range (in)	Avg (in)
All	269	100.0		
Vertical	234[a]	87.0	0.03-42.0	2.5
Horizontal	25	19.3	0.1-20.0	3.3
Vertical and horizontal	17	6.3	0.3-13.7	5.1
			0.6-20.0	2.7

Note: 1 in = 25.4 mm.

[a]The number of piers with movement included seven piers that raised vertically. These piers are not included in the total with vertical movement.

Table 7. Summary of pier movements by foundation type.

Foundation Type	Movement Type	Frequency: No. of Piers	Frequency: Percentage Moved	Range (in)	Avg (in)
Spread footings	All	145	100.0		
	Vertical	134[a]	92.4	0.1-42.0	1.8
	Horizontal	19	13.1	0.5-20.0	3.1
	Vertical and horizontal	7	4.8	0.8-9.0	3.8
				0.6-20.0	4.9
Piles	All	115	100.0		
	Vertical	92[a]	80.0	0.03-18.0	3.6
	Horizontal	33	28.7	0.1-16.0	3.2
	Vertical and horizontal	10	8.7	0.3-18.0	6.0
				0.6-4.04	1.3

Note: 1 in = 25.4 mm.

[a]The number of piers with movement includes seven piers that raised vertically. These are not included for vertical movements.

piers located in or near the embankment. The magnitudes of horizontal movements, however, were significantly larger for piers located in or near the embankment: They averaged 3.2 in (81.3 mm) compared with only 1.1 in (27.9 mm) for the piers located away from the embankment. This would suggest that, in designing bridge piers in or near the toe of embankments, more consideration needs to be given to the increased horizontal stresses that exist in these areas.

INFLUENCE OF FOUNDATION MOVEMENTS ON BRIDGE STRUCTURES

The investigation of the influence of bridge foundation movements on bridge structures was designed to determine what types and magnitudes of movements most frequently result in structural damage. The variables considered were (a) type of movement (vertical alone, horizontal alone, or vertical and horizontal in combination), (b) magnitude of movements (maximum differential vertical movements between two successive abutments or piers and maximum horizontal movements), (c) span type, (d) type of structural material (steel or concrete), (e) number of spans, and (f) abutment type. A general summary of the types of structural damage and the number of bridges that were reported to have experienced these is presented below:

Type of Damage	No. of Bridges
Damage to abutments	69
Damage to piers	18
Vertical displacement	45
Horizontal displacement	68
Distress in superstructure	117
Damage to rails, curbs, sidewalks, parapets	30
Damage to bearings	34
Poor riding quality	12
Not given or corrected during construction	10
None	81

It should be noted that many of these structures experienced multiple damaging effects.

Although most of the words and phrases used to describe structural damage in the preceding table and subsequent tables are self-explanatory, for the purposes of this paper some explanation is required for the terms "vertical displacement," "horizontal displacement," "distress in the superstructure," and "damage to bearings." Vertical displacement, when applied to structural damage, includes the raising or lowering of the superstructure above or below planned grade or a sag or heave in the deck. Structures that require shimming or jacking as well as truss structures with increased camber are also included. Horizontal displacement, when applied to structural damage, includes the misalignment of bearings and the superstructure or beams jammed against the abutments. Also included in this category of damage are bridges whose superstructure extended beyond the abutment, where beams required cutting, or where there was a horizontal movement of the floor system. Distress in the superstructure consists of cracks or other evidence of excessive stress in beams, girders, struts, and diaphragms as well as cracking and spalling of the deck. Other types of damage included in this category are the shearing of anchor bolts; the opening, closing, or damage of deck joints; and cases where the cutting of relief joints was required. Damage to bearings includes the tilting or jamming of rockers as well as cases where rockers have pulled off bearings or where movement resulted in an improper fit between bearing shoes and rockers that required repositioning. Also included in this category are deformed neoprene bearing pads, sheared anchor bolts in the bearing shoes, and the cracking of concrete at the bearings. A complete description of the terminology and simplifying assumptions used in the analysis is given in the report by Moulton, GangaRao, and Halvorsen (14).

As indicated in the preceding table, the types of structural damage that occurred most frequently were distress in the superstructure, damage to abutments, horizontal displacement, vertical displacement, and damage to bearings. It should be noted that, with the exception of vertical displacement and damage to abutments, all of these most frequently occurring types of structural damage could involve some type of damage to joints and bearings based on the definitions adopted for this study. Those structures with only abutment movements had a high frequency of distress in the superstructure and a somewhat lower incidence of horizontal displacement and abutment damage. Distress in the superstructure also occurred very frequently for bridges with only pier movements and for bridges with both abutment and pier movements.

In terms of the type of foundation movement, it was found that most types of structural damage appear to occur for those bridges in which both vertical and horizontal movements occur simultaneously. Horizontal displacement, abutment damage, and distress in the superstructure occurred relatively frequently for bridges with both vertical and horizontal movements. In contrast, structures for which

only vertical movement was reported had the lowest frequency of damaging structural effects, and a substantial number of structures had no damage at all.

This same general trend was evident in terms of magnitudes of movements in that even moderate differential vertical movements, up to 4 in (101.5 mm), tended to produce a relatively low incidence of structural damage. Of those 155 bridges with maximum differential vertical settlements of less than 4 in, 79 bridges experienced no damage whatsoever. The majority of the remaining structures experienced primarily abutment damage in the form of minor cracking, minor opening or closing of construction joints, and relatively minor distress in the superstructure. For differential vertical movements in excess of 4 in, distress in the superstructure tended to be the predominant structural effect. There was an increased incidence of vertical displacement and poor riding quality for differential vertical movements of 8 in (203.2 mm) and greater. However, it should be pointed out that poor riding quality was reported for only 12 out of the 314 bridges considered.

Bridges that experienced either horizontal movement alone or horizontal movement in conjunction with differential vertical movement had a high frequency of damaging structural effects, even for relatively small horizontal movements, which suggests that horizontal movements are much more critical than vertical movements in causing structural damage. For those structures with horizontal movements alone, movements of from 1.0 to 2.0 in (25.4-50.8 mm) commonly caused distress in the superstructure (in more than two-thirds of the cases). In the majority of these cases, the resulting damage involved the opening or closing of deck joints. The bearings were also affected in more than a third of these structures. Abutment damage and horizontal displacement appeared to begin occurring with greater frequency for horizontal movements of 2 in and greater.

It was more difficult to correlate structural damage with magnitudes of substructure movements for those cases where vertical and horizontal movements occurred simultaneously because of the possible interaction of the two types of movements. However, a detailed review of the actual causes of the various types of distress in the bridges revealed that it was most commonly the horizontal component of the movement that was responsible for the reported damage. Thus, as suggested earlier, horizontal movements appear to be much more critical than differential vertical settlements in causing most types of structural distress. This tends to confirm the findings of Walkinshaw (8) and Bozozuk (9).

In terms of span type (simply supported or continuous), the data showed that distress in the superstructure was the most common structural effect reported for both continuous and simply supported bridges. However, this type of distress was reported more frequently for the continuous structures than for the simply supported bridges. The data also showed that abutment damage was the second most frequently reported effect for the simply supported structures and was reported in approximately half as many of the continuous structures. For both types of spans, the most frequent and most serious types of structural distress appeared to be related to horizontal movements.

The data on the frequency of occurrence of the various types of bridge damage in terms of structural material showed that distress in the superstructure was reported much more frequently for concrete structures than for steel structures. However, the steel structures had a higher frequency of abutment damage, horizontal displacement, and damage to bearings. In terms of vertical and horizontal movements, steel bridges with differential vertical movement alone had a lower incidence and severity of structural damage than did concrete bridges. This situation was reversed for those bridges that experienced horizontal movements only and vertical and horizontal movements simultaneously. More than half of the steel bridges with horizontal movement only experienced distress in the superstructure and damage to bearings. Again, it was found that even relatively small horizontal movements--on the order of 1-2 in--produced more frequent and more severe structural damage than did much larger differential vertical movements regardless of the type of structural material.

The data on the frequency of occurrence of each of the various types of structural distress, in terms of abutment type, showed that structures on full-height abutments tended to have the highest incidence of abutment damage but a relatively low incidence of distress in the superstructure, damage to bearings, and vertical and horizontal displacement. Although those bridges on perched abutments generally had the highest occurrence of the more serious types of structural damage, they also had by far the largest number that experienced no structural damage. This is something of a paradox since, as reported earlier, perched abutments tended to undergo a larger and wider range of movements than did the full-height abutments. However, a detailed examination of the data revealed that it was primarily differential vertical abutment movements in excess of 4 in that caused damage to bridges with perched abutments. The most damaging effects were produced primarily by horizontal movements of 1-4 in in magnitude, and these effects were particularly serious when these horizontal movements were accompanied by larger differential vertical movements--i.e., differential settlements in excess of 4 in. The relatively high vertical movements experienced by the spill-through abutments (Table 3) were found to be largely responsible for the high incidence of superstructure distress reported for bridges with this type of abutment.

TOLERANCE OF BRIDGES TO FOUNDATION MOVEMENTS

The subjectivity of the term "tolerable" may be one reason for the lack of generally accepted tolerable movement criteria. Movements that are considered to be tolerable by one engineer may be considered to be intolerable by another. In an attempt to eliminate some of this subjectivity, TRB Committee A2K03 related tolerance to movements to maintenance requirements, and thus defined intolerable movement as follows (8): "Movement is not tolerable if damage requires costly maintenance and/or repairs and a more expensive construction to avoid this would have been preferable." For the sake of consistency, this definition was also adopted for the study reported here.

The variables considered in the investigation of the tolerance of various bridge structures to foundation movement included (a) type of structural damage, (b) type of movement, (c) magnitude of movements (maximum differential vertical movement between successive units of the substructure, maximum angular distortion, and maximum horizontal movement), (d) span type, (e) type of structural material, (f) number of spans, and (g) type of abutment. Again, space limitations require that only selected results of this investigation be presented here. The report by Moulton, GangaRao, and Halvorsen (14) gives a more complete presentation and discussion of the results.

Overall, of the 280 structures for which data on tolerance to foundation movements were available or could reasonably be assumed, the movements were considered tolerable for 180 bridges and intolerable for 100. The data given in Table 8 show that, of all the structural effects associated with foundation movements that were considered tolerable, damage to abutments and distress in the superstructure appear most frequently. In most instances, the reported damage involved relatively minor cracking and/or the opening or closing of construction joints in the abutments and cracking and spalling of concrete decks. However, there were a surprising number of instances in which the opening of deck joints was reported as being tolerable. Of course, as would be expected, the foundation movements associated with all 81 bridges that experienced no structural damage were considered tolerable.

For those 100 bridges with intolerable movements, Table 8 shows that almost half were reported to have distress in the superstructure. Horizontal displacement, vertical displacement, and damage to bearings were also reported quite frequently. In addition, almost one-quarter of those bridges with intolerable movements had abutment damage. As might have been expected, a larger number of bridges with intolerable movements exhibited multiple damaging effects than did bridges with tolerable movements. The intolerable structural effects that occurred most frequently in combination were distress in the superstructure, horizontal displacement, damage to abutments, vertical displacement, and damage to bearings. A detailed study of the bridge damage data revealed that in the majority of cases there was a direct interrelation between these most frequently occurring categories of structural damage and that most were related to horizontal movements or horizontal movements in combination with vertical movements. Although a variety of damaging incidents were reported, by far the most frequently occurring sequence of events involved the inward horizontal movement of abutments closing the expansion joints in the deck and causing serious damage to the bearings.

The results of the analysis of tolerance to bridge foundation movements in terms of type and magnitude of movement are presented in Table 9. With regard to movements in general, it was found, as might have been expected, that the intolerable movements generally tended to be substantially larger than the tolerable movements. The data given in Table 9 show that moderate magnitudes of differential vertical movements occurring by themselves were most often considered tolerable, whereas vertical and horizontal movements that occurred simultaneously were most commonly considered to be intolerable. Almost 98 percent of the differential vertical settlements less than 2 in (50.8 mm) and 91.2 percent of those less than 4 in (101.6 mm) were considered to be tolerable. However, although there

Table 8. Tolerance of bridges to structural damage.

	Tolerable Movement			Intolerable Movement		
	Bridges with Damage		Bridges with Multiple Damage[a]	Bridges with Damage		Bridges with Multiple Damage[a]
Structural Damage	No.	Percent		No.	Percent	
Damage to abutments	37	20.6	17	24	24.0	23
Damage to piers	8	4.4	7	8	8.0	8
Vertical displacement	3	1.7	2	42	42.0	21
Horizontal displacement	22	12.2	17	37	37.0	31
Distress in superstructure	49	27.2	28	46	46.0	39
Damage to rails, curbs, sidewalks, and parapets	17	9.4	16	8	8.0	8
Damage to bearings	8	4.4	6	17	17.0	17
Poor riding quality	1	0.1	1	11	11.0	4
Not given or corrected during construction	6	3.3	0	2	2.0	0
None	81	31.1	0	0	0.0	0
Total bridges in category	180			100		

[a] Multiple damage refers to the number of bridges in this category that had structural damage in addition to the indicated effects.

Table 9. Range of movement magnitudes considered tolerable or intolerable.

	No. of Bridges with Given Type of Movement							
					Vertical and Horizontal			
	Vertical Only		Horizontal Only		Vertical Component		Horizontal Component	
Interval[a] (in)	Tolerable	Intolerable	Tolerable	Intolerable	Tolerable	Intolerable	Tolerable	Intolerable
0.0-0.9	52	0	3	0	9	1	8	0
1.0-1.9	40	2	5	1	9	3	7	10
2.0-3.9	33	10	1	10	6	4	8	10
4.0-5.9	1	8	2	0	2	5	0	8
6.0-7.9	3	5	1	3	0	2	0	1
8.0-9.9	0	5	0	3	0	2	0	2
10.0-14.9	2	5	0	2	0	6	0	2
15.0-19.9	1	4	0	0	0	3	0	1
20.0-60.0	0	0	0	0	0	4	1	0
Total	132	39	12	19	26	30	24	34

[a] For vertical moments, magnitudes refer to maximum differential vertical movement. For horizontal movements, magnitudes refer to maximum horizontal movement of a single foundation element.

Table 10. Ranges of magnitudes of longitudinal angular distortion considered tolerable or intolerable.

Angular Distortion Interval ($x10^{-3}$)	No. of Bridges of Given Type and Tolerance					
	All Bridges		Simple Span		Continuous Span	
	Tolerable	Intolerable	Tolerable	Intolerable	Tolerable	Intolerable
0-0.99	43	1	17	1	23	0
1.0-1.99	36	5	7	0	25	4
2.0-2.99	32	0	4	0	19	0
3.0-3.99	14	1	5	0	7	1
4.0-4.99	10	4	2	0	5	4
5.0-5.99	2	6	0	1	2	5
6.0-7.99	2	7	1	2	1	4
8.0-9.99	1	3	0	1	1	1
10.0-19.99	3	20	2	4	1	12
20.0-39.9	1	8	1	5	0	2
40.0-59.9	0	3	0	2	0	1
60.0-79.9	0	2	0	1	0	1
Total	144	60	39	17	84	35

were some larger differential vertical settlements that were considered tolerable, the tolerance to differential vertical movements generally decreased significantly for values greater than 4 in. In terms of horizontal movements alone, of those bridges with maximum movements less than 2 in, the movements were considered tolerable in 88.8 percent of the cases. However, a large majority (81.8 percent) of the maximum horizontal movements of 2 in and greater were found to be intolerable. Furthermore, Table 9 indicates that even horizontal movements less than 2 in were only reported as being tolerable in 60.0 percent of the cases when accompanied by differential vertical movements. In fact, a more detailed analysis of the data revealed that, for simultaneous horizontal and vertical movements of this type, the horizontal movements were only reported as being tolerable in the great majority of cases when their magnitudes approached 1 in (15.4 mm) and less.

Although the sample sizes were smaller, the same general trends with respect to the magnitude of tolerable and intolerable foundation movements, given in Table 9 and described above, were observed to hold regardless of span type (simply supported or continuous), number of spans, and structural materials (steel or concrete). However, the apparent lack of tolerance to horizontal movements tended to be slightly more pronounced for all continuous structures and for concrete bridges.

The influence of span length on the tolerance of bridges to foundation movements was studied in terms of longitudinal angular distortion (maximum differential vertical settlement divided by span length). It was found that, for 204 of the 280 bridges with tolerance data, the data were sufficiently complete to permit this type of analysis. Of these 204 bridges, the movements were reported to be tolerable for 144 and intolerable for 60. Table 10 summarizes the frequency of occurrence of the various ranges of magnitudes of angular distortion considered tolerable and intolerable for all types of bridges included in this portion of the study and for bridges by span type. When all of the bridges in the analysis are considered, all 43 of the angular distortions less than 0.001 and 94.6 percent of the 132 angular distortions less than 0.004 were considered to be tolerable. However, only 42.9 percent of the values of angular distortion between 0.004 and 0.01 and 7.1 percent of those over 0.01 were considered to be tolerable. This would suggest that, on the basis of the field data, an upper limit on angular distortion of 0.004 would be reasonable. However, when the data are subdivided by span type, Table 10 indicates that the continuous bridges tended to be more sensitive to angular distortion than the simply supported bridges. Although this result was expected, it was anticipated that there would be a more dramatic difference than that shown in Table 10. For the continuous bridges, 93.7 percent of the 79 angular distortions less than 0.004 were considered to be tolerable whereas only 25.0 percent of those over 0.004 were considered to be tolerable. In contrast, for the simply supported bridges, 97.2 percent of the angular distortions less than 0.005 were reported as being tolerable.

When the data given in Table 10 were broken down in terms of material type, they suggested that the concrete bridges might be slightly more tolerant to angular distortion than the steel bridges. Thus, the reported trend for the concrete bridges to experience more frequent and more severe superstructure damage than the steel bridges as a result of foundation movements did not show up in the tolerance data. This implies that the frequently reported distress in the superstructure of concrete bridges was quite often considered to be tolerable. A detailed breakdown of the data in Table 8, in terms of material type, provided verification for this observation.

IMPROVED DESIGN AND CONSTRUCTION PRACTICE

One of the most surprising results of this study was the relatively large number of pile-supported foundations that experienced movements. This suggested unsatisfactory performance of the piles in resisting the loads to which they were subjected. However, it should be recognized that these data on foundation movements are biased in the sense that they represent the observed behavior of only those bridge foundations that have experienced some type of movement. Consequently, the data are insufficient to permit any inferences to be drawn concerning the relative performance of different foundation systems (i.e., piles versus spread footings). Moreover, many of the case histories studied lacked sufficient detail on the design and construction of the pile foundations to permit a reliable evaluation of the reasons for their poor performance. An effort is being made to obtain additional information on these bridges in order to determine what factors might have contributed to the inability of the pile foundations to resist the applied loads without movements.

In the meantime, however, there are simple design and construction measures that can be used to improve the effectiveness of pile foundations in minimizing bridge movements. One of the most important considerations is the recognition of the way in which piling derives its support from the underlying and surrounding soil and rock. The results of this

study have shown that this is particularly critical with respect to resisting horizontal movements. Thus, if a pile foundation is to be used, it must be carefully designed to resist all of the forces to which the unit of the substructure is subjected. This includes lateral earth pressures as well as vertical dead and live loads. We cannot count on developing any significant amount of horizontal resistance from vertical piles if these piles are expected to derive their lateral support from the passive resistance of soil that may itself be subject to horizontal deformation. Therefore, appropriate consideration should be given to the design of batter piles to resist horizontal loading. Every effort should be made to use modern techniques for the analysis, design, and construction of pile foundations (26-32). The implementation of improved methods of analysis and design in recent years has done much to improve the reliability of pile foundations. The judicious use of test piles and pile load tests (26,33) can also help to ensure that a pile foundation will perform as designed.

One of the most common causes of foundation movements revealed by this study was movement of underlying embankment materials and/or their foundations. In fact, this basic cause of movement was identified as being either totally or partly responsible for the movements of more than 150 foundation elements. These data suggest that, when abutments or other substructure units are to be founded on embankments, whether on spread footings or piles, the embankment should be specifically designed to resist postconstruction deformation either by settlement of the embankment material, consolidation of the underlying foundation soil, or sliding associated with slope or foundation instability.

Postconstruction settlement of the embankment material can be minimized by careful placement and control of compaction (34). Specifying well-compacted, select (granular) borrow in the area immediately beneath the substructure elements has proved to be beneficial in many instances. The application of preloading (17-19,35) and/or soil improvement techniques (36-38) has also been very effective in minimizing postconstruction settlements of compressible foundation soils. The specification of a "waiting period", after embankment construction and before the construction of the foundation elements, is highly recommended. The use of simple instrumentation, such as settlement platforms or settlement stakes, during this waiting period can provide positive information on the rate of settlement and guidance as to when it is safe to proceed with the foundation construction without the risk of serious postconstruction settlement. It should be recognized that, if the embankment is properly designed and constructed to minimize or eliminate potential movements, then one of the most commonly cited reasons for founding on piles has been eliminated and it may be found that spread footing will provide an adequate foundation at substantial savings. Certainly, the cost-effectiveness of this approach (15) should always be investigated.

The results of this study have shown enough problems arising from the instability of embankment slopes and/or their foundations to suggest that the practice of using standard slopes should be abandoned in favor of a formal slope stability analysis and design procedure such as that used in the design of earth dams. In this procedure, the foundation soils and borrow materials are sampled and tested to obtain conservative estimates of postconstruction strength parameters that are then used to perform appropriate stability analyses (39,40). The slope is then adjusted until a suitable factor of safety--say, 1.5--is obtained. In the design of embankments at stream crossings, the possibility of stream bed scour at the toe of the slope should always be considered, and measures should be taken to protect against its occurrence.

One of the most common categories of problems revealed by this study was the opening or closing of bridge deck joints and the damage to bearings caused by horizontal movements of abutments and piers. Although appropriate implementation of the recommendations given above will certainly alleviate this problem by reducing the magnitude of potential horizontal movements, it is unlikely that all horizontal movements can be entirely eliminated by these techniques. This is particularly true for the case of outward movement of perched abutments founded on piles driven through embankments placed over deep compressible soils. Because this phenomenon is not well understood, the occurrence and magnitude of movements of this type are difficult to predict reliably. Consequently, it might be advisable to anticipate some horizontal movements in addition to those normally expected from thermal expansion and contraction and design the joints and bearings to tolerate them. Under some circumstances, it may be desirable to consider minimizing or eliminating the problem through the adoption of the integral-abutment concept. This scheme, which has been used for structures up to approximately 350 ft (106.7 m) in length (41), involves the construction of the abutment integrally with the end of the superstructure. The superstructure, the abutment, and its foundation are designed to tolerate the stresses and deformation associated with thermal expansion and contraction. Thus, this technique eliminates the use of expansion joints and bearings at the abutments. In those instances where expansion joints and some kind of bearings are considered necessary, consideration would be given to the use of elastomeric bearings, particularly for short- and medium-span structures. If assurance of the elimination of postconstruction movements cannot be provided economically, or if expensive maintenance or replacement of bearings is anticipated, then the provision of jacking pads and other structural details that will assist future jacking operations may be desirable.

SUMMARY AND CONCLUSIONS

The data presented in this paper show that a substantial number of highway bridges throughout the United States and Canada have exhibited a rather wide range of both vertical and horizontal movements of substructure elements. Generally, abutment movements occurred much more frequently than pier movements. Although both the frequency and magnitude of vertical movements were often substantially greater than horizontal movements, the horizontal movements generally tended to be more damaging to bridge superstructures. The data suggest that more consideration needs to be directed to the potential effects of horizontal movements during the design stage, particularly for perched and spill-through abutments on fills and piers located near the toe of approach embankments. Furthermore, care should be exercised in the design and construction of approach embankments in order to eliminate this important potential source of damaging postconstruction movements.

The study also showed that spread footing foundations were used slightly more frequently than pile foundations for abutments. However, many more piers were founded on piles than on spread footings. Although the movements of spread footing foundations occurred a little more frequently, the movements of pile foundations had slightly greater magnitudes.

This suggests the need for a more detailed examination of those cases of pile movements in order to determine the reasons for the failure of the pile foundations to serve their intended function of eliminating or minimizing substructure movements.

The results of this study have shown that, depending on type, length, and stiffness of spans and the type of construction material, many highway bridges can tolerate significant magnitudes of total and differential vertical settlement without becoming seriously overstressed, sustaining serious structural damage, or suffering impaired riding quality. However, it was found that many of the bridges involved in this study were susceptible to structural damage, particularly to joints and bearings, from relatively small horizontal movements of abutments and piers, and the level of these damages was more severe when the horizontal movement was accompanied by vertical movement.

In many instances, it was possible to identify the cause or causes of the bridge movements and the resulting structural damage. The primary causes of substructure movements usually fell into three general categories: (a) movements of approach embankments and/or their foundations, (b) unsatisfactory performance of pile foundations, and (c) inadequate resistance to lateral earth pressures, causing horizontal movements of abutments. The potential movements arising from these sources can be minimized or eliminated by using the relatively simple design and construction techniques suggested above and thus reducing the potential for structural damage and the resulting maintenance.

REFERENCES

1. A.W. Skempton and D.H. MacDonald. Allowable Settlement of Buildings. Proc., Institute of Civil Engineers, London, England, Part 3, Vol. 5, Dec. 1956, pp. 727-768.
2. D.E. Polshin and R.A. Tokar. Allowable Non-Uniform Settlement of Structures. Proc., 4th International Conference on Soil Mechanics, London, England, Aug. 1957, Vol. 1, pp. 402-405.
3. J. Feld. Tolerance of Structures to Settlement. Journal of Soil Mechanics and Foundations Division, ASCE, Vol. 91, No. SM3, May 1965, pp. 63-77.
4. R. Grant, J.T. Christian, and E.H. Vanmarcke. Differential Settlement of Buildings. Journal of Geotechnical Engineering Division, ASCE, Vol. 100, No. GT9, Sept. 1974, pp. 973-991.
5. J.B. Burland and C.P. Wroth. Settlement of Buildings and Associated Damage: State-of-the-Art. Proc., Conference on Settlement of Structures, Cambridge, England, Pentech Press, London, England, 1974, pp. 661-654.
6. R.A. Grover. Movements of Bridge Abutments and Settlement of Approach Pavements in Ohio. TRB, Transportation Research Record 678, 1978, pp. 12-17.
7. P. Keene. Tolerable Movements of Bridge Foundations. TRB, Transportation Research Record 678, 1978, pp. 1-6.
8. J.L. Walkinshaw. Survey of Bridge Movements in the Western United States. TRB, Transportation Research Record 678, 1978, pp. 6-10.
9. M. Bozozuk. Bridge Foundations Move. TRB, Transportation Research Record 678, 1978, pp. 17-21.
10. A.G. Stermac. Discussion of Bridge Foundations Move by M. Bozozuk. TRB, Transportation Research Record 678, 1978, p. 21.
11. L.K. Moulton. Movement of Highway Bridges and Their Effects on Design, Construction and Maintenance. Proc., Bridge Maintenance and Rehabilitation Conference, Morgantown, WV, 1980, pp. 271-313.
12. L.K. Moulton and J.R. Kula. Bridge Movements and Their Effects. Public Roads, Vol. 44, No. 2, 1980.
13. H.V.S. GangaRao and L.K. Moulton. Tolerable Movement Criteria for Highway Bridges. Public Roads, Vol. 44, No. 4, 1981, pp. 140-147.
14. L.K. Moulton, H.V.S. GangaRao, and G.T. Halvorsen. Tolerable Movement Criteria for Highway Bridges: Volume I--Interim Report. FHWA, Rept. FHWA/RD-81/162, Dec. 1981, 127 pp.
15. S.J. Sequirant. An Evaluation of the Performance and Cost Effectiveness of the Use of Spread Footings in Fill Embankments for the Support of Highway Bridge Abutments in the State of Washington. Department of Civil Engineering, Univ. of Washington, Seattle, M.S. thesis, 1979.
16. A.G. Stermac, M. Davata, and K.G. Selby. Unusual Movements of Abutments Supported on End-Bearing Piles. Canadian Geotechnical Journal, Vol. 5, No. 2, May 1969.
17. H.P. Aldrich. Precompression for Support of Shallow Foundations. Journal of Soil Mechanics and Foundations Division, ASCE, Vol. 91, No. SM2, 1965, pp. 5-20.
18. H.Q. Golder and A.B. Sanderson. Bridge Foundation Preloaded to Eliminate Settlement. Civil Engineering, Vol. 31, No. 10, Oct. 1961, pp. 62-65.
19. S.J. Johnson. Precompression for Improving Foundation Soils. Journal of Soil Mechanics and Foundations Division, ASCE, Vol. 96, SM1, 1970, pp. 73-110.
20. E.S. Barber. Observed Settlements of Highway Structures Due to Consolidation of Alluvial Clay. Public Roads, Vol. 26, No. 11, Dec. 1951, pp. 217-224.
21. L. Bjerrum, W. Johnson, and C. Ostenfeld. The Settlement of a Bridge Abutment on Friction Piles. Proc., 4th International Conference on Soil Mechanics and Foundation Engineering, London, Vol. 2, 1957, pp. 14-18.
22. A.B. George, F.W. Sherrell, and M.J. Tomlinson. The Behavior of Steel H-Piles in Slaty Mudstone. Geotechnique, Vol. 26, May 1976, pp. 95-104.
23. W.P. Kimball. Settlement Studies of Huey P. Long Bridges. Civil Engineering, Vol. 10, No. 3, March 1940, pp. 145-148.
24. R. Marche and Y. Lacroix. Stabilities des culees de ponts estabilies sur des peiux traversant une couche molle. Canadian Geotechnical Journal, Vol. 9, No. 1, Feb. 1972, pp. 1-24.
25. N.D. Nicu, D.R. Antes, and R.S. Kessler. Field Measurements on Instrumented Piles Under an Overpass Abutment. HRB, Highway Research Record 354, 1971, pp. 90-102.
26. H.D. Butler and H.E. Hoy. The Texas Quick-Load Method for Foundation Load Testing: Users Manual. FHWA, Rept. FHWA-IP-77-8, 1977, 59 pp.
27. G.G. Goble and F. Rausch. Wave Equation Analysis of Pile Driving, WEAP Program: Volume I--Background. FHWA, Rept. FHWA-IP-76-14.1, July 1976, 124 pp.
28. G.G. Goble and F. Rausch. Wave Equation Analysis of Pile Driving, WEAP Program: Volume II--Users Manual. FHWA, Rept. FHWA-IP-76-14.2, July 1976, 120 pp.
29. G.G. Goble and F. Rausch. Wave Equation Analysis of Pile Driving, WEAP Program: Volume III--Users Manual. FHWA, Rept. FHWA-IP-76-14.3, July 1976, 127 pp.
30. G.G. Goble and F. Rausch. Wave Equation Analy-

sis of Pile Driving, WEAP Program: Volume IV--Narrative Presentation. FHWA, Rept. FHWA-IP-76-14.4, July 1976, 66 pp.
31. A. Kezdi. Pile Foundations. In Foundation Engineering Handbook (H.F. Winterkorn and H.-Y. Fang, eds.), Van Nostrand Reinhold Co., New York, 1975, pp. 556-600.
32. Design of Pile Foundations. NCHRP, Synthesis of Highway Practice 42, 1977, 68 pp.
33. Piles Under Axial Compressive Load: Standard Method of Testing Designation D1143-74. In Annual Book of ASTM Standards, ASTM, Part 19, 1980, pp. 236-246.
34. Bridge Approach Design and Construction Practices. NCHRP, Synthesis of Highway Practice 2, 1969, 30 pp.
35. R.D. Holtz. Preloading by Vacuum: Current Prospects. TRB, Transportation Research Record 548, 1975, pp. 26-29.
36. Soil Improvement: History, Capabilities, and Outlook. Committee on Placement and Improvement of Soils and the Geotechnical Engineering Division, ASCE, New York, 1978.
37. R.D. Barksdale and R.C. Bachus. Methodology for the Design and Construction of Stone Columns. Presented at FHWA Research Review Conference, Springfield, VA, 1980.
38. J.K. Mitchell. Soil and Site Improvement Techniques to Enhance the Use of Shallow Foundations. Presented at FHWA Research Review Conference, Atlanta, GA, 1977.
39. A.W. Bishop. The Use of the Slip Circle in the Stability Analysis of Slopes. Geotechnique, Vol. 5, No. 1, 1955, pp. 7-17.
40. J.M. Ducan and A.L. Buchignani. An Engineering Manual for Slope Stability Studies. Department of Civil Engineering, Univ. of California, Berkeley, March 1975, 83 pp.
41. D.H. Beeson. Integration of Maintenance Needs into Preconstruction Procedures. FHWA, Rept. FHWA-TS-77-216, April 1978, pp. 104-105.

Publication of this paper sponsored by Committee on Sealants and Fillers for Joints and Cracks.

Caltrans Prestressed Concrete Pipe Culvert Research: Design Summary and Implementation

ALFRED E. BACHER, ALBERT N. BANKE, AND DANIEL E. KIRKLAND

A summary of the design and implementation of a California Department of Transportation (Caltrans) research project on the use of prestressed concrete pipe in culverts is presented. The Cross Canyon installation has 96-in prestressed concrete pipe culvert under 200 ft of overfill. The following design summary conclusions were made: (a) Method A (compacted structure backfill) loadings of 140V:140H and 140V:42H are adequate; (b) fill heights versus soil pressures were approximately linear; (c) there was excellent correlation between theoretical and experimental moments, thrusts, and displacements; (d) the 96-in prestressed pipe was grossly overdesigned; and (e) earth load stresses are additive to those from prestressing. In the future, Caltrans proposes to introduce a new criterion, dimension ratio, for prestressed concrete pipe design. In addition, implementation of Section 1.16 (Prestressed Concrete-Soil Structure Interaction System) of the AASHTO bridge specifications is recommended. It is concluded that prestressed concrete pipe should continue to be used for unstable drainage site conditions.

In 1963, the California Department of Transportation (Caltrans), in cooperation with the Federal Highway Administration, initiated a $3.5 million culvert research program to assess the structural behavior of culverts embedded in deep embankments. Included in this extensive culvert research program was a prestressed concrete pipe project located in Cross Canyon. Culvert size was 96 in, and overfill height was 200 ft.

The prestressed concrete pipe research project was initiated because prestressed pipe, with its semirigid structural characteristics, offered an alternative type of underground structure with the potential for appreciable savings in material. It could sustain deformation of 0.5 to 1.0 percent without impairment of its structural capability. Furthermore, it had sufficient wall thickness to offer assurance against catastrophic wall failures.

Caltrans has used prestressed concrete pipe culverts for special designs involving unstable earth slide conditions. Examples include the extension of the 15-ft West Fork Liebre Gulch reinforced concrete arch culvert, which had suffered severe distress during construction, with a 12.5-ft-diameter prestressed pipe and replacement of a failed triple reinforced concrete box at San Pablo Creek with triple 11-ft-diameter prestressed pipes. Prestressed concrete pipe design had been historically based on Marston-Spangler design criteria. Concern that these criteria were not appropriate for culvert design under high overfills and special design conditions led to Caltrans' undertaking this prestressed concrete pipe culvert research.

CROSS CANYON PROJECT

Description of Installation

The Cross Canyon prestressed concrete pipe research installation consists of a functional 96-in prestressed concrete pipe, designated zone 11, with instrumented plans A, B, and C; and zone 12, a control segment, placed in the same fill. The center pipe segment in zone 11 was instrumented with electric resistance strain gauges at each octant point. Rebar strains in the concrete pipe were measured as were strains in the concrete pipe core. The three planes of instrumentation were placed 6 and 7 ft apart, respectively, for planes A, B, and C (see Figures 1 and 2).

Soil stress meters were embedded in the surface of the concrete pipe at all three planes and in the soil surrounding the concrete pipe. The upper half of the pipe contained meters at 45° intervals, and the lower half had meters at 30° circumferential spacings. Strain gauges were placed in plane A only.

A new, specially designed Cambridge Meter, obtained from Robertson Research, Limited, was in-

Figure 1. Cross Canyon prestressed pipe culvert installation.

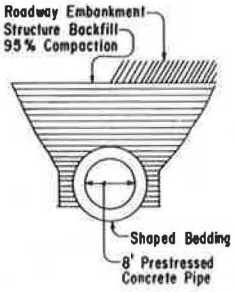

Figure 2. Effective densities: zone 11, planes A, B, and C.

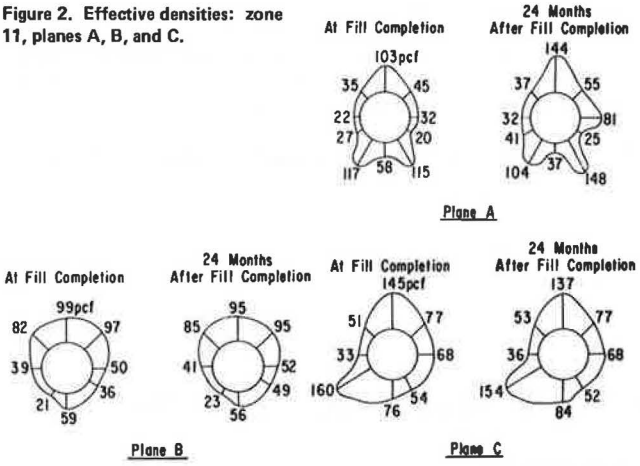

Figure 3. Soil pressures: zone 11.

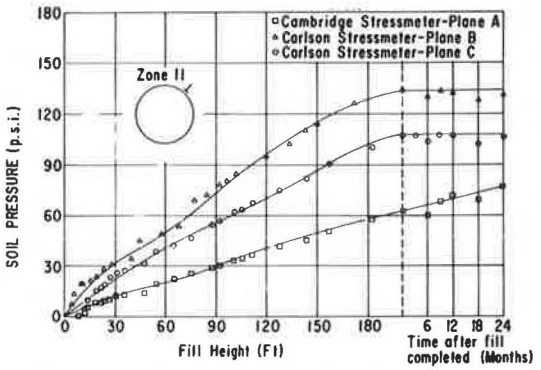

Figure 4. Theoretical and experimental moments: zone 11, plane A.

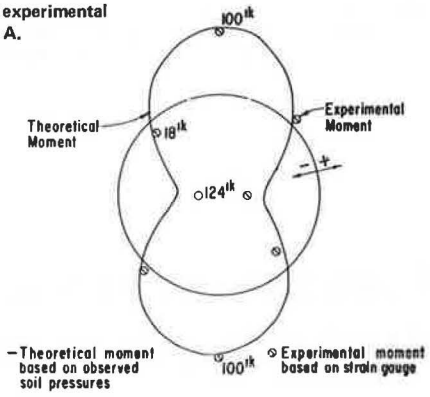

stalled in zone 11, plane A. This device measures both normal pressures and circumferential shears on the pipe wall. Displacements, settlements, rigid body rotations, and joint movements were measured manually. Zone 11 was placed in a trench condition and was surmounted by 10 ft of structure backfill. Shaped bedding with a 120° bedding angle was also provided.

Design Summary and Applications

The plots of the unadjusted effective densities of planes A, B, and C of zone 11 at Cross Canyon are conclusive in the following respects. The stresses produced by observed effective densities for method A (compacted backfill structure), planes A and C, can be approximated by using an idealized loading of 140V:42H. Plane B exhibited lesser circumferential effective densities and a maximum of 99-pcf effective density at the crown. The lateral effective densities ranged between 22 and 81 pcf in planes A, B, and C.

The effective density increase after fill completion was negligible in planes B and C but did increase significantly in plane A (Figure 1). This anomaly represents the one instance in Caltrans Method A rigid pipe culvert research when such an increase did occur. However, the increased readings of 144 pcf at position 1 and 148 pcf at position 5 are only slightly larger than the 140 pcf currently specified by Caltrans.

There is approximate linearity of the soil stress versus fill height plots up to fill completion for position 2 on planes A, B, and C (see Figure 3). Note that for plane A there was an increase in effective density after fill completion.

The asymmetry of effective densities common to all Caltrans rigid culvert research results to date (1, Section I, Volumes 1, 3, and 6; Section II, Part 1; Section III, Volume 2; Section IV, Volumes 1 and 2; Section V, Volumes 11 and 12; and Section IX) was also exhibited on planes A, B, and C of zone 11. Cambridge Meter circumferential shear readings were but one of the indications of the condition of asymmetrical loading. A computational effort was made to establish rotational, horizontal, and vertical equilibrium at zone 11.

The correlation between the experimental moments, based on soil-stress readings, and the theoretical moments, based on strain gauges, using the neutral point method was excellent for plane A (see Figure 4). These moments were of considerable magnitude--i.e., 100 ft-kip.

In all previous Caltrans rigid culvert research, there had been little success in correlating the theoretical and experimental thrusts based on soil pressure readings and strain gauges, respectively. However, at plane A, zone 11, with thrusts as high as 64 kips, excellent correlation was achieved (see Figure 5).

As an indication of the gross overdesign of the 96-in prestressed concrete pipe at Cross Canyon, with a wall thickness of 24 in, the maximum deflection observed was 0.08 in (see Figure 6). The theoretical displacement based on observed soil pressures has excellent correlation with the theoretical displacements based on extensometer measurements. No cracking was observed at zone 11.

Further confirmation of the gross overdesign was provided by the theoretical prestressing steel stresses obtained for outer wrap (there were two layers of prestressed steel), due to earth load only, based on measured soil pressures/neutral point analysis (see Figure 7). The maximum tensile stress of 9300 psi, due to earth load only, is indicative of gross overdesign of the 24-in wall thickness of the 96-in prestressed concrete pipe at Cross Can-

Figure 5. Theoretical and experimental thrusts: zone 11, plane A.

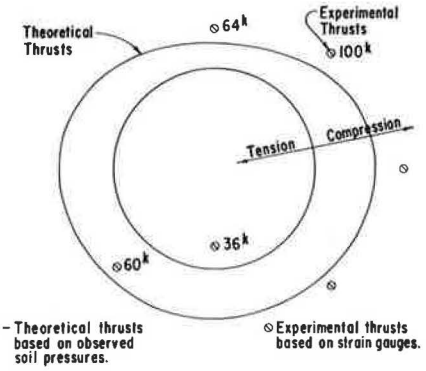

Figure 6. Theoretical and experimental displacements: zone 11, plane A.

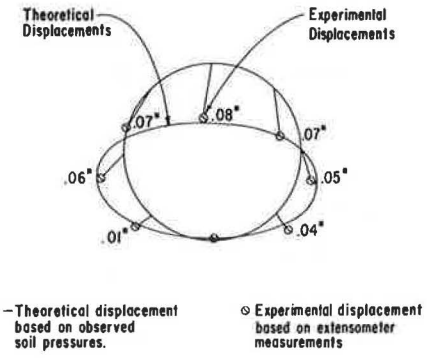

Figure 7. Prestressing steel stress due to load only: zone 11, plane A.

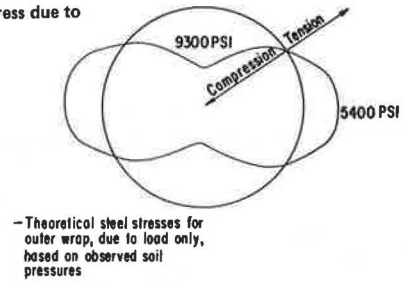

Figure 8. Inner reinforcing bar, compressive stress: zone 11.

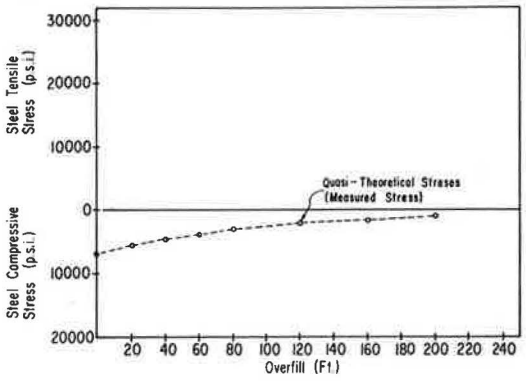

Figure 9. Outer reinforcing bar, compressive stress: zone 11.

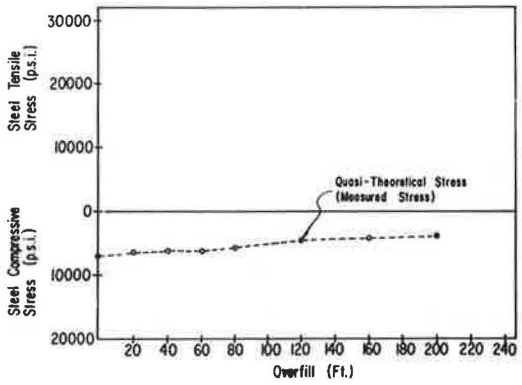

yon. This is further supported by the fact that the 1000D pipe with an 8-in wall thickness of the dummy 84-in reinforced concrete pipe at this same site was sufficient structurally to withstand 200 ft of overfill.

A comparison has been made between the 96-in prestressed concrete pipe furnished at Cross Canyon, based on D-load equivalency, and a 1000D reinforced concrete pipe. By using Paris coefficients and the working stress method, for a prestressed concrete pipe designed for a field load of 230 000 lb/lineal ft and a 90° bedding angle, the equivalent D-load obtained is 15 000D. A comparable 1000D prestressed pipe would have a 7-in wall and 0.45-in²/ft prestressed steel.

Two cages of bar reinforcing steel were also included in zones 11 and 12 to facilitate the research of this prestressed concrete pipe. That this prestressed concrete pipe is grossly overdesigned is supported by the fact that compressive stresses only were observed for the inner and outer cages of the bar reinforcing (see Figures 8 and 9). Initially, the prestressing had resulted in a compressive stress of 6800 psi in the bar reinforcing steel. Subsequent placement of earth overfill reduced the compressive stresses to 700 psi in the inner reinforcing bar cage.

Tensile stress was observed only on the concrete inner fiber after the overfill exceeded 110 ft (see Figures 10-13). Initially, the prestressing had resulted in a 735-psi compression on the inner and outer concrete fibers. The net tensile stress of 220 psi observed in the concrete inner fiber at the time of fill completion is less than the 450-psi allowable tensile stress for concrete. The existence of low tensile stresses was affirmed by the fact that no cracking was observed in zone 11.

It is apparent that the use of prestressed concrete pipe for a high fill poses a situation in which the prestressing stresses are added to the stresses induced by the earth overfill. The design of the prestressed concrete pipe was based on Marston-Spangler criteria; experimentally, the installed pipe was found to be overdesigned.

The primary use for prestressed concrete pipe to date has been for internal pressure conditions. Ameron Pipe Products, for example, has placed more than 300 miles of prestressed concrete pipe as pressure pipe. Prestressed concrete pipe has been used by Caltrans in special designs because of its semirigid structural characteristics. Except for Cross Canyon, it has been placed where overfills were less than 90 ft and has performed extremely well.

IMPLEMENTATION

Based on reinforced concrete pipe research at Mountainhouse and Cross Canyons, Caltrans has imple-

Figure 10. Concrete inner fiber, compressive stress: zone 11.

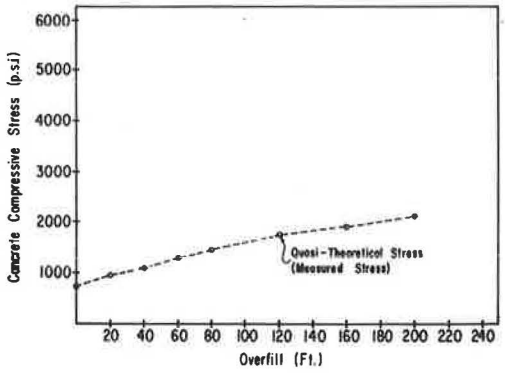

Figure 11. Concrete outer fiber, compressive stress: zone 11.

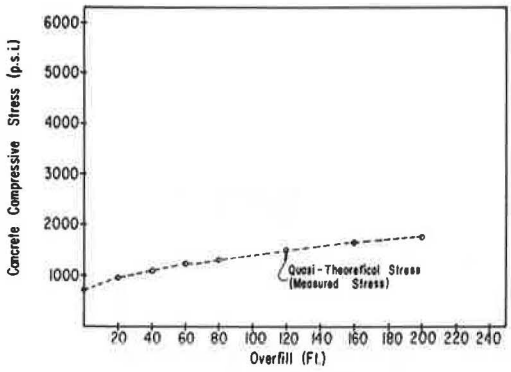

Figure 12. Concrete inner fiber, tensile and compressive stress: zone 11.

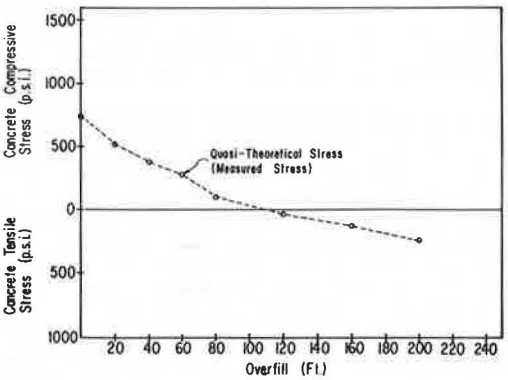

Figure 13. Concrete outer fiber, tensile and compressive stress: zone 11.

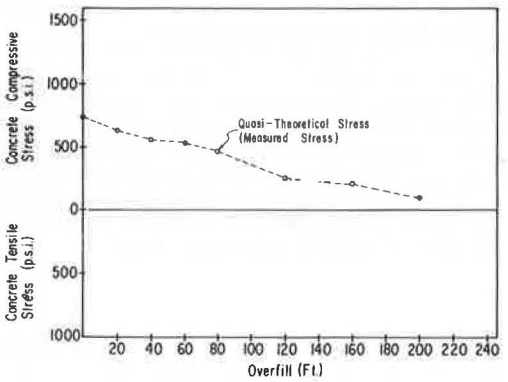

Figure 14. Caltrans criteria for unit load on culverts, where dimension ratio is 1.0-11.9.

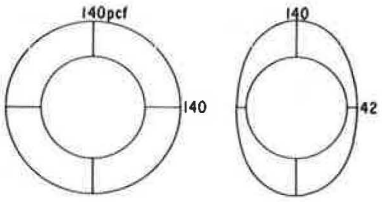

Figure 15. AASHTO criteria for unit load on culverts.

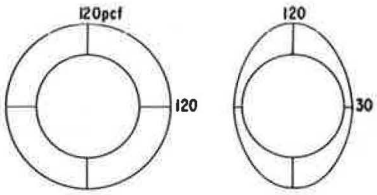

Figure 16. Dimension ratio.

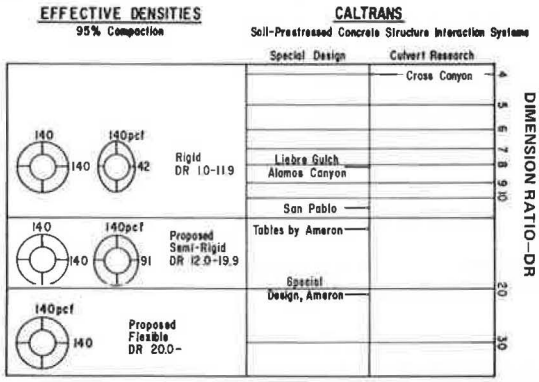

mented design loadings of 140V:140H and 140V:42H for reinforced concrete pavement. They are considered equally applicable to prestressed concrete pipe design, where the dimension ratio is 1.0-11.9 (see Figure 14).

The American Association of State Highway and Transportation Officials (AASHTO) has recently revised its Article 1.2.2A, Loads on Culverts (2), to specify two loading conditions for rigid culverts: 120V:120H and 120V:30H (see Figure 15).

FUTURE CONSIDERATIONS

1. Caltrans proposes to introduce a new criterion, dimension ratio, for prestressed concrete pipe design (see Figure 16). Dimension ratio is defined as the internal diameter in inches divided by the wall thickness in inches. Caltrans reinforced concrete pipe research at Cross Canyon, previously reported, has emphasized the importance of the dimension ratio. With a dimension ratio of 4.0, the previous assumption by Caltrans that a prestressed concrete pipe always acts as a semirigid structure was not supported by this research. With a wall thickness of 24 in and an inside diameter of 96 in, zone 11 is, in effect, a rigid culvert. Ameron has developed tables based on a dimension ratio of 13.0--i.e., a semirigid condition. The initial proposed loadings are 140V:140H and 140V:91H for semirigid culvert design. Caltrans is currently developing a curvilinear relation between varying lateral effective densities and dimension ratios.

2. Initiation and development of Section 1.16 of the AASHTO bridge specifications (2)--Prestressed

Concrete-Soil Structure Interaction Systems--are recommended.

SUMMARY

The primary use of prestressed pipe to date has been for pressure pipe installations. In Caltrans, it has been limited to special drainage designs and has been considered a semirigid design. The prestressed concrete pipe research reported in this paper, coupled with the reinforced concrete pipe research by Hydro-Conduit using pipes that share common dimension ratios and Ameron prestressed concrete pipe designs, gives further support to the dimension ratio concept.

Prestressed concrete pipe continues to offer an acceptable alternative for special drainage designs--i.e., where there is an unstable soil condition in a potential slide area. Under high fills it is not recommended, since there is admittedly the adverse effect of the earth loads being added to the prestressing forces.

ACKNOWLEDGMENT

The Caltrans Culvert Committee and Ameron cooperated and participated fully in the initiation of the prestressed concrete pipe culvert research at Cross Canyon and the selection of the design parameters to be considered. Walt Creasmon of Ameron contributed significantly to the initiation of the prestressed concrete pipe research proposal and, most recently, to this paper on design summary and implementation.

REFERENCES

1. R.E. Davis, F.M. Semans, D.W. Spannagel, and A.E. Bacher. Rigid Pipe Proof Testing Under Excess Overfills with Varying Backfill Parameters. California Department of Transportation, Sacramento, Oct. 1978 to July 1982.
2. Standard Specifications for Highway Bridges, 12th ed. AASHTO, Washington, DC, 1977.

Publication of this paper sponsored by Committee on Culverts and Hydraulic Structures.

Effect of Heavy Loads on Buried Corrugated Polyethylene Pipe

REYNOLD K. WATKINS, RONALD C. REEVE, AND JAMES B. GODDARD

Corrugated polyethylene pipe, developed originally in 4- to 12-in diameters for land drainage, is now manufactured in larger diameters for other uses of buried conduits such as culverts, air ducts, and service conduits. Tests were conducted on pipes with 15-, 18-, and 24-in inner diameter to investigate the structural performance and performance limits of these larger-diameter pipes when subjected to external soil pressures. For pipes in typical native soil backfill, compacted by typical methods to greater than 80 percent standard density (AASHTO T-99), less than 1 ft of soil cover (called minimum cover) was found to be adequate protection against H-20 (32-kip/axle) loads and up to 54-kip/axle "super-loads". The soil envelope does not have to be select material. At less than minimum cover, the performance limit is either (a) excessive pipe deflection or (b) localized reversal of curvature directly under the wheel load. Under high soil cover, both the performance and performance limit are pipe deflection (out-of-roundness), which is a function of the total vertical soil pressure and is equal to or slightly less than vertical-soil strain in the backfill material on both sides of the pipe, herein referred to as sidefill. In compacted soil backfill, pipe deflection is less than 10 percent for either H-20 loads on minimum soil cover or vertical pressures up to 2500 psf under high soil cover. Pipe stiffness is roughly equal to steel and is greater than aluminum in 16-gage, 2-2/3 x 1/2 corrugations.

Corrugated plastic pipe is one of the leading pipe materials used for land drainage in the United States. It was introduced in the late 1960s, beginning with small inner diameters (ID) (3 and 4 in), which were used primarily for agricultural land drainage. During the 1970s the uses for corrugated plastic pipe greatly increased. Sizes up to 15-in diameter were developed, and applications were extended to highway drainage and to various residential and commercial construction uses, including foundation drainage, home sewage disposal, and grain aeration. With the introduction of 18- and 24-in pipe in 1981, the uses for corrugated plastic pipe again expanded to a still wider range of applications, including mining, culverts for roads and driveways, and other types of entrance and ditch crossing applications.

In 1979, field loading tests were conducted at Hamilton, Ohio, to evaluate the structural performance of 12-in corrugated polyethylene pipe for various types of culvert installations (1). With the recent development of the larger pipe diameters (18 and 24 in), the following additional questions arise.

Are there any structural limitations pertaining to these larger-diameter pipes when they are subjected to heavy external soil pressures? Subdrainage pipe is often backfilled with gravel or similar material that provides a filter for the inflow of ground water but also provides radial support for the pipe. If the pipe is used for purposes other than subdrainage (i.e., culvert), a select backfill material is not needed as a filter. But is it needed as support for the pipe? Most drainage pipe is installed in trenches and at shallow depths that can be excavated by a backhoe or wheel trencher or plowed in with a drainage plow. The most critical pipe loadings are surface wheel loads usually no heavier than H-20 truck loads, the highest legal highway wheel loadings. Can buried polyethylene pipe, with minimum cover, resist the super heavy wheel loads of construction equipment, off-highway trucks, etc.? Can corrugated polyethylene pipe be buried under very high embankments or in very deep trenches? What about pipe stiffness?

To answer these questions, field tests were conducted at London, Ohio, by Utah State University (USU) in cooperation with Advanced Drainage Systems, Inc., to investigate the effect of heavy loads passing over shallow buried corrugated polyethylene pipe. An additional series of tests conducted at USU used a pressure soil test cell to simulate the effect of great depths of cover, which in some cases can result in very high soil pressures. Comparative

tests were conducted by the Wadsworth Testing Laboratory of Canton, Ohio, and by USU on the stiffness of functionally equivalent corrugated pipes of steel, aluminum, and polyethylene.

NOTATION

The following notation is used in this paper:

- D = nominal pipe diameter = inside diameter (in),
- d = depth of corrugation (in),
- Dm = mean diameter of pipe = D + d (in),
- B = width and height of select soil envelope, usually gravel (in) (in this study, width and height were equal),
- H = height of cover above the top of the pipe (in),
- H/D = ratio of height of cover to nominal pipe diameter (dimensionless),
- Δy = vertical pipe deflection (in),
- $\Delta y/D$ = ratio of decrease in vertical diameter to the original circular diameter (dimensionless),
- γ = soil density based on AASHTO T99, applied to native soil in situ, or after compaction of soil backfill (pcf),
- P = vertical soil pressure at the top of the pipe (psf),
- ϵ = vertical soil strain (in/in), and
- $F/\Delta y$ = pipe stiffness (lb/in of length ÷ in of deflection).

MINIMUM COVER TESTS

Procedure

A test course of seven pipe runs was set up at a site near London, Ohio, as shown in Figure 1. Each pipe run consisted of two 20-ft sections coupled together at the midpoint (the midpoint was not a measurement point). The objective of the testing program was to determine, for buried corrugated polyethylene pipe, the relation of pipe deflection to height of soil cover under large wheel loads at various backfill densities.

Loads

A single-axle H-20 load, 16 kips/dual wheel, was used as the basic load, but "super-loads" up to 27 kips/wheel, as might be applied by heavy off-highway equipment, were also investigated. The standard truck H-20 rear axle load of 32 kips was simulated by use of a John Deere model 762 scraper. The front wheels of the loaded scraper (16 kips each) were centered directly over the pipe as shown in Figure 2.

Deflection

The pipe deflection under each wheel was measured by using a spring-loaded, direct-reading deflectometer (see Figure 3). Deflection was measured to the nearest 1/16 in at five loading positions at 3-ft spacings on each side of the midpoint of each 40-ft pipe run, which made a total of 10 measuring points/pipe. As the testing proceeded, it became apparent that deflections were less than 5 percent even when the height of cover was less than 12 in. To obtain a wider range of deflections, it was decided to remove cover from the shallow end of each pipe run and to test the pipe with the H-20 load at zero cover.

Cover

The pipes were installed in sloping trenches and backfilled to the original soil level (as shown in Figure 1) to provide a continuously decreasing height of cover from one end of each pipe run to the other. The height of cover was determined from elevations taken along the pipe before and after backfilling.

Materials

Three sizes of corrugated polyethylene pipe were tested: 15-, 18-, and 24-in diameters. The recently developed 18- and 24-in-diameter pipes are manufactured with a slightly angled helical corrugation of approximately 2°. These sizes were compared with the annularly corrugated 15-in-diameter pipe manufactured by the continuous extrusion and corrugating process. The pipes used in the tests were representative of standard production material. The high-density polyethylene resins used in the manufacture of the pipes complied with the requirements of Type III, Class C, category 5 as defined and described in ASTM D1248. The pipe stiffness values recorded on the test specimens exceeded the proposed minimum pipe stiffness requirements of large-diameter pipe of 40 psi at 5 percent deflection and 30 psi at 10 percent deflection.

As shown in Figure 1, the testing was designed for three soil densities: 75, 85, and 95 percent American Association of State Highway and Transportation Officials (AASHTO) standard density. The native soil at the site was used as backfill on six of the seven pipe runs. Uncompacted gravel backfill (AASHTO coarse aggregate 57, uncompacted) was used on run 3. The backfill soil was a mixture of two strata: a 2.5-ft stratum of sandy clay silt (Unified Soil Classification CL) and a sandy silty clay from below that depth (CL).

The soil backfill around the pipe was compacted by mechanical power tampers as shown in Figure 4. For pipe runs 1, 2, 5, 6, and 7, the soil was compacted in successive lifts of about 6-10 in each, depending on the desired degree of soil density. More lifts and more passes achieved greater density. The soil backfill for pipe run 4 (75 percent specified density) was dumped on and around the pipe with a loader and spread with a dozer blade; there was no compaction except the slight compaction due to the D-6 crawler dozer passing over the completed backfill with a track pressure less than or equal to 3 psi. A specified density of 75 percent usually indicates uncompacted or very lightly compacted soil. The density of the soil was checked with a Troxler nuclear densitometer at several stations along the pipe and at various levels as the backfilling progressed.

Results

The results of the tests for minimum cover on 24-in-diameter pipe subjected to H-20 loads are shown in Figures 5 and 6, where $\Delta y/D$ is plotted as a function of both height of soil cover in inches and the dimensionless soil cover term H/D. The dashed curves are power curves of the form ($y = bx^m$) that represent the best-fit curves of the data for the 24-in pipe at the three average soil densities of the field tests--95.8, 91.8, and 75.0 percent. Because the soil densities attained on pipes 5 and 7 were nearly equal, the data were combined for analysis.

For purposes of design, plots of 95 percent confidence levels were evaluated by using the 24-in pipe data for soil densities of 75, 80, 85, 90, and 95 percent standard AASHTO density. These are shown in Figure 6. The 95 percent confidence level plot is that plot below which 95 percent of all test data fall. The test data for pipe 3, uncompacted gravel

Figure 1. Minimum cover test layout at London, Ohio.

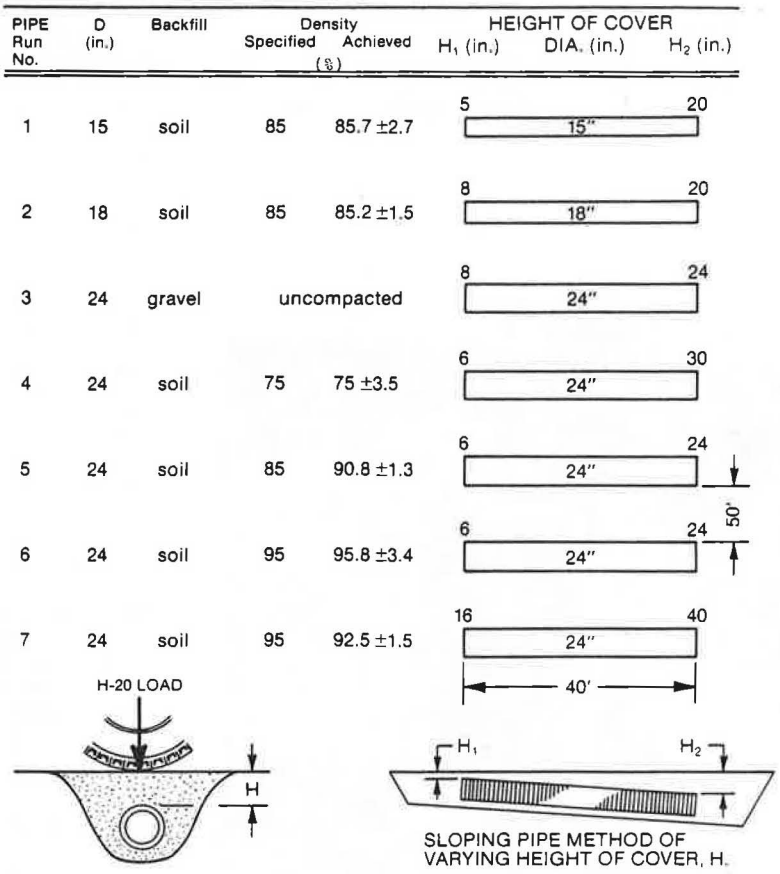

Figure 2. H-20 standard truck load (32-kip axle load), simulated with John Deere scraper, being positioned for deflection measurement.

Figure 3. Spring-loaded, direct-reading deflectometer.

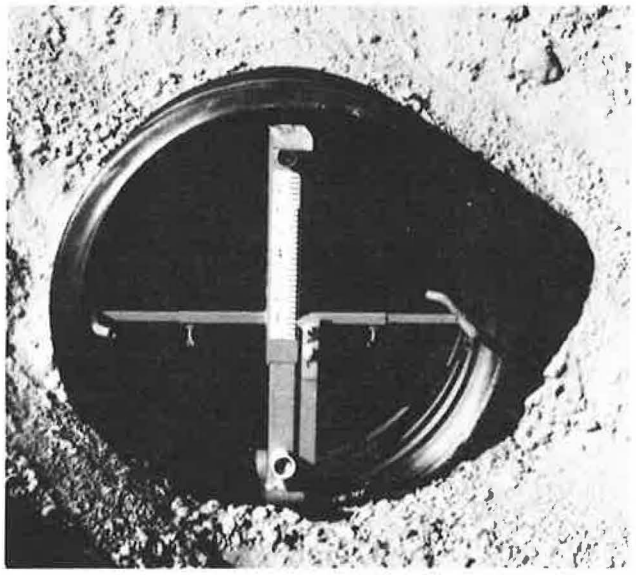

backfill, are also shown in Figure 6. These data fall within the range of cover from 20 to 30 in. The performance of the gravel backfill was similar to that of soil backfill at 95 percent density.

For most pipe installations, the maximum allowable ratio of deflection would be set at $\Delta y/D$ = 10 percent by the design engineer. This includes a safety factor of 2 based on an assumed performance limit of $\Delta y/D$ = 20 percent. Thus, the safety factors inherent in Figure 6 for 24-in pipe are generally adequate for design.

For comparison of all three diameters, Figure 7 shows the 95 percent confidence levels for minimum cover at 85 percent soil density for all three diameters under H-20 loads. The apparent reversal of positions of the 15- and 18-in curves left of H = 16 in indicates that localized anomalies begin to affect the deflection at very low soil cover. It was observed that with less than a foot of soil cover the deflection is sensitive to tire tread and tire pressure, surface finish (cut by blade after compaction or filled, i.e., backraked by blade), surface

soil type, moisture content, etc. This is to be expected since at very shallow heights of cover live loads are not uniformly distributed to the underground conduits. It is also noteworthy that to the right of H = 16 in the 24-in-ID plot is lower than the other two, which indicates that a 24-in-ID pipe is relatively deeper in the pressure bulb under an H-20 dual wheel than are the smaller pipes. For the H-20 load, separate plots of $\Delta y/D$ versus H for each pipe size are proposed as shown in Figure 7. Further details concerning the effects of loads are given by Watkins and Reeve (2).

Figure 4. Compacting backfill with powered tamper.

Based on the assumption that the effects of the backfill density on the 24-in pipe are similar for the 15- and 18-in sizes, a curve-fitting technique was used to interpolate the relation between percentage deflection and height of cover for intermediate soil densities of 80, 85, and 90 percent. These relations for 15-, 18-, and 24-in pipes are given in Tables 1-4. The values in Tables 1 and 2 are average values from the best-fit curves. The values given in Tables 3 and 4 are at the 95 percent confidence level. Tables 1 and 3 give percentage deflection for various heights of cover, and Tables 2 and 4 give height of cover for various percentage deflections. Tables 3 and 4, at the 95 percent confidence level, should be used for design.

Super-Loads

In some applications, loads from off-highway-type vehicles, such as large scrapers, may need to be taken into account in the design process. A superload of 54 kips on one axle was achieved by teetering a loaded John Deere model 762 scraper on its blade. This was done by using the blade as a fulcrum to raise the tractor axle off the ground with the machine's hydraulic system. The blade bore on timber blocks cut to simulate single-wheel imprint areas of 12x24 in each. Where the soil cover was less than 6 in, the 27-kip wheel loads sheared through the pipe. For pipe 4 at 75 percent soil density and soil cover ranging from 20 to 24 in, the pipe deflection ranged from 3 to 7.5 percent. Where the cover exceeded about 12 in, the pipe deflection was not significantly greater than that for the H-20 standard AASHTO truck loading.

HIGH SOIL PRESSURE TESTS

The USU soil pressure test cell (see Figures 8 and 9) was used to evaluate the structural performance of 4-ft-long test sections of the 15-, 18-, and 24-in-diameter corrugated polyethylene pipe sizes

Figure 5. Deflection versus cover height for 24-in pipe under H-20 loading at three average backfill densities.

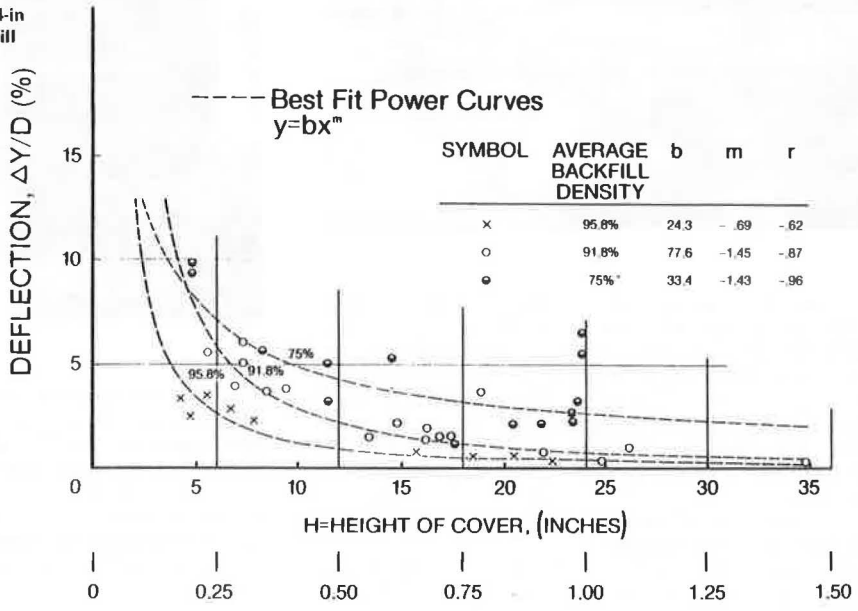

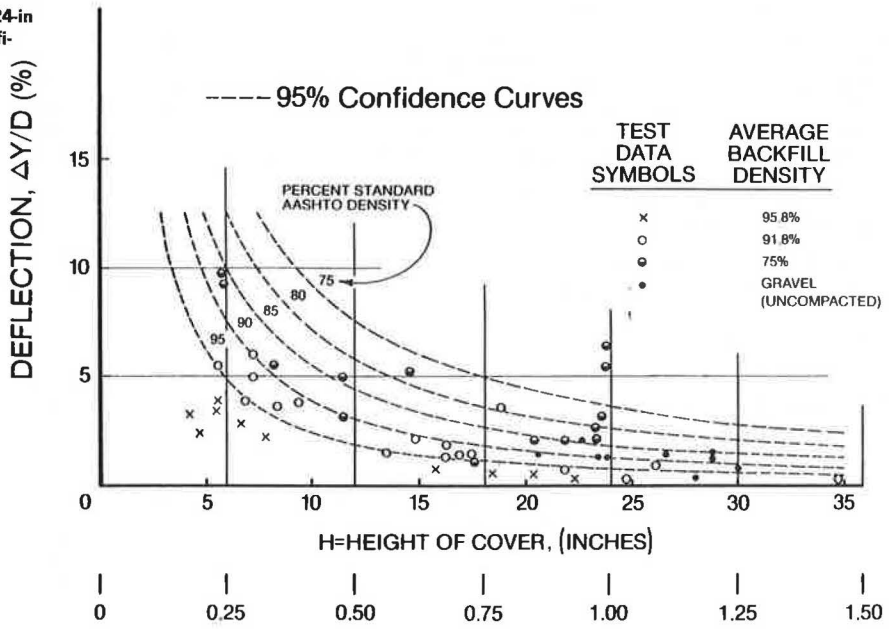

Figure 6. Deflection versus cover height for 24-in pipe under H-20 loading with 95 percent confidence level curves for five backfill densities.

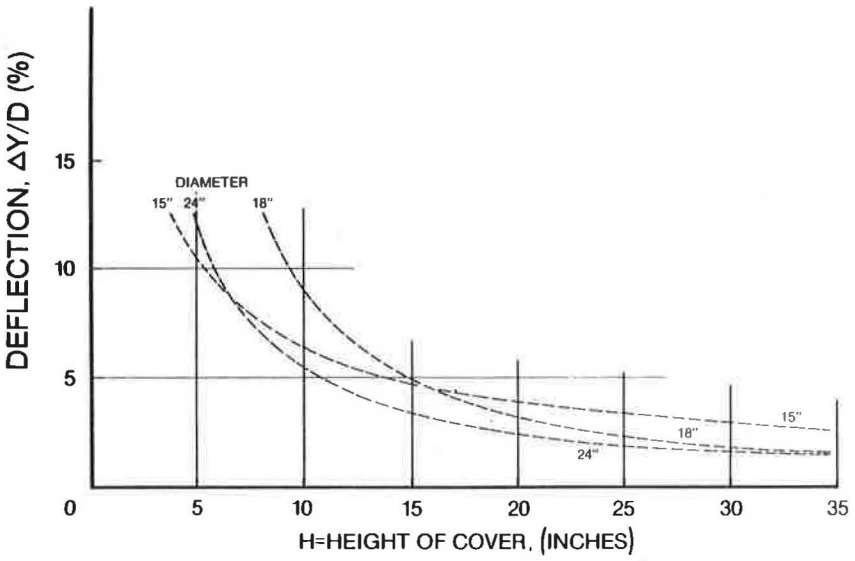

Figure 7. Plots of 95 percent confidence values for deflection versus cover height at 85 percent soil density under H-20 loading.

Table 1. Average deflection values by cover height for 15-, 18-, and 24-in pipe diameters and 80, 85, and 90 percent backfill densities.

Cover Height (in)	Avg Deflection (%)								
	15 in			18 in			24 in		
	80%	85%	90%	80%	85%	90%	80%	85%	90%
3		12	10						
4	11	9	8						10
5	9	8	7				11	10	7
6	8	7	6				9	8	6
7	7	6	5			10	8	7	5
8	6	6	5	13	11	8	7	6	4
9	6	5	4	11	9	7	6	5	4
10	5	5	4	9	7	6	6	4	3
11	5	4	4	8	6	5	5	4	3
12	5	4	3	7	6	4	5	3	3
13	4	4	3	6	5	4	4	3	2
14	4	4	3	6	4	3	4	3	2
15	4	3	3	5	4	3	4	3	2
16	4	3	3	5	4	3	3	2	2
17	4	3	3	4	3	3	3	2	2
18	4	3	3	4	3	2	3	2	2
19	3	3	2	4	3	2	3	2	1
20	3	3	2	3	3	2	3	2	1

(the USU tests are referred to as high soil pressure tests). In the test cell, performance limits were identified and related to corresponding vertical soil pressures that may be associated with high earth fill in typical cohesionless soils. The objective of this testing was to find the relation between deflection and high soil pressures at various soil densities with and without select soil (gravel) envelopes immediately around the pipe.

The test schedule was as follows:

Test No.	Pipe ID (in)	Envelope B (in)	Soil Backfill Density (%)
1	24	None	85
2	24	None	75
3	15	27x27	75
4	18	27x27	75
5	18	27x27	85
6	18	27x27	95
7	15	None	75

Procedure

High vertical pressure was applied in the soil cell by hydraulic rams that had sufficient capacity to simulate depths of soil cover to more than 100 ft. The load was applied in increments, and observations

Table 2. Minimum cover height versus pipe deflection for 15-, 18-, and 24-in pipe diameters and 80, 85, and 90 percent backfill densities.

	Minimum Height of Cover (in)								
Deflection	15 in			18 in			24 in		
(%)	80%	85%	90%	80%	85%	90%	80%	85%	90%
1	95	75	63	44	36	30	55	32	25
2	38	30	25	28	23	19	28	18	14
3	22	18	14	21	18	15	18	13	10
4	15	12	10	17	15	13	14	10	8
5	11	9	7	15	13	11	11	9	7
6	9	7	6	13	12	10	9	8	6
7	7	6	5	12	11	9	8	7	5
8	6	5	4	11	10	8	7	6	5
9	5	4	3	10	9	8	6	5	4
10	4	4	3	9	8	7	6	5	4
11	4	3	3	9	8	7	5	5	4
12	3	3	2	8	7	6	5	4	3

Table 3. Pipe deflection at 95 percent confidence level versus cover height for 15-, 18-, and 24-in pipe diameters and 80, 85, and 90 percent backfill densities.

	Deflection (%)								
Cover Height	15 in			18 in			24 in		
(in)	80%	85%	90%	80%	85%	90%	80%	85%	90%
3			12						
4		12	10						12
5	13	10	8					12	9
6	11	9	7				13	10	7
7	10	8	6			13	11	8	6
8	9	8	6			10	9	7	5
9	8	7	5		11	8	8	6	5
10	8	6	5	12	9	7	7	6	4
11	7	6	5	10	8	6	6	5	4
12	7	6	4	9	7	5	6	4	3
13	6	5	4	8	6	5	5	4	3
14	6	5	4	7	6	4	5	4	3
15	6	5	4	6	5	4	5	3	2
16	5	5	4	6	5	3	4	3	2
17	5	4	4	5	4	3	4	3	2
18	5	4	4	5	4	3	4	3	2
19	5	4	3	4	3	3	4	3	2
20	5	4	3	4	3	2	3	2	2

Table 4. Minimum cover height at 95 percent confidence level for 15-, 18-, and 24-in pipe diameters and 80, 85, and 90 percent backfill densities.

	Minimum Cover Height (in)								
Deflection	15 in			18 in			24 in		
(%)	80%	85%	90%	80%	85%	90%	80%	85%	90%
1									
2	66	53	43	32	27	23	32	24	17
3	38	19	23	25	21	17	22	17	13
4	25	20	15	20	17	15	17	13	10
5	19	14	11	18	15	13	14	11	8
6	14	11	8	16	13	11	12	9	7
7	12	9	6	14	12	10	10	8	6
8	10	7	5	13	11	9	9	7	6
9	8	6	4	12	10	9	8	7	5
10	7	5	4	11	10	8	7	6	5
11	6	5	3	10	9	8	7	6	4
12	6	4	3	10	8	7	6	5	3

Figure 8. USU high vertical soil pressure test cell, showing setup for testing corrugated plastic pipe.

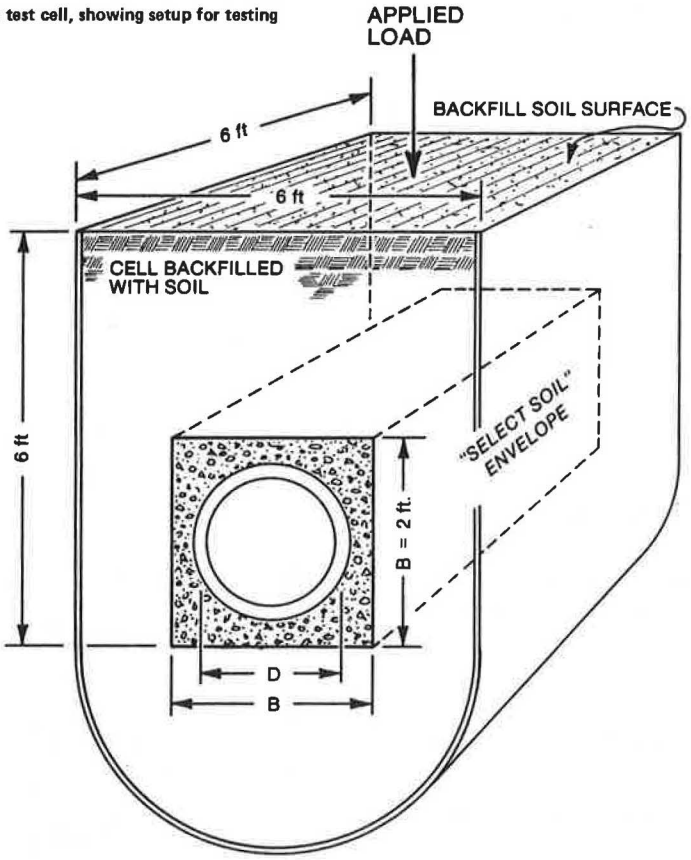

Figure 9. USU high vertical soil pressure test cell in operation.

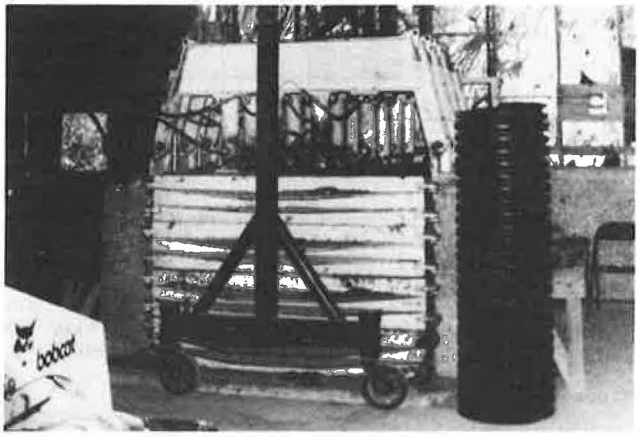

such as visual distress and deflection were recorded at each increment of load.

The native soil used in these tests was fine sand with about 20 percent silt. The select soil envelope was gravel with some coarse sand, all less than 0.5-in sieve mesh. The soil densities in the laboratory were measured with a densitometer in a procedure similar to that used in the field tests.

Results

The tests produced the following results and general observations.

Deformation

The performance limit was ratio of deflection $\Delta y/D$. No wall buckling, wall crushing, cracking, or tearing occurred. At deflections greater than about 25-30 percent, a longitudinal dimpling in the inside crests of corrugations could be detected at nine and three o'clock. As a performance limit this was discounted in favor of prior deflection of 20 percent, proposed by Spangler as "failure". That no wall crushing occurred under these extremely high pressures in the soil cell is remarkable. This confirms recent observations that polyethylene pipes do not fracture under constant strain (constant deformation) because stress decreases (stress relaxes) faster than strength decreases. In this case, the soil envelope assured constant deformation at each load increment.

Deflection versus vertical soil pressure for 24-, 18-, and 15-in pipe, respectively, is shown in Figures 10-12. Silty sand backfill was used in the tests, with a 0.375- to 0.5-in gravel envelope for the 24- and 18-in pipes and with and without a gravel envelope for the 15-in pipe.

Flexible Pipe Ring

Corrugated polyethylene pipe has a flexible cross section (ring) despite the corrugations. Therefore, under load, deflection is essentially equal to vertical soil strain:

$$\Delta y/D = \varepsilon$$

where $\Delta y/D$ is the ratio of vertical decrease in diameter to nominal pipe diameter and ε is vertical soil strain. The corrugations serve to hold the shape of the pipe ring during placement of the sidefill. But, as vertical soil pressure is applied, the flexible ring simply conforms with the soil. The only exception occurs in loose soil (75 percent density). The slight hump at the lower end of each

Figure 10. Vertical deflection versus vertical soil pressure for 24-in pipe in high pressure soil cell.

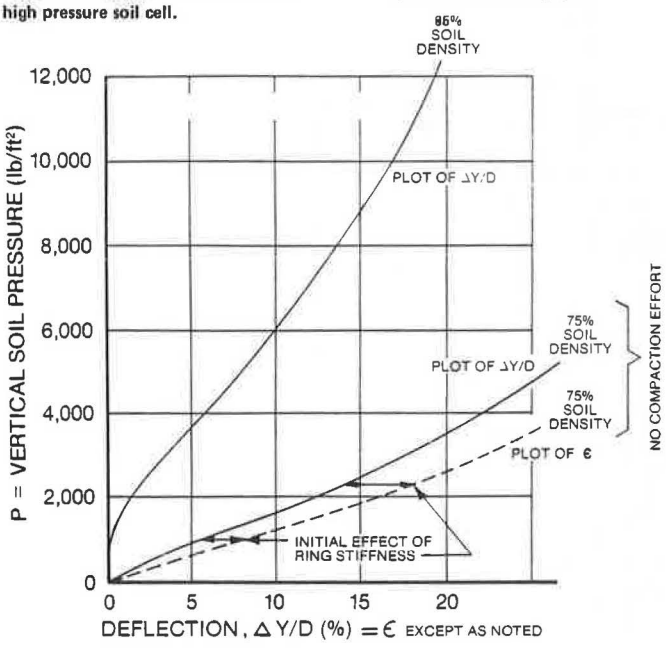

Figure 11. Vertical deflection versus vertical soil pressure for 18-in pipe in high pressure soil cell.

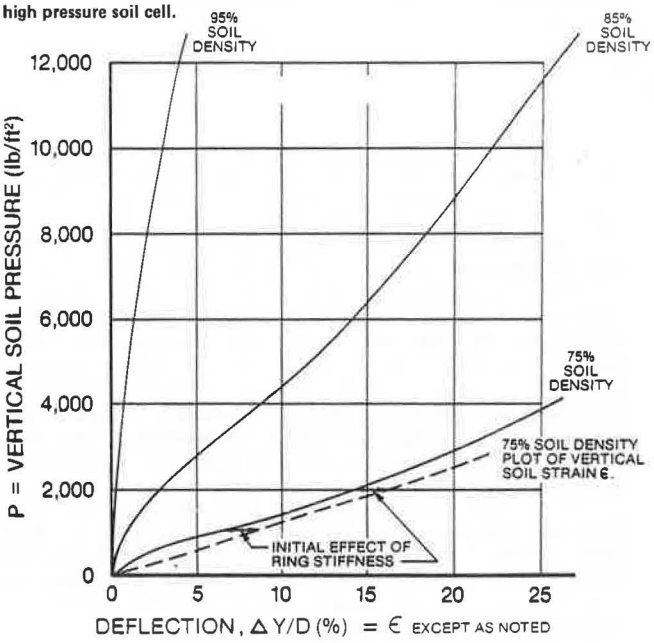

deflection plot indicates some initial resistance by the corrugations before the soil is dense enough to dominate deflection.

Select Gravel Envelope

The select gravel envelope reduced deflection slightly in very loose soil (see Figure 13). If the B/D ratio is roughly 1.8--or, say, 2--then the maximum reduction in deflection achieved by using a select gravel envelope is less than one-third. There is some benefit in using a gravel envelope to reduce deflection but only if the native soil is unusually compressible and if the B/D ratio is 2 or greater. On the other hand, where the entire backfill is

Figure 12. Vertical deflection versus vertical soil pressure for 15-in pipe in high pressure soil cell.

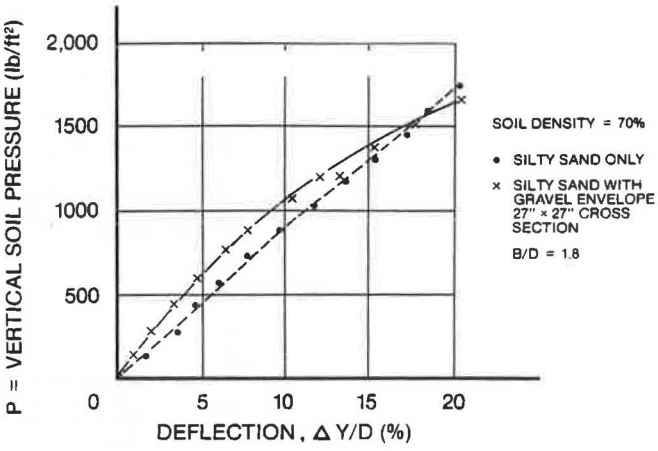

Figure 13. Effect of B/D on deflection (not significant in loose soil for B/D < 2).

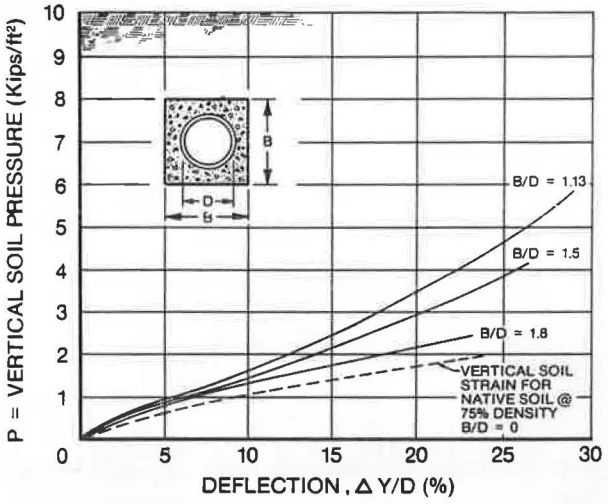

gravel, the high internal friction of the gravel forms a semirigid structure and carries virtually the total load with minimal pipe deflection. The response of total gravel backfill is essentially the same as native soil backfill at 95 percent density.

Minor Variables

Observations indicate that minor variables that influence pipe performance are (a) pipe diameter and (b) select soil envelope.

Pipe Diameter

The data plots in Figures 10 and 11 show a tendency toward steeper plots for the 24-in pipe than for the 18-in pipe. All other conditions appear to remain equal. This does not mean that pipe stiffness is significantly greater for the 24-in pipe nor that pipe stiffness has significant effect on deflection. In fact, all deviations in pipe deflection for any soil density and pressure are within one standard deviation of vertical soil strain at the same density and pressure for all diameters. Uniformity of soil density may be a modifying factor. The wider corrugations of the 24-in pipe may allow higher soil densities between the corrugations. The larger pipe

Figure 14. Pipe stiffness ratio.

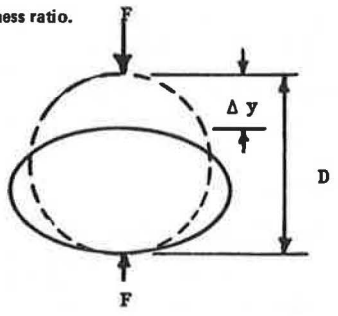

diameter may also permit more compaction lifts--i.e., more uniformity--on each side than a smaller pipe. Certainly, the relative positions of soil lifts to pipes are not identical for the 18- and 24-in pipes.

Select Soil Envelope

Figure 13 shows how much the pipe deflection is resisted by the select soil (gravel) envelope for various values of B/D. However, the deviation of these plots from each other is not statistically significant. Standard deviations due to other major variables are greater than the deviation of the three plots from their mean. In fact, the apparent influence of B/D on Δy/D is just the reverse of what would be anticipated. A larger sample is needed if significance is to be tested. But the more important observation is that the gravel envelope where B/D is small serves little purpose structurally in maximum cover design except to ensure integrity of the soil support about the pipe, including the spaces under the haunches and between the corrugations.

COMPARATIVE PIPE STIFFNESSES

Pipe stiffnesses were measured for functionally equivalent corrugated pipes of aluminum, steel, and polyethylene in diameters of 15, 18, and 24 in. The metal pipes were 16-gage, 2-2/3x1/2 corrugations. The following can be concluded from the tests:

1. The differences between calculated and measured values of pipe stiffness are so great that the use of calculated values for design is suspect. It is recommended that the industry adopt measured values of pipe stiffness F/Δy for design except in cases where it is proved that calculated values, such as $F/\Delta y = 53.77\ EI/D^3$, are essentially the same as measured values.
2. Pipe stiffness at 5 percent deflection is greater than pipe stiffness at 10 percent by roughly one-third; i.e., 52 pii at 5 percent and 37 pii at 10 percent. For design, it is recommended that pipe stiffness at 5 percent be used.
3. Pipe stiffnesses vary as much as three to one between aluminum and steel. Pipe stiffness for polyethylene is about the same as for steel. Ultimate loads follow roughly the same ratios. It is noteworthy that pipe stiffness is of value in maintaining the shape of the pipe ring during construction and in resisting heavy surface loads under minimum soil cover.

The question arises, Does creep reduce the pipe stiffness of polyethylene? The answer is yes. However, creep does not occur during short periods of load such as those experienced during installation or under live surface loads. The strength in resisting sudden loads is not reduced by creep. At constant pipe deformation, stresses decrease (relax) at a faster rate than strength. Therefore, polyethylene pipes supported by good soil are not prone to structural failure as a function of time of service. This would not be true in plastic soil. Service life (50-year) strength should be used for design in this case.

The differences between measured and calculated values of pipe stiffness can be explained by the following.

Longitudinal Seams

If the seam can rotate as a longitudinal hinge, then the pipe stiffness ratios (F/Δy no hinge to F/Δy hinge) are as follows (see Figure 14):

Location of Single Seam (hinge)	Pipe Stiffness Ratio
Top or bottom	2.4
Springline (either one)	1.6

These values are limiting cases because seams are not hinges. However, they do show the sensitivity of pipe stiffness to a longitudinal seam that does not develop full resistance to moment. Even when a plastic hinge starts to form, the partial rotation allows a reduction in F/Δy. Corrugations do not nest perfectly in overlap. Rotation of seams in buried pipes is often observed in the field.

Locked-In Stresses near Yield Point

Because corrugated metal pipes are cold-formed, circumferential stresses can be high enough that with little deflection the yield point is exceeded, especially at the springlines when outside locked-in stress is in tension. Even without a locked-in stress, a 21-in-diameter aluminum pipe reaches a yield point of 35 ksi before the deflection reaches 3.4 percent. The same pipe in steel reaches yield point, 40 ksi, at only 1.4 percent. Clearly, F/Δy measured at 5 percent deflection and greater is less than the calculated value, $F/\Delta y = 53.77\ EI/D^3$.

In order to form a fully developed plastic hinge, a moment of $M_p = 1.44\ M_e$ is needed. M_e is the elastic moment at which the yield point is just reached. It is the start of a plastic hinge. In other words, if the elastic yield point is reached in aluminum at the top and bottom when the deflection is 3.4 percent, then plastic hinges form at top and bottom when deflection is 1.44 (3.5) = 5 percent. Plastic hinges are incipient on the springlines at deflections no greater than 9 percent; i.e., 5 percent (M_B/M_A) = 5 percent $[\pi(\pi - 2)/2]$ = 9 percent. At 9 percent deflection, the specimen will collapse under the parallel plate load because four plastic hinges cause instability. Pipe stiffness drops to zero at collapse.

Deflection

The deflection itself causes moments that increase at a greater rate than the applied parallel plate load. Due to elliptical pipe deformation, the pipe stiffness at 10 percent deflection is only 90 percent of the pipe stiffness for a circle.

Because this effect combines with the plastic hinge effect, locked-in stress, and longitudinal seam effect, the low measured values of $F/\Delta y$ compared with the traditional $F/\Delta y = 53.77\ EI/D^3$ are readily understood.

Nonelliptical Pipe

First-mode deflection of a pipe in soil is the el-

lipse. The ellipse causes the least circumferential stress for any given deflection. Unfortunately, the ellipse is ideal but buried pipe is not. The parallel plate test is even less so. Because the pipe is not elliptical, stresses are greater for a given load and pipe stiffness is less than for an ellipse.

DISCUSSION OF RESULTS

The minimum cover tests were designed to evaluate the localized effect of large asymmetrical loads on the pipe-soil structure. The high soil pressure tests were designed to evaluate performance under uniformly applied vertical pressures.

For buried pipe that is confined by considerably more than the minimum soil cover, the distribution of pressure on the pipe is uniform for live load as well as dead load. The deflection is symmetrical. This is not true at soil cover equal to or less than the minimum soil cover. For practical pipe design under super-heavy surface loads, methods of evaluating vertical soil pressure P on the select soil envelope are available. For Cooper E-80 locomotive loading, the values are listed in the Handbook of Steel Drainage and Highway Construction Products (3, p. 87). For heavy off-highway wheel loads, the Boussinesq method of analysis is adequate.

Performance Criteria

Considerable importance is attached to the finding in these tests that polyethylene pipe has structural qualities quite unlike those of concrete or metal pipes.

First, polyethylene pipe is flexible. It conforms with the soil around it. The density of the sidefill material is important. Under load, the deflection of the pipe equals the vertical compressive strain of the sidefill material. If the sidefill material is compacted to a high density at time of installation, any increased strain due to the applied load is minimal. So also is the pipe deflection. Note the results for 95 percent soil density at high pressures in Figure 11: At 12 000 psf the deflection was less than 4 percent.

Second, polyethylene does not have a definite yield point as do metals. For metal pipes, once the yield point is reached, permanent set occurs with wall crushing and/or buckling. As demonstrated in the high-pressure tests on polyethylene pipes, there was no wall crushing or buckling. At these extremely high pressures, the failure mode was pipe deflection, which was equal to vertical strain or settlement in the sidefill soil.

The constraining influence of the sidefill material on pipe performance is illustrated by field deflection measurements after skimming down to zero cover and application of a 16-kip wheel load. The deflections at zero cover, for the 24-in pipe at sidefill densities of 75, 90.8, and 95.8 percent, were 7.2, 4.2, and 3.3 percent, respectively. For the 15-in pipe at a sidefill density of 85.7 percent, deflection was 13.3 percent. For the 18-in pipe at a sidefill density of 85.2 percent, deflection was 12.5 percent. Removal of the top cover did not substantially affect the pipe deflection. The sidefill material at the installed density still performed in restraining the pipe and in supporting the applied load.

Design Considerations

For a non-specification-type application, such as driveway culverts or other entrance crossings, a usual practice is to push the native soil backfill into place and give little attention to sidefill compaction. For loosely applied backfill in most soils, densities will be no more than about 75 percent. It has been demonstrated that with a little care the sidefill density can be increased to around 80 percent by simply "walking in" the sidefill material in 6- to 8-in lifts.

For specification-type installation, the 95 percent confidence values given in Tables 3 and 4 should provide a basis for design with adequate safety factor. The pipe deflection can be held within an allowable limit by adjusting the height of the cover and/or sidefill density.

Corrugated polyethylene pipe is manufactured with corrugations deep enough to hold its circular cross section during installation. After experience with many installations, the manufacturers have developed pipe stiffness comparable to that of functionally equivalent corrugated steel pipes.

Creep is the relaxation of stress with time. This is a favorable property in that any stress concentrations during installation tend to relax. The slip of riveted seams in metals accomplishes a similar favorable relaxation. Under constant stress, polyethylene yields. If some long-term surface load follows the pipe down, or if the soil envelope is fluid, then the allowable stress must be based on the 50-year-service-life strength of the yielding polyethylene.

Of course, polyethylene cannot resist high bearing stresses resulting from large rocks lodged against it.

REFERENCES

1. R.K. Watkins and R.C. Reeve. Structural Performance of Buried Corrugated Polyethylene Tubing. Presented at 30th Annual Highway Geology Symposium, Portland, OR, 1979.
2. R.K. Watkins and R.C. Reeve. Effect of Heavy Loads on Buried Corrugated Polyethylene Pipe. Advanced Drainage Systems, Inc., Columbus, OH, March 1982.
3. Handbook of Steel Drainage and Highway Construction Products. American Iron and Steel Institute, Washington, DC, 1977.

Publication of this paper sponsored by Committee on Culverts and Hydraulic Structures.

Computer Modeling of the Cross Canyon Culvert

LAWRENCE C. RUDE

The CANDE finite element computer program was used to determine the effectiveness of three different soil models in predicting the behavior of an underdesigned reinforced concrete culvert installed under a deep fill. The analysis consisted of comparing the predicted behavior with the actual behavior of a dummy culvert installed at Cross Canyon, California, by using several different types of soil models. The actual behavior was obtained from information published by the California Department of Transportation. Comparisons included prefailure and postfailure behavior of the pipe culvert. An overburden-dependent soils model most accurately predicted the behavior of the culvert.

The California Department of Transportation (Caltrans) has conducted many research projects involving monitoring of culverts installed in deep embankments. In one of these projects a dummy reinforced concrete culvert was placed in the same embankment at Cross Canyon, California (1, Section I, Volumes 1 and 2; Section III; Section IV, Volume 1; and Section V, Volumes 7 and 9), with a functioning, 243.8-cm (96-in) diameter, prestressed concrete culvert. The dummy culvert had a 213.3-cm (84-in) inside diameter and was grossly underdesigned for the 55-m (180-ft) overfill. Backfill parameters and pipe strength were varied in ten different zones throughout the dummy pipe test section. Dummy sections were installed 3 m (10 ft) above and to the side of the functioning culvert. The reinforced concrete pipe was instrumented with displacement measuring devices, strain gauges, and soil stressmeters. This paper reports comparisons of finite element analyses performed by using the CANDE computer program (2) and the published behavior of one instrumented section (zone 6).

FIELD INSTALLATION

The dummy reinforced concrete had a wall thickness of 20.3 cm (8 in). The area of reinforcing steel was 275 cm^2/m (1.30 in^2/ft) for the inner cage and 184 cm^2/m (0.87 in^2/ft) for the outer cage. The culvert had a D-load rating of 2500 D. The load rating is the load in pounds per unit length of pipe divided by the internal diameter in feet that develops a 0.254-mm (0.01-in) wide crack 30.5 cm (12 in) long when force is applied by using a standard three edge bearing test. Development of the 0.254-mm crack is the accepted strength criterion. Based on the traditional Spangler design procedure (3), this pipe could be safely installed in a trench situation under overfills of 6-9 m (19-29 ft), depending on bedding conditions.

At zone 6, the reinforced concrete pipe was placed in a shallow trench made in previously placed fill material. Well-compacted structure backfill was installed adjacent to the pipe to provide increased lateral support. A layer of fine aggregate was placed beneath the pipe. Figure 1 shows bedding and backfill conditions for zone 6.

The structure backfill consisted of a well-graded gravelly sand with approximately 22 percent of material by weight finer than 0.074 mm (0.003 in). The largest particles were less than approximately 50.8 mm (2 in) in diameter. The wet unit weight of the structure backfill was 2113 kg/m^3 (131 pcf).

Only one gradation curve was available for embankment material; this curve shows that the material was a well-graded, gravelly, silty sand. The largest particle size was 64 mm (2.5 in), and 22 percent passed the 0.074-mm sieve. Liquid limit was 23, and unit weight was 2169 kg/m^3 (134.5 pcf).

Results of laboratory triaxial tests on embankment and structure backfill materials were also published. Parameters have been derived for implementation of the Kondner-Duncan soil model in finite element computer codes. This model is the result of work by Kondner (4), Duncan and Chang (5), and Kulhawy, Duncan, and Seed (6). A cursory review of triaxial test data and a statistical analysis of the Kondner-Duncan model parameters indicated that, due to the number of samples and the standard deviation of the results, there was no significant statistical difference between embankment and structure backfill materials.

INSTRUMENTATION

Dummy test sections were instrumented to determine soil pressures acting on the external surface of the

Figure 1. Bedding and backfill conditions.

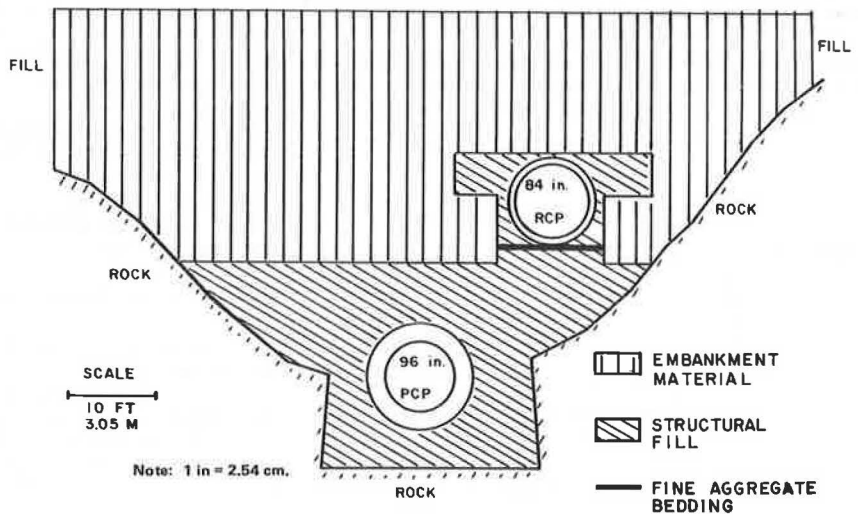

pipe, strains in the pipe wall, and displacements of the internal wall surface. Vertical settlements and soil stresses in the embankment were not obtained at zone 6.

Strain readings were taken for concrete and reinforcing steel. Weldable SR-4 gauges were placed on the inner and outer surfaces of inner and outer reinforcing bar cages. Concrete strain meters were placed at the midplane of the wall. Typically, eight points at 45° intervals around a section were instrumented with strain gauges.

Carlson and Cambridge contact stressmeters were installed at the outer surface of the concrete pipe. The Carlson meters provided normal pressures and the Cambridge meters normal and tangential pressures.

For measurement of interior wall displacements, steel balls were fastened at eight equally spaced points about the perimeter. An extensometer was used to determine 14 chord measurements, from which horizontal and vertical displacements could be calculated.

COMPUTER PROGRAM

The CANDE finite element computer program was used to perform all calculations described in this paper. CANDE is a FORTRAN program specifically made for the analysis and design of buried culverts. The program operates on three levels: (a) a modified elasticity solution developed by Burns and Richards (7), (b) a finite element procedure with automatic mesh generation, and (c) a finite element procedure in which the mesh is as defined by the user. The program has an executive routine that provides for the selection of common types of pipe culverts and five soil models. The common pipe types include steel, aluminum, concrete, plastic, and nonstandard. The soils models are linear elastic, orthotropic linear elastic, overburden dependent, extended Hardin, and an extended Hardin model for use with triaxial soil test data.

In this project, only the concrete pipe routine was used. The dummy pipe was assumed to have the nonlinear stress-strain relation shown in Figure 2. Cracking is handled by allowing only a small tensile strain (ϵ_t), usually taken as zero. For compressive loading, a trilinear curve is used. ϵ_y represents the strain at the elastic limit ($1/2\ f_c'/E_1$), where f_c' is the unconfined compressive strength in pounds per square inch and E_1 is the linear Young's modulus as defined by $E_1 = 33 \times \delta_w^{1.5}\ f_c'$, where δ_w is unit weight in pounds per cubic foot. ϵ_c represents the concrete strain at the ultimate strength, usually 0.002, and ϵ_u is the strain at crushing.

The concrete pipe was modeled in the finite element computer program by beam-column elements. To account for tension cracking and crushing of the concrete and yielding of the reinforcing steel, sectional properties of the beam column (area, centroid location, and moment of inertia) were changed to satisfy equilibrium and compatibility with the assumed stress-strain law for the concrete. Traditional assumptions of concrete analyses were maintained: (a) Circumferential strains varied in a linear fashion through the pipe wall section, (b) shear deformation was not included, and (c) longitudinal stresses and strains were neglected.

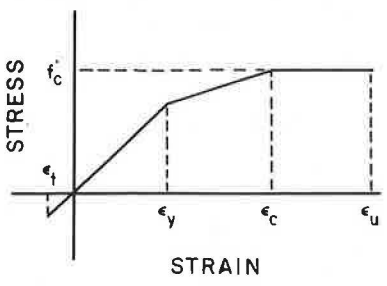

Figure 2. Stress and strain curve for concrete.

The soil was modeled by using plane-strain quadrilateral and triangular elements. The quadrilateral element, a nonconforming element developed by Hermann (8), was two triangular elements, each a quadratic interpolation function. The quadrilateral element has four nodes with a vertical and horizontal degree of freedom at each node and is generated from the triangular elements by applying constraints to ensure compatibility and static condensation procedures.

Several types of soil models were used during the course of the project: (a) linear elastic, (b) overburden dependent, and (c) extended Hardin. In the linear elastic model, the matrix [C] is constant and is completely defined by two parameters: Young's modulus (E) and Poisson's ratio (ν). The [C] matrix relates stress to strain, where C_{11}, C_{12}, C_{21}, C_{22}, and C_{33} are material constants defined below for plane strain conditions:

$$\begin{bmatrix} \sigma_x \\ \sigma_y \\ \tau \end{bmatrix} = \begin{bmatrix} C_{11} & C_{12} & 0 & \epsilon_x \\ C_{21} & C_{22} & 0 & \epsilon_y \\ 0 & 0 & C_{33} & \gamma \end{bmatrix} \quad (1)$$

where

σ_x = vertical stress,
σ_y = horizontal stress,
τ = shearing stress,
ϵ_x = vertical strain,
ϵ_y = horizontal strain, and
γ = shearing strain.

$$C_{11} = C_{22} = [E(1 - \nu)]/[(1 + \nu)(1 - 2\nu)] \quad (2)$$

$$C_{21} = E\nu/[(1 + \nu)(1 - 2\nu)] = C_{12} \quad (3)$$

$$C_{33} = E/[2(1 + \nu)] \quad (4)$$

In the overburden-dependent model, the nonlinear behavior of soil is characterized by secant values of the soil stiffness modulus that vary as a function of overburden pressure. The two parameters needed to characterize the soil are the secant constrained modulus (M_s) and the coefficient of horizontal earth pressure (K_o). In confined compression conditions, lateral deformations are prevented and $K_o = \nu/(1 - \nu)$. Poisson's ratio (ν) is generally constant under this type of loading condition. The coefficients of the plane strain constitutive matrix are $C_{11} = C_{22} = M_s$, $C_{12} = C_{21} = M_s K_o$, and $C_{33} = M_s(1 - K_o)/2$. The secant confined modulus is related to secant Young's modulus (E_s) by

$$\{(1 - \nu)/[(1 + \nu)(1 - 2\nu)]\}\ E_s = M_s \quad (5)$$

Reasonable estimates of E_s as a function of overburden pressure are available from the CANDE engineering manual and from Duncan (9). Values from the CANDE manual are presented below for structure backfill (granular soil with good compaction) and embankment material (mixed soil with good compaction) (1 psi = 6.89 kPa):

Overburden Pressure (psi)	E_s (psi) Structure Backfill	Embankment Material
5	1130	600
10	1300	850
15	1500	1000
20	1650	1100
25	1800	1200
30	1900	1250
40	2100	1350
50	2250	1450

Poisson's ratio (ν) for the CANDE values is 0.3-0.35 for structure backfill and 0.35-0.40 for embankment material.

Values of E_s recommended by Duncan (9) for a compacted SW soil are as follows:

Overburden Pressure (psi)	E_s (psi)
5	833
10	1040
20	1260
30	1440
40	1570

Duncan's values are approximate averages of the values suggested by the CANDE manual. Chang, Espinoza, and Selig (10) have suggested revisions of values provided in the CANDE manual. Only the suggested values of E_s and ν given in the two tables above were used during this project.

The third type of soil model used in this study was the extended Hardin model. The model originally developed by Hardin (11) relates shear stress (τ) to shear strain (γ) by a secant shearing modulus (G_s), where $\tau = G_s\gamma$. The secant shearing modulus (G_s) is expressed in hyperbolic form as $G_s = G_{max}/(1 + \gamma_h)$, where γ_h is the hyperbolic shear strain. The advantage of the original model was that the coefficients (given below) were related to fundamental soil parameters (plasticity index, degree of saturation, void ratio, and soil type). The general relations of Hardin's work are as follows:

$$G_{max} = S_1\sqrt{\sigma_m} \tag{6}$$

$$\gamma_h = \gamma/\gamma_r\left\{1 + [a/\exp(\gamma/\gamma_r)^{0.4}]\right\} \tag{7a}$$

$$\gamma_r = G_{max}/c_1 \tag{7b}$$

where

γ = shear strain;
σ_m = spherical stress = $(\sigma_{11} + \sigma_{22} + \sigma_{33})/3$;
γ_r = reference strain;
S_1 = soil parameter related to void ratio = 1230F;
a = soil parameter related to soil type and degree of saturation = 3.2 for granular soil, 2.54(1 + 0.02S) for mixed soil, and 1.12(1 + 0.02S) for cohesive soil;
c_1 = soil parameter related to void ratio, plasticity index, and degree of saturation = $(F^2R^2)/[0.6 - 0.25(PI)^{0.6}]$;
F = $(2.973 - e)/(1 + e)$;
R = 1100 for granular soil and 1100 - 6S for mixed or cohesive soil;
e = void ratio;
S = degree of saturation ($0 \leq S \leq 100$); and
PI = plasticity index ($0 \leq PI < 1.0$).

Hardin's law was extended in the CANDE engineering manual by adding a functional relation for Poisson's ratio. As in Hardin's work, a hyperbolic relation was developed for a secant Poisson's ratio (ν_s):

$$\nu_s = (\nu_{min} + \gamma_p\nu_{max})/(1 + \gamma_p) \tag{8a}$$

$$\gamma_p = q\,\gamma/\gamma_r \tag{8b}$$

where

ν_{min} = minimum Poisson's ratio at zero shear strain,
ν_{max} = Poisson's ratio at failure, and
q = dimensionless parameter for curve shape.

The CANDE program can be used with recommended values for soil parameters, or the user may define them from triaxial tests.

ANALYSIS

The computer analysis of zone 6 of the Cross Canyon culvert was done in two phases. In the first phase, Lee (12) modeled the dummy pipe in the conventional fashion by assuming vertical symmetry and only represented the culvert as a series of semicircular connected beam elements. Quadrilateral elements, representing the soil, extended above, below, and to the right of the culvert. In the second analysis phase, the entire cross section of the canyon, including the 243.8-cm (96-in) functioning culvert, was included. This grid is shown in Figure 3.

Lee compared results of calculations by using the CANDE program with the measured performance of zone 6. He obtained the most appropriate overburden soil modulus by a trial-and-error procedure until he reduced the difference between the measured and computed performance of the culvert. Lee's recommended values for structure backfill and embankment are given below (1 psi = 6.89 kPa):

Overburden Pressure (psi)	E_s (psi) Structure Backfill	Embankment Material
5	6900	5100
10	7500	5500
15	7900	5900
20	8400	6200
25	8700	6500
30	9000	6800
40	9500	7200
50	9960	7600

Poisson's ratio (ν) for Lee's values is 0.20 for structure backfill and 0.24 for embankment material.

Lee's values are much stiffer than those recommended by Duncan or the CANDE manual. Lee felt he must follow Chang's lead and develop a new overburden model because the existing recommended values produced poor comparisons between calculated and measured performance of the culvert. He also derived an overburden-dependent model from the published triaxial soil test data, but again calculated performance did not agree with measured performance. Lee came to these conclusions by using a conventional symmetrical finite element grid that modeled only culvert and soil and not a grid that incorporated the entire canyon cross section.

In the second phase of the analysis, the grid shown in Figure 3 was used. Beam elements were used to represent the 213.4-cm (84-in) dummy concrete culvert. Two layers of quadrilateral elements were used to represent the 243.8-cm (96-in) functioning prestressed culvert. The soil was represented by triangular and quadrilateral elements. The grid

Figure 3. Finite element grid.

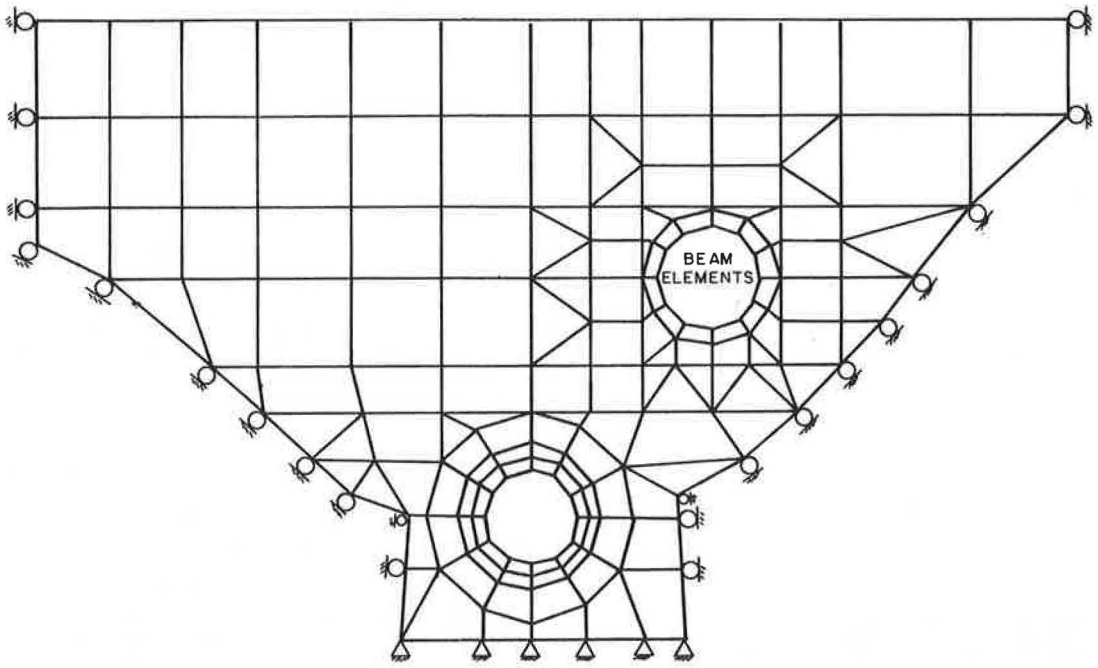

extended to an elevation of 5.5 m (18 ft) above the top of the dummy culvert. Fill placed above this elevation was represented by a surcharge pressure applied to the top of the mesh.

Based on published soil test data, there was no statistically significant difference between structure backfill and embankment material. For the preliminary results presented in this paper, the soil was thus considered to be homogeneous. The concrete in the 213.4-cm pipe was modeled as a nonlinear material. The concrete in the 243.8-cm functioning culvert was modeled as linearly elastic. As previously mentioned, the three types of soil models were linear elastic, overburden dependent, and extended Hardin.

For the linear elastic model, a value of 96.46 MPa (14 000 psi) was selected as an average value for Young's modulus for the fill. This was the initial tangent Young's modulus determined from a triaxial compression test when the overburden pressure was one-half the final overfill. A Poisson's ratio of 0.20 was used.

Two overburden-dependent models used average values of Lee's results and overburden pressures suggested by Duncan (Duncan's values of Young's modulus for a well-graded sand compacted to 95 percent of its maximum dry density were given previously). A Poisson's ratio of 0.2 was used. The comparison of the two overburden-dependent models also provided a method of checking Lee's suggested values.

The following table defines the input parameters for the extended Hardin soils model:

Parameter	Value
Soil type	Mixed
Minimum void ratio	0.1
Maximum void ratio	0.49
Poisson parameter q	0.260
Degree of saturation	0.46
Plasticity index	0.020
Density (lb/ft^3)	131

BEHAVIOR OF DUMMY CULVERT

Vertical and horizontal diameter changes of the 213.4-mm (84-in) reinforced concrete pipe installed at zone 6 at Cross Canyon are shown in Figure 4. The changes in vertical diameter increase in a linear fashion up to an overfill of 30.5 m (100 ft). For overfills greater than 30.5 m (100 ft), the vertical diameter changes in a nonlinear fashion. The change in horizontal diameter varies essentially in a linear fashion with increasing fill height.

Development of a 0.25-mm (0.01-in) crack 30.5 cm (12 in) long has long been an industrial strength criterion. Such a crack was not recorded until the overfill had reached 30.3 m (99.3 ft). Delamination was observed in different segments at an average overfill of 27.7 m (91 ft). Delamination, or "bowstringing", occurs when reinforcing steel with a minimal amount of embedment and subjected to tensile stresses on the concave section of the pipe straightens and forces the inner surface concrete to separate from the central concrete core. The yield strength of the reinforcing steel was reached at approximately 19.5 m (64 ft). The break of the slope of the vertical diameter change in Figure 4 was most likely due to delamination. A similar discontinuity, though less pronounced, is visible in the horizontal diameter change curve. The pipe was considered to have reached failure at an overfill of 30.3 m (99.3 ft).

Shown in Figure 4 are vertical diameter changes computed by using the three types of soil models. Only two data points were plotted for each soil model, one at 29.6 m (97 ft) and the other at 54.6 m (179 ft). At the 29.6-m overfill, the linear elastic model and overburden-dependent model, based on Duncan's recommended values, produce reasonable estimates of deflection. At an overfill of 54.6 m (179 ft), the Duncan overburden-dependent model overestimated the vertical diameter by 19.6 percent. The other two soil models grossly underesti-

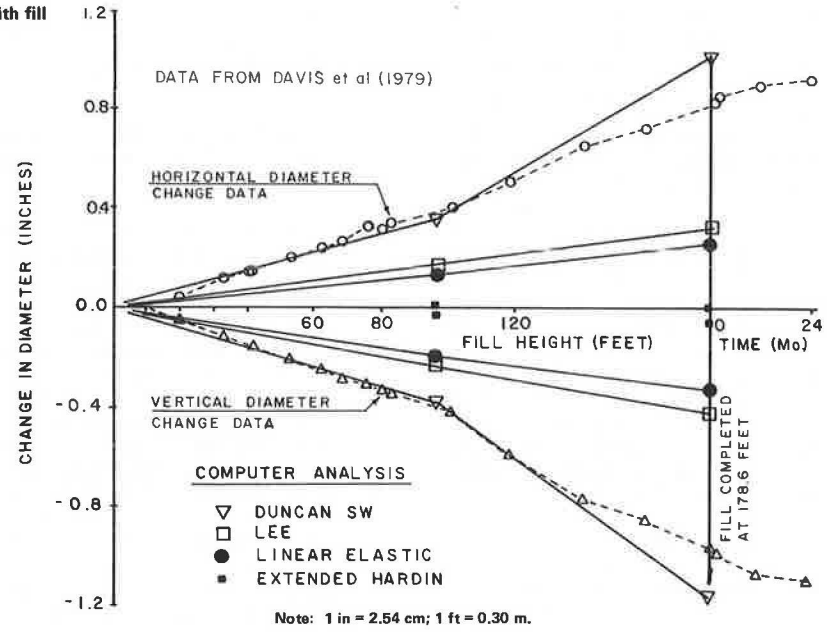

Figure 4. Diameter changes with fill height.

mated the vertical diameter changes. The errors for the linear elastic model and for Lee's overburden model at an overfill of 54.5 m (178 ft) for the vertical diameter change were 66 and 57 percent, respectively. The extended Hardin model predicted only negligible diameter changes.

In summary, results were obtained by using only one construction increment. An appropriate pressure was applied to the top of the finite element grid to represent different overfills. The computer program did not take into account reinforcing steel movements due to delamination. Duncan's recommended values produced reasonable comparisons in the second phase of the analysis, when the boundary conditions included the canyon walls and the presence of the functioning culvert. The lack of these boundary conditions was most likely the reason for the unsatisfactory results achieved by using recommended overburden-dependent moduli in the first phase of the analysis. Hence, accurately representing boundary conditions is important in backfiguring or improving soil modulus values.

Duncan's overburden model was used to compare measured culvert behavior with observed behavior when the pipe was well within its allowable overfill. Deflections, bending moments, and external normal pressures were compared for an overfill of 12.5 m (41 ft). Computed vertical and horizontal diameter changes were -3.8 mm (-0.149 in) and 3.2 mm (0.126 in), respectively. Actual diameter changes were -3.86 mm (-0.152 in) and 3.68 mm (0.145 in). Average percentage error between the measured results and the calculated results was 14 percent.

Figure 5 shows computed and actual bending moments around the pipe culvert. Actual bending moments were computed from strain readings. As the figure shows, computed and actual bending moments compare favorably at the crown and invert but not at the springing line on the left side of the diagram.

Figure 6 shows a comparison between computed and measured normal pressures acting on the external surface of the dummy culvert. Measured normal pressures were determined from Carlson and Cambridge stressmeters. Field data showed a maximum pressure at the invert and another maximum pressure at 10 o'clock with respect to the crown. High pressure at the invert was probably due to the contact stress

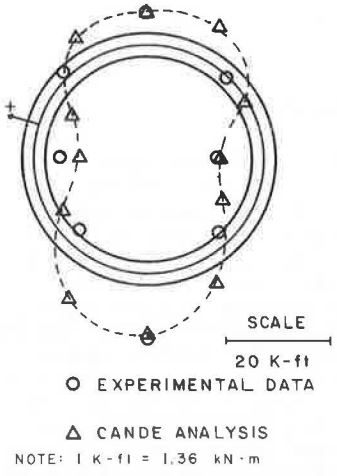

Figure 5. Comparison of experimental and computed bending moments.

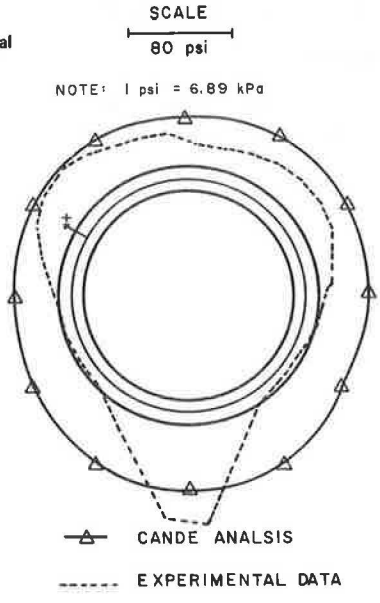

Figure 6. Comparison of computer and experimental normal pressures.

between the pipe and the aggregate bedding. Except at the invert, the computed normal pressures were greater than any other measured normal pressures. Computed pressures do not necessarily produce a conservative design since the horizontal pressures provide a restraint against lateral movement. A decrease in lateral pressure would increase lateral movement and alter the wall bending moments.

My research (13) has shown that finite element analysis of buried culverts performed by using a linear elastic soil model is very dependent on the proper selection of Poisson's ratio for the soil. To show the effects of Poisson's ratio on Duncan's model, additional calculations were made for an overfill of 27 and 54.6 m (90 and 178 ft) for Poisson's ratios of 0.1 and 0.3. Vertical and horizontal diameter changes were compared with field data. The results, summarized below, show that Poisson's ratio affects diameter changes but does not produce as great an error as is produced when another soil model is used (1 ft = 0.3 m):

		Error (%)	
Overfill (ft)	Poisson's Ratio	Vertical Diameter Change	Horizontal Diameter Change
90	0.1	29	0
	0.2	-1	17
	0.3	15	35
178	0.1	7	-16
	0.2	-21	-26
	0.3	31	40

CONCLUSIONS

Three different types of soil models were compared for their effectiveness in predicting the behavior of an underdesigned reinforced concrete culvert installed in a deep fill. The extended Hardin model, a linear elastic model, and two overburden-dependent models were used. The overburden-dependent model recommended by Duncan predicted the actual behavior with the least error. The analysis was performed by using the CANDE computer program. Only one construction increment was used in conjunction with a surcharge pressure applied to the top of a relatively shallow finite element grid to simulate additional overburden. The program reasonably predicted prefailure and postfailure behavior of the pipe culvert. The need to accurately represent the actual boundary conditions in backfiguring overburden-dependent values was also shown.

REFERENCES

1. R.E. Davis, F.M. Semans, D.W. Spannagel, and A.E. Bacher. Rigid Pipe Proof Testing Under Excess Overfills with Varying Backfill Parameters. California Department of Transportation, Sacramento, Oct. 1978.
2. M.G. Katona, J.M. Smith, R.J. Odello, and J.R. Allgood. CANDE: A Modern Approach for the Structural Design and Analysis of Buried Culverts. Civil Engineering Laboratory, Naval Construction Battalion Center, Port Hueneme, CA, Oct. 1976.
3. M.G. Spangler and R.L. Handy. Soil Engineering. Intext Educational Publications, New York, 1973, pp. 658-729.
4. R.L. Kondner. Hyperbolic Stress-Strain Response: Cohesive Soils. Journal of Soil Mechanics and Foundations Division, ASCE, Vol. 89, No. SM1, Jan. 1963, pp. 115-143.
5. J.M. Duncan and C.Y. Chang. Non-Linear Analysis of Stress and Strains in Soils. Journal of Soil Mechanics and Foundations Division, ASCE, Vol. 96, No. SM5, Sept. 1970, pp. 1629-1653.
6. F.M. Kulhawy, J.M. Duncan, and H.B. Seed. Finite Element Analysis of Stresses and Movements in Embankments during Construction. U.S. Army Engineer Waterways Experiment Station, Vicksburg, MS, Contract Rept. 569-8, 1969.
7. J.Q. Burns and R.M. Richards. Attenuation of Stresses on Buried Culverts. Proc., Symposium on Soil-Structure Interactions, Tucson, AR, Univ. of Arizona Engineering Research Laboratory, Sept. 1964, pp. 378-392.
8. L.R. Hermann. Efficiency Evaluation of a Two Dimensional Incompatible Finite Element. Journal of Computers and Structures, Vol. 3, 1973, pp. 1377-1395.
9. J.M. Duncan. Design of Circular and Elongated Flexible Metal Culverts. Presented at 55th Annual Meeting, TRB, 1976.
10. C.S. Chang, J.M. Espinoza, and E.T. Selig. Computer Analysis of Newton Creek Culvert. Journal of Geotechnical Division, ASCE, Vol. 106, No. GT5, Proc. Paper 15438, May 1980, pp. 513-556.
11. B.O. Hardin. Characterization and Use of Shear Stress-Strain Relations for Airfield Subgrade and Base Coarse Materials. Air Force Weapons Laboratory, Kirtland Air Force Base, NM, Final Rept. AFWL-TR-71-60, June 1971.
12. C.Y. Lee. Computer Analysis of Cross Canyon Culvert. Virginia Polytechnic Institute and State Univ., Blacksburg, M.S. thesis, 1981.
13. L.C. Rude. Measured Performance of a Laboratory Culvert. Journal of Geotechnical Engineering Division, ASCE, Vol. 108, No. GT12, Dec. 1982, pp. 1624-1641.

Publication of this paper sponsored by Committee on Culverts and Hydraulic Structures.